Barcelona 2014

UNIVERSITAT POLITÈCNICA DE CATALUNYA

Advanced Electrospun Scaffolds based on Biodegradable Polylactide and Poly(Butylene Succinate) for Controlled Drug Delivery and Tissue Engineering

Elena Llorens Domenjó

Advanced Electrospun Scaffolds based on Biodegradable Polylactide and Poly(Butylene Succinate) for Controlled Drug Delivery and Tissue Engineering

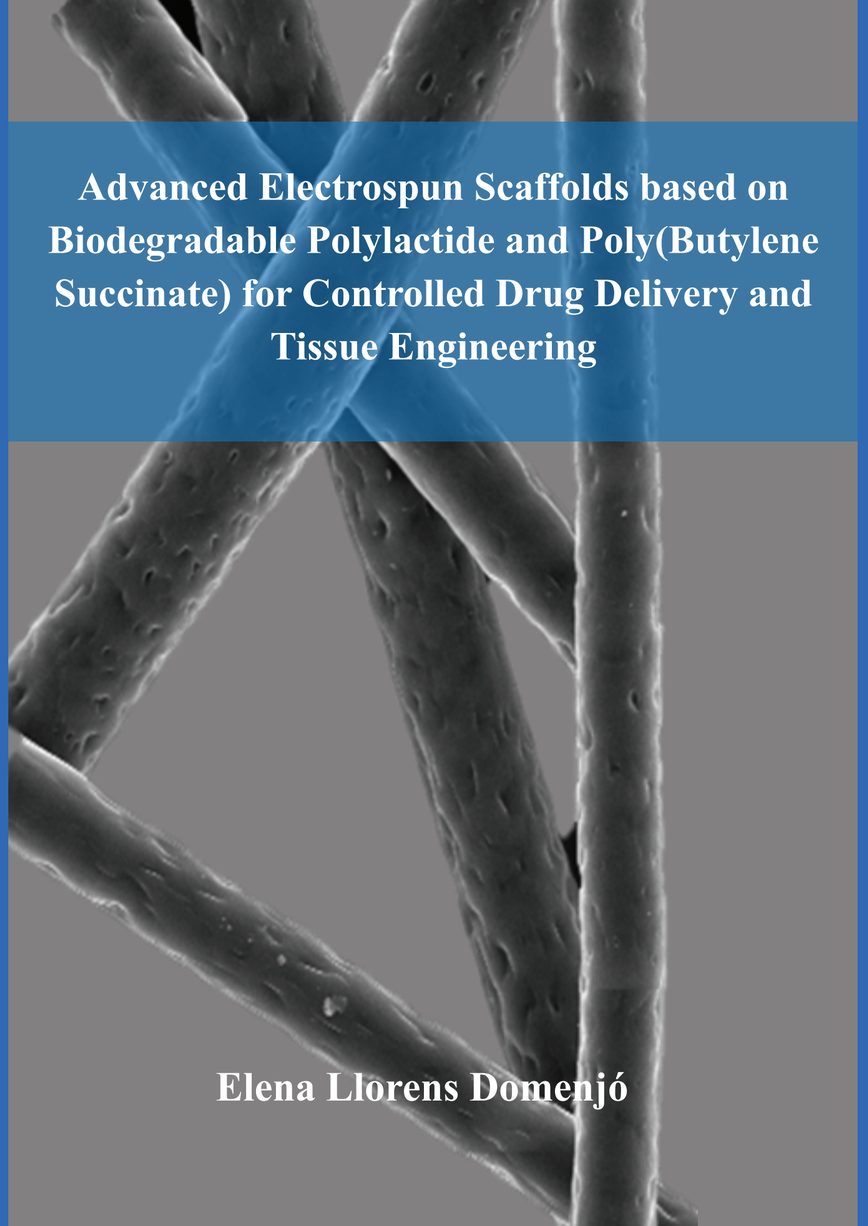

Elena Llorens Domenjó

Elena Llorens, was born in Lleida in 1985, is passionate about reading, traveling and science. She graduated in Chemistry and Biochemistry in Universitat Rovira i Virgili. After the experience in different industries in material processing and chemical analysis, she decided to increase her knowledge in polymer science starting a Master in Polymers and Biopolymers, which gave her the chance to initiate a PhD program in Universitat Politècnica de Catalunya.
But her ambition on how the industries are managed, motivated her to do a Master in Business Academy and Master in Leadership and Management Skills.
Given the opportunity to work in a chemical company, now is time to deepen her detailed knowledge in the polymer industry, after having gained an experience and solid research background in biomaterials and polymers for more than four years.

“Advanced Electrospun Scaffolds based on Biodegradable Polylactide and Poly(Butylene Succinate) for Controlled Drug Delivery and Tissue Engineering”

Elena Llorens Domenjó

Advisors

Dr. Jordi Puiggalí Bellalta Dr. Luis J del Valle Mendoza

Universitat Politècnica de Catalunya

Departament d’Enginyeria Química

Escola Tècnica Superior d’Enginyeria Industrial de Barcelona

Barcelona 2014

Ph.D. Thesis submitted to obtain degree of Doctor in Polymers and Biopolymers Program

"La lógica te llevará de la A a la B.

La imaginación te llevará a todas partes"

Albert Einstein

Abstract

As one of the most promising developments of micro/nanotechnology, electrospinning has gathered a great deal of interest in the last decades. The electrospinning technique allows the preparation of fiber matrices in controlled conditions, with diameters ranging from micron to nanoscale. Basically, electrospinning can produce fibers through the action of an external electric field that creates an electrically charged jet from a polymer solution drop and fibers after the rapid evaporation of the solvent. This versatile technique has allowed processing a wide variety of polymers. However, a large number of variables must be taken into account as they can directly influence the characteristics of the resulting fibers. These variables are either related to the material and solution properties (e.g., solubility, molecular weight, viscosity, etc.) or to the specific processing parameters (applied voltage, flow rate or tip-collector distance). Scaffolds constituted by electrospun fibers have a large specific surface area, light weight and high porosity, and, consequently, are interesting for a wide variety of applications including nanocomposites and biomedical such as tissue templates, prosthesis and drug delivery systems.

In this Thesis, micro/nanofibers conveniently modified were prepared by electrospinning to get novel materials for biomedical applications. Four blocks were mostly covered in this dissertation with different focus on drug delivery and/or tissue engineering.

In the first block, polylactide (PLA) was electrospun in micro/nanofibers and loaded with four different molecules with antioxidant activity (i.e. vitamin B_6 in pyridoxine and pyridoxal forms, *p*-coumaric acid and caffeic acid). The influence of different antioxidant molecules was studied regarding their physical properties, morphology, *in-vitro* drug release profiles and biocompatibility. As the antioxidant activity was previously assessed, it was interesting to test these new materials as an application to inhibit oxidative DNA damage caused by free radicals initiators. This damage was evaluated *in-vitro* and *in-vivo* by measuring the conversion of supercoiled plasmid DNA into open circular and linear forms. It was demonstrated that these antioxidants, in solution, could significantly inhibit the oxidative DNA damage and could maintain their protective role *in-vitro* and *in-vivo* against oxidative DNA damage when they were loaded in PLA nanofibers. Thus, these electrospun mats appear to be interesting for their use in the purification of plasmidic or genomic DNA.

In the second block, PLLA matrices loaded with two or three drugs were prepared in order to get a multifunctional activity. Thus, antioxidant, anti-inflammatory and antimicrobial molecules were considered in order to prevent chain oxidation processes in different biomolecules (proteins, DNA, etc.), avoiding the subsequent local inflammatory process and reducing the potential risk of microbial infection of wounds, respectively. These matrices have a special interest due to the synergies and antagonisms, which may occur during the simultaneous release of different drugs. In all cases, antimicrobial activity was tested and the biocompatibility of derived scaffolds evaluated.

The third block deals on the possibility of preparing biodegradable scaffolds from non electrospinable polymers that have advantages like conductivity/electroactivity or bactericide activity. In the first case, PLA nanofibers were successfully loaded with polyhexamethylenebiguanide hydrochloride (PHMB), which is a low molecular weight polymer with a well-known bactericide activity. Finally 3D biodegradable scaffolds had a well proven antibacterial activity and a release that was highly dependent on the hydrophilicity of the medium. In the second case, hybrid scaffolds constituted by different ratios of polylactide as a biodegradable polymer and poly(3-thiophene methyl acetate) (P3TMA) as an electroactive polymer were studied. The incorporation of P3TMA slightly affected the fiber morphology and lead to a significant electroactivity when its weight percentage was close to 50 wt-%. Obviously, scaffolds with higher percentages were not able to be prepared due to the low molecular weight of the conducting polymer.

Finally, in the fourth block, electrospun scaffolds were obtained using a sacrificial polymer (e.g., polyethyleneglycol (PEG)) that could easily be subsequently removed by solubilization in aqueous media. This block considered three possibilities: a) Preparation of scaffolds constituted by different ratios of PLA and PEG electrospun fibers, b) Preparation of scaffolds constituted electrospun fibers having different PLA and PEG contents; c) Preparation of scaffolds constituted by coaxial electrospun fibers with different core-shell polymer distributions. In general, all procedures gave interesting results since porosity of scaffolds was increased and cell colonization logically favoured. The three considered procedures gave also the possibility of preparing scaffolds with different drug release behaviors.

Acknowledgements

There are many people I am grateful to for making it possible for me to earn my Ph.D. degree. First and foremost, I would like to start thanking my supervisors, Prof. Dr, Jordi Puiggalí, for taking a chance and believe in me when he give me the opportunity to work in this laboratory, his wisdom and ideas on how to deepen the understanding of my work were invaluable; and Dr. Luis J. del Valle, for his guidance, inspiration and constant encouragement and patience throughout the project. His unfailing optimism and enthusiasm for science made the most difficult problems very exciting endeavors. Both of them have taken considerable amount of time and energy to teach me, and their ideas and suggestions always lead to a better understanding of my thesis topic. They have always pushed me to work hard and challenged my mind with insightful questions.

I would like to thank Dr. Lourdes Franco for her time invested in explaining and helping me with the calorimetric analysis. I am exceedingly grateful to Dr. María Teresa Casas and Dr. Trifon Trifonov for training me in microscope techniques, Dr. Montse Domínguez and Dr. Alfonso Rodríguez-Galan for the XPS and RMN analysis, respectively. Their support and encouragement enriched my experience.

I must also extend thanks to research fellow labmates: Angélica, Sara, Yolanda, Ricard, Silvia, Heliazar, Sergi, Gustavo, Georgina, Ester, Dani… I always love the talks we had, the food we shared, and the challenges we worked through together. They have all contributed to this study in some way. I know I would not be at this point without all their help.

Lastly, I want to express my biggest appreciation to my parents and sister, for their unconditional love and selfless support through all these years. They sacrificed too much to rise me up and always give me full support to pursue my dreams. No matter where I am and what I am going to be, I know they always be with me. I give my heartfelt thanks to my dearest friends: Montse, Natàlia and Virgínia. Those tears and laughter shared with you are priceless memories that I treasure deep in my heart. A special thank you to Javi, who being always there in the most difficult times to listen me despite thinking that I am like a broken record. His endless love and happiness are invaluable for me.

Publications

Llorens, E.; del Valle, L. J.; Díaz, A.; Casas, M. T.; Puiggalí, J. **Polylactide Nanofibers Loaded with Vitamin B6 and Polyphenols as Bioactive Platform for tissue Engineering**. *Macromol. Res*. **2013**, *21* (7), 775-787.

Llorens, E.; Armelin, E.; Pérez-Madrigal, M. M.; del Valle, L.J.; Alemán, C.; Puiggalí; J. **Review: Nanomembranes and Nanofibers from Biodegradable and Conducting polymers.** *Polymers*. **2013**. *5* (3), 1115-1157.

Llorens, E.; del Valle, L. J.; Puiggalí, J. **Inhibition of Radical-Induced Oxidative DNA Damage by Antioxidants Loaded in Electrospun Polylactide Nanofibers**. *Macromol. Res*. **2014**, *22* (4), 388-396.

Llorens, E.; del Valle, L. J.; Ferran, R.; Rodríguez-Galán, A.; Puiggalí, J. **Scaffolds with Tuneable Hydrophilicity from Electrospun Microfibers of Polylactide and Poly(ethylene glycol) Mixtures: Morphology, Drug Release Behavior and Biocompatibility**. *J. Polym. Res*. **2014**, *21* (2), 360-375.

Llorens, E.; Pérez-Madrigal, M.M.; Armelin, E.; Alemán, C.; del Valle, L.J.; Puiggalí; J. **Electrospun Nanofibers from Biodegradable Polylactide and Conducting Poly(thiophenen methyl acetate) Mixtures.** *RSC Adv*. **2014**, *4*, 15245-15255.

Llorens, E.; Calderón, S.; Rodríguez-Galán, A.; del Valle, L. J.; Puiggalí, J. **Polybiguanide (PHMB) Loaded in PLA Scaffolds Displaying Superhydrophobic, Biocompatibility and Antibacterial Properties**. *Mater. Sci. Eng. C.* Submitted.

Llorens, E.; Bellmunt, S.; del Valle, L. J.; Puiggalí, J. **Scaffolds Constituted by Mixed Polylactide and Poly(Ethylene Glycol) Electrospun Microfibres.** *J. Polym. Res.* Submitted.

Llorens, E.; Ibañez, H.; del Valle, L. J.; Puiggalí, J. **Biocompatibility and Drug Release Behavior of Scaffolds Prepared by Coaxial Electrospinning of Poly(Butylene Succinate) and Polyethylene Glycol**. *Mater. Sci. Eng. C.* Submitted.

Llorens, E.; del Valle, L. J.; Puiggalí, J. **Electrospun Scaffolds of Polylactide with a Different Enantiomeric Content and Loaded with Anti-Inflammatory and Antibacterial Drugs**. *Express Polym. Lett.* Submitted.

Llorens, E.; del Valle, L. J.; Puiggalí, J. **Multifunctional Ternary Drug-Loaded Electrospun Scaffolds**. *J. Appl. Polym. Sci.* Submitted.

Contributions to Conferences

Llorens, E.; Puiggalí, J.; del Valle, L. J. **Loading of Polylactyde Electrospun Nanofibers with Antioxidant Agents: Evaluation of the Effect on Cells under Oxidative Stress Conditions and Applications for DNA Purification**. 4th International Conference "Smart Materials, Structures and Systems". CIMTEC. Poster. Montecatini Terme, Tuscany, Italy, **2012**.

Llorens, E.; Calderón, S.; Puiggalí, J.; del Valle, L. J. **Electrospun Polylactyde Scaffolds with Multifunctional Activity (Antimicrobial, Antioxidant and Anti-Inflammatory): Properties and Delivery.** 5th International Conference on Molecular Materials. MOLMAT. Poster. Barcelona, **2012**.

Llorens, E.; Ferran, R.; Franco, L.; Rodríguez-Galán, A.; Puiggalí, J.; del Valle, L. J. **Electrospun Hybrid Scaffolds Composed of PLA/PEG Mixtures for Tissue Engineering and Drug Delivery**. 3rd International Symposium Frontiers in Polymer Science. Poster. Sitges, **2013**.

Llorens, E.; Calderón, S.; Puiggalí, J.; del Valle, L. J. **Antibacterial Activity of Polyhexamethylene Biguanide Loaded in PLA Electrospun Microfibers**. 3rd International Symposium Frontiers in Polymer Science. Poster. Sitges, **2013.**

Table of Contents

ABSTRACT I
ACKNOWLEDGEMENTS III
PUBLICATIONS V
CONTRIBUTIONS TO CONFERENCES VII
TABLE OF CONTENTS IX
ABREVIATIONS AND ACRONYMS XIII
1. INTRODUCTION 3
1.1 Biomaterials 3
1.1.1 Poly(lactic acid) (PLA) 4
1.1.2 Polybutylene succinate (PBS) 5
1.1.3 Polyethylene glycol (PEG) 6
1.1.4 Conducting Polymers 7
1.2 Biomedical Applications 8
1.3 Tissue Engineering 9
1.4 Drug Delivery 12
1.5 Other Applications 13
1.5.1 Surgical Fixation Devices 13
1.5.2 Wound Dressings 14
1.6 Electrospinning 15
1.6.1 Brief history 15
1.6.2 Electrospinning set-up 17
1.6.3 Electrospinning parameters 18
1.6.4 Advances on the electrospinning technique 19
1.7 Electrospinning of biodegradable polymers as bioactive systems 21
1.7.1 Biodegradable polymer loaded with drugs 21
1.7.2 Biodegradable polymer meshed with conductive polymers 23
1.8 References 25
2. OBJECTIVES 33
3. ANTIOXIDANT LOADED BIODEGRADABLE SCAFFOLDS AND POTENTIAL APPLICATION FOR DNA PURIFICATION 39
3.1 Polylactide Nanofibers Loaded with Vitamin B_6 and Polyphenols as a Potential Bioactive Platform for Tissue Engineering 43
3.1.1 Introduction 44
3.1.2 Experimental Section 47
3.1.3 Results and Discussion 51
3.1.4 Conclusions 69
3.1.5 References 70

3.2 Inhibition of Radical-Induced Oxidative DNA Damage by Antioxidants Loaded in Electrospun Polylactide Nanofibers 73
3.2.1 Introduction 74
3.2.2 Experimental Section 76
3.2.3 Results and Discussion 79
3.2.4 Conclusions 90
3.2.5 References 91

4. MULTIFUNCTIONAL BIODEGRADABLE FIBER SCAFFOLDS _____ 93

4.1 Electrospun Scaffolds of Polylactide with a Different Enantiomeric Content and Loaded with Anti-Inflammatory and Antibacterial Drugs 97
4.1.1 Introduction 98
4.1.2 Experimental Section 100
4.1.3 Results and Discussion 104
4.1.4 Conclusions 119
4.1.5 References 120
4.2 Electrospun Ternary Drug-Loaded Multiactive Scaffolds 123
4.2.1 Introduction 124
4.2.2 Experimental Section 126
4.2.3 Results and Discussion 130
4.2.4 Conclusions 146
4.2.5 References 147

5. PREPARATION OF BIODEGRADABLE SCAFFOLDS INCORPORATING NON-ELECTROSPINABLE POLYMERS _____ 151

5.1 PLA Scaffolds Incorporating Bactericide Polybiguadine (PHMB) 155
5.1.1 Introduction 1556
5.1.2 Experimental Section 158
5.1.3 Results and Discussion 162
5.1.4 Conclusions 178
5.1.5 References 179
5.2 Electrospun Nanofibers from Biodegradable Polylactide and Conducting Poly(3-Thiophene Methyl Acetate) Mixtures 183
5.2.1 Introduction 184
5.2.2 Experimental Section 186
5.2.3 Results and Discussion 190
5.2.4 Conclusions 206
5.2.5 References 207

6. BIODEGRADABLE POLYMER MATRICES INCORPORATING POLYETHYLENE GLYCOL AS A SACRIFICIAL POLYMER_____209

6.1 Scaffolds with Tuneable Hydrophilicity from Electrospun Microfibers of Polylactide and Poly(Ethylene Glycol) Mixtures: Morphology, Drug Release Behavior and Biocompatibility 213

6.1.1 Introduction 214
6.1.2 Experimental Section 216
6.1.3 Results and Discussion 220
6.1.4 Conclusions 236
6.1.5 References 237
6.2 Scaffolds Constituted by Mixed Polylactide and Poly(Ethylene Glycol) Electrospun Microfibers 241
6.2.1 Introduction 242
6.2.2 Experimental Section 245
6.2.3 Results and Discussion 248
6.2.4 Conclusions 2600
6.2.5 References 2611
6.3 Biocompatibility and Drug Release Behavior of Scaffolds Prepared by Coaxial Electrospinning of Poly(Butylene succinate) and Polyethylene Glycol 265
6.3.1 Introduction 266
6.3.2 Experimental Section 269
6.3.3 Results and Discussion 273
6.3.4 Conclusions 289
6.3.5 References 290
6. CONCLUSIONS 293
General Conclusions 295

Abreviations and Acronyms

A

AAPH	2,2'-Azobis(2-methylpropionamidine) dihydrochloride
ANOVA	Analysis of variance
ATR	Attenuated total reflectance

C

CA	Contact angle
CAF	Caffeic acid
CC_{50}	Cytotoxic concentration to reduce cell population by 50%
CCV	Control cyclic voltammetry
$CDCl_3$	Deuterated chloroform
CFU	Colony forming units
CHX	Chlorhexidine (1,1'-hexamethylene-bis-5-(4-chlorophenyl) biguanide
COS-7	Kidney fibroblast cells derived from African Green Monkey
CUM	*p*-Coumaric acid
CUR	Curcumine

D

d	Doublet
DCM	Dichloromethane
DH5α	*Escherichia coli* DH5α, strain for routine cloning applications
DMEM	Dulbeccos' modified eagle medium
DMF	*N*,*N*-dimethylformamide
DMSO	Dimethylsulfoxide
DSC	Differential scanning calorimetry
DTGA	Derivative thermogravimetric analysis

E

E	Tensile modulus
E.coli	*Escherichia coli*
ECM	Extracellular matrix
EDTA	Ethylenediaminetetraacetic acid
EtOH	Ethanol

F

FTIR	Fourier transform infrared

H

h	Hour(s)
HEP-2	Epithelial cells derived from human laryngeal carcinoma

I

I	Intensity
IC_{50}	Half maximal Inhibitory Concentration

J

J	Coupling constant

K

K_H	Higuchi release constant
K_1	First order release constant

L

L	Litre(s)
LB	Luria Bertrani

M

m (in NMR)	Multiplet
M	Molar
M.luteus	*Micrococcus luteus*
MDCK	Madin-Darby canine kidney cells

MG-63	Human osteosarcoma cells
M_n	Number-average molecular weight
MRC-5	Human fetal lung fibroblast cells
MTT	3-(4,5-dimethylthiazol-2-yl)-2,5-diphenyl-2H-tetrazolium bromide
M_w	Weight-average molecular weight
min	Minute(s)
	N
n	Number of repeat units
NMR	Nuclear magnetic resonance
	P
P3TMA	Poly(3-thiophen methyl acetate)
PBS	Poly(butylene succinate)
PBS	Phosphate saline buffer solution
PCL	Poly(ε-caprolactone))
PDI	Polydispersity index
PEG	Poly(ethylene glycol)
PHMB	Polyhexamethylenebiguanide hydrochloride
PHT or P3HT	Poly(3-hexylthiophene)
PL	Pyridoxal hydrochloride
PLA	Polylactic acid
PLGA	Poly(lactic-*co*-glycolic acid)
HFIP	1,1,1,3,3,3-Hexafluoroisopropanol
PN	Pyridoxine hydrochloride
PPy	Polypyrrole
PS	Polystyrene
pUC19	Plasmid DNA
ppm	Parts per million

Q

q	Scattering vector

R

RCS	Refrigeration cooling system
ROP	Ring-opening polymerization

S

s	Singlet
SS	Phosphate saline buffer solution
SEC	Size exclusion microscopy
SEM	Scanning electron microscopy

T

t	Time
t (in NMR)	Triplet
TBE	Tris-Borate-EDTA buffer
T_C	Crystallization temperature
TCM	Trichloromethane
TCPS	Tissue culture plate of polystyrene
TCS	Triclosan
TEM	Transmission electron microscopy
T_g	Glass transition
TGA	Thermogravimetric analysis
T_m	Melting temperature
Tris	Tris(Hydroxymethyl)aminomethane
TRX	6-hydroxy-2,5,7,8-tetramethylchroman-2-carboxylic acid (Trolox)

U

UV	Ultra-violet spectroscopy

V

VERO	Kidney epithelial cells derived from African green monkey

W

W/O	Water-in-oil
WAXD	Wide-angle X-ray diffraction

X

XPS	X-ray photoelectron spectroscopy

#

3TAA	3-Thiophene acetic acid
3TMA	3-Thiophenen methyl acetate
δ (in IR)	Bending
r (in IR)	Rocking (s – symmetric, as – asymmetric)
ν (in IR)	Vibration (s – symmetric, as – asymmetric)
ΔC_p	Increment of heat capacity
ΔH_c	Increment of enthalpy of crystallization
ΔH_m	Increment of enthalpy of fusion
χ_c	Degree of crystallinity
χ_{MAP}	Mobile amorphous phase fraction
χ_{RAP}	Rigid amorphous phase fraction
σ	Tensile strength
γ	Tensile elongation

1.

Introduction

1. Introduction

1.1 Biomaterials

The term of biomaterial refers to any material, natural or man-made, that comprises whole or part of a living structure or biomedical device, which performs, augments, or replaces a natural function.[1] To interact with biological systems, the biomaterials must be biocompatible, meaning that they must have the ability to perform an appropriate host response in a specific application. New materials are designed to elicit an effective interaction with tissues, provoking physiological responses such as cell growth and/or differentiation at the site of implantation.[2]

The biomaterials used as implants can be divided into permanent or temporary biomaterials.[3] Permanent biomaterials are used to replace damaged tissues for an undetermined period of time, but in some situations the support only is needed to temporarily fill the damaged region until tissue recomposition is completed, or guided by the regeneration process. With temporary biomaterials, the term biodegradable can be applied to polymers and the solid devices that undergo dispersion *in vivo* as a result of macromolecular degradation.[4] Biodegradable polymers can be attacked by biological elements so that the integrity of the system is affected, forming fragments and other degradation products that can be removed from the site of action but not necessarily from the body.[4] Another revelant feature for materials used as temporary devices is the bioresorbability, in this case degradation is followed by a reduction in the size of the biomaterial and resorbed *in vivo*, which means that materials can be removed by cellular activity (e.g., phagocytosis) in the organism.

Nowadays, biodegradable polymers have gained increasing attention due to their greater demand for diverse biomedical applications including regenerative medicine, tissue engineering, controlled drug delivery and gene therapy.[5] Some polymers of this type are polylactide (PLA), polycaprolactone (PCL), polyglycolide (PGL) and their copolymers [e.g., poly(lactic-*co*-glycolic acid) (PLGA)] (**Figure 1.1**). These are the most commonly used synthetic polymers despite the ongoing efforts focused on designing novel biomaterials with enhanced performance.[6]

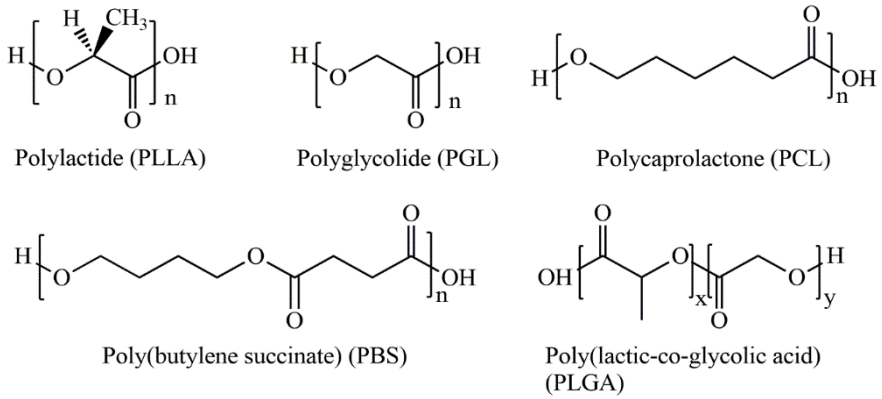

FIGURE 1.1

Scheme showing the chemical structure of some biodegradable polymer used in biomedicine.

The synthetic polymeric biomaterials based on aliphatic polyesters are probably the most employed. These polymers can be classified in two main groups:

- Poly(hydroxyalkanoate)s: Synthetized by polymerization of hydroxy acids or by ring-opening polymerization of cyclic monomers, e.g., poly(lactic acid) (PLA) and poly(glycolic acid) (PGA).
- Poly(alkylene dicarboxylate)s: Synthetized through a polycondensation reaction between a diol (HO-R_1-OH) and a dycarboxylic acid (HOOC-R_2-COOH) or the corresponding diester (e.g., poly(butylene succinate) (PBS) and poly(butylene adipate) (PBA)).

A large number of biodegradable polyesters are commercially available but merely polymers with reasonably short aliphatic chains can be used as biodegradable polymers for biomedical applications. These polyesters are often mildly hydrophobic and degrade by bulk erosion through the hydrolizable ester bonds.[7] Poly(α-esters) have been the most heavily researched degradable biomaterials to date[7] due to their relatively easy synthesis (via both ring-opening and polycondensation reactions) and commercial availability.

1.1.1 Poly(lactic acid) (PLA)

Poly(lactic acid) offers unique features of biodegradability, biocompatibility, bioresorbability, thermoplastic processability and eco-friendliness. These features allow potential applications as ecological materials, surgical implant materials, drug delivery systems and, porous scaffolds for the growth of neo-tissues.[8, 9] PLA is also being used because its good performance, excellent properties and low price.[10] Various devices have been commercialized from different PLA types including degradable sutures, drug delivery microparticles, nanoparticles, and porous scaffolds for cellular applications.

The diversification of PLA applications is such that a single polymer can be useful in many applications by simple modifications of their physical-chemical structure. In many cases, the polymer can be blended or copolymerized with other polymeric or non-polymeric components to achieve the desired behaviour.[11] The surface properties of materials play a critical role in determining its applications, especially when biocompatibility is required. Different surface modification strategies - such as physical, chemical, plasma and radiation[12] induced methods - have been employed to reduce degradation time and create desirable surface properties.[13]

PLA can be used as biodegradable polymer implants, which remain temporarily in the body and disappear upon degradation. However, PLA is unsuitable for sutures because its degradation rate is very slow.[14] On the contrary, PLA is the preferred material for applications where a long retention of the strength is required. These include ligament and tendon reconstruction, and stents for vascular and neural reconstruction.[15] Three-dimensional porous scaffolds of PLA have been created for culturing different cell types, and used in cell-based gene therapy for cardiovascular diseases.

1.1.2 Poly(butylene succinate) (PBS)

Polybutylene succinate (PBS) was synthetized in 1990 and commercialized under the trademark Bionolle®.[16] PBS is one of the most accessible biodegradable polymers. It is an aliphatic polyester with good processability, and easy preparation and flexibility, with degradation products that are non-toxic. Thus, succinic acid is an intermediate in the biological tricarboxylic acid (TCA) cycle. In addition, PBS could degrade into CO_2 and H_2O through naturally occurring enzymes and microorganisms.[17-20]

PBS is a semicrystalline polyester with a melting point higher than that of PLA. Its mechanical and thermal properties depend on the crystal structure and the degree of crystallinity.[21] The relatively poor mechanical flexibility of PBS limits the applications of 100% PBS-based products. However, this feature can be overcome by blending with PLA or starch in order to provide similar properties than polyolefins.[21] Specifically, materials with a good tensile and impact resistance, and moderate stiffness and strength can be achieved. By changing the polymer composition in the blend of PBS/PLA, the mechanical properties can be adjusted to suit the required application.[22] These blends, have been extensively studied for commercial applications in agriculture, fishery, forestry, construction, and other industrial fields as a conventional plastic.[23] Applications of PBS or its blends have also been proposed as a support for different approaches in the medical field.[24]

PBS can be easily produced in a wide variety of forms and structures, such as yarns, non-wovens, films and mono-filaments that provide, as above explained, excellent mechanical properties that are comparable with those of polyethylene or polypropylene.[37, 40] In light of its biodegradability and harmless degradation products, PBS is an excellent choice to use as scaffolds support in tissue regeneration.[25]

1.1.3 Polyethylene glycol (PEG)

Scaffolds of bio-based polymers are interesting as reinforcement for tissue engineering applications, but they have also some limitations. The most significant is associated to their dense structure that limits cell infiltration. These biomaterials are inherently resistant to non-specific cell adhesion and protein adsorption. Thus, they provide a blank slate upon which ECM-derived signals can be systematically introduced spatially and temporally manipulated to control cell behavior and tissue regeneration.

To overcome this problem, an extensive research has been conducted to use sacrificial biopolymers that allow the creation of desired holes in scaffolds or templates.[26] PEG (**Figure 1.2**) is a polymer with great interest because it presents outstanding properties, e.g., solubility in water and in organic solvents, lack of toxicity, absence of antigenicity and immunogenicity, which are essential for biomedical applications, including surface modification, bioconjugation, drug delivery and tissue engineering.[27, 28]

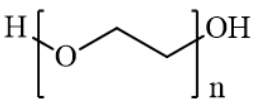

Poly(ethylene glycol) (PEG)

FIGURE 1.2
Chemical structure of poly(ethylene glycol).

The combination of the above mentioned strategies may ultimately result in PEG-based scaffolds containing the necessary cues that recapitulate the dynamic environment of ECM and lead to the regeneration of tissues.[29]
Continuous enhancement of PEG-based biomaterial strategies, towards the design of scaffolds, is highly reliant on their ability to a separate control of the incorporation of multiple biofunctional signaling molecules from alterations in degradation kinetics and mechanical properties. Furthermore, it is important to tune, temporally and spatially, the design of mechanical and biofunctional signals to promote rapid and guided neovascularization (new blood vessel formation) prior to complete material degradation.[29]

The PEG-drug conjugates have several advantages: prolonged residence in the body, a decreased degradation by metabolic enzymes and a reduction or elimination by immunogenic protein.[30] While the advantages of PEG in biomedical applications are lengthy, it should be considered its non-degradable structure as the primary disadvantage for its use in biomedical applications.

1.1.4 Conducting Polymers

Conducting polymers (CPs) provide a type of processable materials with characteristics that range between those of semiconductors and metals (e.g., electrical and optical properties). Furthermore, the attractive properties associated with conventional polymers such as low density, stability, lightness, easy of synthesis and processing, have given a wide range of applications in the microelectronics industry (e.g., batteries,[31] electrochromic devices,[32] supercapacitors,[33] electroluminescence[34] and photovoltaic cells[35]), in biological field (e.g., biomedical engineering[36] and drug delivery[37]) and mechanical and chemical sensors (e.g., biosensor).[38] The main focus in the use of these polymers lies in the scope of their low manufacturing cost.

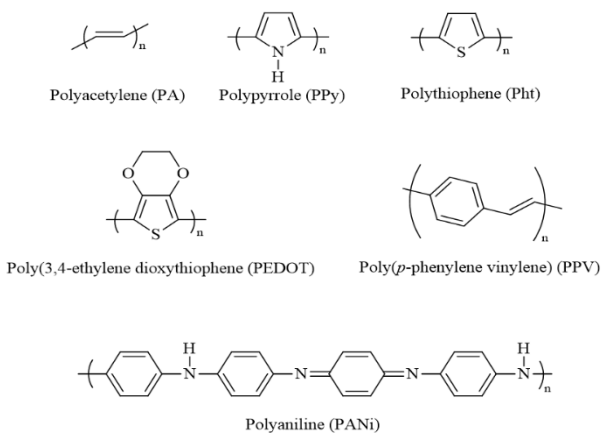

FIGURE 1.3
Scheme showing the chemical structure of main conduncting polymers (CP).

The most common CPs include polyacetylene (PA), polypyrrole (PPy), polythiophenes (PThs), polyaniline (PANi), and poly(p-phenylene vinylenes) (PPVs) (**Figure 1.3**), although not all of them have been considered for biomedical uses.[6]

There is an increasing interest to explore the utility of incorporating conducting polymers into biomaterials to take advantage of the beneficial effect of electrical stimulation on tissue regeneration such as skeletal nerve or other living tissues.[6]

Mainly, PPy and their derivatives are the most widely studied polymers due to their easy synthesis, good chemical and thermal stabilities, low oxidation potential and high conductivity.[39] Furthermore, the long-term environmental stability enhances its interest for many industrial applications (e.g., antistatic, electromagnetic shielding, actuator and polymer battery) despite some uses may be limited by the inherently poor solubility in common solvents. The interest of PPy for biomedical applications has been highlighted by Langer *et al*.[31] who

showed that the electrical stimulation from the application of an external electrical field through a PPy film could significantly improve the spreading in cultured neurons. Then, it has been shown its ability to improve the effect of nerve growth factor (NGF) for inducing neuronal differentiation of PC12 cells in electric stimulation.[40]

However, in the last two decades some PTh derivatives with excellent electrical and electrochemical properties, characteristic chemical structure, as well as very high environmental stability, have been reported.[41, 42] Among them, PEDOT, is the most important due to its high conductivity (up to 400-600 $S \cdot cm^{-1}$), good thermal and chemical stability, fast redox processes and excellent biocompatibility.[43] Consequently, this CP has attracted considerable interest based on its properties and many applications have been rapidly developed, e.g., antistatic coatings, electrode material in supercapacitors, hole injection layer in organic light-emitting diodes, and solar cells.[44] Poly(3-thiophene methyl acetate) (P3TMA) is another polythiophene derivative that is characterized by bearing carboxylate substituents in the 3-position of the heterocyclic ring. The P3TMA can be easily prepared via oxidative chemical[45] and photochemical[46] reactions and appears a suitable candidate for being processed by electrospinning since has a good solubility in organic solvents like chloroform. Furthermore, it has currently been demonstrated that it's very stable free-standing nanomembranes. Electroactive and biodegradable properties can be achieved by combining P3TMA and polyesters, such as poly(tetramethylene succinate), and even thermoplastic polyurethanes and poly(vinylidene fluoride).[47, 48]

Finally, PANi is an electroactive conjugated polymer with three primary oxidation states (leucoemeraldine, emeraldine and pernigranilin[49, 50]) that shows very good environmental stability. PANi became an important studied subject since 1980 because of its significant potential for technological applications such as in batteries (as electrodes), electromagnetic shielding, capacitors, sensor, corrosion inhibitors, actuators and electrochromic devices.[51] For example, PANi and its derivatives were found to be able to function as biocompatible substrates, upon which both H9c2 cardiac myoblasts and PC12 pheochromocytoma cells can adhere, grow and differentiate.[52]

1.2 Biomedical Applications

Nowadays, a variety of polymers are used for biomedical applications such as tissue engineering scaffolds,[53] filtration membranes[54, 55] and in drug delivery systems. Naturally occurring polymers normally exhibit better biocompatibility and low immunogenicity than synthetic polymers.[56] A strong reason is the inherent capacity for binding cells since they carry specific protein sequences such as RGD.[57] Scaffolds fabricated from natural polymers promise better clinical functionality, although problems like their partial denaturation should be taken into account. Synthetic polymers often offer many advantages over natural polymers as they can be

tailored to give a wider range of properties such as necessary mechanical properties and desired degradation rate.[58]

One of the main areas of research in biomedical applications is drug delivery where controlled release is an efficient process of delivering drugs in medical therapy. Also, the effective release of therapeutic agents towards alleviating medical conditions is one aspect of polymeric biomaterials design.

Tissue engineering (TE) is being one of the most important areas of research in health care, which has revolutionized medical engineering and has the potential to push the limitations even further in future. TE is a growing interdisciplinary scientific area that involve the knowledge from biology, medicine, engineering and material science field[59] towards the development of biological substitutes to create, repair or replace tissue function.

1.3 Tissue Engineering

Human body is a complex and well organized system consisting of tissues and organs. The extracellular matrix (ECM) is a complex of separate different tissues, which form a supportive network of nanometer-sized proteins and glycosaminoglycans.[59, 60] Adequate nutrients, oxygen and the suitable environment for the cell growth should be available in the tissues (**Figure 1.4**).

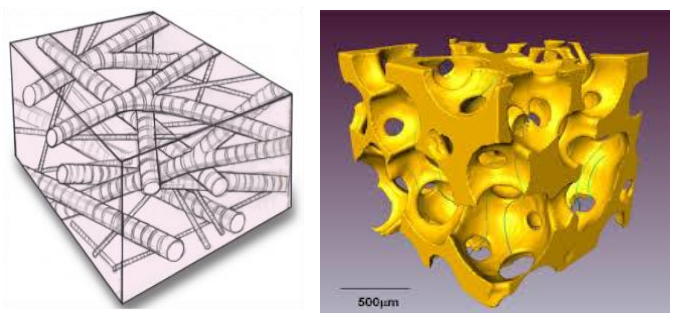

FIGURE 1.4
Representacion of fibers forming a 3D structure in comparison with a representative ECM porous scaffold.

It is widely understood that cell behavior is affected through indirect effects of surface chemistry and free surface energy on the adsorption of specific ECM proteins, required by cells for attachment via integrin receptor binding.[29] ECM and cell-cell interactions determine the ability of cells to build tissues and maintain tissue-specific functions. An important objective of tissue engineering is to create an appropriate temporary cellular environment until repair or regeneration occurs. Currently, tissue engineering is based on the use of biomaterials formed as scaffolds, which provide a 3D framework for the cells to attach and develop *in-vitro*.[61]

In this way, the cell and the carrier are the two main components of tissue engineered products. The success rate of tissue engineering depends on the carriers which are designed as scaffolds. The basic requirements for a functional scaffold are: (a) high degree of porosity; (b) large surface area-to-volume ratio; (c) biodegradability, so a second surgery is not required to remove implant due to the degradation rate that mimic the rate of neo-tissue formation;[62] (d) structural integrity to prevent the pores of the scaffold from collapsing during neo-tissue formation and provide appropriate mechanical properties;[63] (e) no cell toxicity and biocompatibility, meaning that it will integrate in the host tissue without eliciting a major immune response. Thus, the scaffold acts as a temporary support for the cells to adhere, proliferate, migrate and differentiate. It can also be understood that the scaffold mimics the ECM both architecturally and functionally.

Nowadays, the scaffolding is essential in this endeavor to act as a three-dimensional template for tissue ingrowths by mimicking ECM.[64] Key scaffold characteristics can be tailored to the specific application by careful selection of the polymers used in its preparation, additional scaffold components, and the fabrication technique. Many different types of scaffolds have been used to achieve different goals. Typically, researchers use polymers which biodegrade slowly into non-toxic by-products as tissue regenerates. Scaffolds are modified to form an interface with healing tissue cells and usually include biopolymers, which direct the correct signals to the tissue regeneration cells. So, there is a large capacity for tailoring a scaffold architecture and biological activity towards the needs of a particular tissue.

To improve an engineered tissue, different techniques have been used during the last few decades. The highlight of TE strategies aims to design templates with specific mechanical and biological properties in order to imitate ECM. A polymeric scaffold is designed by means of various processing methods such as solvent casting,[65] salt leaching,[66] phase separation,[67] self-assembly,[68] gas foaming[69] and electrospinning.[59,53-55] **Table 1.1** summarizes the most important techniques used.

TABLE 1.1. Scaffold fabrication techniques in tissue engineering applications.[70]

Method	Polymers	Unique factors	Applications
Biodegradable porous scaffold fabrication			
Solvent casting/ Particulate-leaching.	Absorbable polymers (PLLA, PLGA, collagen, etc.).	Biodegradable controlled porous scaffold.	Cardiac and vascular tissue engineering.
Gas foaming.	PLLA, PLGA and PDLLA.	Controlled porosity and pore structure sponge.	Drug delivery and tissue engineering.
Microsphere fabrication			
Solvent evaporation technique.	PLGA and PLAGA.	High-density cell culture, due to the extended surface area.	Bone repair.
Freeze drying.	PLGA, PLLA, PGA, PLGA/PPF, Collagen and Chitosan.	3D porous sponge structure, durable and flexible.	Tissue engineering scaffolds.
Injectable gel scaffold fabrication			
Hydrogel-based injectable scaffolds.	Hydrophilic/hydrophobic diblock and triblock copolymer combinations of PLA, PGA, PLGA, and PEG. Copolymers of PEO and PPO and polyoxamer, alginates, collagen, chitosan, HA and fibroin.	Biomimetically, exhibit biocompatibility and cause minimal inflammatory responses, thrombosis, and tissue damage.	Cartilage, bone tissue engineering, and drug delivery.
Hydrogel scaffold fabrication			
Micromolding.	Alginate, PMMA, HA and PEG.	Microgels, biologically degradable with mechanical and physical complexity.	Insulin delivery, gene therapy, bioreactor, and immunoisolation.
Photolithography.	Chitosan, fibronectin, HA, PEG, PNIAAm, PAA, PMMA, PAam, and PDMAEM.	Microwells, microarrays, controlled size and shape.	Microdevices, biosensors, growth factors, matrix components, forces, and cell-cell interactions.
Keratin scaffold fabrication			
Self-assembling.	Keratin.	Biocompatibility.	Drug delivery, wound healing, soft tissue augmentation,synthetic skin, coatings for implants, and scaffolds for tissue engineering.
Fibrous scaffold fabrication			
Electrospinning.	PGA, PLA, PLGA, PCL copolymers, collagen and elastin.	High surface area, Biomechanical performance and biocompatibility.	Drug delivery, wound healing, soft tissue synthetic skin, and scaffolds for tissue engineering.
Automation and direct organ fabrication			
Rapid prototyping (PR)/Computer-aided design (CAD).		Patient-specific scaffolds and automated scaffold assembly algorithm.	Develop a program algorithm that can be used to design scaffold internal architectures.

1.4 Drug Delivery

Polymeric drug delivery systems are advantageous because they can be controlled to deliver drugs efficiently to a localized area.[65] Design of the polymeric structure is a basic point to stablish appropriate interactions with the drug, to get a desired degradation rate and to provide a good mechanism for its removal from the body. Molecular weight, crystallinity, lability of bonds, and degradability play an important role for achieving controlled release. Polymers may be excreted directly via kidney (renal clearance) or biodegraded (metabolic clearance) into smaller molecules.

The goal of all sophisticated drug delivery systems is to distribute intact medications to specifically targeted parts of the body through a mean which can control the therapy administration via either a physiological or a chemical trigger. To achieve this goal, researchers are turning to advances in the worlds of micro- and nanotechnology. During the past decade, polymeric microspheres, polymer micelles and hydrogel-type materials have been shown to be effective in enhancing drug targeting specificity, lowering systemic drug toxicity, improving treatment absorption rates, and providing protection for pharmaceuticals against biochemical degradation.[71]

Basically, two broad categories of polymer systems have been studied: reservoir devices and matrix devices. The former involves the encapsulation of a pharmaceutical product within a polymer shell, whereas the latter describes a system in which a drug is physically entrapped within a polymer network.

Typically, drug release rates are controlled by release mechanisms of drugs. There are three primary mechanisms by which active substances can be released from a controlled delivery system: (i) diffusion, which can be different for reservoir and matrix devices (**Figure 1.5**). In the first case, the drug is surrounded by the polymer film, while in the second case, the drug is uniformly dispersed throughout the polymer matrix; (ii) chemical reaction: a chemical-controlled system is a system that changes its chemical structure when exposed to biological fluid. This system is carried out by polymer degradation or chemical cleavage of drug molecules from a polymer backbone via hydrolysis or enzymatic degradation; and (iii) solvent activation: a polymeric matrix absorbs water or body fluid and then swells, resulting in the diffusion of drug through the swollen network into the external environment.

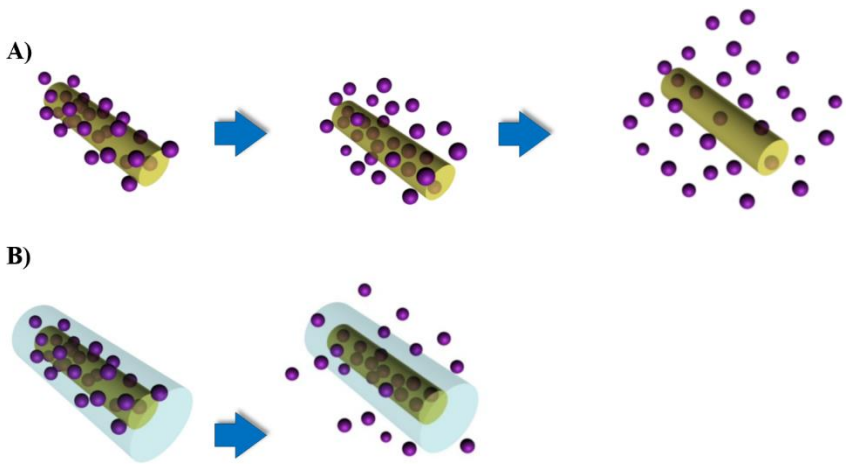

FIGURE 1.5

Schematic illustration showing the release of the anti-inflammatory drug from electrospun nanofibers (**a**) without and (**b**) with an alginate hydrogel coating.

Currently, modern research is aimed to explore the use of biodegradable polymer systems as the matrix system. These drug deliverers degrade into biologically acceptable compounds, often through the process of hydrolysis, which subsequently leave their incorporated medications behind. This erosion process occurs either in bulk (wherein the matrix degrades uniformly) or at the polymer surface (whereby release rates are related to the polymer surface area). For example, the PLGA in its degradation process involves the breakdown of polymers into lactic and glycolic acids. These acids are eventually reduced by the Kreb's cycle to carbon dioxide and water, which the body can easily expel. Hence, a second surgery is not required to remove the reservoir or matrix devices.[71]

1.5 Other Applications

1.5.1 Surgical Fixation Devices

In a situation of a healing wound, a broken bone or a damaged blood vessel, surgical fixation devices (e.g., sutures, clips, pins, plates and vascular grafts) are the corresponding support devices. About 40 types of biodegradable polymers and their copolymers are currently identified as alternatives to metal implants since these have clear disadvantages such as the sensitivity of patients to metal and the need for a removal operation. For instance, PGA, and PLGA copolymers have been successfully used as absorbable sutures because they can be processed as strong filaments and hydrolyzed *in-vitro* and *in vivo*. The most commercially utilized absorbable sutures are a multifilament PGA (Dexon®), the copolymer PLLA (8%)-co-PGA (92%) (Vicryl®) and poly(*p*-dioxanone) (PDS®).

Related to surgical sutures, the development of materials with adequate properties to be used as a coating is also highly interesting. These coating could contain different agents (e.g., triclosan,

chlorhexidine) that could render and additional activity (e.g., antibacterial or anti-inflammatory responses).[72]

1.5.2 Wound Dressings

When the skin is injured, the human body initiates a process that eventually leads to an epithelialization (regeneration of epithelial tissue) of the wound area and reestablishment of the skin barrier function.[73] The subsequent processes are ECM degradation and re-synthesis of tissue cells, which eventually results in a scar. The four phases of the wound healing process are inflammation; reconstruction; epithelialization; and maturation.

In the inflammatory phase, the body prepares itself for healing by removing foreign matter and dead cells. After any injury to the skin that breaches the epidermis, damaged blood vessels will constrict within seconds to limit blood loss. When a blood vessel is damaged, sub-endothelial tissue is exposed resulting in the aggregation of platelets (platelet plug). The platelets at the wound site will release growth factors, which attract white blood cells and stimulate the release of other chemical mediators, e.g., cytokines, which are necessary for wound healing. Consequently, macrophages contained within the surrounding blood vessels are readily moved into the tissue via vasodilation. The final and longest state, maturation phase, is a progressive decrease in the vascularity of the wound which becomes more organized and then gains strength as the collagen matures. Maturation of a wound may take months to complete and in large open wounds, it can take years.

The time period for each phase depends on the wound type. All four physiological processes occur in the healing of all soft tissue injuries, e.g., chronic ulcerative wounds (leg ulcers, pressure sores), traumatic wounds (lacerations, skin flaps, abrasions, burns), and surgical wounds. However, concentrations of reactive oxygen species (ROS) such as hydroxyl radicals (·OH), singlet oxygen (O_2), hydroperoxyl radicals (·OOH), and hydrogen peroxide (H_2O_2) can produce "oxidative stress". Chronic and severe oxidative stress conditions may delay the healing condition due to prolonged inflammation. Thus, the wound healing process may be assisted by the use of antioxidant wound dressings that reacts specifically with excess ROS, leading to the reduction of oxidative stress. The ROS inhibitors impregnated into the wound dressings include flavonoids, vitamin E, carnosin, mexidol, trypsin, and dieton.[74]

1.6 Electrospinning

1.6.1 Brief history

Scientists have been interested in the use of electrostatic force to deform liquid for centuries.[75] In the late 1500's William Gilbert set out to describe the behaviour of the known magnetic and electrostatic phenomenon.[75] He distinguished between the force arising from a loadstone and the force from rubber amber[76] and invented the term electricity to describe the force from amber. One of his more obscure observations was that when a suitably charged piece of amber was brought near a droplet of water it would form a cone shape and small droplets would be ejected from the tip of the cone. This is the first recorded observation of electrospraying.

Throughout the 20th century, electrodynamic atomization[77-79] was studied and patents for a process similar to electrospinning were accepted as early as 1902 by William James Morton,[80, 81] which demonstrate the application of high voltage electrostatic fields to both electrospray and electrospun colloids fluids, separating the fluids into fine particles and fibers which could be collected on rotating collectors (**Figure 1.6 a**, **b**).

A series of patents were awarded to A. Formhals between 1934 and 1940[82, 83] who applied an electrospinning process for the production of yarns for the textile industry. The patents described the use of polymers dissolved in an organic solvent. Another patent awarded in 1936 by C.L. Norton[84] described the collection of fibers on a rotating collector (**Figure 1.6 c**), a process adopted by many electrospinning setups nowadays.

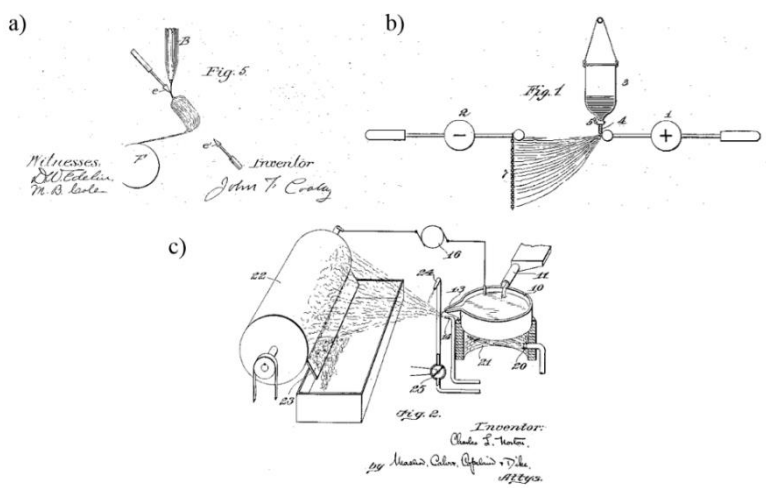

FIGURE 1.6

Dispersion of fluids by electrohydrodynamic atomization. Images taken from patents awarded to J.F. Cooley (a) and W. J. Morton (b) in 1902. A rotating collector was used as the target to collect electrospun filaments and fibres. Images taken from a patent awarded to C. L. Norton in 1936 (c).

Interest to use electrospinning for the textile research continued to increase from this point onwards. On 1969, Taylor performed one of the first systematic studies on how the electrostatic field competes with the surface tension of spherical viscous polymer droplets placed at the tip of a needle, pulling the droplet first into a cone shape, and then, as the field strength was increased, ejecting a stream of solution from the tip of the cone.[85] In 1981, Larrondo and Manley were the first to demonstrate that a molten polymer could be electrospun in a similar fashion,[86-88] a finding backed up by more recent discoveries.[89] In the late 1980's the electrospinning effect was further studied by Reneker group, who established how the unstable whipping effect was caused by the jet elongation in the electric field and how changing the strength of the electric field and the proportion of solvent to polymer affected nanofibre size and production.[90]

Despite these early discoveries, electrospinning did not gain a lot of interest and was not utilized commercially until the 90s. It is only after the emergence of nanotechnology, in the 1990s, that electrospinning gained increasing attention as a way of manufacturing fibers at the nanoscale range. Researchers have looked at the potential of electrospinning to produce complex and highly functionalized systems, which could be used in a variety of scientific and commercial applications. The possibilities presented by electrospinning in the fields of bio-medical research, electronics, catalysis, environmental and energy storage applications (**Figure 1.7**) led to an almost exponential increase in the number of scientific publications since the 90s[91, 92].

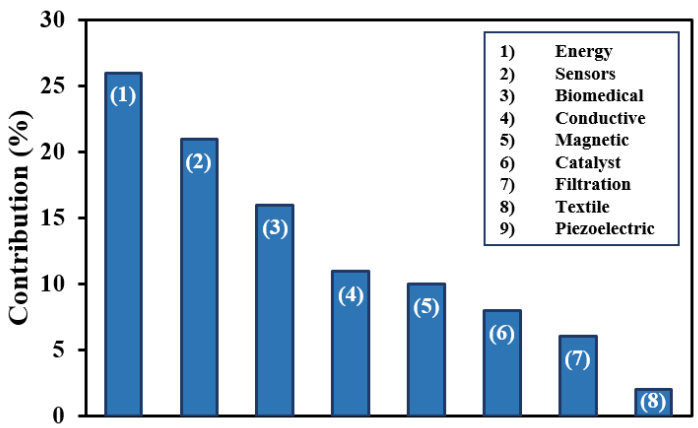

FIGURE 1.7

Statistics on the literature published on the advanced applications of electrospun fibers in the period 2001–2014 (search made through Web of Knowledge using as keywords: Electrospinning + area of application).

1.6.2 Electrospinning set-up

Ultrathin fibers from a wide range of polymer materials can be easily prepared by electrospinning[92-102] (**Figure 1.8**). This electrostatic technique involves the use of a high voltage field to charge the surface of a polymer solution droplet, held at the end of a capillary tube, and induce the ejection of a liquid jet towards a grounded target (collector).

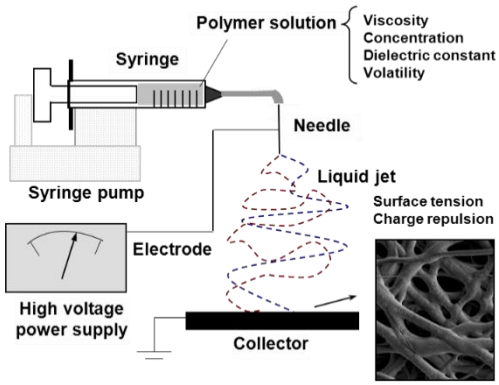

FIGURE 1.8

Scheme showing the electrospinning process.[6]

The single jet initially formed is divided into multiple filaments by radial charge repulsion, which results in the formation of solidified ultrathin fibers as the solvent is evaporating. Morphology of fibers obtained onto the collector depends on the solution properties (e.g., viscosity, dielectric constant, volatility, concentration) and operational parameters (e.g., strength of the applied electrical field, deposition distance, flow rate).[92, 95, 97-99] Electrospinning of some polymers may be problematic, and may require a detailed study of appropiate experimental conditions for fiber production.

Selection of the experimental conditions can lead to fibers with diameters that can range from several micrometers to few nanometers in an extremely rapid process (millisecond scale).[94] The technique is also characterized by a huge material elongation rate and high cross-sectional area reduction that favors molecular orientation within the fiber. Electrospinning becomes nowadays a simple one step approach for producing active matrices with high surface area.[94] The electrospun fibers can provide interconnected porous networks, which are interesting for drug, gene or cell delivery, artificial blood vessels, wound dressings and substrates for tissue regeneration, immobilization of enzymes and catalyst systems.

Non-woven mats of electrospun nanofibers can mimic the extracellular matrices (ECM) since their architecture becomes similar to the collagen structure of the ECM (a 3D network of collagen nanofibers with diameters between 50 and 500 nm). In addition, electrospun synthetic materials can offer several advantages for tissue regeneration: correct and controllable

topography (e.g., 3D porosity, nanoscale size, and alignment), encapsulation and local sustained release of drugs (e.g., growth factors, antioxidants, anti-inflammatory agents), and surface functionalization. Electrospun nanofiber-mats can also be used for the development of complex nanosensory systems to detect biomolecules (e.g., glucose-recognition) in a less than nanomolar concentrations.[103]

1.6.3 Electrospinning parameters

Numerous parameters have been identified as affecting the final properties of electrospun fibers: polymer-solvent solution, processing and environmental parameters. Conditions are largely dependent on the dissolution parameters and hence the process parameters have to be empirically determined for each solution system.

Most of these parameters have a range in which electrospinning of polymeric solutions is suitable. However, due to the sensitivity of the fiber morphology to small changes in these parameters, optimization is usually necessary for controlling the process and yield desired fiber morphologies and diameters. The optimization process can be difficult since the control of one parameter can lead to unwanted changes in another (e.g., adding a salt to increase conductivity can result in a change in the solution viscosity, making mutual optimization of these parameters difficult). Understanding the effects of each parameter on the electrospinning becomes a large part of this investigation. In this section, the key parameters of electrospinning and their effect on electrospun fiber morphologies is shortly discussed with reference to literature (**Table 1.2**).

TABLE 1.2. Electrospinning parameters (solution, processing and environmental) and their effects on fiber morphology.[53]

Parameters	Effects on fiber morphology
Solution	
Viscosity/Concentration	▪ Low concentrations/viscosities yielded defects in the form of beads and junctions; increasing concentrations/viscosities reduced the defects. ▪ Fiber diameter increased with the increase of concentration.
Molecular Weight	▪ The increase of molecular weight caused a reduction in the number of beads and droplets.
Surface Tension	High surface tension resulted in instability of jets. No conclusive link was found with fiber diameter.
Conductivity/Surface Charge density	▪ Increasing the conductivity aided the production of uniform bead-free fibers and decreased the fiber diameter.
Dielectric constant	▪ Successful spinning occurred in solvents with a high dielectric constant.
Processing	
Voltage	▪ Fiber diameter decreased with increasing voltages.
Tip to collector distance	▪ An optimal distance seems to be required to get uniform fibers. Beads are formed at distances either too short or too long.
Feed Rate	▪ Fiber diameters decreased by decreasing the flow rate. Beads are usually generated when too high flow rates are applied.
Environmental	
Temperature	▪ Fiber dimeters decreased with temperature as a consequence of the solution viscosity decrease.
Humidity	▪ High humidity resulted in the appearance of circular pores on the fibers.

1.6.4 Advances on the electrospinning technique

The basic set-up for electrospinning is so simple that it has already found widespread use in many research laboratories. Due to the bending instability, a typical electrospinning jet deposits fibers in a random mat. Nevertheless, there are several applications where fibers should be deposited in a more controlled fashion. Thus, several techniques for influencing the layout of the fiber deposition have been developed. These can generally be grouped in two categories: mechanical and electrical.

The collector can be further divided into the rotating device or a configuration of electrodes (**Figure 1.9**). The major category of electrospinning setups configuring aligned nanofibers employs a rotating device as the collector. Several geometries have also been designed and used. The purpose of the rotating device is to stretch mechanically the fibers and favour their alignment along the periphery of the drum. These configurations include a solid cylindrical collector, which can rotate about its axis.[104]

Because the electrospinning jet is charged, it is also possible to exert some control over the deposition process using electric fields. Typically, a single grounded conducting substrate is used to collect the fibers (**Figure 1.9 a**). The grounded area can be restricted in a controlled fashion using a patterned electrode that induces the accumulation of fibers on the grounded electrode.[104] One interesting collector configuration consists on a rotating disc and a small aluminium table attached to the disk edge (**Figure 1.9 b**). This system allows obtaining double- and triple-layer highly aligned crossbar structures. If two conducting collecting electrodes separated by an insulating gap are used, the jet will dance between the electrodes and produce a uniaxially aligned array of fibers.[105, 106] Other collection techniques that rely on such behavior have been devised, such as the use of dual ring electrodes to collect a uniaxially aligned array of fibers (**Figure 1.9 d**) and the rotation of one of the collection rings that allowed the production of multi-filament yards. Another approach to manipulate the deposition of electrospun fibers is the control of the electric field using external electrodes between the tip and the collecting substrate (**Figure 1.9 c**). Taking this idea one step further, a time-varying electric field was applied to several electrodes to steer the electrospinning jet to "draw" individual fibers.[107]

Another remarkable approach is based on the deposition of fibers in a circumferentially oriented way by employing an auxiliary electric field placed in a certain configuration. As an example, the production of tubular structures can be mentioned. It was reported that the indicated geometry can be achieved the asymmetric deposition of a rotating and charged drum between two charged plates or by the connexion of an auxiliary electrode (grid) made of a plurality of connected aluminium foil strips away from collector drum.

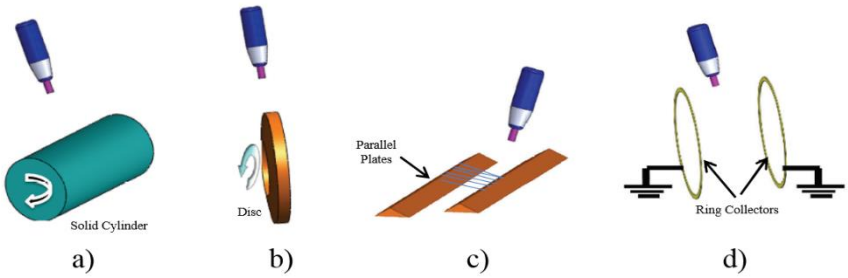

FIGURE 1.9

Collector configurations: a) solid cylinder; b) disc collector; c) parallel plates and, d) dual rings.[104]

The most basic electrospinning system uses a single metallic needle as the source to support the liquid droplet (the "spinneret" or tip). Other more complex systems have been developed and multicomponent fibers have been produced using electrospinning systems with modified spinnerets. These structures may include a core and a variable number of shells that allows getting bicomponent and multicomponent structures (**Figure 1.10**). The phenomenon mainly comprised of coaxially pumping out two chemically dissimilar solutions. The phenomenon needs a precise control of the system and processing parameters to achieve a well-defined core-shell structure (**Figure 1.10 a**). Coaxial fibers, which in many cases can be subsequently processed into hollow tubes, may be produced using a coaxial electrospinning spinneret.[108] The other variation of this configuration[109] depicted in **Figure 1.10 b** includes gas as a shell material. The gas flow applies additional drawing action on the polymer jet during the electrospinning process. The dispensing system disperses two solutions from a single needle, thus fabricating bicomponent nanofibers (**Figure 1.10 c**).

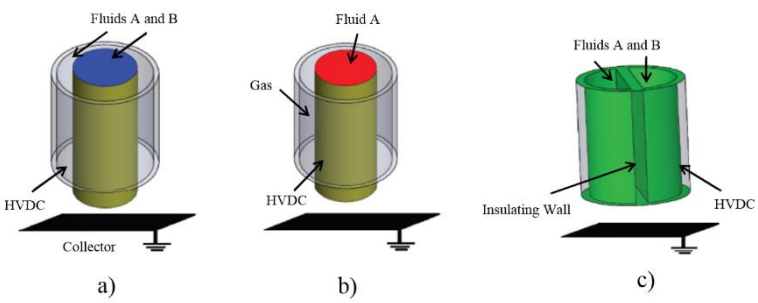

FIGURE 1.10

Multicomponent fibers set-up: a) core-shell, b) gas as a shell material in core-shell structure and c) bicomponent electrospinning system.[104]

One aspect of typical electrospinning setups that limits commercialization is low mass throughput. Electrospinning processes tend to operate at mass flow rates between μg/min to mg/min. Several techniques have been developed to overcome this problem, all of which use an

array of multiple electrospinning spinnerets operating in parallel. This technique is usually manifested in systems employing an array of needles that are fed by the same electrospinning solution.[110]

1.7 Electrospinning of biodegradable polymers as bioactive systems

1.7.1 Biodegradable polymer loaded with drugs

Electrospinning offers great flexibility in terms of material selection for drug delivery applications, being a wide variety of drugs physically or chemically formulated within electrospun fibers or on their surfaces. These include for example antibiotics,[111-115] anti-cancer drugs,[111-115] proteins,[118, 119] and DNA.[120-122] The drug release mechanism can be associated with polymer degradation and diffusion pathway. Specifically, the release profile of drug from electrospun fibers may be tuned by the polymer composition and fiber morphology.[123]

Many strategies can be used to control the release of proteins and growth factors from fiber scaffolds. When biodegradable polymers are used, a common approach is to load the growth factors (e.g., bioactive molecules) on the material and use the combined effects of diffusion and erosion to mediate the release kinetics. Fiber meshes inherently have an appropriate structure to maximize surface area. Additionally, the hydrophilicity can be optimized by using surface-modification methods. In general, it is accepted that hydrophobic materials are more compatible with the biological systems.

The electrospinning process, being solvent based, allows the mixing of drugs and bioactive agents before the production of micro/nanofibers. However, the solvent needs to be harmless for the loaded bioactive agent, and must not compromise its functionality. Depending on the chemical interactions between drug and polymer carrier, different modes of interaction may be explored:[124]

- Drug as particles or inclusions trapped in the fiber structure.
- Blend of drugs and carrier materials integrated into one mesh of composite fibers.
- Carrier material electrospun into a tubular form in which the drug particles are encapsulated.
- Drug adsorbed onto fiber mats.

Drug-release systems can be tailored to tune the release kinetics, to regulate local distribution and to minimize toxic side effects, thereby enhancing the effectiveness of the bioactive agent released.[125] Electrospinning also allows control of the fiber diameter, to some extent, and control the release of kinetics by the diameter of the fibers, both in diffusion- and in degradation-controlled release. Moreover, the electrospinning process, being based in solvents, does not involve high temperatures which is particularly useful for heat-sensitive drugs. Furthermore, it

enables minimizing the initial burst release and the possibility of delivering uniform and highly controlled doses of bioactive agents at the wound side by tuning the surface properties of the fibers.[126] **Table 1.3** summarizes the main electrospun fibers meshes proposed as drug-delivery.

Specifically, the reported data suggests that many studies explored the loading of antibiotics onto fiber meshes, but only few reported the loading of antitumor or growth factors or other specific drugs. The materials that have been proposed as fiber drug carriers are restricted to the group of biodegradable synthetic polymers.[127]

TABLE 1.3 Electrospinnig particles employed as drug-delivery systems.[59, 128, 129]

Delivery Systems	Incorporated Drug	Scaffold Material
Antymicotic	Griseofulvin	PMCA
	Tetracycline hydrochloride	PCL, PLA, PVA, PLGA, PEVA
Antimicrobic	Triclosan	PS-DVB, PLA[130]
	Chlorhexidine	CA[131]
Antibiotic	Mefocin® (cefoxitin)	PLA, PLGA, PLGA/PLA/PEG-*b*-PLA
	Cefazolin	PLGA
	Itraconazole	HPMC
	Gentamicyn sulfate	PCL
	Biteral (ornidazol)	PCL
	Rifampin (rifadin)	PLLA
	Mupirocin	PLLA[132]
	Amphotericin B	PLA-PCL[133]
Antitumor	Paclitaxel	PLLA, PLGA
	Doxorubicin	PLGA
	Curcumin	PLLA[134, 135]
Antiinflammatory	Ibuprofen	PLGA, PLA-*g*-CHN
	Ketoprofen	PVP[136], PVA[137]
	Curcumin	PCL[138]
	Diclofenac sodium	PCL, PLA-CL, PVA, PAM14
	Dexamethasone	PLA-CL[139]
Analgesic	Paracetamol	PDLLA
Anticoagulant	Heparin	PCL, PLGA
Antioxidant	Vitamin A and E	CA
	Resveratrol (phytoalexin)	PCL
	Curcumin	PCL[138]
	Gallic Acid	PLLA[140]
Growth Factor	NGF	PCLEEP
	BMP-2	PLGA/HA[141], Chitosan
Protein	BSA	PVA[142], PCL/PEG (Shell) – Dextran/BSA (core)[143]
DNA	Plasmid DNA	PLA-PEG, PLGA, LEL
Enzyme	α-chymotrypsin	PS, PSMA[144]

1.7.2 Biodegradable polymer meshed with conductive polymers

Electrically conducting polymers are considered important because of their unique properties as mentioned above. Recently, several groups have demonstrated the preparation of conducting polymer nanofibers via electrospinning. Obtention of conductive nanofibers by electrospinning is not trivial and different strategies have been undertaken: (a) Incorporation of conductive particles [e.g., carbon nanotubes (CNT)] into the fibers, being usually necessary a surface treatment of particles in order to increase their affinity for the polymer matrix; (b) Direct electrospinning of conducting polymers with problems related to their stiffness and low solubility; (c) Blending the conducting polymer with another electrospinnable polymer (used as a carrier), being the detriment of the electronic properties the major inconvenience; and (d) Coating electrospun nanofibers with conductive materials.[6]

Spin coating is a useful technique for preparing uniform thin films with thicknesses below 10 nm. Basically a polymer solution is placed on a flat substrate, which is then rotated at high speed in order to spread the fluid by centrifugal force (**Figure 1.11**). The thickness of the film depends on the angular speed of spinning and the amount and concentration of the solution. Usually a sacrificial layer is deposited over the permanent support. The formed film is separated by destroying this layer after the fabrication procedure.

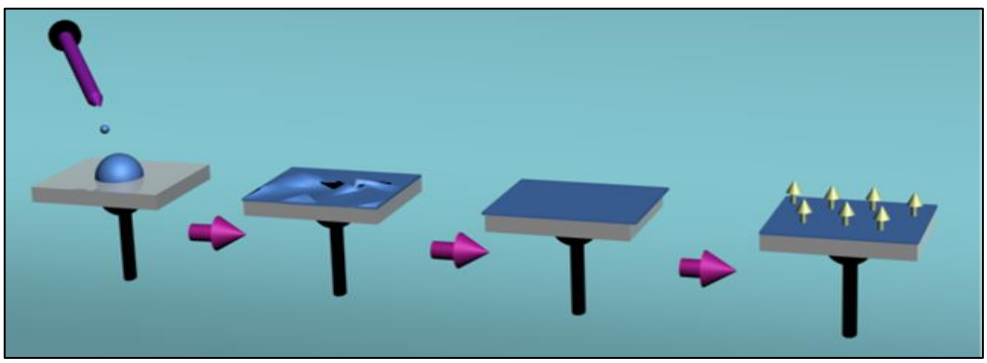

FIGURE 1.11

Spin coating process involves the following steps: (a) Solution deposition; (b) Substrate acceleration; (c) Constant spinning rate; and (d) Drying and separation (not shown).[6]

It is difficult to use a conducting polymer alone in the electrospinning process due to the low molecular weight and its high crystallinity.[145] Therefore, despite the expected reduction in electrical characteristics, blends of polymers and electrospinnable additives have usually been used.[146] In such mixtures, the selection and composition of the conducting polymer has become very limited. On one hand, if the ratio of the conducting polymer is too low, the fabricated nanofibers tend to have poor electrical characteristics or no electrical properties at all.[147] On the other hand, if the ratio of the conducting polymer is too high, it becomes difficult to prepare conducting nanofibers because of the rigid structure of the polymer backbone and low solubility.

Other promising investigations about the use of polymer matrices as drug transport devices have also been undertaken. For example, the use of conducting/electroactive polymers as a medium-sensing and bioactive molecule-releasing system. Drug delivery with these conducting polymer membranes is achieved through the controlled ionic transport of counterions (dopants) in and out of the membranes. Specifically, redox reactions regulate the necessary electrochemical switching, thus allowing electrostatically entrapped anionic dopants (such as the biological molecule ATP, which has been investigated for various cardiovascular therapies) to be either retained or released. In fact, initial studies that mainly involved a polypyrrole-based polymer membranes have proved quite promising. Results indicated that the drug delivery rate, chemical sensing, and electrochemical triggering can all be and precisely controlled.[6]

1.8 References

[1] D.F. Williams, Proceedings of a Consensus Conference of the Europe a Society for Biomaterials, Elsevier, England, 1987.

[2] E.S. Place, J.H. George, C.K. Williams, M.M. Stevens, Chem Soc Rev, 38 (2009) 1139-1151.

[3] P. Tormala, T. Pohjonen, P. Rokkanen, P I Mech Eng H, 212 (1998) 101-111.

[4] A. Rodrigues Santos, Bioresorbable polymers for tissue engineering, in: D. Eberly (Ed.) Tissue Engineering, InTech, 2010.

[5] L.S. Nair, C.T. Laurencin, Prog Polym Sci, 32 (2007) 762-798.

[6] E. Llorens, E. Armelin, M.M. Pérez-Madrigal, L.J. del Valle, C. Aleman, J. Puiggali, Polymers, 5 (2013) 1115-1157.

[7] B.D. Ulery, L.S. Nair, C.T. Laurencin, J Polym Sci Part B Polym Phys, 49 (2011) 832-864.

[8] B. Gupta, N. Revagade, J. Hilborn, Prog Polym Sci, 32 (2007) 455-482.

[9] H. Yamane, K. Sasai, Polymer, 44 (2003) 2569-2575.

[10] R.E. Drumright, P.R. Gruber, D.E. Henton, Adv Mater, 12 (2000) 1841-1846.

[11] Y. Cheng, S. Deng, P. Chen, R. Ruan, Front Chem China, 4 (2009) 259-264.

[12] J.S. Loo, C.P. Ooi, F.Y. Boey, Biomaterials, 26 (2005) 1359-1367.

[13] A.J.R. Lasprilla, G.A.R. Martinez, B.H. Lunelli, A.L. Jardini, R.M. Filho, Biotechnol Adv, 30 (2012) 321-328.

[14] Q. Wang, J. Liu, C. Wang, L. Ma, Y. Liu, J. Li, J. Liu, World Congress on Medical Physics and Biomedical Engineering, Springer Berlin Heidelberg, Beijing, China, 2012.

[15] L. Durselen, M. Dauner, H. Hierlemann, H. Planck, L.E. Claes, A. Ignatius, J Biomed Mater Res, 58 (2001) 666-672.

[16] T. Fujimaki, Polym Degrad Stabil, 59 (1998) 209-214.

[17] J. Nicklin, K. Graeme-Cook, T. Paget, R.A. Killington, Instant Notes in Micriobiology, BIOS Scientific Publishers Limited, Oxford, 1999.

[18] K. Bahari, H. Mitomo, T. Enjoji, F. Yoshii, K. Makuuchi, Polym Degrad Stabil, 61 (1998) 245-252.

[19] T. Hashitani, E. Yano, Y. Ando, Fujitsu Sci Tech J, 38 (2002) 112-118.

[20] V. Tserki, P. Matzinos, E. Pavlidou, D. Vachliotis, C. Panayiotou, Polym Degrad Stabil, 91 (2006) 367-376.

[21] R. Babu, K. O'Connor, R. Seeram, Progr Biomater, 2 (2013) 8.

[22] L. Liu, J. Yu, L. Cheng, W. Qu, Compos Part A-Appl S, 40 (2009) 669-674.

[23] W.S. Lyoo, J.H. Kim, W.S. Yoon, B.C. Ji, J.H. Choi, J. Cho, J. Lee, S.B. Yang, Y. Yoo, Polymer, 41 (2000) 9055-9062.

[24] R. Vasita, D.S. Katti, Int J Nanomedicine, 1 (2006) 15-30.

[25] N. De Geyter, R. Morent, Non-Thermal Plasma Surface Modification of Biodegradable Polymers, in: D.N. Ghista (Ed.) Biomedical Science, Engineering and Technology, InTech, 2012.

[26] C. Somerville, Annu Rev Cell Dev Biol, 22 (2006) 53-78.

[27] J.H. Lee, H.B. Lee, J.D. Andrade, Prog Polym Sci, 20 (1995) 1043-1079.

[28] N.A. Alcantar, E.S. Aydil, J.N. Israelachvili, J Biomed Mater Res, 51 (2000) 343-351.

[29] G. Papavasiliou, S. Sokic, M. Turturro, Synthetic PEG Hydrogels as Extracellular Matrix Mimics for Tissue Engineering Applications, in: R.H. Sammour (Ed.) Biotechnology - Molecular Studies and Novel Applications for Improved Quality of Human Life, InTech, 2012.

[30] F.M. Veronese, G. Pasut, Drug Discov Today, 10 (2005) 1451-1458.

[31] G. Decher, Science, 277 (1997) 1232-1237.

[32] X. Qin, H. Wang, X. Wang, S. Li, Z. Miao, N. Huang, Q. Chen, Mater Sci Eng C, 29 (2009) 1453-1457.

[33] J.B. Schlenoff, S.T. Dubas, Macromolecules, 34 (2001) 592-598.

[34] E. Blomberg, E. Poptoshev, P.M. Claesson, F. Caruso, Langmuir, 20 (2004) 5432-5438.

[35] Y. Guo, W. Geng, J. Sun, Langmuir, 25 (2009) 1004-1010.

[36] G. Decher, J.D. Hong, J. Schmitt, Thin Solid Films, 210 (1992) 831-835.

[37] M. Kolasińska, P. Warszyński, Appl Surf Sci, 252 (2005) 759-765.

[38] A. Ulman, An Introduction to Ultrathin Organic Films: From Langmuir–Blodgett to Self-Assembly, Academic Press, Boston, 1991.

[39] A.F. Diaz, K.K. Kanazawa, G.P. Gardini, J Chem Soc Chem Commun, (1979) 635-636.

[40] A. Kotwal, C.E. Schmidt, Biomaterials, 22 (2001) 1055-1064.

[41] G. Inzelt, Conducting Polymers: A new era in electrochemistry, Springer, Berlin, 2008.

[42] G.G. Wallace, G.M. Spinks, L.A.P. Kane-Maguire, P.R. Teasdale, Conducting Electroactive Polymers: Intelligent Polymer Systems, CRC Press, New York, 2008.

[43] N. Rozlosnik, Anal Bioanal Chem, 395 (2009) 637-645.

[44] L. Groenendaal, G. Zotti, P.H. Aubert, S.M. Waybright, J.R. Reynolds, Adv Mater, 15 (2003) 855-879.

[45] E. Armelin, A.L. Gomes, M.M. Perez-Madrigal, J. Puiggali, L. Franco, L.J. del Valle, A. Rodriguez-Galan, J.S.D. Campos, N. Ferrer-Anglada, C. Aleman, J Mater Chem, 22 (2012) 585-594.

[46] A.L. Gomes, M.B.P. Zakia, J. Filho, E. Armelin, C. Aleman, J.S.D. Campos, Polymer Chemistry, 3 (2012) 1334-1343.

[47] M.M. Perez-Madrigal, E. Armelin, L.J. del Valle, F. Estrany, C. Aleman, Polym Chem, 3 (2012) 979-991.

[48] M.M. Perez-Madrigal, M.I. Giannotti, G. Oncins, L. Franco, E. Armelin, J. Puiggali, F. Sanz, L.J. del Valle, C. Aleman, Polym Chem, 4 (2013) 568-583.

[49] T.J. Skotheim, R.L. Elsenbaumer, J.R. Reynolds, Handbook of Conducting Polymers, 2nd ed., Marcel Dekker, New York, 1998.

[50] P. Chandrasekhar, Conducting Polymers, Fundamentals and Applications: A Practical Approach, Kluwer Academic Publishers, Boston, 1999.

[51] A.F. Diaz, J.A. Logan, J Electroanal Chem, 111 (1980) 111-114.

[52] P.R. Bidez, S.X. Li, A.G. MacDiarmid, E.C. Venancio, Y. Wei, P.I. Lelkes, J Biomat Sci-Polym E, 17 (2006) 199-212.

[53] Q.P. Pham, U. Sharma, A.G. Mikos, Tissue Eng, 12 (2006) 1197-1211.

[54] C. Burger, B.S. Hsiao, B. Chu, Annu Rev Mater Re, 36 (2006) 333-368.

[55] N. Bhardwaj, S.C. Kundu, Biotechnol Adv, 28 (2010) 325-347.

[56] S.K. Sahu, A.K. Prusty, Int J Curr Pharm Res, 3 (2010) 08-12.

[57] M.D. Pierschbacher, E. Ruoslahti, Nature, 309 (1984) 30-33.

[58] M. Hakkarainen, Adv Polym Sci, 157 (2002) 113-138.

[59] S. Agarwal, J.H. Wendorff, A. Greiner, Polymer, 49 (2008) 5603-5621.

[60] C.Y. Xu, R. Inai, M. Kotaki, S. Ramakrishna, Tissue Eng, 10 (2004) 1160-1168.

[61] B. Sharma, J.H. Elisseeff, Ann Biomed Eng, 32 (2004) 148-159.

[62] F. Rosso, G. Marino, A. Giordano, M. Barbarisi, D. Parmeggiani, A. Barbarisi, J Cell Physiol, 203 (2005) 465-470.

[63] D.W. Hutmacher, Biomaterials, 21 (2000) 2529-2543.

[64] L.E. Freed, G. Vunjaknovakovic, R.J. Biron, D.B. Eagles, D.C. Lesnoy, S.K. Barlow, R. Langer, Bio-Technol, 12 (1994) 689-693.

[65] S. Selvam, W.V. Chang, T. Nakamura, D.M. Samant, P.B. Thomas, M.D. Trousdale, A.K. Mircheff, J.E. Schechter, S.C. Yiu, Tissue Eng Part C-Me, 15 (2009) 463-474.

[66] B.P. Ma, J.H. Elisseeff, Taylor & Francis Group, CRC Press, Boca Raton, FL, 2006.

[67] P. van de Witte, P.J. Dijikstra, J.W.A. van der Berg, J. Feijen, J Membrane Sci, 117 (1996) 1-31.

[68] G.M. Whitesides, J.K. Kriebel, B.T. Mayers, in: W.T.S. Huck (Ed.) Nanoscale Assembly, Springer US, 2005, pp. 217-239.

[69] A. Salerno, M. Oliviero, E. Di Maio, S. Iannace, P.A. Netti, J Mater Sci-Mater M, 20 (2009) 2043-2051.

[70] B. Dhandayuthapani, Y. Yoshida, T. Maekawa, D.S. Kumar, Int J Polym Sci, (2011).

[71] C.T. Vogelson, Nanotechnology, 4 (2001) 49-52.

[72] R. Zurita, J. Puiggali, A. Rodriguez-Galan, Macromol Biosci, 6 (2006) 58-69.

[73] P. Martin, Science, 276 (1997) 75-81.

[74] G.I. Klebanov, O.B. Lyubitsky, S.E. ll'ina, E.O. Medusheva, V.V. Ryltsev, V.N. Filatov, Biochemistry (Moscow) Supplement Series B: Biomedical Chemistry, 1 (2007).

[75] W. Gilbert, The Magnet, Bernard Quaritch, London, 1628.

[76] W.M. Saslow, Electricity, Magnetism and Light, Academic Press, 2002.

[77] J. Zelany, Phys Rev Lett, 3 (1914) 69-91.

[78] W.A. Macky, P R Soc Lond a-Conta, 133 (1931) 565-587.

[79] B. Vonnegut, R.L. Neubauer, J Coll Sci Imp U Tok, 7 (1952) 616-622.

[80] W. Morton, in: U. Patent (Ed.), 1902.

[81] J.F. Cooley, Charles Patent Office, Massachusetts, 1902.

[82] A. Formhals, in: U. patent (Ed.), USA, 1934.

[83] A. Formhals, in: U. Patent (Ed.), USA, 1944.

[84] C.L. Norton, in: U. Patent (Ed.), 1944.

[85] G. Taylor, Proc R Soc Lon Ser-A, 313 (1969) 453-&.

[86] L. Larrondo, R.S.J. Manley, J Polym Sci Pol Phys, 19 (1981) 909-920.

[87] L. Larrondo, R.S.J. Manley, J Polym Sci Pol Phys, 19 (1981) 921-932.

[88] L. Larrondo, R.S.J. Manley, J Polym Sci Pol Phys, 19 (1981) 933-940.

[89] J. Lyons, C. Li, F. Ko, Polymer, 45 (2004) 7597-7603.

[90] J. Doshi, D.H. Reneker, J Electrostat, 35 (1995) 151-160.

[91] A. Greiner, J.H. Wendorff, Angew Chem Int Edit, 46 (2007) 5670-5703.

[92] D. Li, Y.N. Xia, Adv Mater, 16 (2004) 1151-1170.

[93] D.H. Reneker, I. Chun, Nanotechnology, 7 (1996) 216-223.

[94] D.H. Reneker, A.L. Yarin, H. Fong, S. Koombhongse, J Appl Phys, 87 (2000) 4531-4547.

[95] A. Frenot, I.S. Chronakis, Curr Opin Colloid Interface Sci, 8 (2003) 64-75.

[96] Y. Dzenis, Science, 304 (2004) 1917-1919.

[97] K. Jayaraman, M. Kotaki, Y.Z. Zhang, X.M. Mo, S. Ramakrishna, J Nanosci Nanotechnol, 4 (2004) 52-65.

[98] S.R. Dhakate, B. Singla, M. Uppal, R.B. Mathur, Adv Mater Lett, 1 (2010) 200-204.

[99] S. Sharma, Adv Mater Lett, 4 (2013) 522-533.

[100] R. Dersch, M. Steinhart, U. Boudriot, A. Greiner, J.H. Wendorff, Polym Adv Technol, 16 (2005) 276-282.

[101] I.S. Chronakis, J Mater Process Tech, 167 (2005) 283-293.

[102] J.M. Deitzel, J. Kleinmeyer, D. Harris, N.C.B. Tan, Polymer, 42 (2001) 261-272.

[103] A. Tiwari, D. Terada, C. Yoshikawa, H. Kobayashi, Talanta, 82 (2010) 1725-1732.

[104] R. Sahay, V. Thavasi, S. Ramakrishna, Journal of Nanomaterials, 2011 (2001) 17.

[105] D. Li, Y. Wang, Y. Xia, Nano Lett, 3 (2003) 1167-1171.

[106] D. Li, Y. Wang, Y. Xia, Adv Mater, 16 (2004) 361-366.

[107] L.M. Bellan, H.G. Craighead, J Vac Sci Technol B, 24 (2006) 3179-3183.

[108] D. Li, Y.N. Xia, Nano Lett, 4 (2004) 933-938.

[109] Y. Lin, Y. Yao, X. Yang, N. Wei, X. Li, P. Gong, R. Li, D. Wu, J Appl Polym Sci, 107 (2008) 909-917.

[110] S.A. Theron, A.L. Yarin, E. Zussman, E. Kroll, Polymer, 46 (2005) 2889-2899.

[111] K. Kim, Y.K. Luu, C. Chang, D. Fang, B.S. Hsiao, B. Chu, M. Hadjiargyrou, J Control Release, 98 (2004) 47-56.

[112] E.R. Kenawy, G.L. Bowlin, K. Mansfield, J. Layman, D.G. Simpson, E.H. Sanders, G.E. Wnek, J Control Release, 81 (2002) 57-64.

[113] E.R. Kenawy, F.I. Abdel-Hay, M.H. El-Newehy, G.E. Wnek, Mater Chem Phys, 113 (2009) 296-302.

[114] X.L. Xu, W. Zhong, S.F. Zhou, A. Trajtman, M. Alfa, J Appl Polym Sci, 118 (2010) 588-595.

[115] N. Yan, X. Zhang, Q. Cai, X. Yang, X. Zhou, B. Wang, X. Deng, J Biomater Sci Polym Ed, 23 (2012) 1005-1019.

[116] X.L. Xu, X.S. Chen, P.A. Ma, X.R. Wang, X.B. Jing, Eur J Pharm Biopharm, 70 (2008) 165-170.

[117] J. Xie, C.-H. Wang, Pharm Res, 23 (2006) 1817-1826.

[118] N. Charernsriwilaiwat, P. Opanasopit, T. Rojanarata, T. Ngawhirunpat, Int J Pharm, 427 (2012) 379-384.

[119] J.J. Won, R. Nirmala, R. Navamathavan, H.Y. Kim, Int J Biol Macromol, 50 (2012) 1292-1298.

[120] M. Chen, S. Gao, M. Dong, J. Song, C. Yang, K.A. Howard, J. Kjems, F. Besenbacher, ACS Nano, 6 (2012) 4835-4844.

[121] H. Nie, C.-H. Wang, J Control Release, 120 (2007) 111-121.

[122] D. Liang, Y.K. Luu, K. Kim, B.S. Hsiao, M. Hadjiargyrou, B. Chu, Nucleic Acids Res, 33 (2005) e170.

[123] T.J. Sill, H.A. von Recum, Biomaterials, 29 (2008) 1989-2006.

[124] Z.M. Huang, Y.Z. Zhang, M. Kotaki, S. Ramakrishna, Comp Sci Technol, 63 (2003) 2223-2253.

[125] M. Goldberg, R. Langer, X.Q. Jia, J Biomat Sci-Polym E, 18 (2007) 241-268.

[126] A. Martins, R.L. Reis, N.M. Neves, Int Mater Rev, 53 (2008) 257-274.

[127] J.I. Langford, A.J.C. Wilson, J App Crystallogr, 11 (1978) 102-113.

[128] Z. M., P. M.P., R. S., Int J Nanomedicine, 8 (2013) 2997-3017.

[129] A. Martins, J.V. Araújo, R.L. Reis, N.M. Neves, Nanomedicine, 2 (2007) 929-942.

[130] L.J. del Valle, A. Diaz, M. Royo, A. Rodriguez-Galan, J. Puiggali, Express Polym Lett, 6 (2012) 266-282.

[131] L. Chen, L. Bromberg, T.A. Hatton, G.C. Rutledge, Polymer, 49 (2008) 1266-1275.

[132] R.A. Thakur, C.A. Florek, J. Kohn, B.B. Michniak, Int J Pharm, 364 (2008) 87-93.

[133] G. Buschle-Diller, J. Cooper, Z. Xie, Y. Wu, J. Waldrup, X.J. Ren, Cellulose, 14 (2007) 553-562.

[134] E. Thangaraju, N.T. Srinivasan, R. Kumar, P.K. Sehgal, S. Rajiv, Fiber Polym, 13 (2012) 823-830.

[135] Y. Chen, J. Lin, Y.N. Fei, H.B. Wang, W.D. Gao, Fiber Polym, 11 (2010) 1128-1131.

[136] D.G. Yu, X. Wang, X.Y. Li, W. Chian, Y. Li, Y.Z. Liao, Acta Biomater, 9 (2013) 5665-5672.

[137] E.R. Kenawy, F.I. Abdel-Hay, M.H. El-Newehy, G.E. Wnek, Mat Sci Eng a-Struct, 459 (2007) 390-396.

[138] J.G. Merrell, S.W. McLaughlin, L. Tie, C.T. Laurencin, A.F. Chen, L.S. Nair, Clin Exp Pharmacol P, 36 (2009) 1149-1156.

[139] N.M. Vacanti, H. Cheng, P.S. Hill, J.D.T. Guerreiro, T.T. Dang, M.L. Ma, S. Watson, N.S. Hwang, R. Langer, D.G. Anderson, Biomacromolecules, 13 (2012) 3031-3038.

[140] P. Chuysinuan, N. Chimnoi, S. Techasakul, P. Supaphol, Macromol Chem Physic, 210 (2009) 814-822.

[141] H. Nie, M.-L. Ho, C.-K. Wang, C.-H. Wang, Y.-C. Fu, Biomaterials, 30 (2009) 892-901.

[142] J. Zeng, A. Aigner, F. Czubayko, T. Kissel, J.H. Wendorff, A. Greiner, Biomacromolecules, 6 (2005) 1484-1488.

[143] H.L. Jiang, Y.Q. Hu, P.C. Zhao, Y. Li, K.J. Zhu, J Biomed Mater Res B, 79B (2006) 50-57.

[144] T.E. Herricks, S.H. Kim, J. Kim, D. Li, J.H. Kwak, J.W. Grate, S.H. Kim, Y.N. Xia, J Mater Chem, 15 (2005) 3241-3245.

[145] A. Laforgue, L. Robitaille, Chem Mater, 22 (2010) 2474-2480.

[146] J.H. Choi, J. Lee, J. Choi, D. Jung, S.E. Shim, Synthetic Met, 160 (2010) 1415-1421.

[147] N.J. Pinto, A.T. Johnson, A.G. MacDiarmid, C.H. Mueller, N. Theofylaktos, D.C. Robinson, F.A. Miranda, Appl Phys Lett, 83 (2003) 4244-4246.

2.
Objectives

2. Objectives

The present doctoral dissertation mainly aims to investigate the functionalization of three-dimensional templates of micro/nanofibers obtained from biodegradable polymers. These matrices will be loaded with bioactive molecules with a specific activity, such as antimicrobial, anti-inflammatory, antioxidant and/or anticancerigen. The incorporation of these molecules in the fibers is intended to provide a pharmacological functionality to the matrix and a controlled release of the loaded drugs. Moreover, the incorporation of polymers with specific properties like conductivity, and electroactivity while biodegradability is mantained will be also considered. Therefore, four specific objectives will be considered:

First Block: Antioxidant loaded biodegradable scaffolds and potential application for DNA purification

Antioxidants have been chosen to be loaded into biodegradable scaffolds to prevent tissue damage. This process is called stress-oxidative, where cells and DNA should be controlled or treated in order to enhance tissue regeneration. The targets of this block are:

i. Preparation of 3D scaffolds from electrospun polylactide nanofibers loaded with antioxidants (*i.e.*, vitamin B_6 in pyridoxine and pyridoxal form and two polyphenols, caffeic and *p*-coumaric acids) to prevent oxidative stress of cells colonizing the material.

   Study of the morphology and the physicochemical characterization of new loaded matrices, with the determination of drug release kinetics, and the evaluation of antioxidant bioactivity.

ii. a) Evaluation of the effect of the selected compounds to inhibit oxidative damage in solution of plasmid DNA.

   b) Preparation of electrospun nanofiber matrices loaded with antioxidants and evaluation of their ability to inhibit oxidative DNA damage.

   c) Study of the application of new matrices as support for the purification of DNA subjected to oxidative stress.

Second Block: Multifunctional biodegradable fiber scaffolds

Development of multifunctional electrospun materials for regenerative medicine applications. These are based on polylactide fibers that are loaded with active agents of different nature and with diverse therapeutic effects. The targets of this block are:

i. Preparation of electrospun scaffolds from PLAs having slightly different ratios between L- and D-lactide units.
   Evaluation of dual and ternary systems involving triclosan (TCS) as an antibacterial agent, ketoprofen (KTP) as a conventional anti-inflammatory drug and *p*-coumaric (CUM) as an antioxidant drug.
ii. Modulation of the therapeutic effect caused by the simultaneous incorporation of different drugs.
iii. Evaluation of the influence of the polymer matrix crystallinity on the release behavior.

Third Block: Preparation of biodegradable scaffolds that incorporate non-electrospinable polymers

Several polymers with highly interesting properties like conductivity/electroactivity or having bactericide activity cannot be electrospun directly. Therefore, the development of scaffolds based on blends of such polymers and biodegradable polymers may render new materials with highly promising properties for their application in the biomedical field. The targets of this block are:

i. a) Development of biodegradable scaffolds containing PHMB as bactericide agent and optimization of electrospinning conditions for different PLA/PHMB ratios.
   b) Study of micro/nanofiber morphology and physicochemical characterization of PLA/PHMB scaffolds.
   c) Evaluation of the release kinetics, antimicrobial activity against both Gram negative and Gram positive bacteria (i.e. *E. coli* and *M. luteus*) and biocompatibility of PLA/PHMB scaffolds.
ii. Establishment of the electrospun conditions required to get continuous micro/nanofibers from mixtures of P3TMA with PLA as well as performing a basic characterization of morphology and properties (e.g., ability to store charge and biocompatibility) of the derived scaffolds.

Fourth Block: Biodegradable polymer matrices incorporating polyethylene glycol as a sacrificial polymer

PEG can be considered a good sacrificial polymer due to its high solubility in aqueuos media. Scaffolds incorporating PEG will increase their porosity and favour cell colonization after exposure to such media. The targets of this block are:

i. a) Optimization of electrospinning conditions to get PLA/PEG scaffolds from polymer mixtures in a wide range of compositions (i.e., PEG content varying from 10 to 70 *wt*-%).

b) Evaluation of the solubility of the newly prepared scaffolds in different aqueous media since scaffold texture may be drastically affected and biocompatibility altered depending on the composition and the washing process.

c) Getting information concerning the distribution of PEG and PLA phases.

d) Study of drug loading and release profiles in media with different hydrophobicity.

ii. a) Preparation of scaffolds constituted by electrospun fibers of PLA and PEG. This process allows an easy modulation without any restriction of the ratio between both kind of fibers and even makes feasible the combination of fibers with highly different morphologic features.

b) Evaluation of the biocompatibility of new scaffolds and the bactericide effect caused by incorporation of drugs with well-differentiated hydrophobic/hydrophilic character such as triclosan (TCS) and polyhexamethylene biguanide hydrochloride (PHMB).

iii. a) Study of coaxial electrospun scaffolds constituted by PEG and PBS with different core-shell distributions.

b) Evaluation of the morphological changes caused by the rapid solubilization of PEG in aqueous media.

c) Evaluation of scaffolds as drug delivery systems considering the independent load of drugs with different characteristics (e.g., triclosan and curcumin) in the two polymer components.

3.

Antioxidant loaded biodegradable scaffolds and potential application for DNA purification

The work described in this chapter previously appeared in:

[1] Llorens, E.; del Valle, L. J.; Díaz, A.; Casas, M. T.; Puiggalí, J. *Macromol Res*. **2013**, *21* (7), 775-787.

[2] Llorens, E.; del Valle, L.; Puiggalí, J. *Macromol Res*. **2014**, *22* (4), 388-396.

3.1

Polylactide Nanofibers Loaded with Vitamin B_6 and Polyphenols as a Potential Bioactive Platform for Tissue Engineering

Electrospun polylactide nanofibers loaded with different antioxidants (i.e. vitamin B_6 in pyridoxine and pyridoxal form, p-coumaric acid and caffeic acid) are prepared from N,N-dimethylformamide/dimethylsulfoxide solutions. Morphology, structure and crystallinity are evaluated by TEM, SEM, X-ray diffraction and DSC techniques. Fibers are highly amorphous but able to cold crystallize easily due to the high molecular orientation induced by the electrospinning process. The drug molecules are incorporated into the polymeric matrix or formed isolated crystals. A fast release of loaded drug occurs within the first 8 h in hydrophobic medium; but, a slow and sustained release during several days occurs in a hydrophilic medium. Cells attachment on the loaded scaffolds are unaffected by the incorporation of the antioxidants. In contrast, cells proliferation increases with high antioxidative activity against free radicals responsible for cell damage. These new electrospun scaffolds provide high protection of cells against oxidative stress and resulting in innovative 3D fibrous platforms for tissue growth and proliferation

3.1.1 Introduction

One of the most important current problems in tissue engineering is the rejection of biomaterial scaffolds introduced in human body. The main cause of rejection is that the immune system identifies foreign material within the body and attempts to destroy it.[1] However, there is another problem concerning biomaterials, i.e. the generation and harmful effects of reactive oxygen species (ROS) in transplanted organs, which has been demonstrated experimentally.[2]

ROS include different oxidizing molecules like hydrogen peroxide (H_2O_2), superoxide anions (O_2^-) and free radicals such as hydroxyl ($HO^\cdot$) and peroxyl ($R\text{-}COO^\cdot$), which are usually highly reactive and short-lived. ROS form as a natural by-product of the normal metabolism of oxygen and have important roles in cell signalling, inflammatory responses and apoptosis (or programmed cell death).[3] ROS levels can increase dramatically in some specific situations, damaging cell structures significantly. This is known as oxidative stress. This problem can affect cellular components including lipids (by oxidation of their polyunsaturated fatty acids), DNA, proteins, carbohydrates and other biological molecules, leading to many pathological processes.[4, 5]

Fortunately, biological systems can protect themselves against harmful effects of ROS by production of molecules with antioxidant performance. Antioxidant activities essentially suppress the formation of ROS or oppose their reaction. Cellular antioxidants typically correspond to enzymes such as superoxide dismutases, catalases, lactoperoxidases, glutathione peroxidases and peroxiredoxins, and also to small molecules like ascorbic acid (vitamin C), tocopherol (vitamin E), pyridoxine (vitamin B_6), pyridoxal (vitamin B_6 analogue), uric acid and glutathione.[6]

In recent years, there has been an increased interest in the application of antioxidants to medical treatment as information linking the development of human diseases to oxidative stress is constantly gathered. The generally accepted hypothesis is that in any biological system proper balance must be maintained between the formation and removal of reactive oxygen. Within this context, it has also been stated that success in organ transplantation may be related to the use of molecules with antioxidant activity.[7, 8]

The growing need for organ replacement has led to the development of tissue engineering techniques. Specifically several biodegradable polymers have been designed as temporary support for growth and differentiation of cells to form regenerated tissues.[9-12] Thus, three-dimensional (3D) structures can be typically produced by several methods such as particle leaching,[13-15] emulsion freeze-drying,[16] and phase separation.[15, 17] Despite significant advances, there are, however, potential limitations such as lack of desired mechanical stability and porosity. Electrospun scaffolds offer an attractive approach for mimicking the natural extracellular matrix and even for controlling final porosity.[18] These 3D structures facilitate cell

attachment and tissue regeneration while preserving the expression or differentiation of cellular phenotypes.[6, 7]

Although very few reports about the preparation of scaffolds loaded with antioxidants are available, some merit attention, e.g., those concerning mats of electrospun cellulose acetate fibers containing asiaticoside or curcumin,[19] vitamin A acid or vitamin E,[20],as well as polyesters like polycaprolactone and polylactide loaded with curcumin,[21] and gallic acid,[22] respectively. Animals and humans require a constant supply of vitamin B_6 in their diet because this vitamin is a vital cofactor for the metabolism of amino acids and lipids, as well as the synthesis of neurotransmitters (e.g., histamine and haemoglobin). Moreover, it supports DNA repair against free radical damage.[23, 24] Vitamin B_6 or pyridoxine is the derivative of 3-hydroxy-2-methylpyridine. It includes three chemically, metabolically, and functionally related forms, i.e. pyridoxol, pyridoxal and pyridoxamine, in which alcohol, aldehyde, and amine group are respectively located at the fourth position of the pyridine ring (as shown in **Figure 3.1.1** for the pyridoxine and pyridoxal structures).[25] On the other hand, hydroxycinnamic acid is the major subgroup of phenolic compounds, which can be found in a wide variety of fruits, vegetables and herbs. These compounds (e.g., the caffeic[26] and *p*-coumaric[27] acids in **Figure 3.1.1**) are also well recognized, effective antioxidants because they assist in preventing ROS damage by scavenging free radicals.[28]

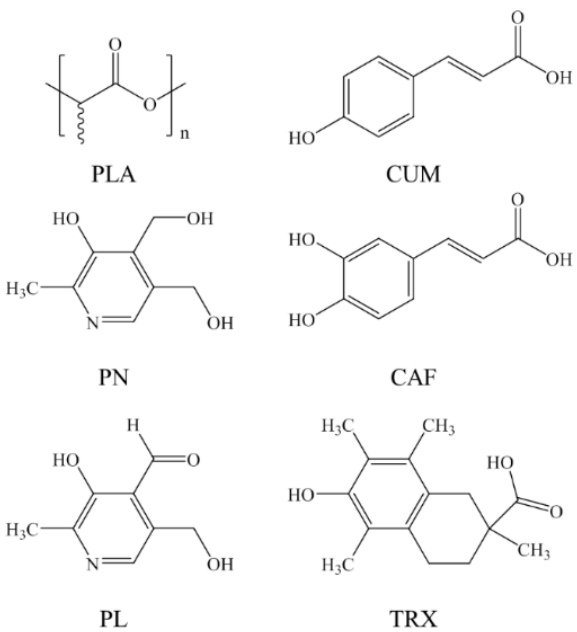

FIGURE 3.1.1

Chemical structure of polylactic acid (PLA), pyridoxine hydrochloride (PN), pyridoxal hydrochloride (PL), *p*-coumaric acid (CUM), caffeic acid (CAF), and 6-hydroxy-2,5,7,8-tetramethylchroman-2-carboxylic acid or trolox (TRX).

The main goal of this work is to prepare 3D scaffolds from electrospun polylactide nanofibers loaded with antioxidants (*i.e.*, vitamin B_6 in pyridoxine and pyridoxal form and two polyphenols, caffeic and *p*-coumaric acids) to prevent oxidative stress of cells colonizing the material. For this purpose, the morphology and physicochemical characterization of the new loaded matrices, together with drug release kinetics, are studied and antioxidant bioactivity is evaluated.

3.1.2 Experimental Section

Materials

Polylactide (PLA), a product of Natureworks (polymer 2002D), was kindly supplied by Nupik International (Polinyà, Spain). According to the manufacturer, this PLA has a D content of 4.25%, a residual monomer content of 0.3%, a density of 1.24 $g \cdot cm^{-3}$, a glass transition temperature (T_g) of 58 ºC and a melting point of 153 ºC. N,N- dimethylformamide (DMF), dimethylsulfoxide (DMSO), pyridoxine hydrochloride (PN).[25] pyridoxal hydrochloride (PL),[25] trolox (6-hydroxy-2,5,7,8-tetramethylchroman-2-carboxylic acid) (TRX), 2,2'-azobis(2-methylpropionamidine) dihydrochloride (AAPH), 3-(4,5-dimethylthiazol-2-yl)-2,5-diphenyl-2H-tetrazolium bromide (MTT) were purchased from Sigma-Aldrich (St. Louis, USA). Caffeic acid (3,4-dihydroxycinnamic acid) (CAF) and p-coumaric acid (p-hydroxycinnamic acid) (CUM) were purchased from Acros Organics (New Jersey, USA). HEp-2 (epithelial cells derived from human laryngeal carcinoma), MDCK (kidney epithelial cells derived from Madin-Darby Canine) and Cos-7 (kidney fibroblast cells derived from African green monkey) and MG-63 (human osteosarcoma cells) were purchased from ATCC (USA).

Antioxidant Loaded PLA Nanofibers from Electrospinning

Nanofibers of PLA unloaded and loaded with an antioxidant (PN, PL, CAF or CUM) were prepared by the electrospinning technique under optimal operational parameters obtained experimentally. To this end, 1 g of PLA was dissolved in 9 mL of anhydrous DMF and the polymer solution was maintained for 12-16 hours at 70 ºC to obtain a clear solution. Then, 1 mL of DMSO containing the corresponding drug (0.1 g) was added and the mixture was vortexed to obtain an electrospinable solution with a 10 and 1 *w*/*v*-% concentration of PLA and antioxidant, respectively. Controls consisting of PLA only and a sample containing a typical drug (TRX) with potent antioxidant activity were prepared by the same procedure. It should be pointed out that TRX is a synthetic analogue derivative of vitamin E and cannot be applied to biomedical use (i.e., only research and not human use). A plastic syringe of 10 mL (Becton Dickson, Spain) was filled with the polymer solution; electrospinning was then carried out between the needle (18G; Terumo, Belgium) connected to the anode and the static collector connected to the cathode. The DC voltage was applied using a high voltage supply (ES30-5W model, Gamma High Voltage Research, USA). The flow was controlled using a KD100 infusion syringe pump (KD Scientific Inc., USA). The polymer jet was collected on an aluminium foil and on coverslips of 14 mm diameter to evaluate cell adhesion and proliferation. All electrospinning experiments were conducted at room temperature.

Morphology and Crystallinity of Drug Loaded PLA Nanofibers

The diameter of electrospun fibers was measured with a Philips TECNAI 10 transmission electron microscope (TEM) at an accelerating voltage of 80 kV and using a SIS MegaView II digital camera. Fibers were directly electrospun on 400 mesh Cu grids coated with a thin carbon film. Inspection of fiber surfaces was performed by scanning electron microscopy using a Focus Ion Beam Zeiss Neon 40 instrument (Carl Zeiss, Germany). Carbon coating was accomplished with a Mitec K950 Sputter Coater (dotted with a film thickness monitor *k*150x). Samples were viewed at an accelerating voltage of 5 kV. Wide angle X-ray diffraction patterns were acquired at the CRG beamline (BM16) of the European Synchrotron Radiation Facility of Grenoble. The beam was monochromatized to a wavelength of 0.098 nm. Scaffold samples were confined between Kapton films. The WAXD detector was calibrated with diffractions of a standard of an alumina (Al_2O_3) sample. The diffraction profiles were normalized to the beam intensity and corrected considering the empty sample background. Calorimetric data were obtained by differential scanning calorimetry with a TA Instruments Q100 series equipped with a refrigeration cooling system (RCS). Experiments were conducted under a flow of dry nitrogen with a sample weight of approximately 5 mg and the calibration of equipment was performed with indium. Heating runs were carried out at a rate of 20 ºC·min^{-1}.

Antioxidante Release Experiments

Controlled release measurements were performed with mats of electrospun samples cut into square pieces (20 x 20 x 0.1 mm^3). They were weighed and incubated in 50 mL tubes containing 30 mL of the release medium at 37 ºC and orbital shaking (200 rpm) for 1 week. Sörensen's buffer (pH 7.4) containing a 70 *v/v*-% of ethanol and alternatively TBE buffer (89 mM Tris, 89 mM boric acid, 2 mM EDTA, pH 8.4) were assayed as release media. Drug concentration in the release media was evaluated by UV spectroscopy using a UV-3600 (Shimadzu, Japan). Calibration curves were obtained by plotting the absorbance measured at the corresponding wavelengths against drug concentration. Samples (1 mL) were drawn from the release medium at predetermined intervals and an equal volume of fresh medium was added to the release vessel. All the drug release tests were carried out using three replicates to control the homogeneity of the release, and the results obtained from the samples were averaged.

Porosity of Antioxidant Loaded PLA Scaffolds

The porosity of the nanofiber scaffolds was measured using the liquid intrusion method.[29] Scaffolds (n = 3) were weighed prior to immersion in ethanol (liquid intrusion). Vacuum was applied for 10 min, and the scaffolds were left on a shaker table for 1 hour to allow diffusion of ethanol into the void volume. The scaffolds were taken out and reweighed. The porosity was calculated according to **Equation 1**:

$$P = \left[\frac{(S_w - S_d)}{d_{EtOH}}\right] / \left[\frac{(S_w - S_d)}{d_{EtOH}} + \frac{S_d}{d_{PLA}}\right] \quad (1)$$

where S_w, S_d are the weights of the wet and dry scaffolds, respectively, and d_{EtOH} and d_{PLA} the densities of ethanol (0.789 g·mL^{-1}) and amorphous PLA (1.24 g·mL^{-1}), respectively. The latter density was selected due to the low crystallinity and drug content of PLA scaffolds.

In-vitro Biocompatibility Assays: Cell Adhesion and Proliferation

HEp-2, MDCK, and Cos-7 cells were cultured in Dulbecco's modified Eagle medium (DMEM) supplemented with 10% fetal bovine serum, 1% penicillin/streptomycin and 2 mM L-glutamine at 37 ºC in a humidified atmosphere with 5% CO_2 and 95% air. The culture medium was changed every two days and, for sub-culture, the cell monolayers were rinsed with phosphate buffered saline (PBS) and detached by incubation with trypsin-EDTA (0.25%) at 37 ºC for 2-5 min. Cell concentration was established by count with a Neubauer camera using 4% trypan-blue as dye vital. The detached cells with viability ≥ 95% were used for cultures the conditions for biocompatibility assays.

The unloaded and antioxidant loaded electrospun PLA nanofibers were collected on circular coverslips (diameter 1.4 cm). These samples were placed into the wells of a multiwell culture plate and sterilized by UV-radiation in a laminar flux cabinet for 15 min. To fix the samples in the well, a small drop of silicone (Silbione® MED ADH 4300 RTV, Bluestar Silicones France SAS, Lyon, France) was used as the adhesive. The samples were incubated with 1 mL of the culture medium in culture conditions for 30 min to equilibrate the material. Finally, the medium was aspired and the material was evaluated for cell adhesion and proliferation by exposing cells to direct contact with the material surface.

To assess cell adhesion, aliquots of 50-100 µL containing 5x10^4 cells were seeded onto the electrospun samples in the wells. The plate was incubated in culture conditions for 30 min to allow cell attachment to the material surface. Then, 1 mL of the culture medium was added to each well and the plate was incubated for 24 h. Finally, cell viability was determined by the MTT assay.[9, 10] Controls were performed by cell culture on the polystyrene surface of the plate (TCPS).

Cell proliferation was evaluated by a similar procedure to the adhesion assay, but the aliquot of 50-100 µL contained 2x10^4 cells. The cultures were maintained for 7 days to allow cell growth and adequate cell confluence in the well. The media were renewed every two days. Finally, viability was determined by the MTT assay.

Each sample was evaluated using five replicates and the results were averaged and graphically represented. The statistical analysis was performed by one-way ANOVA to compare the means of all groups; *t*-Test was then applied to determine a statistically significant difference between two studied groups. The tests were performed with a confidence level of 95% ($p < 0.05$).

To obtain SEM images, samples from adhesion and proliferation assays were processed as follows. First, they were fixed in 2.5% glutaraldehyde-PBS overnight at 4 ºC, and then

dehydrated by washing in an alcohol battery (30º, 50º, 70º, 90º, 95º and 100º) at 4 ºC for a minimum of 30 min per step. Finally, the samples were dried and covered by carbon sputtering for SEM examination.

Antioxidative Effect of PLA Scaffolds Loaded with Vitamin B_6 and Polyphenols

This assay was performed to determine the protective potential of antioxidant loaded PLA nanofibers and to compare the results with unloaded PLA nanofibers. Samples were exposed to oxidative stress induced by AAPH. This water soluble compound has a well-recognized capability to generate free radicals at a constant rate.[30]

MG-63 cells were cultured and manipulated as described above for other cell lines. An aliquot of 50-100 µL containing $2x10^4$ cells was seeded onto the electrospun samples. The plate was incubated in culture conditions for 30 min to allow cell attachment to the material. Then, 1 mL of the culture medium was added to each well and the plate was incubated for 48 h. The medium was subsequently replaced with a fresh one supplemented with different concentrations of the AAPH radical initiator and the culture was continued for 24 h. Finally, all the media were replaced again with a fresh medium without AAPH and supplemented with the MTT reactive to determine cell viability.[9, 10] TCPS controls without and with AAPH were performed to obtain the highest and lowest viability, respectively. The results were statistical analyzed as described above.

3.1.3 Results and Discussion

Morphology of Antioxidant Loaded Electrospun PLA Nanofibers

Selection of an appropriate solvent system is crucial for a successful electrospinning process. DMF has the advantage of having a high dielectric constant, and furthermore is fully miscible with DMSO, which is essential to dissolve the antioxidants tested. A DMF/DMSO mixture (9:1, *v/v*) was consequently employed as a solvent for all experiments. It is also well known that fiber diameter is strongly influenced by polymer concentration which was, like drug concentration, kept constant (10 *w/v*-% and 1 *w/v*-%, respectively) in all the assays.

Electrospinning experimental conditions were optimized to avoid problems like bead formation and obtain a similar diameter distribution in the nanometric range for all samples, which provides rapid release and an antioxidant effect.

The selection of the spinning voltage was essential to ensure a stable, conical liquid jet which minimized bead formation. The distance between the target and the syringe tip was kept close to 12.5 cm, and the flow was found to be drastically affected by the viscosity of the solvent. Thus, a low flow (0.5 - 1 $mL \cdot h^{-1}$) was required in contrast with typical values close to 5-10 $mL \cdot h^{-1}$, which were previously reported for electrospinning of PLA from chloroform:acetone (2:1, *v/v*) mixtures and similar concentrations.[9, 10]

TABLE 3.1.1. Optimal spinning conditions applied for the different studied samples and average fiber diameter values.

Sample	Voltage [kV]	Flow [$mL \cdot h^{-1}$]	Distance[a] [cm]	Fiber Diameter[b] [nm]	Porosity[c] [%]
PLA	17.5	1	12.5	92 ± 1	69 ± 10
PLA-PN	17	0.5	12.5	101 ± 3	85 ± 5
PLA-PL	17	0.5	12.5	124 ± 3	77 ± 12
PLA-CUM	17.5	1	12.5	86 ± 2	49 ± 17
PLA-CAF	19	1	12.5	81 ± 2	82 ± 5
PLA-TRX	17.5	1	12.5	63 ± 1	84 ± 1

[a] Between the syringe tip and the collector
[b] Average value and standard deviation determined from TEM micrographs
[c] Average value and standard deviation determined from liquid intrusion method

Table 3.1.1 summarizes the optimized operational parameters (voltage, flow and needle-collector distance) as well as the derived diameter size. **Figure 3.1.2** contains optical micrographs of electrospun samples obtained under the selected optimum conditions and the histograms of the diameter distributions. Measured values confirm the success of electrospinning to obtain fibers in the nanometric scale, and specifically point out a diameter

range between 63 and 124 nm. Diameters of fibers were highly dependent on the characteristics of the added drug, and consequently the influence of operational variables cannot be discussed independently. For example, an unreliable conclusion could be inferred from the largest diameter (i.e. 101-124 nm) attained at the lowest flow (i.e. 0.5 $mL \cdot h^{-1}$) if the change of drug (i.e. vitamin B_6 instead of polyphenols) is not taken into account.

It is worth noting that the selected solvent system made it possible to obtain nanometric fibers despite working with a relatively high polymer concentration (for example, when a chloroform:acetone mixture was used, the PLA concentration that gave rise to fibers with a similar diameter was lower than 2.5 *w/v*-%).[10]

Incorporation of drugs clearly influenced the diameter of electrospun PLA fibers. Specifically, vitamin B_6 in PN and PL form increased the diameter of fibers from 92 to 101 and 123 nm, respectively. In contrast, larger antioxidant molecules having a carboxylic group such as CUM, CAF and TRX decreased the fiber diameter (86, 81 and 63 nm, respectively). Apparently, diameter sizes increased in the reverse order of the drug molecular volume (TRX > CUM/CAF > PN/PL, as shown in). The possible dissociation of TRX, CAF and CUM into ionic species can increase the charge density on the surface of and/or within the ejected polymer jet. The increased charge density should impose greater elongation and thinning forces on the jet as it travels through the electric field to the collector, leading to the formation of smaller fiber diameters. A similar explanation was proposed for the gallic acid-loaded PLA fibers, which were thinner than those of PLA.[22]

Scaffolds were highly porous (70-85%) although the size of pores was small due to the reduced diameter of the constitutive nanofibers. However, no correlation was found between this size and the diameter of nanofibers (**Table 3.1.1**).

SEM electron micrographs of **Figure 3.1.3** compare the surface morphology of the nanofibers. A surface rough with multiple holes was characteristic of the unloaded PLA (**Figure 3.1.3 a**) and even of samples having PN and PL drugs. However, the micrographs of PLA-PN samples also highlight the presence of isolated drug crystals distributed along the fibers (**Figure 3.1.3 b**), even after the partial melting of the polymer under the electron flux (**Figure 3.1.3 b**, inset). PLA-PL fibers were also characterized by the presence of protrusions that could correspond to vitamin B_6 crystals which seemed better integrated in the fiber structure (**Figure 3.1.3 c**). PLA-CUM fibers had a rough morphology with bumps protruding above the surface (**Figure 3.1.3 d**) in a similar way to PLA-PL fibers. PLA fibers loaded with CAF again had a rough surface and polyphenol crystals that were perpendicularly embedded in the fibers (**Figure 3.1.3 e**). Finally, PLA-TRX fibers had a smooth appearance (**Figure 3.1.3 f**) where the presence of drug crystals could not be clearly detected.

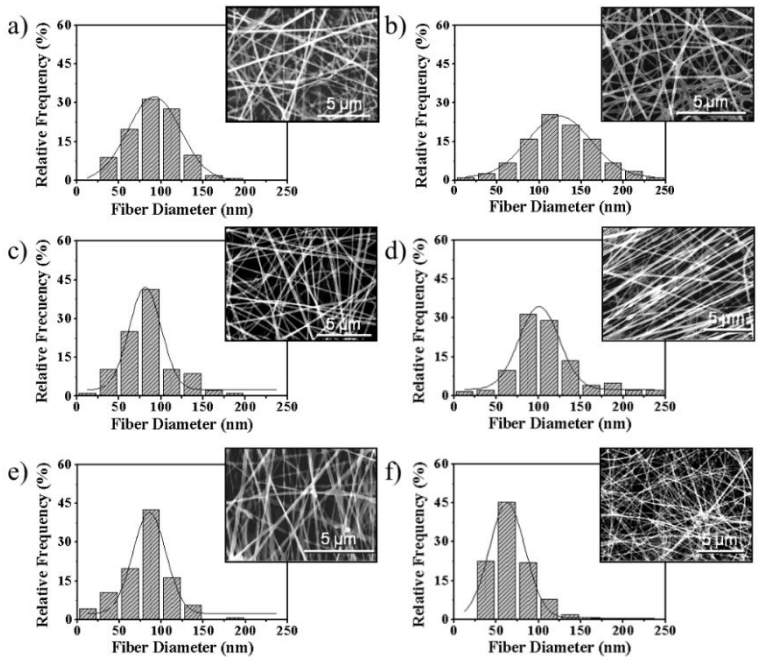

FIGURE 3.1.2

Scanning electron micrographs (images) and frequency distribution (graphics) of the fiber diameter of electrospun PLA (a), PLA-PN (b), PLA-PL (c), PLA-CUM (d), PLA-CAF (e) and PLA-TRX (f) nanofibers.

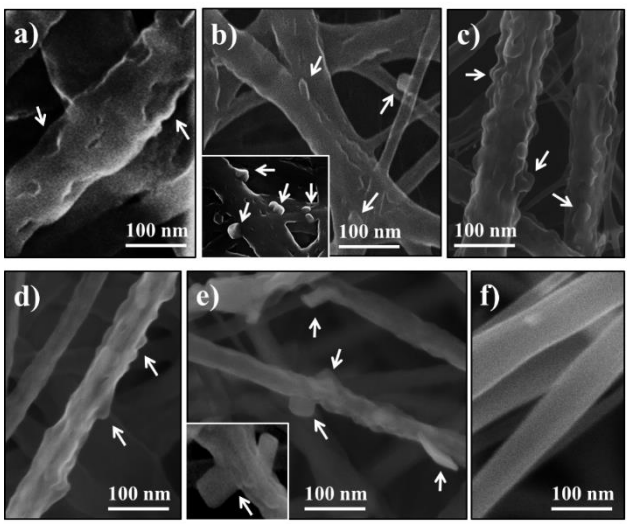

FIGURE 3.1.3

Representative SEM images of scaffolds showing morphological details of the fiber surfaces. (a) PLA fibers with holes (arrows). (b) PLA-PN fibers with PN crystals (arrows). Inset shows how the crystals remain embedded after partial melting of fibers under the electron flux. (c) PLA-PL fibers with large numbers of protrusions (arrows). (d) PLA-CUM fibers with embedded crystals protruding from the surface (arrows). (e) PLA-CAF fibers with flat crystals protruding perpendicularly from the surface (arrows). Inset shows a detail of the crystal arrangement. (f) PLA-TRX fibers with a smooth surface.

X-Ray Diffraction Data of Antioxidant Loaded Electrospun PLA Nanofibers

X-ray diffraction was used to assess how antioxidants became incorporated into the PLA nanofiber samples (i.e. giving isolated crystals or mixing in either the amorphous or crystalline phases of PLA). **Figure 3.1.4** compares WAXD profiles of all studied mats with those corresponding to isolated drug.

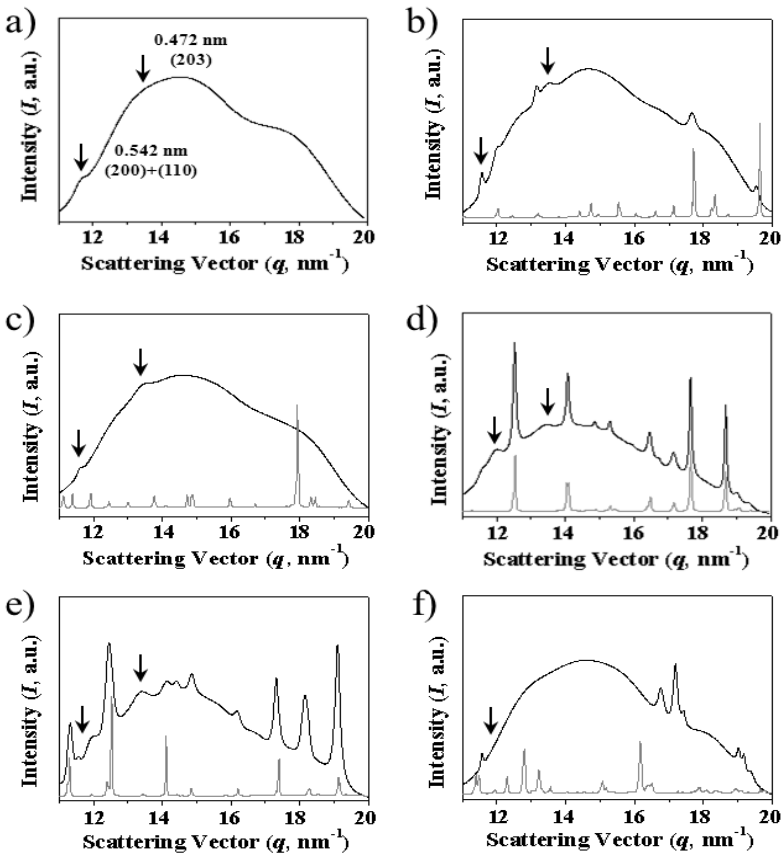

FIGURE 3.1.4

WAXD patterns (intensity, *I*, versus the scattering vector, $q = [4\pi/\lambda] \sin(\theta) = 2\pi/d$, where θ is the scattering angle and *d* the Bragg spacing) of electrospun microfibers (top black line) and the corresponding loaded antioxidant (bottom gray line): a) PLA, b) PLA-PN, c) PLA-PL, d) PLA-CUM, e) PLA-CAF, and f) PLA-TRX. Arrows indicate peaks that could be associated with the PLA crystalline phase.

The pattern of electrospun PLA nanofibers revealed the presence of dominant amorphous halos and the almost complete absence of crystalline PLA Bragg reflections. Predominant Bragg peaks associated with the expected α-form (10_3 helical conformation) of PLA should appear at 0.542 and 0.472 nm and corresponded to the (200)+(110) and (203) reflections.[9, 31-33] These were hardly observed in the PLA sample or in the drug loaded scaffolds, in agreement with the low degree of crystallinity determined from DSC measurements, as will be explained below.

No peaks associated with PL crystals were observed in the diffractograms of PLA-PL samples (**Figure 3.1.4 c**), suggesting that this drug was well mixed in the polymeric matrix, as also inferred from morphological observations (**Figure 3.1.3 c**). On the contrary, crystalline reflections with a relatively low intensity (**Figure 3.1.4 b**) were detected in the PN loaded scaffolds; note that in this case a low number of crystals were observed in the electron micrographs (**Figure 3.1.3 b**).

Samples loaded with CUM and CAF polyphenols gave rise to X-ray profiles (**Figures 3.1.4 d** and **3.1.4 e**) where the characteristic reflections of the corresponding drug crystals appeared with high intensity. Differences on the peak width allowed deducing a smaller size of CAF crystals (i.e. those with the higher width) according to the Scherrer equation.[34] The relative intensity of peaks associated with CAF crystals changed slightly in the loaded scaffold with respect to the powder drug (**Figure 3.1.4 e**), suggesting that crystals were deposited in the PLA nanofibers in a preferred orientation, as also suggested by the morphological observations (**Figure 3.1.3 e**). Finally, the X-ray profile of the PLA-TRX sample revealed the absence of TRX crystals, indicating that these antioxidant molecules were well integrated in the polylactide matrix. However, the appearance of new Bragg reflections also merits attention because it suggested that a new phase can occur by the interaction between TRX and PLA molecules.

Thermal Behaviour of Antioxidant Loaded Electrospun PLA Nanofibers

Table 3.1.2 contains the main calorimetric data obtained from the heating run of antioxidant loaded electrospun samples. Heating traces of these samples are shown in **Figure 3.1.5** together with the trace corresponding to the heating run of a PLA sample after being processed in a controlled way (i.e. cooled at a rate of 10 ºC·min^{-1} from the melt state).

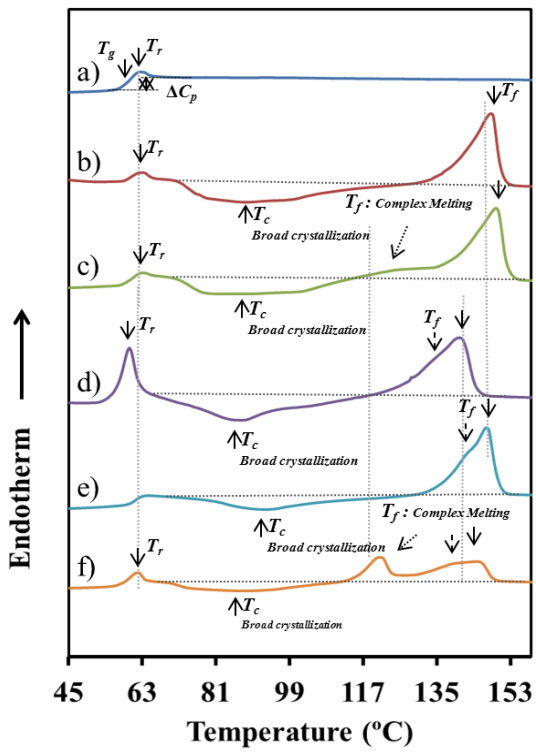

FIGURE 3.1.5

DSC heating runs (20 ºC·min^{-1}) corresponding to: PLA sample after being cooled from the melt state to room temperature at 10 ºC·min^{-1} (a), PLA-PN (b), PLA-PL (c), PLA-CUM (d), PLA-CAF (e) and PLA-TRX (f).

TABLE 3.1.2. **Selected calorimetric data from the heating scan performed with the different PLA electrospun samples.**

Sample	T_g [ºC]	ΔCp [J·g^{-1}·ºC^{-1}]	ΔH_r [J·g^{-1}]	T_c [ºC]	ΔH_c [J·g^{1}]	T_m [ºC]	ΔH_m [J·g^{-1}]	ΔH_m - ΔH_c [J·g^{-1}]	χ_c	χ_{MA}	χ_{RA}
PLA[a)]	60.0	0.62	2.7	-	-	-	-	-	-	0.86	0.14
PLA	61.1	0.50	3.8	89.7	24.0	148.3	24.8	0.8	0.01	0.79	0.20
PLA-PN	60.5	0.19	2.7	87.6	23.3	148.1	26.9	3.6	0.03	0.31	0.66
PLA-PL	60.8	0.40	1.7	85.2	21.7	149.4	32.6	10.9	0.10	0.63	0.27
PLA-CUM	58.3	0.20	12.2	86.9	25.3	140.4	28.4	3.1	0.03	0.32	0.65
PLA-CAF	59.7	0.15	1.3	92.9	16.3	147.1	23.4	7.1	0.07	0.25	0.68
PLA-CUM	59.8	0.20	3.9	87.1	18.6	120.3, 142.2	35.9	17.3	0.16	0.32	0.52

[a)] For comparative purposes data corresponding to a heating run of a PLA sample after being cooled from the melt state are also given.

Several features deserve attention:

- All electrospun samples had a broad exothermic peak (70-120 ºC) indicative of the cold crystallization of PLA. Its appearance, enthalpy and specific temperature range depended on the sample nature (i.e. the antioxidant added to PLA). The high molecular orientation attained in the electrospun fibers facilitated the crystallization process, as previously reported,[9, 33] which was not observed when the PLA sample was processed by slow cooling from the melt state (**Figure 3.1.5 a**). On the contrary, unloaded electrospun PLA samples again were able to crystallize (**Table 3.1.2**).

- Electrospun samples showed melting peaks which were mainly due to the cold crystallization process. The difference between melting and cold crystallization enthalpies was low, and consequently samples crystallized with high difficulty during the electrospinning process. The degree of crystallinity (X_c) of the electrospun samples could be evaluated from the above enthalpic difference and the reported melting enthalpy (106 $J \cdot g^{-1}$) for a 100% crystalline sample.[35, 36] Significant crystallinity differences were found between the electrospun samples although these values were always relatively low. Specifically, samples loaded with TRX and PL had the highest values (i.e. 17.3 and 10.9%, respectively). It should be pointed out that these were the only samples where no crystals of the added drug were detected in the X-ray profiles. Note also that all samples attained moderate crystallinity (i.e. 22-34%) after the cold crystallization process.

- The melting process, which was relatively complex, gave rise to a main peak (149-140 ºC) together with a small shoulder, and in some cases to an additional minor peak at a lower temperature. The main peak temperature changed slightly depending on the loaded drug and specifically on its capability to be incorporated into the crystalline structure. This capability was higher for the CUM molecules, as deduced from the higher decrease in the melting temperature and even in the crystallinity (**Table 3.1.2**). The shoulder and the main peak detected in the heating runs seem to correspond to the characteristic PLA double melting peak, which is associated with a recrystallization process where thinner lamellae become thicker. The minor peak observed in two cases (i.e. PLA-TRX and PLA-PL samples) at a temperature close to 120 ºC is indicative of the existence of highly defective crystals (i.e. those with a significantly lower thickness or a high drug content).

- All PLA heating traces had a clear glass transition, as could be presumed for practically amorphous samples (i.e. those obtained before cold crystallization), and also a relaxation endothermic peak that usually appeared later. This peak is indicative of the trend of the metastable PLA glassy material to achieve equilibrium thermodynamic conditions with a lower specific volume, enthalpy and entropy, which logically render a material with higher stiffness. The glass transition temperature was practically constant for all samples, and consequently the incorporation of the aromatic drug molecules did not facilitate the mobility

of the rigid PLA molecules. However, the strong impact on the relaxation process for the PLA-CUM sample is worth noting.

- The amorphous phase of PLA is complex and should usually be analyzed assuming a biphasic model where a mobile amorphous phase (MAP), responsible for the heat capacity jump in the glass transition region, and a rigid amorphous phase (RAP) associated with the hindered molecular motions of chains within lamellar stacks, can be distinguished. Specifically, these fractions are determined as $X_{MAP} = \Delta C_p/\Delta C_P^0$ and $X_{RAP} = 1\text{-}X_c\text{-}X_{MAP}$, where ΔC_p and ΔC_P^0 correspond to the heat capacity jump of the studied sample and a fully amorphous PLA (i.e. 0.623 $J\cdot g^{-1}\cdot {}^oC^{-1}$). Results in **Table 3.1.2** again show significant differences between all loaded PLA samples and, interestingly, a loss of correlation between X_c and X_{RAP} fractions since both should change in a similar way (i.e. both should increase or decrease). Discrepancies suggest the existence of interfaces between drug crystals and PLA that increased the X_{RAP} fraction.

Spectral Characteristics Related to the Antioxidants Release from PLA Electrospun

The release of molecules loaded in an electrospun matrix is intimately related to the morphology and structure of the constituting fibers and also to the environment where such release occurs. After the analysis of the characteristics of the loaded PLA nanofibers, it seemed interesting to study the behavior in solution of the selected drugs. To this end, two media of different hydrophobicity/hydrophilicity were selected to vary the affinity with the released drug. Specifically, a Sörensen-ethanol (3:7, *v/v*; pH 7.4) mixture and a TBE buffer (pH 8.4) were taken as examples of hydrophobic and hydrophilic release media, respectively. UV-Vis spectroscopy was used to quantify the amount of released antioxidant and to detect spectral/electronic changes undergone by the released molecules (**Figure 3.1.6**). The PBS buffer was also tested as release hydrophilic medium (data not shown), and the release kinetic results were similar to those obtained in Sörensen-ethanol (3:7, *v/v*; pH 7.4) buffer; however, TBE buffer has the advantage of facilitating the detection of vitamins and polyphenols by UV-Vis spectroscopy due to electronic changes in these molecules by the presence of the borate ions in the buffer. For this reason, TBE buffer was chosen as the hydrophilic medium for release assays.

The spectrum of PN in the hydrophobic medium (**Figure 3.1.6 a**) is characterized by two bands at 280 nm and 325 nm associated with the presence of the 3-hydroxyl group (i.e. that directly linked to the pyridine ring). In aqueous solution, the spectrum became clearly dependent on the pH.[37] A single maximum at 292 nm is characteristic when pH values are equal to or lower than 3, but it gradually decreased and two new bands appeared at 255 and 325 nm as the pH was raised to 7.4, which is precisely the value of the medium tested. This splitting is characteristic of the presence of the hydroxyl groups since it was never observed for 3-methoxy derivatives.[37] In contrast, the absorption spectra of PN in the pH 8.4 TBE hydrophilic buffer (**Figure 3.1.6 b**) showed a single band at 292 nm, which can be explained by the presence of the borate ions in

the buffer. The borate-PN complex, which has been reported in previous works, consisted of the coordination of bore atoms with two PN molecules through their oxygen atoms in positions 3 and 4. This complex kept the physiological activity of PN and was thermostable in neutral solutions.[37, 38]

The PL and PN spectra in the hydrophobic and hydrophilic media (**Figures 3.1.6 c** and **3.1.6 d**, respectively) were similar, although a new band appeared near 400-410 nm, most probably because of the presence of the aldehyde group of PL.

The spectra of CUM in the Sörensen-ethanol medium correspond to a single band with a maximum at 285 nm and a shoulder at 310 nm (**Figure 3.1.6 e**). This main band can be attributed to the 3-hydroxyl aromatic substitution and basically remains unchanged when the hydrophilic medium is used (**Figure 3.1.6 f**). The spectrum of CAF with 3 and 4- hydroxyl aromatic substitutions is clearly different since now two bands appear at 285 nm and 310 nm in the Sörensen-ethanol buffer (**Figure 3.1.6 g**). A notable change in the spectrum occurred in the hydrophilic medium since the intensity of the peaks is reversed and specifically the intensity of the peak at 310 nm increases significantly (**Figure 3.1.6 h**).

The TRX molecules in both hydrophobic and hydrophilic media (**Figures 3.1.6 i** and **3.1.6 j**) have identical spectral characteristics defined by a single band at 291 nm (Sörensen-ethanol buffer) and 289 nm (TBE buffer). Note that the molecule has only a hydroxyl substitution, and therefore a simple spectrum should be expected.

Finally, for all antioxidants, lineal plots of absorbance (measured at the specific wavelength corresponding to the maximum determined for each release medium) versus drug concentration were obtained (insets of **Figures 3.1.6 a**-**3.1.6 j**) and used to estimate the drug concentration in the subsequent release experiments.

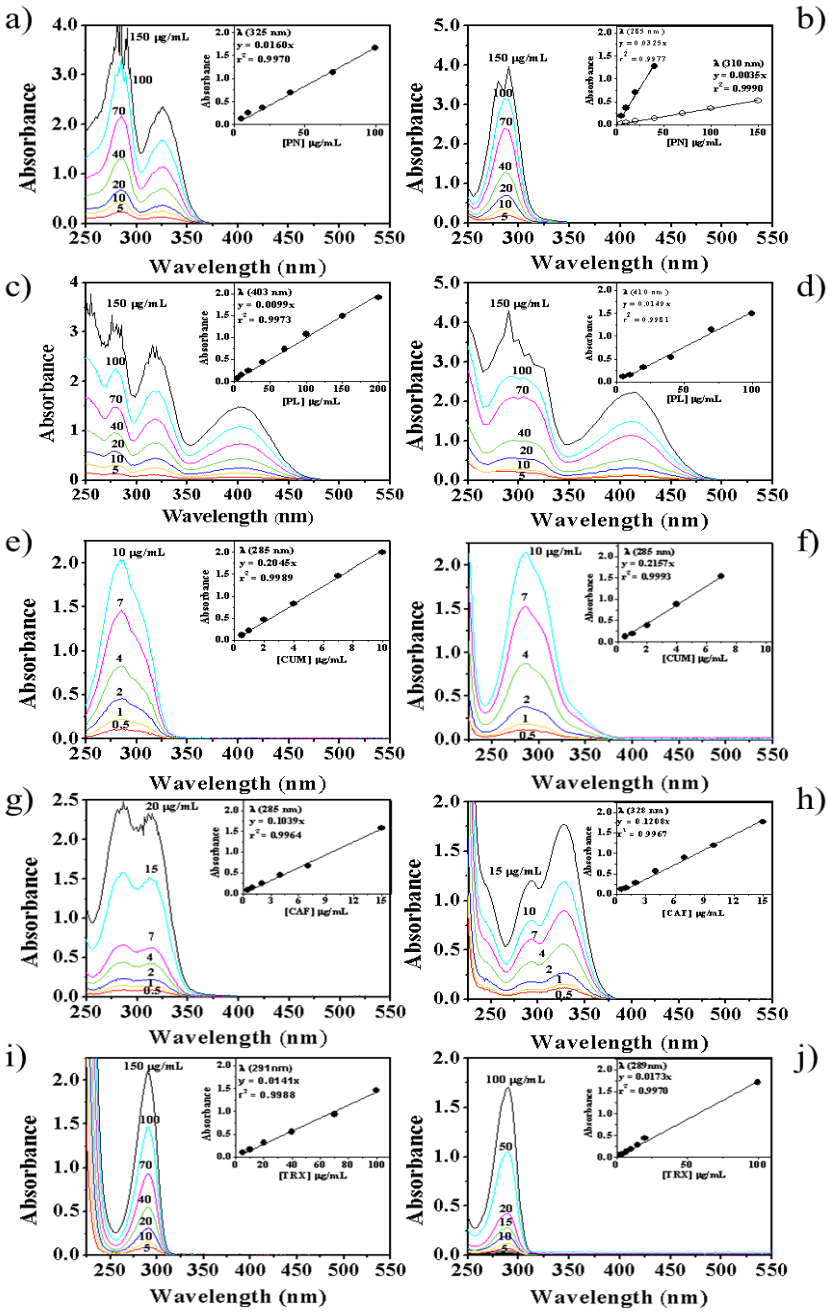

FIGURE 3.1.6.

UV-Vis spectral characteristics of the antioxidants used in this work: PN (a, b), PL (c, d), CUM (e, f), CAF (g, h), and TRX (i, j). Antioxidants were dissolved in a Sörensen-ethanol buffer (3:7, v/v) hydrophobic medium (a, c, e, g, and i) and in a TBE buffer hydrophilic medium (b, d, f, h and j). The UV-Vis spectra of each antioxidant were recorded at different concentrations, and a regression analysis was performed for quantification at a characteristic wavelength of each drug (inset).

The release kinetics can be calculated from experimental results by several theoretical models, typically first-order,[39, 40] Higuchi[41, 42] and their combination.[43] The release generally occurred in two different steps, i.e. rapid release of molecules that should be deposited mainly on the high surface area of nanofibers and slow release that should involve the diffusion of molecules through the polymer bulk towards the release medium. In this way, a combined model based on the Higuchi and first-order models (**Equation 2** and **3**) is usually used to describe the first (0-60%) and second (40-100%) parts of the release, respectively:

$$M_t/M_0 = k_h t^{1/2} \qquad (0 \leq M_t/M_0 \leq 0.6) \qquad (2)$$

$$\ln(1 - M_t/M_0) = a - k_1 t \qquad (0.4 \leq M_t/M_0 \leq 1.0) \qquad (3)$$

where k_h is the Higuchi release constant, k_1 is the first-order release constant, a takes into account the release in the first step, M_t is the percentage of drug released at time t, and M_0 is the drug equilibrium percentage (considered as the maximum drug percentage).

The release of the studied drugs in the two media is graphically shown in **Figure 3.1.7**, whereas the deduced kinetic constants are summarized in **Table 3.1.3**. In general, the release could be well fitted using only the Higuchi model, although in some specific cases (i.e. PL and TRX in the Sörensen-ethanol medium), this model had a limited range of application, and therefore the second part of the release should be fitted with a first-order kinetics.

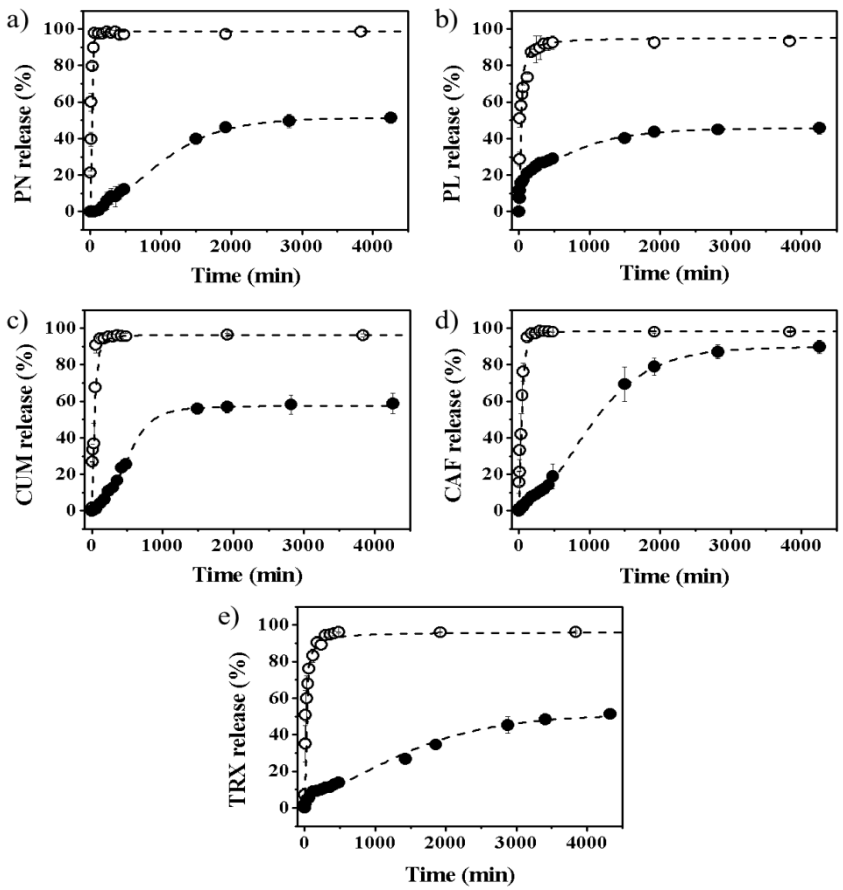

FIGURE 3.1.7

Antioxidant release profiles for five loaded electrospun PLA samples: PLA-PN (a), PLA-PL (b), PLA-CUM (c), PLA-CAF (d), and PLA-TRX (e). The concentration of drug released in a Sörensen-ethanol buffer mixture (3:7, v/v) (open circle) and in a TBE buffer (solid circle) was measured by UV-Vis spectroscopy. Results are mean ± SE (n = 3).

Because of their hydrophobic character (due to their aromatic ring structure), all drugs were rapidly released in the Sörensen-ethanol medium. Thus, 100-95% of the loaded drug was released after only 8 h of exposure to the medium in all cases.

By contrast, in the hydrophilic environment, the release was slower and progressive and an equilibrium condition was established. This was deduced from the asymptotic release percentage obtained in all cases. The release occurred in two different steps, as also deduced from the selected kinetic model. A relatively fast process over an exposure time close to 8 h was firstly observed, corresponding to a release between 15 and 30% of the total loaded drug, with the minimum value found when TRX was loaded. After this period, the release was slower until the above asymptotic value was reached in a period that could extend over three days. This release was around 50% except for the more hydrophilic CAF drug (80%).

TABLE 3.1.3. Release kinetikcs parameters of the Higuchi model (0-60%) for the antioxidant release from PLA scaffolds in hydrophilic and hydrophobic media.

Drug	Sörensen-ethanol (Hydrophobic medium)			TBE (Hydrophilic medium)		
	k_H [$h^{-0.5}$]	*r*	range	k_H [$h^{-0.5}$]	*r*	range
PN	1.033	0.986	0-98%	0.191[b]	0.987	0-100%
PL	1.192[a]	0.93	0-58%	0.098[a]	0.987	0-100%
CUM	0.718	0.959	0-94%	0.175[b]	0.986	0-95%
CAF	0.683	0.988	0-95%	0.229[b]	0.985	0-98%
TRX	0.853[a)]	0.936	0-76%	0.074	0.995	0-100%

Values adjusted in kinetics with an initial gap (not release) during 5 min ([a]) or 60 min ([b])

Kinetic constants were logically higher for the hydrophobic medium. In this case, slight differences were determined for the different drugs, although the values of the kinetic constant found at the beginning of the process suggested a hydrophobic character that decreased in the order PN/PL > CUM/CAF. Similar conclusions were drawn when kinetic constants corresponding to the second part of the release in the hydrophilic medium were compared. Some discrepancies were found for the first part but in this case the process is probably mainly influenced by the physical state of the drug in the PLA matrix (i.e. mixed or forming isolated crystals). For example, CUM formed bigger crystals than CAF and was released faster at the beginning of the process despite its lower hydrophilicity. The peculiar behavior of TRX, which had practically the smallest kinetic rate constants for the two media, indicating affinity between the drug and the PLA matrix (as suggested by SEM, X-ray and DSC observations), is worth noting. Hydrogen bond interactions were probably established between hydroxyl and carboxylic groups of the drug and the PLA ester groups.

Biocompatibility of Antioxidant Loaded Electrospun PLA Nanofibers: Cell Adhesion and Proliferation

PLA nanofiber matrices loaded with antioxidants were evaluated as appropriate scaffolds to support cell adhesion and proliferation. Thus, epithelial cells like MDCK and HEp-2, and fibroblast-like cells such as Cos-7 were seeded in direct contact with the studied materials (**Figure 3.1.8**). Cell adhesion was determined after 24 hours as an early event of cell colonization on the scaffolds while cell proliferation was determined at 7 days as an endpoint that demonstrated cell growth on the materials.

Cell attachment was evaluated considering the ratio between the number of adhered cells and cell viability (i.e. number of cells adhered on the TCPS control) for each cultured well of the plate. In this way, it was clearly established that a high number of cells, close to 80%, adhered to the scaffold surface although this surface corresponded to only 68% of the total well surface. This important feature was found for all tested cells (i.e. Cos-7, MDCK and HEp-2, as shown in **Figure 3.1.8 a**, **3.1.8 c** and **3.1.8 e**, respectively). Specifically, the adhesion/viability ratio of the scaffold, together with the ratio obtained for the remaining plate surface of the well that contained the sample, was similar to the control. In conclusion, the obtained results clearly exclude any possible cytotoxic effect generated by the PLA matrices after being loaded with the selected antioxidants.Cell proliferation was determined as the total growth in the wells containing the electrospun samples. Thus, the three cell lines (Cos-7, MDCK and HEp-2 cells) showed a significant increase in the cell number when the well contained antioxidant loaded PLA scaffolds (**Figure 3.1.8 b**, **3.1.8 d** and **3.1.8 f**). This increase demonstrated that cell growth and/or cell culture had a self-basal oxidative stress[4, 6-8] and that the antioxidant activity of vitamin B_6, its derivative and polyphenols released from the loaded scaffold improved the cellular environment considerably by their radical-scavenging capacity. It should be pointed out that the selected natural antioxidants gave better results than the well-recognized TRX, which was used as a positive control. The effect of the natural antioxidants changed slightly according to their nature and the cells tested. Thus, the highest proliferation was found for MDCK cells grown on CUM loaded scaffolds (i.e. more than 50% compared to the TCPS control), whereas the lowest proliferation corresponded to HEp-2 cells on PLA-CUM scaffolds (i.e. only more than 20% compared to the control). Changes in the antioxidant effect of vitamin B_6, its derivative and polyphenols during prolonged culture could be related to decomposition and pro-oxidative effects of the products of this decomposition.[44]

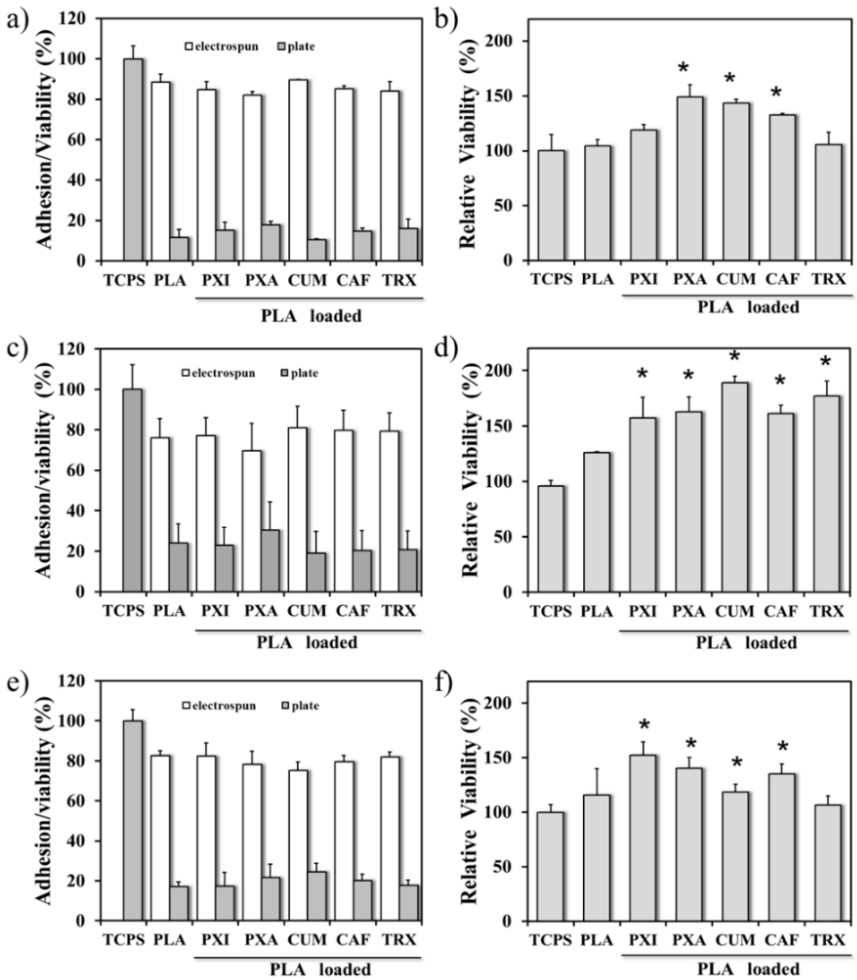

FIGURE 3.1.8

Cell attachment and proliferation on scaffolds of electrospun nanofibers for three cell lines: Cos-7 cells (a) and (b), MDCK cells (c) and (d), and HEp-2 cells (e) and (f). Cell attachment (a, c, and e) was evaluated on the electrospun sample and on the surface of a well not covered with the electrospun sample (i.e. the plate, TCPS). Cell proliferation (b, d, and f) was evaluated in the whole well that contained the electrospun sample. Results are mean ± SD (n = 5). Values differing from controls (TCPS) are indicated by an asterisk, $p < 0.05$ (t-Test).

Morphological observations gave evidence of the formation of a cell monolayer on all the electrospun samples (**Figure 3.1.9 a-3.1.9 f**). The increase in the number of cells grown on the surface of the samples does not exclude a possible alteration or occurrence of defects in the cell monolayer (e.g., stacking of cells in isolate clusters). The micrographs in **Figure 3.1.9** show that representative Cos-7 cells grew normally to contact each other and formed a monolayer structure on the scaffold surface. Furthermore, it is clear that these scaffolds had high fiber density and reduced pore size that restricted the entry of cells into the matrix (**Figure 3.1.9 g**). Invasion and

colonization of the scaffolds by cells were consequently hindered because of their inherent geometry.

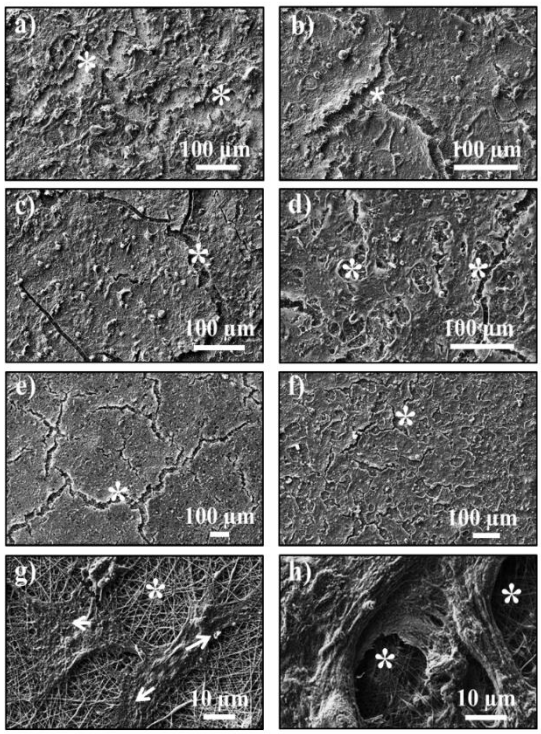

FIGURE 3.1.9

SEM images of the cell monolayer on PLA (a), PLA-PN (b), PLA-PL (c), PLA-CUM (d), PLA-CAF (e), and PLA-TRX (f) during proliferation of Cos-7 cells. The asterisk points out the electrospun nanofibers. Representative images of Cos-7 cells show a morphological detail of the cytoplasmic extension (arrows) demonstrating cell adhesion on the electrospun sample after 24 hours of culture (g), and a layer cell arrangement with a tissue-like morphology after 7 days of culture (h).

Thus, the cells extended lamellipodia to adhere to the electrospun surface (**Figure 3.1.9 g**). However, the cells formed a tissue-like stratum on the scaffold surface (**Figure 3.1.9 h**), which is a promising feature about applications focused on tissue remodeling and regeneration.

Effect of Vitamin B_6 and Polyphenols Loaded PLA Electrospun Nanofibers against the Induction of Oxidative Stress

The main goal for the new loaded PLA matrices is to confer a protective effect against free radicals responsible for cell damage and death by necrosis while the ability to support cell adhesion and growth is maintained or even improved. In this way, an induction experiment of oxidative stress in the cultured cells was carried out in the presence of the scaffold and using AAPH as an agent of oxidative injury.[30]

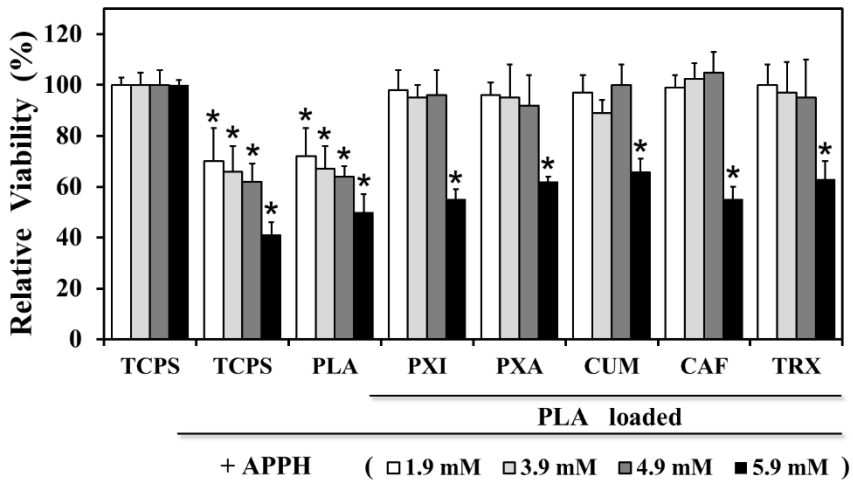

FIGURE 3.1.10

Antioxidant effect of the selected drugs after being loaded into the scaffolds of PLA electrospun nanofibers. The MG-63 cell (fibroblasts-like) culture was performed on the electrospun samples and the control (TCPS, culture plate). All samples were then exposed to AAPH to induce cell oxidative stress. Cell viability was evaluated at 24 h after induction to determine the antioxidant effect of the drugs loaded into the PLA scaffolds. Results are mean ± SD ($n = 5$). Values differing from controls (TCPS) are indicated by an asterisk as $p < 0.05$ (*t*-Test).

Figure 3.1.10 shows the effect of the selected agent on the cultured cells over the TCPS control. The deleterious effect of AAPH is worth noting. A decrease in cell viability is clearly deduced, and obviously depends on the APPH concentration in the culture. Thus, doses between 1.9 mM and 4.9 mM caused a decrease in close to 30-40% in cell viability, whereas a severe reduction (i.e. close to 60%) was found at the highest doses (5.9 mM). A similar behavior was observed when cells were cultured on unloaded PLA scaffolds (**Figure 3.1.10**, PLA group), demonstrating that cell growth in this matrix is unprotected against oxidative stress. However, damage in the cultured cells induced by AAPH could be reverted when cell growth occurred in the antioxidant loaded PLA matrices provided that AAPH doses were lower than the maximum concentration tested (5.9 mM). Note also that the antioxidant effect was obviously limited by the low amount of PN, PL and polyphenols loaded into the scaffolds. No significant statistical differences were found between the antioxidant loaded PLA scaffolds. In any case, the proposed strategy appears suitable to provide new materials that support both cell adhesion and growth, and additionally have a protective activity against oxidative stress.

3.1.4 Conclusions

PLA nanofibers loaded with different antioxidants can be prepared by electrospinning from DMF-DMSO (9:1, *v/v)* mixtures under optimized conditions. Thus, diameters ranging between 63 and 124 nm were attained using polymer and drug concentrations of 10 and 1 *w/v*-%, flows between 0.5 and 1 $mL \cdot h^{-1}$, voltages between 17 and 19 kV and a distance between the collector and the spinneret of 12.5 cm. Fiber morphology (diameter and texture) and crystallinity were dependent on the drug added, which in addition appeared well mixed into the PLA matrix (e.g., the PL analogue of vitamin B_6) or formed isolated crystals (e.g., CUM) depending on its chemical nature.

Hydrophobic medium allowed a fast, practically complete release of all studied drugs (PL, PN, CUM, CAF and TRX), whereas clear differences were found in the release kinetics when a hydrophilic medium was used. Furthermore, in this case, the amount of drug released depended on equilibrium conditions. Specifically, the maximum amount was obtained when the more hydrophilic drug (i.e. CAF) was considered.

Cell proliferation was higher when antioxidant loaded scaffolds were used since the cellular environment was improved by the radical-scavenging capacity of drugs. Furthermore, the new loaded PLA matrices had a protective effect against free radicals responsible for cell damage and death by necrosis even when agents of oxidative injury were added to the cultured cells. In summary, the new antioxidant loaded PLA scaffolds appear suitable to support both cell adhesion and growth, and additionally have a protective activity against oxidative stress.

3.1.5 References

[1] M.D. Jenkins, R.K. Woo, R.S. Greco, Nanoscale Technology in Biological Systems, in: R.S. Greco, F.B. Prinz, R.L. Smith (Eds.) Nanoscale Technology in Biological Systems, CRC Press, Boca Raton, FL, USA, 2004.

[2] W.F. Liu, M. Ma, K.M. Bratlie, T.T. Dang, R. Langer, D.G. Anderson, Biomaterials, 32 (2011) 1796-1801.

[3] H.U. Simon, A. Haj-Yehia, F. Levi-Schaffer, Apoptosis, 5 (2000) 415-418.

[4] C. Leeuwenburgh, J.W. Heinecke, Curr Med Chem, 8 (2001) 829-838.

[5] S.C. Sikka, Front Biosci, 1 (1996) 78-86.

[6] A.R. Collins, Am J Clin Nutr, 81 (2005) 261-267.

[7] H.P. Neeff, E. von Dobschuetz, O. Sommer, U.T. Hopt, O. Drognitz, Transpl Int, 21 (2008) 1081-1089.

[8] W. Jassem, N.D. Heaton, Kidney Int, 66 (2004) 514-517.

[9] L.J. del Valle, R. Camps, A. Diaz, L. Franco, A. Rodriguez-Galan, J. Puiggali, J Polym Res, 18 (2011) 1903-1917.

[10] L.J. del Valle, A. Diaz, M. Royo, A. Rodriguez-Galan, J. Puiggali, Express Polym Lett, 6 (2012) 266-282.

[11] T.J. Sill, H.A. von Recum, Biomaterials, 29 (2008) 1989-2006.

[12] S.A. Sell, P.S. Wolfe, K. Garg, J.M. McCool, I.A. Rodriguez, G.L. Bowlin, Polymers-Basel, 2 (2010) 522-553.

[13] L.J. del Valle, D. Roca, L. Franco, J. Puiggali, A. Rodriguez-Galan, J Appl Polym Sci, 122 (2011) 1953-1967.

[14] A.G. Mikos, M.D. Lyman, L.E. Freed, R. Langer, Biomaterials, 15 (1994) 55-58.

[15] E. Traversa, B. Mecheri, C. Mandoli, S. Soliman, A. Rinaldi, S. Licoccia, G. Forte, F. Pagliari, S. Pagliari, F. Carotenuto, M. Minieri, P. Di Nardo, J Exp Nanosci, 3 (2008) 97-110.

[16] D.J. Mooney, D.F. Baldwin, N.P. Suh, L.P. Vacanti, R. Langer, Biomaterials, 17 (1996) 1417-1422.

[17] H.D. Kim, E.H. Bae, I.C. Kwon, R.R. Pal, J.D. Nam, D.S. Lee, Biomaterials, 25 (2004) 2319-2329.

[18] S. Soliman, S. Sant, J.W. Nichol, M. Khabiry, E. Traversa, A. Khademhosseini, J Biomed Mater Res A, 96A (2011) 566-574.

[19] O. Suwantong, U. Ruktanonchai, P. Supaphol, J Biomed Mater Res A, 94A (2010) 1216-1225.

[20] P. Taepaiboon, U. Rungsardthong, P. Supaphol, Eur J Pharm Biopharm, 67 (2007) 387-397.

[21] J.G. Merrell, S.W. McLaughlin, L. Tie, C.T. Laurencin, A.F. Chen, L.S. Nair, Clin Exp Pharmacol P, 36 (2009) 1149-1156.

[22] P. Chuysinuan, N. Chimnoi, S. Techasakul, P. Supaphol, Macromol Chem Physic, 210 (2009) 814-822.

[23] J.M. Matxain, M. Ristila, A. Strid, L.A. Eriksson, J Phys Chem A, 110 (2006) 13068-13072.

[24] A.S. Chen, T. Taguchi, S. Aoyama, M. Sugiura, M. Haruna, M.W. Wang, I. Miwa, Free Radical Bio Med, 35 (2003) 1392-1403.

[25] IUPAC-IUB, Pure Appl Chem, 33 (1973) 447-452.

[26] I. Gulcin, Toxicology, 217 (2006) 213-220.

[27] M. Stražišar, S. Andrenšek, A. Šmidovnik, Food Chem, 110 (2008) 636-642.

[28] E. Pino, A.M. Campos, C. Lopez-Alarcon, A. Aspee, E. Lissi, J Phys Org Chem, 19 (2006) 759-764.

[29] S. Honarbakhsh, B. Pourdeyhimi, J Mater Sci, 46 (2011) 2874-2881.

[30] I. Elisia, D.D. Kitts, Mol Cell Biochem, 312 (2008) 139-145.

[31] P. De Santis, A.J. Kovacs, Biopolymers, 6 (1968) 299-306.

[32] W. Hoogsteen, A.R. Postema, A.J. Pennings, G. Tenbrinke, P. Zugenmaier, Macromolecules, 23 (1990) 634-642.

[33] J. Zeng, X. Chen, Q. Liang, X. Xu, X. Jing, Macromol Biosci, 4 (2004) 1118-1125.

[34] J.I. Langford, A.J.C. Wilson, J Appl Crystallogr, 11 (1978) 102-113.

[35] T.Y. Cho, G. Strobl, Polymer, 47 (2006) 1036-1043.

[36] J.R. Sarasua, R.E. Prud'homme, M. Wisniewski, A. Le Borgne, N. Spassky, Macromolecules, 31 (1998) 3895-3905.

[37] J.V. Scudi, W.A. Bastedo, T.J. Webb, J Biol Chem, 136 (1940) 399-406.

[38] J.V. Scudi, J Biol Chem, 139 (1941) 707-720.

[39] M. Gibaldi, S. Feldman, J Pharm Sci, 56 (1967) 1238-1242.

[40] J.G. Wagner, J Pharm Sci, 58 (1969) 1253-1257.

[41] T. Higuchi, J Pharm Sci, 50 (1961) 874-875.

[42] T. Higuchi, J Pharm Sci, 52 (1963) 1145-1149.

[43] R.W. Baker, in, John Wiley & Sons, New York, USA, 1987.

[44] S. Andueza, L. Manzocco, M.P. de Pena, C. Cid, C. Nicoli, Food Res Int, 42 (2009) 51-55.

3.2 Inhibition of Radical-Induced Oxidative DNA Damage by Antioxidants Loaded in Electrospun Polylactide Nanofibers

Polylactide (PLA) nanofibers loaded with antioxidants, i.e. vitamin B_6 or pyridoxine (PN) and its analogue pyridoxal (PL), and with hydroxycinnamic acids, i.e. p-coumaric acid (CUM) and caffeic acid (CAF), were prepared by electrospinning technique. Control consisted of nanofibers loaded with trolox (TRX). Experimentally, these new materials were tested on the inhibition of oxidative DNA damage caused by free radicals initiated by 2,2'-azobis(2-amidinopropane hydrochloride) (AAPH). This damage was assessed in-vitro and in-vivo by measuring the conversion of supercoiled pUC19 plasmid DNA to open circular and linear forms. It was found that these antioxidants, in solution, could inhibit oxidative DNA damage significantly and that the antioxidants loaded in the PLA nanofibers maintained in-vitro and in-vivo their protective role against oxidative DNA damage. Thus, electrospun mats derived from PLA nanofibers loaded with the considered compounds have capacity to protect DNA against to oxidative damage and appear interesting for their use in the purification of plasmidic or genomic DNA.

3.2.1 Introduction

Now there is clear evidence that free radical-induced oxidative damage of cell membranes, DNA and proteins is closely associated with aging and several degenerative diseases,[1, 2] such as cancer,[3] atherosclerosis and cataract.[4] Particularly, the oxidative DNA damage produce diverse lesions such as modifications of the bases and sugar cycles to form first adduct radicals and then strand breaks, which are considered the most significant nuclear lesion. The oxidative damage mainly affects the gene expression,[4] cell cycle regulation,[5] and reparation of DNA.[6] Antioxidants, like α-tocopherol (vitamin E), L-ascorbic acid (vitamin C) and β-carotene, might have beneficial effects on protecting DNA against these diseases. Thus, the supplementation of antioxidants has become an attractive therapeutic strategy for reducing their risk of occurrence.[7-9]

Vitamin B_6 is a water-soluble compound that exists in three major chemical forms: pyridoxine, pyridoxal and pyridoxamine. It performs a wide variety of functions and is essential for good health; e.g., vitamin B_6 is required for more than 100 enzymes involved in proteins metabolism, and for haemoglobin synthesis. A deficiency of this vitamin can result in a type of anaemia. Moreover, animal studies have shown that its deficiency can decrease antibody production and suppress the immune response.[10] Recent research has also revealed that DNA damage from deficiency of micronutrients, including vitamin B_6 and other vitamins, is likely to be a major cause of cancer.[11] Vitamin B_6 has a crucial role in 1-carbon metabolism, which involves DNA synthesis and DNA methylation[12] and can modulate gene expression.[13] Although not classified as an antioxidant compound, pyridoxine and its derivatives have recently been shown to have highly effective antioxidant properties.[14]

Hydroxycinnamic acids (e.g., coumaric and caffeic acids) and their derivatives are frequently considered to be among the most valuable antioxidants in natural products and beverages. The presence of phenolic moieties confers to these compounds their free radical scavenging capabilities. In particular, caffeic acid is one of the most active compounds of the family because of the presence of two vicinal hydroxyl groups. The chemical structure of cinnamic acid derivatives (such as conjugated double bond or number and position of hydroxyl groups in the aromatic ring) was evaluated to ascertain their ability to act as free radical scavengers.[15]

Recent advances in biomaterials are related to the use of scaffolds for drug delivery and tissue engineering.[16, 17] Many groups are exploring the development of biomaterial-biochemical composites incorporating biological agents such as growth factor and other cell regulatory molecules.[16, 18] These efforts are carried out to mimic the natural scaffold that for most tissues is the extracellular matrix (ECM).[19] The ECM has a highly porous morphology with a wide pore size distribution that contributes to rigidity and tensile strength of bone, resilience of cartilage, flexibility and hydrostatic strength of blood vessels, and elasticity of skin.

Different approaches use electrospinning from polymer solutions to fabricate scaffolds with micro structured fibres. Electrospinning occurs when the surface tension force of a polymer solution is overcome by an applied electrical force and tiny droplets or fibres are extruded from the solution. This method produces non-woven membranes with individual fibre diameters typically ranging from nano to micro scale. The fibres form a large and interconnected porous network that is ideal for drug, gene, as well as cell delivery [20].

We have recently prepared polylactide (PLA) nanofibers loaded with pyridoxine and pyridoxal, and polyphenols such as *p*-coumaric and caffeic acids to assess their delivery in several release media and to study the biocompatibility of such biomaterials for cell adhesion and growth.[21] It is also of great interest to extend this research study to other oxidative substrates such as DNA, since DNA is also a major target of free radical attack. We herein examine the effects of antioxidant loaded PLA scaffolds on the inhibition of AAPH-induced oxidative damage of plasmid DNA (in this model, the supercoiled and closed circular plasmid DNA are converted by oxidative damage to open circular and/or linear forms). The present work has three main goals: a) Evaluation of the effect of the selected compounds to inhibit oxidative damage in solution of plasmid DNA; b) Preparation of electrospun nanofiber matrices loaded with antioxidants and evaluation of their ability to inhibit oxidative DNA damage; c) Study of the application of new matrices as support for the purification of DNA subjected to oxidative stress.

3.2.2 Experimental Section

Materials

Pyridoxine (PN), Pyridoxal (PL), Trolox (TRX), 2,2'-Azobis(2-amidinopropane hydrochloride (AAPH), *N*,*N*-dimethylformamide (DMF) and dimethylsulfoxide (DMSO) were purchased from Sigma-Aldrich (Sigma-Aldrich Chemical Co., USA) with the highest purity available and used as received. Caffeic acid (3,4-dihydroxycinnamic acid) (CAF) and *p*-coumaric acid (*p*-hydroxycinnamic acid) (CUM) were purchased from Acros Organics (New Jersey, USA). Polylactide (PLA), a product of Natureworks (polymer 2002D), was kindly supplied by Nupik International (Polinyà, Spain).

Preparation and characterization of electrospun PLA fibers

Unloaded and antioxidant (PN, PL, CAF or CUM) loaded PLA nanofibers were prepared by electrospinning under optimal operational parameters obtained experimentally. To this end, an electrospinable solution were prepared with a 10 and 1 *w*/*v*-% concentration of PLA and antioxidant, respectively; and mixed with a DMF-DMSO 90:10 *v*/*v* mixture. The polymer solution was maintained overnight at 70 ºC to obtain a clear solution. Controls consisting of PLA and PLA loaded with TRX were prepared by the same electrospinning procedure. TRX is the usual antioxidant control due to its high activity. It should be pointed out that TRX is a synthetic analogue derivative of vitamin E which cannot be used for biomedical applications (i.e. no human use). A plastic syringe of 10 mL was filled with the polymer solution and then electrospinning was carried out between the needle (18G) connected to the anode and the static collector connected to the cathode. The direct current (DC voltage) was applied using a high voltage supply (ES30-5W model, Gamma High Voltage Research, USA). The flow was controlled using a KD100 infusion syringe pump (KD Scientific Inc., USA). The polymer jet was collected on an aluminium foil. All electrospinning procedures were conducted at room temperature.

Scanning electron microscopy (SEM, Focus Ion Beam Neon-40, Carl Zeiss, Germany) was used to examine the morphology and surface of the electrospun fibers. Fourier transform infrared (FTIR) spectra were recorded on an ATR-IR spectrometer (FT-IR 4100 Serie, Jasco Inc., USA).

Assay for oxidative DNA strand breaks

The pUC19 plasmid (Invitrogen, USA) was cloned in *Escherichia coli* DH5α used as the competent bacterium (Invitrogen, USA). Bacterial growth was carried out in Luria-Bertani (LB) medium supplemented with 100 $\mu g \cdot mL^{-1}$ ampicillin. Plasmid DNA was purified using a commercial kit (Quiagen, USA).

Induction of DNA strand breaks by AAPH was determined by measuring the conversion of supercoiled pUC19 plasmid DNA to open circular and linear forms.[22] Briefly, 2.7 µg of pUC19

plasmid DNA was incubated at 37 ºC for 90 min using 20 µL of a solution containing 3 µL of 0.9 µg·mL^{-1} stock DNA, 0.5-15 µL of 100 mM AAPH stock, and 2-17 µL of phosphate- buffered saline (PBS, 137 mM NaCl, 2.7 mM KCl, 8.1 mM Na_2HPO_4 and 1.5 mM KH_2PO_4) for complement. The reaction was carried out in microtubes of 200 µL at 37 ºC and 200 rpm for 90 min. Following incubation, the samples were mixed with 4 µL of gel loading buffer and immediately loaded into a 1% agarose gel containing TBE (40 mM Tris, 20 mM sodium borate and 2 mM EDTA), and electrophoresed in a horizontal slab gel apparatus in TBE buffer for 1 h (90 V, constant). After electrophoresis, the gels were photographed under UV light. DNA strand breaks were evaluated using the untreated DNA under the same incubation conditions as a control. The GenoSoft software (VWR, USA) was used to quantify all DNA forms in the gel.

Assay for inhibition of oxidative DNA strand breaks

In the inhibition experiments, the selected antioxidants (i.e. PN, PL, CUM, CAF and TRX) were firstly dissolved in ethanol to 1 M concentration and then the solution was diluted with PBS to get a 100 mM stock. An aliquot (0.5-9 µL) of the antioxidant stock was mixed with 3 µL of 0.9 µg·mL^{-1} of pUC19 plasmid DNA stock, 4 µL of 100 mM AAPH stock, and 4-17 µL of PBS for complement (**Scheme 3.2.I a**). Thus, all incubations had approximately a 20 mM AAPH final concentration. The reaction was carried out at 200 rpm and 37 ºC for 90 min. The products of the reaction were evaluated in agarose gel, as indicated above.

Inhibition of oxidative DNA strand breaks using electrospun PLA scaffolds

Antioxidant-loaded electrospun PLA nanofibers were tested to evaluate their inhibitory activity on oxidative stress induced by AAPH. *In-vitro* assays were performed in 1.5 mL microtubes containing an electrospun sample of c.a. 20 mg (a mat of 1 cm x 1cm x 0.1-0.2 cm), and 3 µL of 0.9 µg·mL^{-1} pUC19 plasmid DNA stock, 50 µL of 100 mM AAPH stock, and 200 µL of PBS. Thus, all incubations had approximately a 20 mM AAPH final concentration. A control test was performed in the absence of AAPH to determine the maximum amount of DNA recovered. A negative and a positive control test were conducted with an unloaded electrospun PLA scaffold and a TRX-loaded electrospun PLA scaffold, respectively. The reaction was carried out at 37 ºC and at 200 rpm for 90 min. The products of the reaction were recovered by centrifugation at 4 ºC and 10000 rpm for 5 min. The scaffolds were washed in 100 µL of PBS and the supernatants were recovered by centrifugation. Supernatants from reaction and wash were mixed (350 µL in total), and the DNA was precipitated by addition of 70 µL of 5 M sodium acetate and 875 µL of pure ethanol at -20 °C for 30 min. The precipitated DNA was recovered as a pellet after centrifugation of the microtube at 13000 rpm for 10 min, and was then washed with 70% ethanol (**Scheme 3.2.I b**). Finally, the DNA was dried under vacuum and evaluated by electrophoresis using agarose gel (1%), as indicated above.

In-vivo assay for inhibition of oxidative DNA strand breaks

Plasmid DNA (pUC19) was cloned in *Escherichia coli* DH5α. A clone of pUC19 plasmid DNA was amplified in LB broth supplemented with ampicillin. 15 mL of cultured bacteria in log phase was pelleted and washed in PBS. Plasmid DNA was purified using a commercial kit (Quiagen, USA), and the antioxidant-loaded PLA scaffold was introduced in two different stages during purification. 1) An electrospun of c.a. 20 mg (a piece of 1 cm x 1 cm x 0.1-0.2 cm) was placed in the micro tube containing the bacterial pellet (**Scheme 3.2.I c**), and 200 µL of resuspension buffer was added to resuspend the pellet. Next, 50 µL of 100 mM AAPH stock was added to induce oxidative damage and the reaction was maintained at 37 ºC and 200 rpm for 2 h. Bacterial lysate and plasmid DNA purification were performed according to the instructions of the kit. 2) The electrospun mat was placed in the purification column before equilibration step according to the manufacturer, and settled on the filter in blend form (**Scheme 3.2.I d**). The neutralized bacterial lysate (600 µL) was subsequently loaded in the column and an aliquot of 150 µL of 100 mM AAPH stock was added to achieve an AAPH concentration of 20 mM. In this stage, the column was maintained at 37 ºC for 2 h. Then, plasmid DNA was bond to the filter in the column by centrifugation. The purification of plasmid DNA was continued according to the manufacturer. Finally, the yield and integrity of purified DNA were evaluated by 1% agarose gel electrophoresis.

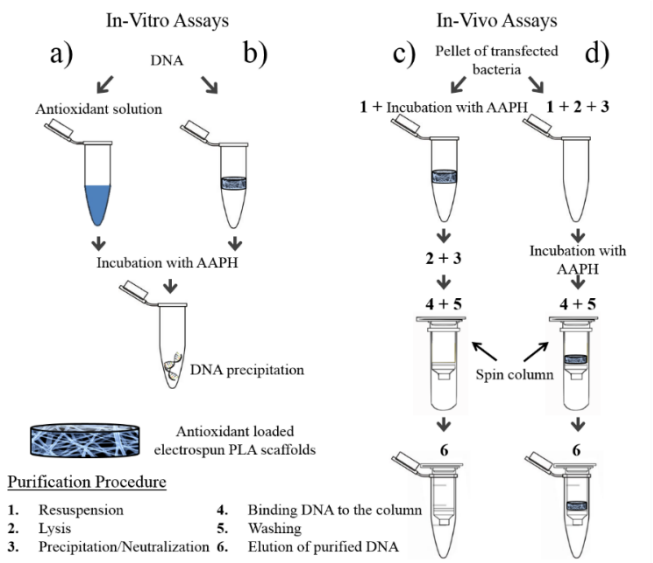

SCHEME 3.2.I

Assay for inhibition of oxidative DNA strand breaks. *In-vitro* assays: (a) using antioxidant solution; and (b) using antioxidant-loaded in electrospun PLA scaffolds. *In-vivo* assays were carried out using transformed *E.coli* DH5α with plasmid DNA: (c) the inhibition was carried out during the bacteria lysis; and (d) the inhibition was carried out during the binding and washing of DNA into the purification filter.

3.2.3 Results and Discussion

Characterization of Antioxidant-Loaded Electrospun PLA

The morphology and diameter of electrospun PLA nanofibers are dependent on several parameters such as solvent characteristics, solution concentration, flow (ϕ), applied voltage (V) and electrospinning distance (h) (i.e. the distance from the tip of the needle to the collector),[23, 24] In addition, incorporation of small percentages of drug in the polymer solution can affect the morphology of electrospun PLA fibres and probably the operational parameters should be modified.[16, 24, 25] **Figure 3.2.1** contains SEM images of the antioxidant-loaded electrospun PLA fiber mats. The fine, continuous morphology and structure of the nanofibers resulted from the optimization of the experimental conditions to avoid undesirable forms of fibers, such as beads on fiber strings, notches and local non-uniformity in the thickness of nanofibers. The best solvent was a mixture of DMF (good solvent for PLA) and DMSO (good solvent for the studied antioxidants) due to the impossibility to find a common solvent for polymer and drugs. The optimal experimental conditions to obtain antioxidant-loaded electrospun PLA nanofibers were similar for all combinations, i.e. values were in the range of 17-19 kV for V, 0.5-1 $mL \cdot h^{-1}$ for ϕ and 12.5 cm for h. **Figure 3.2.1 g** shows that, in all cases, the distribution of fibers was fitted to a Gaussian model. An average diameter of 92 ± 1 nm was determined for unloaded PLA fibers. By contrast, larger diameters were obtained for PLA loaded with PN and PL (101 ± 3 nm and 124 ± 3 nm, respectively). PLA fibers loaded with CUM and CAF had smaller diameters than unloaded PLA fibers (86 ± 2 nm and 81 ± 2 nm, respectively). The diameter of TRX-loaded PLA fibers was the smallest one (63 ± 1 nm).

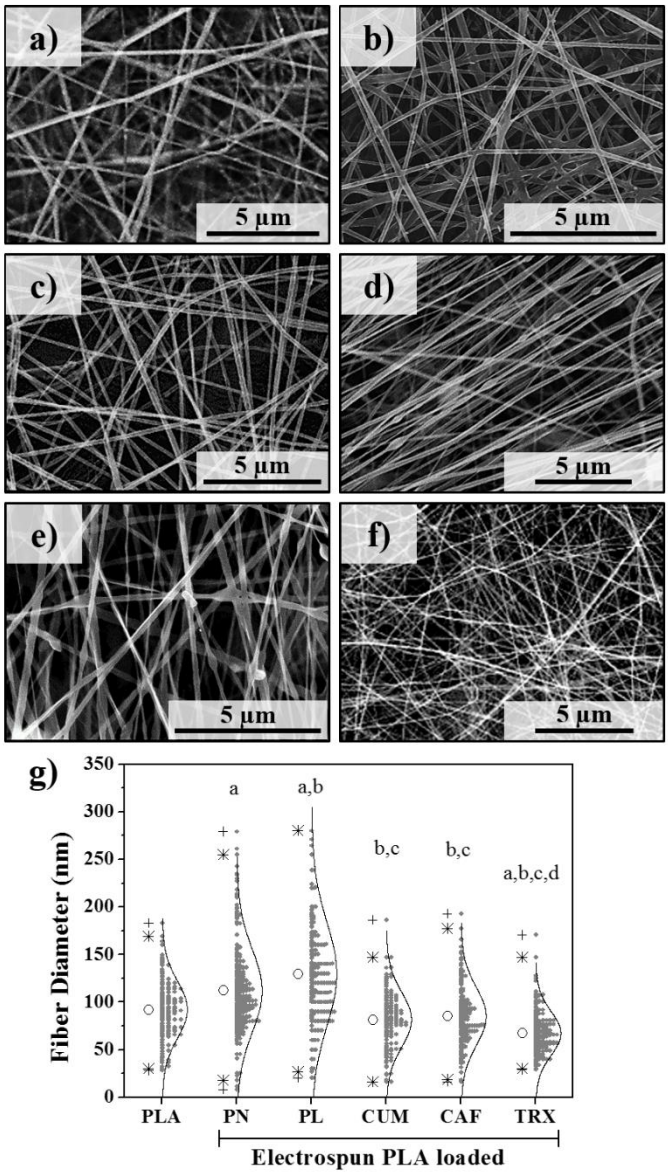

FIGURE 3.2.1

SEM images of electrospun PLA nanofibers unloaded (a) and nanofibers loaded with PN (b), PL (c), CUM (d), CAF (e), and TRX (f). Diameter distribution of the nanofibers (g), the data are plotted in gray circles and fitted to a Gaussian distribution (right). In the chart-box (left), the boxes represent the percentile 25%-75%, the bars represent the range 5%-95%, (*) indicate 1% and 99% of the distribution, and (+) indicate the maximum and minimal values of the data. The letters in the graphic indicate significant differences (Tukey test, $p < 0.05$) in comparison to electrospun PLA (a), and electrospun PLA loaded with PN (b), PL (c), CUM and CAF (d).

The presence of antioxidant molecules in the loaded nanofibers was corroborated by FTIR as shown in **Figure 3.2.2**.

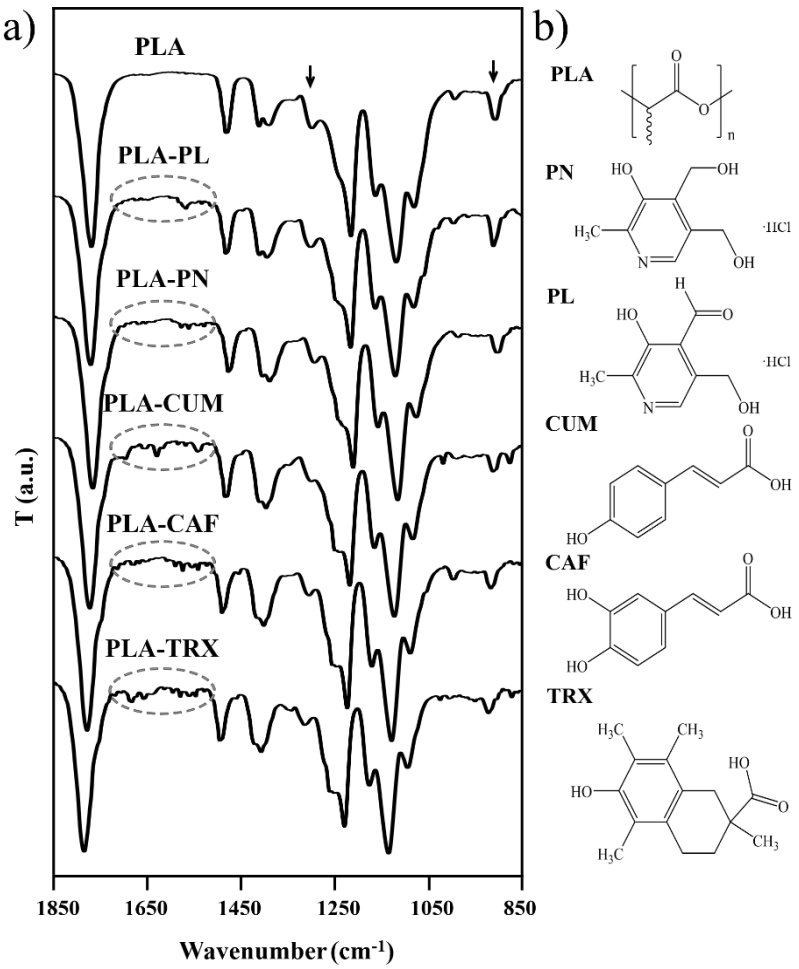

FIGURE 3.2.2

FTIR-ATR spectra of unloaded and antioxidant loaded electrospun PLA scaffolds. The arrows and dotted circle shown representatively spectral changes produced by vitamin B6 (PN and PL), hydroxycinnamic acids (CUM and CAF) and trolox (TRX). (b) Molecular structure of PLA and antioxidants.

The spectra were compared to demonstrate the incorporation of PN and the analogue PL, and al hydroxycinnamic acids in the electrospun PLA nanofibers. In all cases, the typical absorption bands of PLA[26, 27] were observed (i.e. 1759 cm^{-1}, ν(C=O); 1458 cm^{-1}, $\delta_{as}(CH_3)$; 1385 cm^{-1}, $\delta_s(CH_3)$; 1363 cm^{-1}, δ(CH); 1263 cm^{-1}, ν(CH) + ν(C-O-C) for random conformation; 1209 cm^{-1}, ν_{as}(C-O-C) + $r_{as}(CH_3)$ for helical conformation; 1183 cm^{-1}, ν_{as}(C-O-C) + $r_{as}(CH_3)$ for the crystalline phase; and 1128 cm^{-1}, $r_s(CH_3)$; 1082 cm^{-1}, ν_s(C-O-C); 1044 cm^{-1}, $\nu(C\text{-}CH_3)$; 867 cm^{-1}, $r_{as}(CH_3)$ for the amorphous phase) together with small signals associated to the loaded drug.

These were clearer in the 1750-1450 cm^{-1} range where no PLA signals appeared (**Figure 3.2.2 a**), and this is described below. Some differences were also detected in the spectra of the studied samples as a consequence of the different degree of crystallinity and even of the randomness or the helical nature of PLA chains. Thus, bands at 1263 and 867 cm^{-1} appeared with a variable intensity (see arrows in **Figure 3.2.2 a**) and specifically their decrease was associated with a lower proportion of segments with random conformation and a decrease of the amorphous content, respectively.

The FTIR bands for drugs loaded in the PLA nanofiber were identified in the low energy range of the spectra (1750-1450 cm^{-1}), even though their small proportion (9.1 *wt*-% aprox.) with respect to the PLA content. In detail, the PLA-PL spectrum showed characteristic bands at 1679 and 1553, 1538 and 1505 cm^{-1}, assigned the first to the ν(CO) mode for the aldehyde group and the other three to the tautomeric equilibrium between aromatic cycle and aldehyde group. Otherwise, PLA-PN, have the same bands as PLA-PL excepting the bands assigned to the vibration of the aldehyde group.[28, 29] In PLA-CUM spectrum, clearly shows that *p*-coumaric acid is present in PLA nanofiber due to the band of $\nu(CC)_{C=C}$ at 1669 cm^{-1} and the four main aromatic bands $\nu(CC)_{ar}$ located in 1601, 1591, 1512 and 1449 cm^{-1}.[30] The nanofiber PLA-CAF contained some characteristic bands for caffeic acid at 1683 cm^{-1}, ν(CO), 1635 cm^{-1}, ν(CC), and 1617 and 1521 cm^{-1}, $\nu(CC)_{ar}$.[31] Finally, infrared analysis was carried out to determine the structural integrity of the TRX (used as control for antioxidative drugs) loaded in the nanofibers PLA-TRX; two specific bands were recognized at 1718 and 1626 cm^{-1} for ν(CO) of the carboxylic group and ν(CC) of the aromatic ring, respectively.[32]

The PLA electrospun loaded with the antioxidants were characterized by theirs capacity to the antioxidants release. A previous study on the release profiles of antioxidant were carried out by us.[21] Here is important noted that occurs with the antioxidant release during the experiments of DNA protection that are detailed after. **Figure 3.2.3** shows that after 2 hours of incubation in a medium hydrophobic, high amount of antioxidant contained in the matrix was released, but this does not occur when the release medium is hydrophilic.

Here it is important to note that a hydrophilic medium can be transformed into medium hydrophobic by the presence of different biological macromolecules (e.g., amino acids, polypeptides, nucleotides, oligomers, etc.). In this sense, cell extracts can be considered with amphipathic character due to their hydrophilic and hydrophobic components.

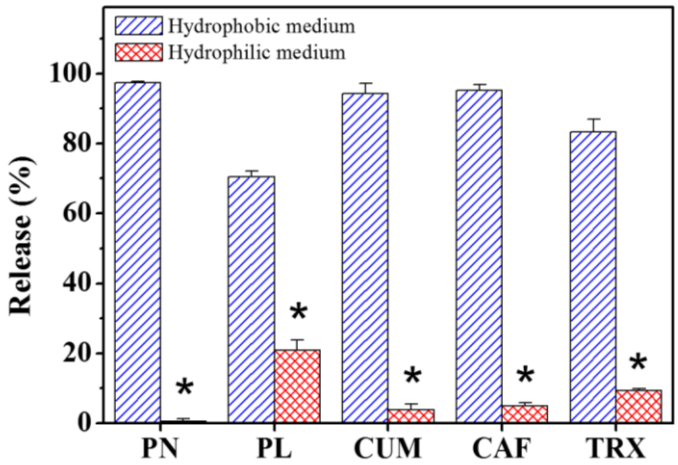

FIGURE 3.2.3

Antioxidant release from five loaded electrospun PLA. The concentration of drug released was measured after 2 hours of incubation in a Sörensen-ethanol buffer mixture (3:7, *v/v*) (hydrophobic medium) and in a TBE buffer (hydrophilic medium). Results are mean ± SE (n = 3). The asterisk (*) indicates $p < 0.05$ between both media.

AAPH-Induced Oxidative Damage of Plasmid DNA

The conversion of supercoiled and closed circular form of plasmid DNA to open circular and further linear forms can be used as a clear indicator of DNA damage. The formation of open circular form of DNA is indicative of single-strand breaks whereas the formation of linear form of DNA is indicative of double-strand breaks (e.g., the *BamHI* restriction enzyme has a single cutting site of both pUC19 DNA strands, resulting in linear DNA).[33, 34] Since AAPH is water-soluble and the rate of free radical generation from AAPH can be easily controlled and measured, this molecule has been extensively used as a free radical initiator for biological studies.[35] Thermal decomposition of AAPH at physiological temperature generates alkyl radicals, which can react with oxygen and produce alkylperoxyl radical (ROO·). This radical can attack plasmid DNA, leading to oxidative DNA damage.[22]

Figure 3.2.4 shows AAPH-induced plasmid DNA strand breaks. It is observed that, at a lower AAPH concentration (2.5-5 mM), the supercoiled DNA band decreases, the open circular DNA band (single DNA chain break) increases and a linear DNA band (double DNA chain break) appears between the supercoiled and the open circular band. At intermediate AAPH concentrations (10-30 mM), the supercoiled DNA band decreases completely and the open circular DNA band decreases gradually, leading to an increase in the linear DNA band. The smear below the linear band suggests the occurrence of multiple breaks in the DNA strands, leading to the formation of low molecular weight fragments. Highly fragmented DNA is predominant when plasmid DNA is treated with high AAPH concentrations (45-75 mM). It can be concluded that the oxidative damage of pUC19 DNA (in general, of plasmid DNA and by

extension of genomic DNA) is concentration-dependent on AAPH, as evidenced by the occurrence of linear DNA (r = 0.93, p > 0.02).

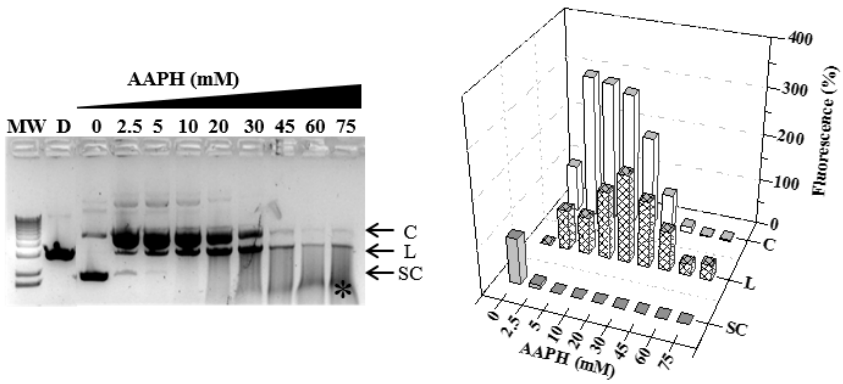

FIGURE 3.2.4

AAPH-induced oxidative damage of plasmid DNA. Electrophoretic pattern of pUC19 DNA after treatment with AAPH in PBS at 37 ºC and pH 7.4 for 90 min. Lane MW: molecular weight marker. Lane D: pUC19 DNA digested with *Bam*HI. The labels C, L and SC correspond to the forms circular, linear and supercoiled of pUC19 plasmid DNA, respectively. The asterisk (*) indicates a severely broken DNA. The 3D-graphic shows the quantification of DNA forms from the electrophoresis.

Inhibition of AAPH-Induced DNA Strand Breaks by Vitamin B_6 and Hydroxycinnamic Acids

Pyridoxal (PL) is a representative analogue of vitamin B_6 or pyridoxine (PN). Studies based on electrochemical and UV-Vis spectroscopy have revealed a supramolecular interaction between DNA nitrogenous bases and PL to form hydrogen bonding.[36, 37] Furthermore, PN and its analogue derivatives enjoy widespread recognition as antioxidant molecules. Thus, we evaluated the ability of PN and PL as scavengers of the free radicals generated by decomposition of AAPH to prevent oxidative DNA damage. As shown in **Figure 3.2.4**, incubation of DNA with 20 mM AAPH for 90 min resulted in complete disappearance of supercoiled DNA, as well as in formation of open circular and linear forms of plasmid DNA. Both single-strand and double-strand DNA breakages seems to take place. The addition of PN and PL at 2.5-45 mM concentration (**Figure 3.2.5 a** and **3.2.5**), respectively) to plasmid DNA attacked with AAPH led to partial or complete inhibition of the conversion of supercoiled DNA to open circular and linear forms. This feature demonstrated that PN and PL are able to protect plasmid DNA against AAPH-induced oxidative damage. The inhibitory concentrations of PN and PL were 10-20 mM and 5-10 mM, respectively. High concentrations of PN and PL not only produced inhibition of oxidative damage, but also promoted the formation of DNA-antioxidant complexes with high molecular weight. These complexes can be understood as aggregates formed by interactions between antioxidants and preferably circular DNA molecules. It is easy to understand that the supercoiled DNA conformation hardly contributes to the formation of these complexes since it

has a highly compact conformation where the nitrogenous bases could be too hidden to establish an effective interaction with PN or PL.[36, 37]

The oxidative activity of AAPH is also inhibited by the presence of *p*-coumaric acid (CUM) and caffeic acid (CAF). The inhibitory concentration was 10-20 mM for both acids (**Figure 3.2.5 c** and **3.2.5 d**), as in the case of vitamin B_6 (PN) and slightly higher than for the PL analogue. High concentration of CUM and CAF leads to the formation of high molecular weight complexes. Moreover, a delay occurs in the mobility of supercoiled and circular DNA bands due to presence of these complexes.

Finally, the activity of trolox (TRX) as the positive control was evaluated (**Figure 3.2.5 e**); TRX is a derivative of vitamin-E and a recognized antioxidant frequently used as control. The inhibitory activity of TRX occurs at the low concentration of 2.5 mM. At high concentrations (20-45 mM) the supercoiled DNA band was relaxed, and the intensity of circular DNA was not changed.[22] Thus, very few DNA-trolox complexes of high molecular weight were formed. These features show that the protective activity of polyphenols against DNA breakage can occur via a specific mechanism which may involve their interaction with DNA bases.

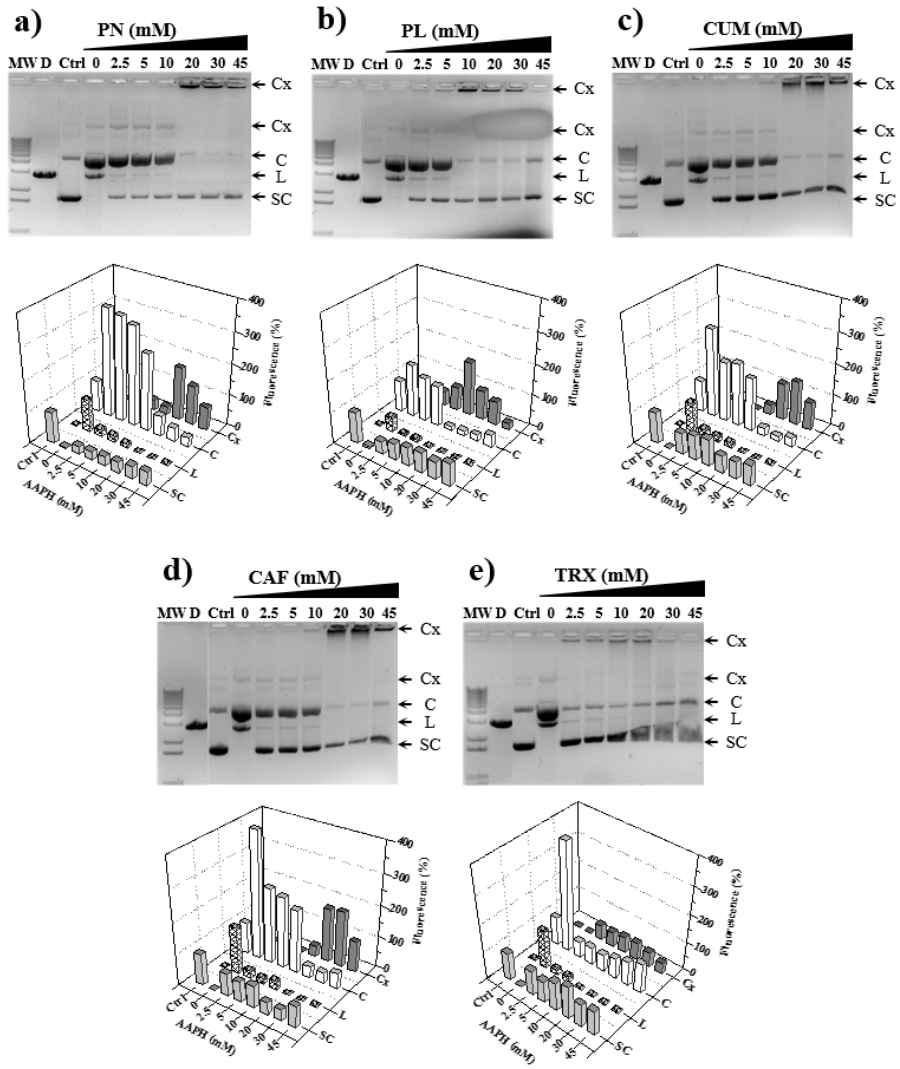

FIGURE 3.2.5

Inhibitory effect of the antioxidants on the AAPH-induced oxidative damage of plasmid DNA. pUC19 DNA strand breaks were induced by 20 mM AAPH in PBS at 37ºC and pH 7.4 for 90 min in the presence of different concentrations of antioxidants: a) PN, b) PL, c) CUM d) CAF, and e) TRX. Agarose gel electrophoretic pattern of plasmid DNA (left) and quantification graphic (right). Lane MW: molecular weight marker. Lane D: pUC19 DNA digested with *Bam*HI. Lane Ctrl: DNA incubated without AAPH and antioxidant (Control).The label Cx corresponds to the formation of DNA-antioxidant complexes.

Inhibition of AAPH-Induced DNA Damage by Antioxidant Loaded Electrospun PLA Nanofiber Mats

Effects on purified DNA

After evaluation of the activity of antioxidants in solution, it was determined whether the electrospun nanofiber loaded with antioxidants can inhibit AAPH-induced oxidative damage of plasmid DNA. AAPH concentration was 20 mM, for all experiments. **Figure 3.2.6** shows that electrospun PLA has no protective effect against this type of damage. This is obvious because supercoiled DNA becomes open-circular and then linear. On the other hand, no significant damage was observed in supercoiled DNA attacked with AAPH in the presence of electrospun PLA scaffolds loaded with PN, PL, CUM and CAF. Moreover, in all cases this was accompanied by an increase in the percentage of circular DNA. However, the absence of the linear DNA band suggests that this increase could correspond to the presence of relaxed DNA. In addition, no complexes of high molecular weight DNA were observed.

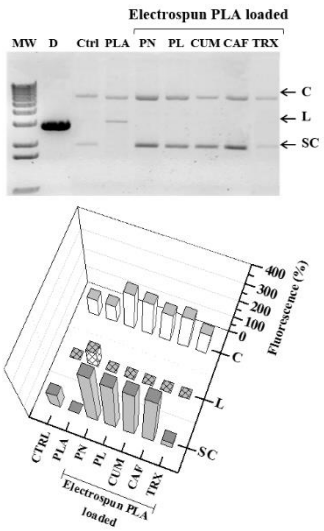

FIGURE 3.2.6

Inhibitory effect of antioxidant-loaded electrospun PLA on pUC19 DNA. pUC19 DNA strand breaks were induced by 20 mM AAPH in PBS at 37ºC and pH 7.4 for 90 min in the presence of electrospun PLA unloaded (lane PLA) and loaded with antioxidants (lane PN, lane PL, lane CUM, lane CAF and lane TRX). After incubation, the DNA was precipitated and running on an agarose gel (above) to evaluate and quantifying (under) the forms of plasmid DNA. Lane MW: molecular weight marker. Lane D: pUC19 DNA digested with *Bam*HI. Lane Ctrl: DNA incubated without AAPH and electrospun.

These results demonstrate that antioxidants loaded in electrospun PLA retain their scavenger function. Furthermore, these fibers avoid an excessive release of antioxidants,[21] preventing the formation of complexes of high molecular weight DNA aggregate. The protective activity of PN, PL, CUM and CAF on DNA is clear because a similar effect was obtained with TRX-loaded electrospun PLA (no band of linear DNA was observed). Furthermore, the protective effect was more effective for the drugs studies. Results would therefore indicate that antioxidant-loaded electrospun PLA is a functional structure capable of protecting *in-vitro* plasmid DNA against oxidative attack.

Effects during Purification of Plasmid DNA from Bacteria

We finally determined the effectiveness of antioxidant-loaded electrospun PLA in two different stages of plasmid DNA purification: 1) The antioxidant-loaded electrospun PLA scaffold was included in the preparation of bacterial lysates for the extraction of plasmid DNA, and 2) antioxidant-loaded electrospun PLA scaffold was settled on the filter in blend form to separate plasmid DNA from other components of the bacterial lysates. In both stages, we included AAPH 20 mM to induce oxidative damage on plasmid DNA (see **Scheme 3.2.I c** and **3.2.I d**).

1) **Figure 3.2.7 a** summarizes the purification results when bacterial lysis was performed in the presence of antioxidant-loaded electro spun PLA (**Scheme 3.2.I c**). It is clear that unloaded electrospun PLA was not efficient in protecting plasmid DNA against AAPH-induced oxidative damage as the linear form of plasmid DNA was observed. By contrast, a significant increase of the circular form of plasmid DNA occurred in presence of antioxidant-loaded electrospun PLA. However, the supercoiled DNA decreases about 50% in comparison to the control (i.e. no AAPH and electrospun PLA). The control based on TRX-loaded electrospun PLA gave similar yields of purified DNA to those obtained with the other antioxidants but the linear form of plasmid DNA was observed, indicating oxidative damage. Thus, it was concluded that TRX inhibits partially AAPH-induced oxidative damage and that the other antioxidants have protective action on plasmid DNA.
2) In the purification column, electrospun PLA was settled on the filter of plasmid DNA binding. Thus, the plasmid DNA bound to the purification matrix was exposed to AAPH to promote oxidative damage. In comparison to the control, the presence of antioxidant-loaded electrospun PLA resulted in a lower percentage of supercoiled DNA and a higher yield of circular DNA (**Figure 3.2.7 b**). The recovery with TRX-loaded electrospun PLA was similar to that of electrospun PLA loaded with PN, PL, CUM and CAF; nonetheless, lineal DNA was only partially recovered.

It is known that oxidative stress is one of the most important causes of many serious diseases, which occurs when the body is exposed to excessive amounts of electrically charged agents, such as aggressive oxygen compounds. By other hand, when the cell tissue is disrupted during DNA purification, genetic material is highly exposed to these aggressive oxygen compounds. The release of the alkylperoxyl radicals (ROO·) from the cell tissue disruption attacks to plasmid

DNA leading to the DNA oxidative damage. Supercoiled DNA can suffer a single strand scissor event to convert supercoiled DNA to open-circular DNA. Progressively, a second strand scissor event converts open-circular DNA into linear DNA.[22]

Finally, the results may justify the addition of antioxidants during DNA purification. Thus, the presence of antioxidants during cell lysate would be a preventive tool against any eventual DNA damage. Furthermore, an effective antioxidant level can be maintained during column binding DNA, preventing the oxidative DNA damage, the loading of these molecules into the nanofibers mats make more powerful this application in existing systems using purification columns.

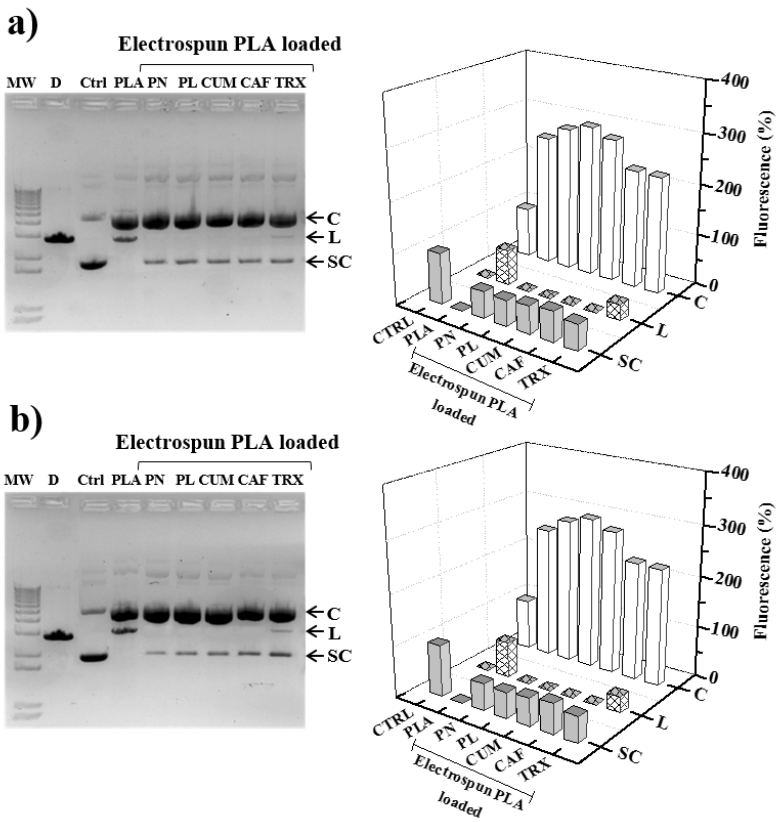

FIGURE 3.2.7

Inhibitory effect of antioxidant-loaded electrospun PLA on pUC19 DNA purified from *Escherichia coli* DH5α. a) The oxidative DNA damage was induced with AAPH: a) in bacteria resuspended, and b) during the binding of DNA to the purification membrane. Electrophoretic pattern of the purified plasmid DNA (left) and theirs quantification (right). Lane MW: molecular weight marker. Lane D: pUC19 DNA digested with *Bam*HI. Lane Ctrl: DNA incubated without AAPH and electrospun.

3.2.4 Conclusions

Electrospun PLA nanofibers loaded with antioxidants, i.e. vitamin B6 or pyridoxine (PN) and its analogue pyridoxal (PL), and hydroxycinnamic acids, i.e. *p*-coumaric acid (CUM) and caffeic acid (CAF) were obtained by electrospinning under conditions optimized for mixtures of PLA in dimethylformamide and antioxidants in DMSO.

AAPH-induced oxidative damage of plasmid DNA can be inhibited *in-vitro* by antioxidants (PN, PL, CUM, and CAF) in solution and by electrospun PLA scaffolds loaded with PN, PL, CUM, and CAF.

Finally, electrospun PLA loaded with PN, PL, CUM or CAF can inhibit oxidative damage of plasmid DNA during purification from bacteria. Thus, *in-vitro* and *in-vivo* results clearly demonstrate the potential application of antioxidant-loaded electrospun PLA to inhibit oxidative damage of plasmid DNA during extraction and purification. This protective activity potentially can also be applied to other macromolecules.

3.2.5 References

[1] T. Finkel, N.J. Holbrook, Nature, 408 (2000) 239-247.

[2] K.J. Barnham, C.L. Masters, A.I. Bush, Nat Rev Drug Discov, 3 (2004) 205-214.

[3] S.P. Hussain, L.J. Hofseth, C.C. Harris, Nat Rev Cancer, 3 (2003) 276-285.

[4] M.S. Cooke, M.D. Evans, M. Dizdaroglu, J. Lunec, Faseb J, 17 (2003) 1195-1214.

[5] J.G. Pizarro, J. Folch, A. Vazquez De la Torre, E. Verdaguer, F. Junyent, J. Jordan, M. Pallas, A. Camins, Free Radical Res, 43 (2009) 985-994.

[6] R.W. Pero, M.W. Anderson, G.A. Doyle, C.H. Anna, F. Romagna, M. Markowitz, C. Bryngelsson, Cancer Res, 50 (1990) 4619-4625.

[7] D.E. Brash, P.A. Havre, P Natl Acad Sci USA, 99 (2002) 13969-13971.

[8] C.A. Rice-Evans, A.T. Diplock, Free Radic Biol Med, 15 (1993) 77-96.

[9] Y.J. Surh, Nat Rev Cancer, 3 (2003) 768-780.

[10] K. Shibata, M. Mushiage, T. Kondo, T. Hayakawa, H. Tsuge, Biosci Biotech Bioch, 59 (1995) 2060-2063.

[11] B.N. Ames, Mutat Res-Fund Mol M, 475 (2001) 7-20.

[12] S.C. Larsson, E. Giovannucci, A. Wolk, Gastroenterology, 128 (2005) 1830-1837.

[13] Y. Natori, T. Oka, Nutr Res, 17 (1997) 1199-1207.

[14] J.M. Matxain, M. Ristila, A. Strid, L.A. Eriksson, J Phys Chem A, 110 (2006) 13068-13072.

[15] E. Pino, A.M. Campos, C. Lopez-Alarcon, A. Aspee, E. Lissi, J Phys Org Chem, 19 (2006) 759-764.

[16] T.J. Sill, H.A. von Recum, Biomaterials, 29 (2008) 1989-2006.

[17] W. Cui, J. Chang, P.D. Dalton, Electrospun Fibers for Drug Delivery, in: Comprehensive Biomaterials, 2011, 445-462.

[18] R.T. Gorsline, P. Tangkawattana, J.J. Lannutti, M. Yamaguchi, C.C. Kaeding, A.L. Bertone, J Biomed Sci Eng, 3 (2010) 908-916.

[19] W.J. Li, C.T. Laurencin, E.J. Caterson, R.S. Tuan, F.K. Ko, J Biomed Mater Res, 60 (2002) 613-621.

[20] Y.K. Luu, K. Kim, B.S. Hsiao, B. Chu, M. Hadjiargyrou, J Control Release, 89 (2003) 341-353.

[21] E. Llorens, L.J. del Valle, A. Diaz, M.T. Casas, J. Puiggali, Macromol Res, 21 (2013) 775-787.

[22] Q.Y. Wei, B. Zhou, Y.J. Cai, L. Yang, Z.L. Liu, Food Chem, 96 (2006) 90-95.

[23] C. Burger, B.S. Hsiao, B. Chu, Annu Rev Mater Res, 36 (2006) 333-368.

[24] L.J. del Valle, R. Camps, A. Diaz, L. Franco, A. Rodriguez-Galan, J. Puiggali, J Polym Res, 18 (2011) 1903-1917.

[25] L.J. del Valle, M. Roa, A. Diaz, M.T. Casas, J. Puiggali, A. Rodriguez-Galan, J Polym Res, 19 (2012).

[26] C. Ribeiro, V. Sencadas, C.M. Costa, J.L.G. Ribelles, S. Lanceros-Mendez, Sci Technol Adv Mat, 12 (2011).

[27] B.D. Kevadiya, G.V. Joshi, H.A. Patel, P.G. Ingole, H.M. Mody, H.C. Bajaj, J Biomater Appl, 25 (2010) 161-177.

[28] F. Bartl, H. Urjasz, B. Brzezinski, J Mol Struct, 441 (1998) 77-81.

[29] J.S. Casas, A. Castineiras, F. Condori, M.D. Couce, U. Russo, A. Sanchez, J. Sordo, J.M. Varela, Polyhedron, 19 (2000) 813-819.

[30] R. Swislocka, M. Kowczyk-Sadowy, M. Kalinowska, W. Lewandowski, Spectrosc-Int J, 27 (2012) 35-48.

[31] Y. Xing, H.Y. Peng, M.X. Zhang, X. Li, W.W. Zeng, X.E. Yang, J Zhejiang Univ Sci B, 13 (2012) 487-493.

[32] L. Gastaldi, E. Ugazio, S. Sapino, P. Iliade, I. Miletto, G. Berlier, Phys Chem Chem Phys, 14 (2012) 11318-11326.

[33] B. Teixeira-Dias, L.J. del Valle, F. Estrany, E. Armelin, R. Oliver, C. Aleman, Eur Polym J, 44 (2008) 3700-3707.

[34] C. Aleman, B. Teixeira-Dias, D. Zanuy, F. Estrany, E. Armelin, L.J. del Valle, Polymer, 50 (2009) 1965-1974.

[35] P. Zhang, S.T. Omaye, Food Chem Toxicol, 39 (2001) 239-246.

[36] S.Q. Liu, M.L. Cao, S.L. Dong, Bioelectrochemistry, 74 (2008) 164-169.

[37] S.Q. Liu, W.H. Sun, L.C. Li, H. Li, X.L. Wang, Int J Electrochem Sc, 7 (2012) 324-337.

4.

Multifunctional biodegradable fiber scaffolds

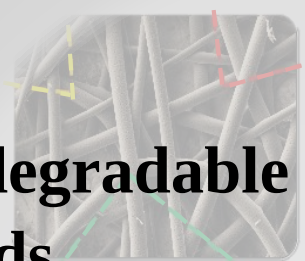

The work described in this chapter previously appeared in:

[1] Llorens, E.; del Valle, L. J.; Puiggalí, J. *Express. Polym. Lett.* Submitted.

[2] Llorens, E.; del Valle, L.; Puiggalí, J. *J. Appl. Polym. Sci.* Submitted.

4.1

Electrospun Scaffolds of Polylactide with a Different Enantiomeric Content and Loaded with Anti-Inflammatory and Antibacterial Drugs

Polylactide (PLA) electrospun microfibers were prepared and loaded with triclosan (TCS), ketoprofen (KTP) or their combination to obtain multifunctional scaffolds with bactericide and anti-inflammatory properties. Continuous and porous fibers with diameters in the micrometer scale and an unimodal distribution were successfully attained using a chloroform:acetone:dimethylsulfoxide mixture capable of effectively dissolving compounds with highly different solubility characteristics such as PLA and the above drugs.

Scaffolds were prepared using two PLA grades having slightly different D-lactide content (i.e. 2 and 4.2 wt-%). It was observed that small differences had a strong influence on physicochemical properties and drug release behavior. Thermal properties of new scaffolds were determined by differential scanning calorimetry and the release evaluated in two media having different hydrophilicity. Dual drug-loaded scaffolds showed a peculiar release that contrasted with single drug-loaded systems and suggested the establishment of intermolecular interactions that delayed TCS and KTP release. Antimicrobial activity of all TCS-loaded electrospun scaffolds was tested and demonstrated against E.coli and M.luteus bacteria. In addition, KTP-loaded samples showed slight bactericide activity. Biocompatibility of scaffolds was evaluated by adhesion and proliferation assays using two epithelial cell lines. Results correlated with drug release observations; interestingly, the dual drug-load systems were able to support high TCS doses without adverse effects.

4.1.1 Introduction

Polylactide (PLA) is currently one of most attractive biodegradable polymers because it is derived from renewable resources, can be easily processed and has many applications ranging from commodity to specialty uses.[1-5] PLA is gaining special attention in the biomedical field. Specifically, devices including degradable sutures, drug releasing micro/nanoparticles, and porous scaffolds for cellular applications can be mentioned.[6-10] The great advantages of PLA are due in part to its ability to degrade into the naturally occurring metabolite lactic acid under physiological conditions, but other exceptional qualities, like biocompatibility, FDA approval for clinical use, low immunogenicity and good mechanical properties must also be considered.

PLA can be obtained by ring-opening polymerization of L-lactide and/or D-lactide, a process that allows obtaining a large number of stereo-copolymers by changing their L/D ratio. Properties of PLA are strongly dependent on its optical purity, for example, PLA can range from semicrystalline to completely amorphous.[11] The degree of crystallinity and even molecular orientation also have a strong influence on PLA biodegradability, specifically, the selection of adequate processing conditions is important to achieve a specific orientation for a given stereoregularity. For example, Lee *et al.* concluded that molecular orientation in amorphous PLA increased with decreasing stretching temperature whereas semycristalline samples required increasing temperatures.[12] It seems that, for amorphous samples, the most important effect concerns the highest orientation when molecular relaxation is hindered by a temperature decrease. For semicrystalline samples, the orientation phenomenon involves the deformation of formed spherulites, and consequently higher temperatures are needed.

Electrospinning is currently one of the simplest methods to draw nano and microfibers from a polymer solution. Basically, the surface tension of a liquid droplet can be counteracted by the electrostatic repulsion due to the charging of the body of the liquid by a sufficiently high voltage. The droplet is stretched and may form a liquid jet if its molecular cohesion is sufficiently high.[13] Scaffolds prepared by electrospinning showed particularly good potential for drug delivery applications due to their large surface area and interconnected pore structure.[14, 15] Moreover, drug release behavior can be easily controlled by the morphology and composition of fibers.[16, 17] Drug-loaded electrospun scaffolds can also be easily fabricated into various shapes (e.g., membranes or tubes) for different applications, such as wound dressing and nerve conduits.[18, 19] To date, most studies of electrospun scaffolds for drug delivery have been focused on sustained release of a single drug. However, it is clear that the use of different drugs is a promising strategy that allows combination therapy and may even induce synergic effects. Studies on dual drug-loaded systems, mainly fibers fabricated by coaxial electrospinning[20] and multilayered electrospun polymer mats,[21] demonstrated different release kinetics from simple systems and/or that the severe initial burst release could be retarded or even negated.

One of the main applications for electrospun scaffolds is its potential use as a matrix for wound healing. The success in wound healing can be handled by the control of various events, such as accelerating tissue regeneration (e.g., by promoting cell proliferation), preventing rejection of

the implanted material (e.g., by improving cell adhesion on the material or by local suppression of the immune cells), or reducing the risk of adverse effects associated with tissue damage (e.g., by preventing infection by opportunistic microorganisms). Thus, the release of two or more different drugs at the proper time and in appropriate doses may be required during treatment for wound healing. For example, post-surgical infection is a common problem after surgical procedures. This requires the release of some drugs, including antibiotics, from the drug-loaded biomaterial in a sustained manner to prevent infections over a short or long period. The rapid release of anti-inflammatory agents and analgesics is also necessary to reduce the cellular immune response and patient's pain, respectively. Thus, it is highly desirable and challenging to develop novel drug delivery carriers that can control the release of multiple drugs with distinct release kinetics.

In the present study, the feasibility of loading active agents of different nature and with diverse therapeutic effects into polylactide fibers is assessed with the aim of developing multifunctional electrospun materials for regenerative medicine applications. A system involving two drugs, triclosan (TCS) as the antibacterial agent and ketoprofen (KTP) as a conventional anti-inflammatory drug, was considered. **Figure 4.1.1** shows the chemical structure of compounds used. Modulation of the therapeutic effect is expected to occur because of the difference in release of these drugs from scaffolds constituted by electrospun fibers. The influence of polymer matrix crystallinity on the release behavior is also determined. To this end, electrospun scaffolds were prepared using PLAs having slightly different ratios between L- and D-lactide units.

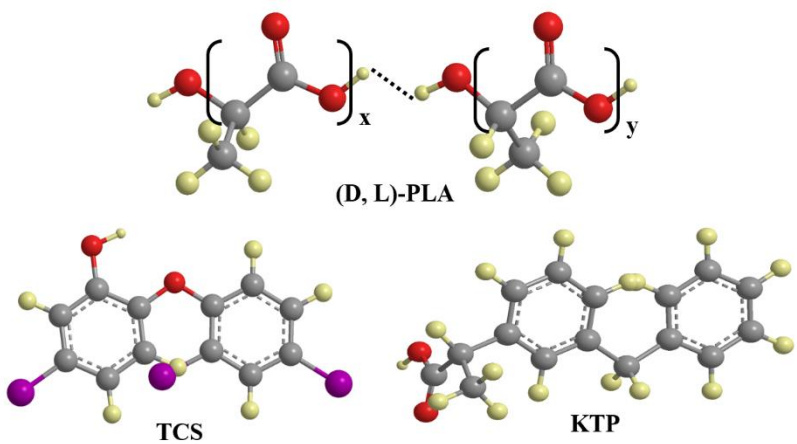

FIGURE 4.1.1

Chemical structures of polylactide (PLA 2002D and PLA 4032D), triclosan (TCS) and ketoprofen (KTP).

4.1.2 Experimental Section

Materials

Two commercial PLA grades from Natureworks® with 95.8 and 98 *wt*-% L-lactic isomer content were used, i.e. PLA 2002D and PLA 4032D, respectively. According to the manufacturer, PLA 2002D is a transparent solid with a density of 1.24 g·cc^{-1}. Its calorimetric and mechanical properties are defined by a glass transition temperature (T_g) of 58 ºC, a melting point (T_m) of 153 ºC, a tensile modulus (E) of 3500 MPa, a tensile strength (σ) of 53-60 MPa and a tensile elongation (γ) of 6%. PLA 4032D has a translucent appearance, a density of 1.24 g·cc^{-1} and very different properties from the sample with higher D-lactide content. Thus, T_g, T_m, E, σ and γ values were reported to be 70 ºC, 160 ºC, 3440-3784 Ma, 103.2-144.5 MPa, 100-180%, respectively. Molecular weights determined by GPC were quite similar, specifically M_n, M_w and polydispersity index were 98,100 g·mol^{-1}, 181,000 g·mol^{-1} and 1.85 for PLA 2002D and 84,200 g·mol^{-1}, 179,400 g·mol^{-1} and 2.13 for PLA 4032D.[22, 23]

Trichloromethane (TCM), acetone, dimethylsulfoxide (DMSO), triclosan or irgasan (TCS), ketoprofen (KTP), 3-(4,5-dimethylthiazol-2-yl)-2,5-diphenyl-2H-tetrazolium bromide (MTT) were purchased from Sigma-Aldrich (St. Louis, USA). VERO (kidney epithelial cells extracted from African green monkey) and MDCK (kidney epithelial cells derived from Madin-Darby Canine) were purchased from ATCC (USA). *Escherichia coli* CECT 101 and Micrococcus luteus CECT 245 bacteria strains were obtained from the Spanish Collection of Type Culture (Valencia, Spain).

Drug loaded PLA electrospun microfibers

Scaffolds constituted by PLA 2002D and PLA 4032D microfibers were prepared by electrospinning, which also allowed loading the two selected drugs (i.e., TCS and KTP). The procedure consisted in dissolving the PLA grade in a chloroform-acetone mixture (2:1 *v*/*v*). For drug-loaded samples, 1 mL of dimethysulfoxide (DMSO) containing the corresponding drug was subsequently added and the mixture was vortexed to obtain an electrospinable solution. Final PLA concentration was 10 *w*/*v*-% whereas for drug loaded samples KTP and TCS concentrations were 1 *w*/*v*-% and 3 *w*/*v*-%, respectively.

A plastic syringe of 5 mL (Becton Dickson, Spain) was filled with the corresponding solution and electrospinning was carried out between the tip of a 18G needle (Terumo, Belgium) connected to the anode and the static collector connected to the cathode. The DC voltage was applied using a high voltage supply (ES30-5W model, Gamma High Voltage Research, USA). The flow rate was controlled using a KD100 infusion syringe pump (KD Scientific Inc., USA). The polymer jet was collected on an aluminum foil and 14 mm diameter coverslips to evaluate cell adhesion and proliferation. All electrospinning procedures were conducted at room temperature.

Morphology and crystallinity of dual drug-loaded PLA microfibers

Diameter measurements and inspection of fiber textures were performed by scanning electron microscopy (SEM) using a Focus Ion Beam Zeiss Neon 40 instrument (Carl Zeiss, Germany). Carbon coating was accomplished with a Mitec K950 Sputter Coater (fitted with a film thickness monitor *k*150x). Samples were viewed at an accelerating voltage of 5 kV.

Calorimetric data were obtained by differential scanning calorimetry (DSC) with a TA Instruments Q100 series equipped with a refrigeration cooling system (RCS). Experiments were conducted under a flow of dry nitrogen with a sample weight of approximately 5 mg and calibration was performed with indium. Heating and cooling runs were carried out at a rate of 20 ºC·min^{-1} and 10 ºC·min^{-1}, respectively.

FTIR spectra were recorded on a FTIR 4100 Jasco spectrophotometer. The samples were placed in an attenuated total reflectance accessory with thermal control and a diamond crystal (Specac model MKII Golden Gate Heated Single Reflection Diamond ATR).

Release experiments

Controlled release experiments were performed with electrospun scaffolds cut into small square pieces (20 x 20 x 0.1 mm^3). The samples were weighed and placed into polypropylene tubes. Two release media with different hydrophobicity and solvent ability were used: a typical phosphate buffer saline or (PBS) and PBS supplemented with 70 *v*/*v*-% of ethanol. The second one was less hydrophilic than PBS and was interesting for simulating the supplement of serum in the medium.[24] Drug-release was carried out in 50 mL of the release medium at 25 ºC for 1 week. Drug concentration in the release medium was evaluated by UV-Vis spectroscopy using a UV-3600 spectrophotometer (Shimadzu, Japan). Calibration curves were obtained by plotting the absorbance measured at the corresponding wavelengths against drug concentration. Samples (1 mL) were drawn from the release medium at predetermined intervals and an equal volume of fresh medium was added to the release vessel. All the drug release tests were carried out using three replicates to control the homogeneity of the release, and the results obtained were averaged.

Antimicrobial test: assay of bacterial growth and adhesion

Escherichia coli (*E.coli*) and *Micrococcus luteus* (*M.luteus*) bacteria were selected to evaluate the antimicrobial effect of TCS and KP loaded electrospun scaffolds. The bacteria were previously grown aerobically to exponential phase in broth culture (5 g·L^{-1} beef extract, 5 g·L^{-1} NaCl, 10 g·L^{-1} peptone, pH 7.2).

Growth experiments were performed in tubes of 15 mL. 10^3 CFU (colony forming units) were seeded in 5 mL of broth culture in the presence of the electrospun scaffolds. The cultures were incubated at 37 ºC and agitated at 80 rpm. After incubation for 24 and 48 h, an aliquot of 100 µL was diluted 10 times with distilled water and the absorbance at 600 nm was measured. The bacterial number was determined using a McFarland curve.

Adhesion experiments were carried out by seeding 10^7-10^8 CFU in 5 mL of broth culture in the presence of the electrospun scaffolds. The cultures were incubated at 37 ºC and agitated at 80 rpm. After incubation, the cultures were aspired and the material washed once with distilled water. Then, 1 mL of sterile 0.01 M sodium thiosulfate was added and the mixture was vortexed for 2 min and left to repose for 30 min in order to remove the bacteria. Finally, 4 mL of broth culture was added and the tubes were incubated at 37 ºC for 24 h and agitated at 80 rpm. The bacterial number was determined as above indicated

All assays were performed in triplicate and the results averaged. ANOVA followed by *t*-Student test were conducted as statistical analysis at a confidence level of 95 % ($p < 0.05$). Additionally, correlation coefficients (r) were calculated to evaluate the relation between antibacterial effect and the drug release.

In-vitro biocompatibility assays: cell adhesion and proliferation

MDCK, and VERO cells were cultured in Dulbecco's modified Eagle medium (DMEM) supplemented with 10% fetal bovine serum, 1% penicillin/streptomycin and 2 mM L-glutamine at 37ºC in a humidified atmosphere with 5% CO_2 and 95% air. The culture medium was changed every two days and, for sub-culture, cell monolayers were rinsed with phosphate buffered saline (PBS) and detached by incubation with trypsin-EDTA (0.25%) at 37ºC for 2-5 min. Cell concentration was determined by counting with a Neubauer chamber using 4% trypan-blue as dye vital. Detached cells with viability ≥ 95% were used for biocompatibility assays.

The unloaded and antioxidant loaded electrospun PLA microfibers were cut into square pieces (10 x 10 x 0.1 mm^3). These samples were placed into the wells of a multi-well culture plate and sterilized by UV-radiation in a laminar flux cabinet for 15 min. To fix the samples in the well, a small drop of silicone (Silbione® MED ADH 4300 RTV, Bluestar Silicones France SAS, Lyon, France) was used as the adhesive. Samples were incubated with 1 mL of the culture medium under culture conditions for 30 min to equilibrate the material. Finally, the medium was aspired and the material was evaluated for cell adhesion and proliferation by exposing cells to direct contact with the material surface.

To assess cell adhesion, aliquots of 50-100 µL containing $5x10^4$ cells were seeded onto the electrospun scaffolds in the wells. The plate was incubated in culture conditions for 30 min to allow cell attachment to the material surface. Then, 1 mL of the culture medium was added to each well and the plate was incubated for 24 h. Finally, cell viability was determined by the MTT assay. Controls were performed by cell culture on the polystyrene surface of the plate (TCPS).

Cell proliferation was evaluated by a similar procedure to the adhesion assay, but the aliquot of 50-100 µL contained $2x10^4$ cells. The cultures were maintained for 7 days to allow cell growth and adequate cell confluence in the well. The media were renewed every two days. Finally, cell viability was determined by the MTT assay.

Each sample was evaluated using five replicates and the results were averaged and graphically represented. The statistical analysis was performed by one-way ANOVA to compare the means of all groups; *t*-Student test was then applied to determine a statistically significant difference between two studied groups. The tests were performed with a confidence level of 95% ($p < 0.05$).

To obtain representative SEM images of samples coming from adhesion and proliferation assays, the following protocol was applied. First, samples were fixed in glutaraldehyde 2.5% in PBS overnight at 4ºC, and then dehydrated by washing in an alcohol battery (30º, 50º, 70º, 90º, 95º and 100º) at 4ºC for a minimum of 30 min per step. Finally, samples were dried and sputter-coated for SEM examination.

4.1.3 Results and Discussion

Morphology of Dual Drug-Loaded PLA Microfibers PLA

Morphology of electrospun fibers depends on both solution properties (e.g., viscosity, surface tension, dielectric constant, volatility and concentration) and operational parameters (e.g., strength of the applied electrical field, tip-collector distance and flow rate).[25-27] Selection of an appropriate solvent system is one of the most crucial points, especially in electrospinning of compounds with highly different characteristics (e.g., polymer and drugs). It should be pointed out that physicochemical properties of the solution can be affected by the incorporation of active drugs and that the system must be accurately chosen to support the load of one or both drugs and render appropriate electrospun fibers.[28]

It was reported that the selection of solvent was also crucial to control the diameter of PLA electrospun fibers. Thus, diameters could be easily varied from 100 nm (i.e., nanometer scale) to 2 µm (i.e. micrometer scale) by using dimethyl formamide and chloroform-acetone (2:1 *v*/*v*) mixture as solvents, respectively, when polymer concentration was kept at 10 *w*/*v*-%.[29, 30] Nevertheless, PLA concentration also played a determinant role because nanofibers could again be obtained when it was lower than 5 *w*/*v*-%.[31]

The above conclusions were taken into account in this study since a micrometer scale was preferred to detect release differences between drugs and from distinct PLA matrices. The main problem was to choose a solvent based on the chloroform-acetone mixture able to dissolve 10 *w*/*v*-% of PLA and the two selected drugs with solubility characteristics different from those of PLA. Note the large difference between Hildebrand parameters reported for PLA[32] (i.e., 9.87 $(cal \cdot cm^{-3})^{0.5}$) and TCS[33] (i.e.,14.38 $(cal \cdot cm^{-3})^{0.5}$). Finally, drugs were dissolved in dimethyl sulfoxide and subsequently added to the former PLA solution to obtain a tricomponent solvent mixture (chloroform:acetone:DMSO 6:3:1 *v*/*v*/*v*) compatible with the selected concentrations of PLA (10 *w*/*v*-%), TCS (3 *w*/*v*-%) and KTP (1 *w*/*v*-%).

Figure 4.1.2 shows the SEM images of the fiber matrices and the corresponding diameter distribution analysis of electrospun fibers prepared under previously optimized operational parameters (i.e. applied voltage, flow rate and tip-collector distance of 15 kV, 10 $mL \cdot h^{-1}$ and 12.5 cm, respectively). A unimodal Gaussian diameter distribution was always determined (insets of **Figure 4.1.2**).

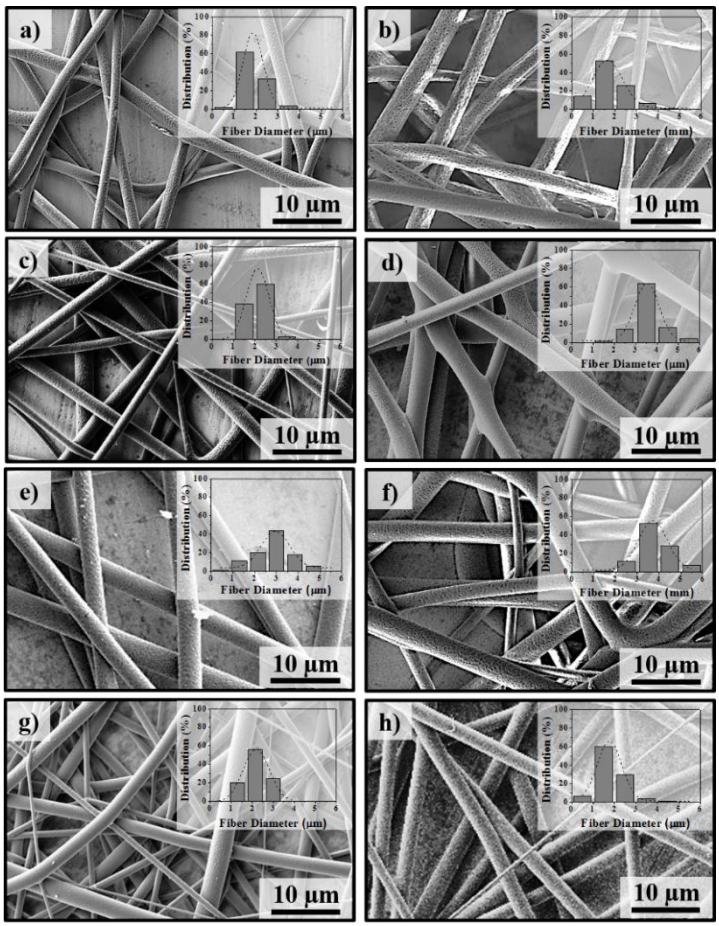

FIGURE 4.1.2

SEM micrographs of unloaded (a,b). triclosan loaded (c,d), ketoprofen loaded (e,f) and dual drug-loaded (g,h) PLA2002D (a,c,e,g) and PLA 4032D (b,d,f,h) electrospun microfibers.

Average diameters determined for all samples are summarized in **Table 4.1.1**. The success of the electrospinning procedure to obtain fibers in the micrometer scale is confirmed in all cases. Differences between unloaded fibers prepared from the two PLA grades were not highly significant (average value of 1.76 µm). However, the incorporation of the drug always led to a diameter increase following the order TCS/KTP < TCS < KTP, with average diameters being 1.98 µm, 2.82 µm and 3.33 µm, respectively. Probably, the physicochemical characteristics of the electrospun solutions were more influenced by the incorporation of bigger KTP molecules (**Figure 4.1.1**). These caused the largest increase on the fiber diameter despite the drug load percentage was the smallest. It should also be pointed out that TCS and KTP drugs caused a significant discrepancy between fiber diameters of samples coming from the two PLA grades, with higher increase being detected for PLA 4032D samples. These changes may reflect a different degree of molecular orientation and even different compactness of the amorphous

phases between the two electrospun polymers. Finally, when the drugs, TCS and KTP, were loaded simultaneously in both PLA samples, diameter values were only slightly higher than those obtained for unloaded fibers. This feature suggests some kind of interaction between TCS and KTP (e.g., hydrogen bonds between hydroxyl and carbonyl groups or stacking between aromatic groups) that could also be favored by higher total drug content with respect to the single drug-loaded systems.

TABLE 4.1.1. Diameters of unloaded and drug loaded electrospun PLA fibers.

Sample	Diameter[a,b] (μm)
PLA 2002D	1.86 ± 0.06
PLA 4032D	1.66 ± 0.05
PLA 2002D + TCS	2.12 ± 0.01
PLA 4032D + TCS	3.53 ± 0.04
PLA 2002D + KTP	2.95 ± 0.02
PLA 4032D + KTP	3.72 ± 0.06
PLA 2002D + TCS/KTP	2.19 ± 0.01
PLA 4032D + TCS/KTP	1.77 ± 0.03

[a]Fibers were obtained using the same electrospinning operational parameters: applied voltage of 15 kV, flow rate of 10 $mL \cdot h^{-1}$ and tip-collector distance of 12.5 cm.
[b]Mean value ± standard deviation.

Figure 4.1.3 shows high-magnification SEM images of the different fibers which reveal a very similar porous texture for all cases.

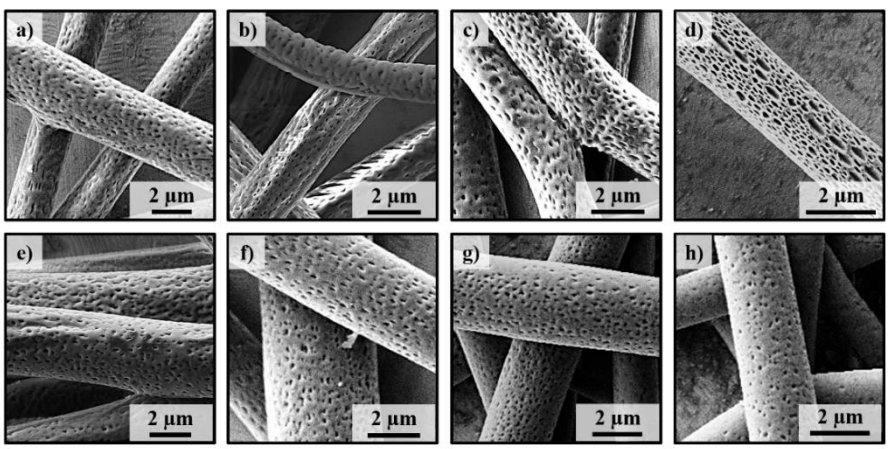

FIGURE 4.1.3

High-magnification SEM micrographs showing the surface texture of unloaded (a,b), triclosan-loaded (c,d), ketoprofen-loaded (e,f) and dual drug-loaded (g,h) PLA 2002D (a,c,e,g) and PLA 4032D (b,d,f,h) electrospun microfibers.

Incorporation of Drugs Into Electrospun Microfibers

FTIR spectra of unloaded and drug-loaded PLA 2002D samples in **Figure 4.1.4** illustrate two interesting points. First, no significant differences exist between typical PLA absorption bands of scaffolds prepared from the two PLA grades or scaffolds loaded with the drugs or their combination. The given spectral region is sensitive to molecular conformation, consequently, it can be concluded that differences between electrospun samples were not large enough to be detected by FTIR. As will be discussed later, although the amorphous content may change slightly with the PLA grade and drug load, it seems that polymer chains attained a similar molecular conformation after the electrospinning process. In fact, processed PLA microfibers were always practically amorphous but a high degree of molecular orientation was induced during electrospinning.[34] Note, for example, that all spectra have similar intensity for the shoulder band at 1209 cm^{-1} (ν_{as}(C-O-C) + $r_{as}(CH_3)$ for a 10_7 helical conformation) and the band at 1263 cm^{-1} (ν(CH) + ν(C-O-C) for a random conformation). Also, the relative proportion between bands at 1385 cm^{-1} ($\delta_s(CH_3)$, amorphous form) and 1363 cm^{-1} (δ(CH), semycrystalline form) became practically invariable.[35]

FTIR spectra were sufficiently sensitive to detect the incorporated drugs despite the relatively low loading percentages. More precisely, TCS was clearly identified in the microfibers through the characteristic peak at 1476 cm^{-1}, attributed to the C=C stretching vibration of benzene rings.[36] However, lesser loaded KTP (i.e. 1 *w/v*-% as opposed to 3 *w/v*-%) could be hardly detected through the strongest peak at 1652 cm^{-1}, attributed to the C=O stretching.[37] Unfortunately, FTIR spectra were not able to detect specific interactions in the dual drug-loaded system due to the low intensity of the involved peaks.

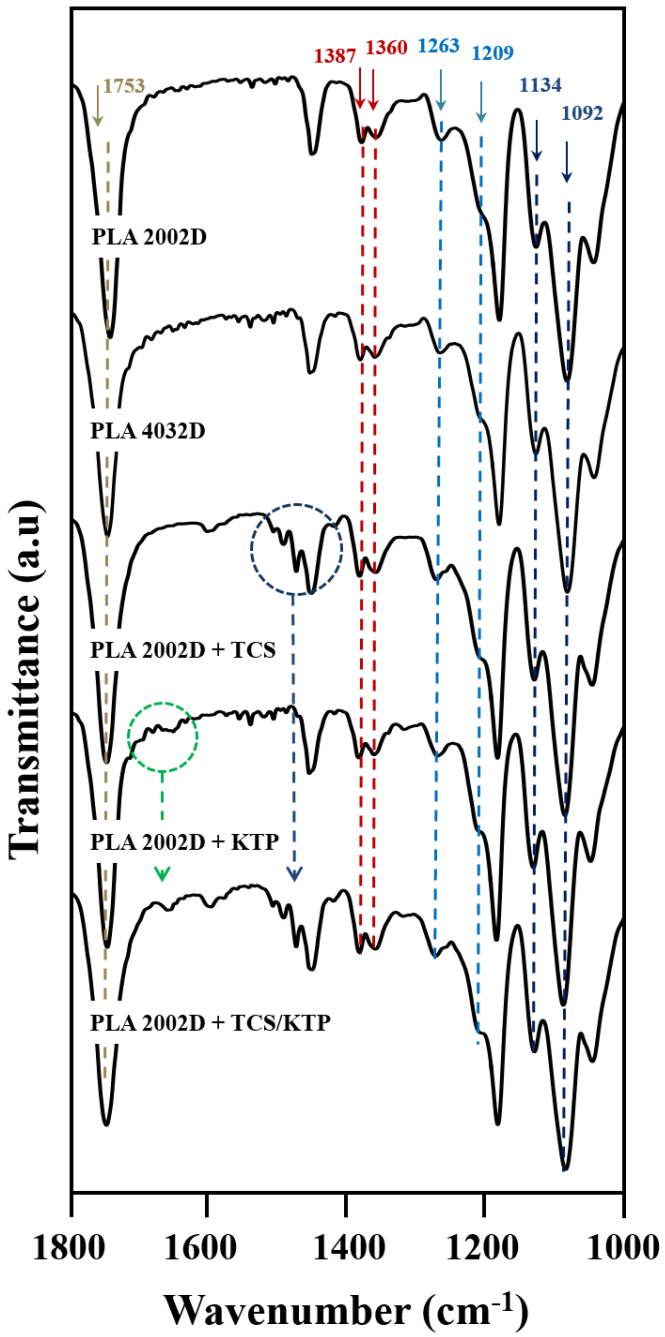

FIGURE 4.1.4

FTIR spectra (1800-1000 cm^{-1} region) of PLA 2002D, PLA 4032D, PLA 2002D + TCS, PLA 2002D + KTP and PLA 2002D +TCS/KTP scaffolds.

Thermal Properties of Unloaded and Drug Loaded PLA Electrospun Scaffolds

Table 4.1.2 summarizes the main calorimetric data obtained from the heating run of unloaded and drug-loaded scaffolds from the two PLA grades, whereas the corresponding DSC traces are shown in **Figure 4.1.5**.

Data corresponding to the two PLA pellets are also given for comparative purposes. It is clear that both samples were manufactured in a semicrystalline form attained after annealing treatment. Values clearly reflect the impact of a small increase of D-lactide content (i.e. from 2 *wt*-% to 4.2 *wt*-%) on both amorphous and crystalline phases, with remarkable changes in glass transition and melting temperatures, respectively. More interestingly, the thermal characteristics of electrospun samples are significantly different from the initial ones. First, both PLA 2002D and PLA 4032D electrospun samples became practically amorphous (degree of crystallinity, X_c, close to 0.07-0.008 as indicated in **Table 4.1.2**) although a remarkable degree of molecular chain orientation could be inferred. Note that cold crystallization peaks can be clearly observed during the heating run of both samples and relatively high degree of crystallinities (i.e. 0.25 and 0.29) could be estimated from the subsequent melting enthalpies. These values were close to those deduced for the corresponding commercial pellet samples and clearly higher than those obtained from the heating run performed with commercial samples after being slowly cooled from the melt state.[29] The high relaxation peak observed for the PLA 4032D electrospun sample, which indicates the great ability of this PLA grade to achieve the equilibrium thermodynamic conditions characterized by higher stiffness and lower enthalpy an volume, is also worth noting. In addition, this close to equilibrium condition led to a fictive glass transition temperature[38] clearly lower than that observed in the initial sample of PLA 4032D (i.e. 62.4 ºC as opposed to 69.3 ºC) and close to those detected for both PLA2002D initial and electrospun samples (59.6 ºC and 59.3 ºC). Cold crystallization took place in a narrow temperature range for PLA 4032D, whereas the use of PLA 2002D involved a wide temperature range suggesting greater difficulty for molecular rearrangement.

TABLE 2. Calorimetric data from the heating scan performed in the electrospun samples prepared with amorphous and crystalline PLA.[a]

Sample	T_m [°C]	ΔCp [J·g^{-1}·°C^{-1}]	T_c [°C]	$\Delta H_c{}^b$ [J·g^{1}]	$T_m{}^c$ [°C]	$\Delta H_m{}^b$ [J·g^{-1}]	ΔH_m - $\Delta H_c{}^b$ [J·g^{-1}]	$\chi_c{}^d$
PLA 2002D[a]	59.6	0.57	-	-	149.3	29.2	29.2	0.28
PLA 2002D	59.3	0.62	106.0	27.0	146.4	26.1	7.6	0.07,0.25
PLA 4032D[a]	69.3	0.23	-	-	167.0	35.0	35.0	0.33
PLA 4032D	62.4	0.55	100.2	22.6	165.9	30.8	8.2	0.08,0.09
PLA 2002D + TCS	41.2	0.53	94.6	8.1	132.6	9.8	1.7	0.02,0.09
PLA 4032D + TCS	39.8	0.50	89.1	22.3	153.9	22.6	0.3	<0.01,0.21
PLA 2002D + KTP	41.3	0.40	78.4	22.8	140.6	23.8	1.0	0.01,0.22
PLA 4032D + KTLP	59.1	0.57	81.5	20.7	160.7	39.5	18.8	0.18,0.37
PLA 2002D + TCS/KTP	51.6	0.47	92.7	13.3	134.1	17.6	4.3	0.04,0.17
PLA 4032D + TCS/KTP	52.6	0.45	109.8	5.0	149.5	23.6	18.6	0.17,0.22

[a]Data obtained from commercial pellet samples.
[b]Values have been rescaled considering the theoretical content of TCS (i.e. 3 *wt*-%) and KTP (i.e. 1 *wt*-%).
[c]Temperature corresponding to the predominant melting peak.
[d]Determined by considering an estimated melting enthalpy of 106 J·g^{-1} for a 100% crystalline sample.[39, 40] Left and right values correspond to crystallinities deduced for the as electrospun material (i.e. considering ΔH_m - $\Delta H_c{}^b$ as the enthalpy associated to crystalline phase of the electrospun sample) and those attained after cold crystallization (i.e. considering ΔH_m as the enthalpy associated to the final crystalline phase), respectively. [e]

Incorporation of drugs had effects on thermal properties that depended on the polymer grade and the drug:

- Incorporation of TCS led to a significant decrease in the melting temperature of the two PLA samples (i.e. close to 13 ºC) suggesting partial incorporation into the crystalline structure. Both loaded samples were practically amorphous after electrospinning but the cold crystallization process was more favorable for the more regular PLA 4032D simple. Final crystallinities were logically lower than those of unloaded samples (i.e. 0.21 as opposed to 0.29 for PLA 4032D and 0.09 as opposed to 0.25 for PLA2002D). TCS also had a plasticizing effect, as suggested by the significant decrease in the glass transition temperature. In addition, the trend to achieve the compact arrangement characteristic of an equilibrium condition was practically supressed for PLA 4032D derived scaffolds since the enthalpy relaxation peak was hardly detected.
- The melting point decrease was less significant (i.e. close to 6 ºC) for scaffolds containing KTP as consequence of their lower drug load. In this case, the most significant feature was the high crystallinity attained after the cold crystallization process, being in the case of PLA 4032 scaffolds, was even greater than for the unloaded sample. It seems that KTP could also act as a nucleating agent, as deduced from the decrease of the cold crystallization temperature and even for the narrower temperature range for the less crystalline PLA 2002D scaffold. Glass transition temperatures and enthalpy relaxation peaks decreased too, suggesting again a plasticizing effect of KTP and greater difficulty in the more compact equilibrium arrangement. Nevertheless, this trend was not completely supressed in the case of PLA 4032D.
- The dual drug-loaded samples showed peculiar DSC traces, which were the result of the effect caused by TCS and KTP. Thus, the decrease in the melting and glass transition temperatures were the highest (12-17 ºC and 25-29 ºC, respectively), enthalpy relaxation was completely suppressed and high crystallinity was attained before (for PLA 4032D sample) and after cold crystallization (for both PLA grades) due to the KTP nucleating effect. The high crystallinity that could again be directly attained in the electrospinning of the PLA 4032D grade in presence of KTP is worth noting. Finally, melting peaks were, in this case, clearly complex due to the presence of crystals with different degrees of perfection (incorporation of impurities or/and different lamellar thicknesses).

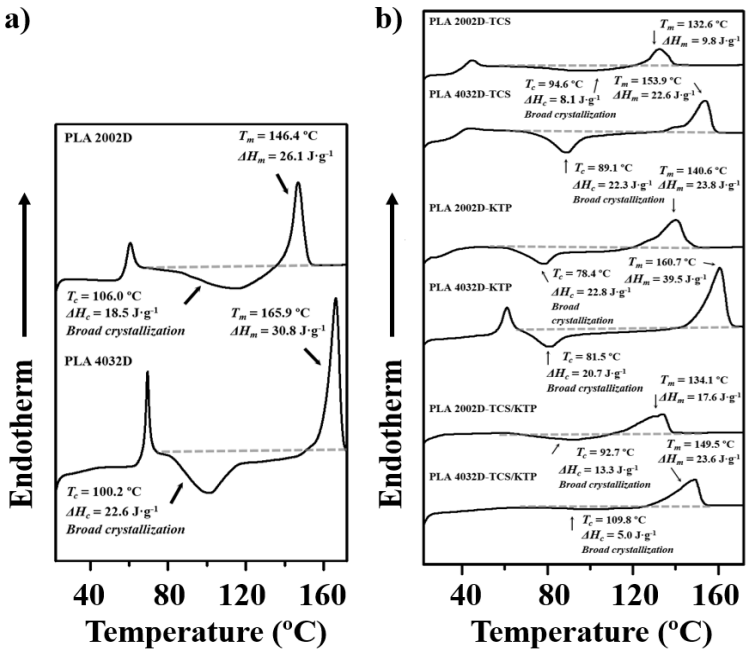

FIGURE 4.1.5

DSC heating runs (20 °C·min^{-1}) of unloaded (a) and drug-loaded (b) PLA 2002D and PLA 4032D electrospun scaffolds.

Drug Release from Scaffolds of PLA with Different D-Lactide Content

A quantitative study was also attempted to follow the release of KTP and TCS from the two different PLA matrices. Release in the less hydrophilic medium containing ethanol (PBS:EtOH 3:7 *v*/*v*) was monitored through the absorbance measurement at 270 and 281 nm for KTP and TCS, respectively, whereas values were measured at 260 and 290 nm for KTP and TCS, respectively, when hydrophilic PBS medium was employed. In all cases, concentrations were evaluated using the coefficient of molecular extinction (ε) calculated for each drug in the corresponding release medium. These values were 7,610 and 6,908 $M^{-1}\cdot cm^{-1}$ for TCS in PBS:EtOH and PBS media, respectively, and 23,604 22,487 $M^{-1}cm^{-1}$ for KTP in PBS:EtOH and PBS media, respectively.

Drug release plots in **Figures 4.1.6** and **4.1.7** highlight differences depending on the PLA grade and logically on the selected medium. In all cases, the release attained a maximum value that mainly depends on the drug equilibrium distribution between the microfibers and the release medium but also on the ability of microfibers to trap the drug efficiently. Hence, the final release percentage was always lower when the more hydrophilic PBS medium was used, in agreement with the hydrophobic character of the drugs and PLA. Furthermore, PLA 2002D microfibers showed the highest release percentages, probably as a consequence of the decrease in trapping

efficiency caused by their lower molecular orientation and less dense molecular arrangement. Thus, for example the release of TCS and KTP from PLA 2002D scaffolds after 8 h of exposure to PBS medium rose 40% and 30%, respectively (**Figure 4.1.6 a**), while these percentages decreased to 30% and 5% for a similar exposure time when PLA 4032D scaffolds were employed (**Figure 4.1.6 c**). A similar trend was observed in PBS:EtOH medium, specifically, the percentages of TCS and KTP release from PLA 2002D scaffolds after 8 h of exposure were, respectively 80% and 60% (**Figure 4.1.7 a**) and from PLA 4032D scaffolds, 50% and 30% , respectively (**Figure 4.1.7 c**). The influence of release medium and type of polymer matrix on drug release was also observed when dual drug-loaded scaffolds were evaluated (**Figures 4.1.6 c, 4.1.6 d, 4.1.7 c** and **4.1.7 d**).

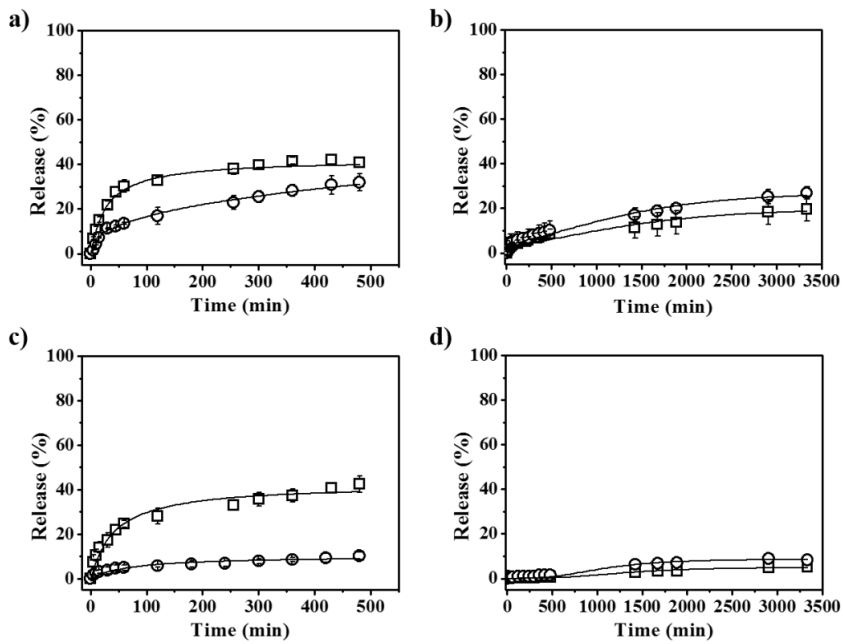

FIGURE 4.1.6

Release curves in PBS medium of TCS (□) and KTP (○) from single drug-loaded (a,c) and dual drug-loaded (b,d) PLA 2002D (a,b) and PLA 4032D (c,d) electrospun scaffolds.

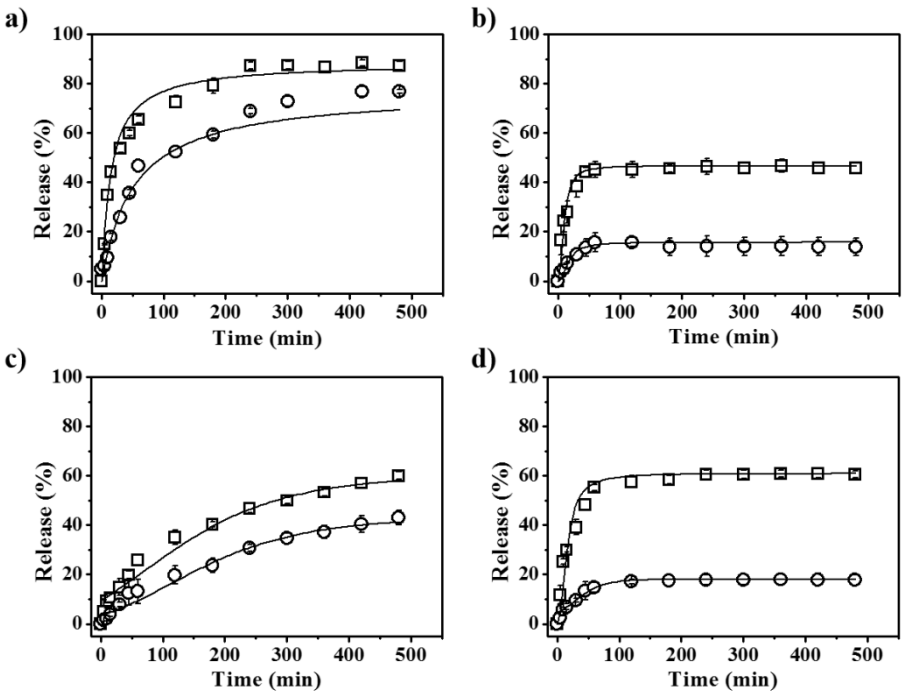

FIGURE 4.1.7

Release curves in PBS:EtOH medium of TCS (□) and KTP (○) from single drug-loaded (a,c) and dual drug-loaded (b,d) PLA 2002D (a,b) and PLA 4032D (c,d) electrospun scaffolds.

An interesting observation about these dual systems is that the release profiles for each drug were different from those determined for single drug-loaded scaffolds. Specifically, a lower release percentage was always found in dual scaffolds. Note that fiber diameters were smaller for these dual systems, and consequently a contrary behavior should be expected if release was only controlled by molecular diffusion. Furthermore, drug release in dual systems seemed to be favored when physicochemical characteristics of the amorphous phase. Thus, decrease of the glass transition temperature or suppression of the aging effect may favour the release. It should be pointed out that crystallinity and molecular orientation seemed too similar in single and dual scaffolds loaded with KTP to justify the large differences found in the corresponding KTP release profiles. Therefore, TCS and KTP molecules should have some kind of intermolecular interactions inside microfibers that change equilibrium distribution or hinder molecular diffusion.

Plots in **Figures 4.1.6** and **4.1.7** also show that release evolves in a gradual manner (i.e. without a significant Burst effect indicative of the presence of drugs deposited on the microfiber surfaces only) until a significant delivery is attained.

In addition to the maximum achievable release, it is also interesting to compare the release rates, which can be easily determined from the experimental results. Several theoretical models have been postulated to fit the experimental release profiles, typically first-order,[41] Higuchi[42] and

their combination.[43] Release generally occurs in two different steps, i.e. a rapid release of molecules that should be deposited mainly on the surface of fibers and a slow release that should involve the diffusion of molecules through the polymer bulk towards the release medium. In this way, a combined model based on the Higuchi and first-order models (**Equations 1** and **2**) is usually used to describe the first (0-60%) and second (40-100%) parts of the release, respectively:

$$M_t/M_0 = k_H\, t^{(1/2)} \qquad (0 \leq M_t/M_0 \leq 0.6) \qquad (\mathbf{1})$$

$$\ln (1 - M_t/M_0) = a - k_1\, t \qquad (0.4 \leq M_t/M_0 \leq 1.0) \qquad (\mathbf{2})$$

where k_H is the Higuchi release constant, k_1 is the first-order release constant, M_t is the percentage of drug released at time t, M_0 is the drug equilibrium percentage (considered as the maximum drug percentage) and a is a constant.

TABLE 4.1.3. Kinetic constants for the first (0-60%) and second part (40-100%) of the TCS and KTP release for selected scaffolds and media.

Sample	Drug	Medium	k_H ($h^{-0.5}$)	k_1 (h^{-1})
PLA 2002D + TCS	TCS	PBS:EtOH	0.78	0.58
PLA 4032D + TCS	TCS	PBS:EtOH	0.35	0.38
PLA 2002D + TCS/KTP	TCS	PBS:EtOH	0.78	0.97
PLA 4032D + TCS/KTP	TCS	PBS:EtOH	0.79	1.10
PLA 2002D + TCS	TCS	PBS	0.47	0.29
PLA 4032D + TCS	TCS	PBS	0.48	1.48
PLA 2002D + TCS/KTP	TCS	PBS	0.15	1.02
PLA 4032D + TCS/KTP	TCS	PBS	0.04	5.61
PLA 2002D + KTP	KTP	PBS:EtOH	0.50	0.39
PLA 4032D + KTP	KTP	PBS:EtOH	0.35	0.40
PLA 2002D + TCS/KTP	KTP	PBS:EtOH	0.25	1.60
PLA 4032D + TCS/KTP	KTP	PBS:EtOH	0.24	1.65
PLA 2002D + KTP	KTP	PBS	0.30	0.37
PLA 4032D + KTP	KTP	PBS	0.10	0.30
PLA 2002D + TCS/KTP	KTP	PBS	0.13	1.26
PLA 4032D + TCS/KTP	KTP	PBS	0.06	2.24

Table 4.1.3 summarizes the values of k_H and k_1 determined for representative scaffolds and release media (i.e. those with a significant release). Basically, the variations of k_1 reflect ability to reach the final equilibrium condition whereas k_H values appear more interesting because they

quantify and allow comparing drugs release speed in the initial phase of delivery. This constant is similar for TCS release in PBH:EtOH medium (0.78-0.79 $h^{-0.5}$) from all scaffolds except from the single-loaded PLA 4032D system, where a slight decrease was detected (0.60 $h^{-0.5}$). This constant clearly decreased (0.29-0.30 $h^{-0.5}$) in PBS medium. Release of KTP proceeded at a slower rate than TCS in both media, with values of 0.22-0.25 $h^{-0.5}$ and 0.10-0.15 $h^{-0.5}$ for PBS:EtOH and PBS media, respectively. The lower rates for each range corresponded to scaffolds prepared from the more regular PLA 4032D matrix. Finally, it is worth mentioning that release of both KTP and TCS proceeded at a very slow rate (0.06 and 0.04 h-0.5, respectively) when dual drug-loaded systems and the more hydrophilic PBS medium were used.

Antibacterial Properties of TCS and KTP Loaded PLA Scaffolds

Antibacterial activity of PLA 2002D and PLA 4032D electrospun scaffolds loaded with TCS and its combination with KTP were tested against *M.luteus* and *E.coli* bacteria (as representative of Gram-positive and Gram-negative bacteria, respectively). It is well known that TCS is a broad-spectrum antiseptic with documented safety and efficacy against both types of bacteria.[44, 45] Basically, TCS blocks the active site of the enol-acyl carrier protein reductase enzyme, which is essential in the synthesis of fatty acids in bacteria.[46]

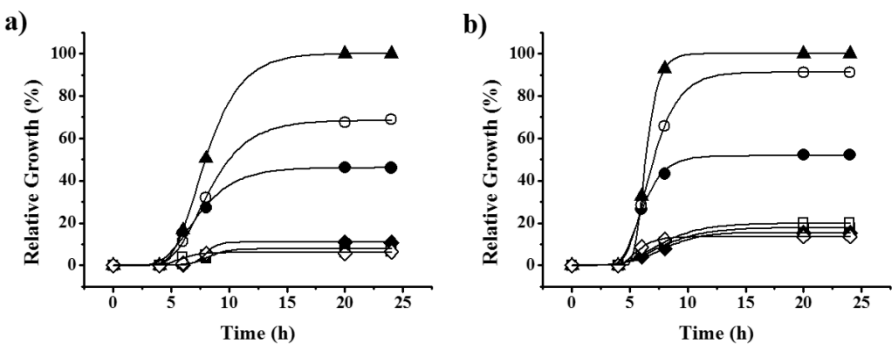

FIGURE 4.1.8

Relative growth of Escherichia coli (a) and Micrococcus luteus (b) on TCS (■,□), KTP (●,○) and TCS/KTP (♦,◊) loaded PLA electrospun scaffolds and polystyrene plate as postive control (▲). Full and empty symbols correspond to PLA 2002D and PLA 4032D samples, respectively.

Bacterial growth curves for *E.coli* and *M.luteus* are shown in **Figures 4.1.8 a** and **4.1.8 b** respectively. An initial lag phase (4-5 hours) followed by an exponential phase associated with binary fission that stopped at growth levels clearly lower than for the positive control is observed. Therefore, for both types of bacteria, the results corroborate that single and dual TCS-loaded scaffolds were active materials for inhibition of bacterial growth. Bacterial growths between 5-10% and 10-20% with respect to the positive control were observed for E. coli and M. luteus, respectively, after 24 hours of culture.

Curves were essentially independent of the polymer matrix, and consequently antibacterial activity was not sensitive to the differences observed in the release experiments. It seems that the high TCS content of scaffolds (i.e. 3 *wt*-%) ensured a sufficient release to inhibit bacterial growth even for matrices with a fairly low release. It is also important to indicate that the incorporation of KTP did not interfere with biological activity of TCS, at least at the assayed concentrations, and made possible the development of multifunctional materials with antibacterial and anti-inflamatory activities.

Interestingly, an intermediate level of inhibition of bacterial growth was also found for scaffolds only loaded with KTP, demonstrating antibacterial activity. In fact, KTP is an active ingredient that inhibits cyclooxygenase, leading to analgesic, anti-inflammatory and antypiretic properties but at the same time it has some bactericide activity through a mechanism that remains unclear.[47, 48] **Figure 4.1.8** clearly shows that the bactericide activity of KTP-loaded scaffolds depended on the selected PLA matrix; specifically, the greatest activity was observed for PLA 2002D. The result is in agreement with the lower crystallinity found for this sample and the higher release compared to the KTP-loaded PLA 4032D scaffold.

Quantification of bacterial adhesion is another checkpoint for the bactericide activity. This activity is demonstrated for all TCS-loaded scaffolds since the percentage of attached bacteria was always statistically lower that than of positive controls, as shown in **Figure 4.1.9**. Nevertheless, the activity was lower against *M.luteus* since Gram-positive bacteria are less sensitive to the effect of triclosan. **Figure 4.1.9** also shows that single KTP-loaded scaffolds were unable to inhibit bacterial adhesion on their surface.

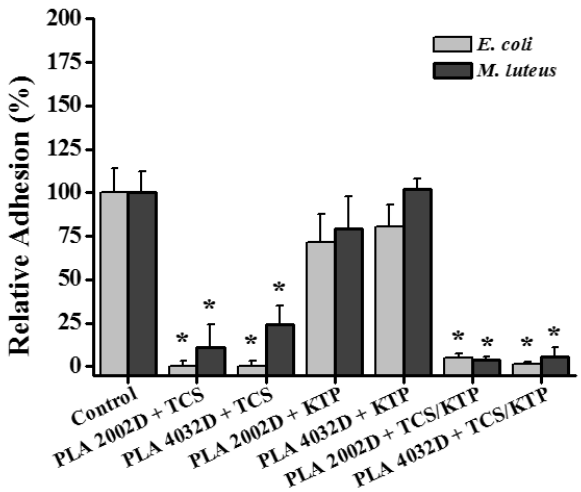

FIGURE 4.1.9

Escherichia coli (light gray) and Micrococcus luteus (dark gray) adhesion on polystyrene plate as positive control and TCS, KTP and TCS/KTP loaded electrospun scaffolds from PLA 2002D and PLA 4032D grades (*p < 0.05 *vs.* control, Tukey's test).

Cell Adhesion and Proliferation on Drug Loaded Scaffolds

Figures 4.1.10 a and **4.1.10 b** show the behavior of two epithelial cell lines (MDCK and VERO) in terms of cell adhesion and proliferation on PLA electrospun scaffolds loaded with TCS and/or KTP. In general, scaffolds allowed adhesion of epithelial cells (**Figure 4.1.10 a**), which is an important event for restarting epithelialization process of a damaged tissue. Nevertheless, a low percentage of cells (18-36% with respect to de control) adhered to the loaded PLA scaffolds. This highly significant difference ($p < 0.001$) was due to the large percentage of loaded TCS (i.e. 3 *w/v*-%), which became cytotoxic to cells in culture.[32] It is remarkable that a large percentage of adhesion was generally observed in dual drug-loaded scaffolds despite having the same TCS content. Only the PLA 2002D scaffold showed a slight significant difference (borderline value with $p < 0.048$). Cytotoxicity can therefore be modulated by incorporating KTP and even by modifying the PLA enantiomer composition. These results are in clear agreement with the release experiments, which indicated a decrease in the amount of delivered TCS when KTP was also incorporated into the microfibers and a higher release when the more amorphous PLA 2002D was employed as a matrix. Finally, a large percentage of cell adhesion was determined for PLA scaffolds loaded with the anti-inflammatory KTP, similarly to the positive control.

Adherent cells kept their proliferative activity and ultimately colonized the material, forming a monolayer tissue. **Figure 4.1.10 b** quantifies cell growth, which was clearly related to the previous cell adhesion event. Thus, the percentage of cells growing on TCS-loaded PLA was still lower than for the positive control (i.e. 42-55%) but the difference was statistically less significant ($p < 0.01$) and relatively moderate. Again, the dual drug-loaded scaffold did not show any statistical difference with respect to the control, and therefore appears to be an appropriate 3D matrix for cell growth.

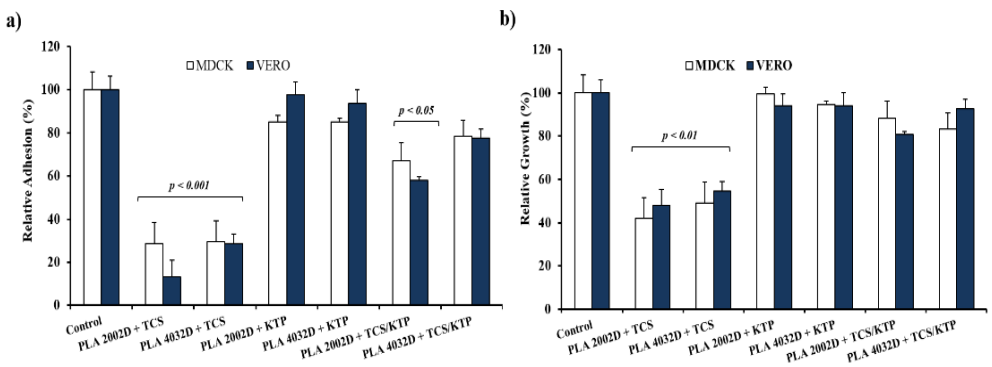

FIGURE 4.1.10

Adhesion (a) and proliferation (b) of MDK (white) and VERO (grey) cells on polystyrene plate as positive control and TCS, KTP and TCS/KTP loaded electrospun scaffolds from PLA 2002D and 4032D grades ($p < 0.001$, $p < 0.01$ and $p < 0.05$ *vs.* positive control, ANOVA-Tukey's test).

4.1.4 Conclusions

Continuous electrospun microfibers of polylactide containing antibacterial and anti-inflammatory agents (i.e. triclosan and ketoprofen) can be successfully prepared using optimized processing parameters and a mixture of chloroform, acetone and dimethylsulfoxide as solvent. Thermal properties of electrospun microfibers were highly dependent on small variation in the D-lactide content of PLA and the incorporation of small ratios of TCS and/or KTP. Specifically, microfibers containing KTP and prepared from the more regular PLA 4032D sample were crystalline as a result of the molecular orientation induced by the electrospinning process and the nucleating effect of the incorporated drug.

Release of TCS and KTP from PLA electrospun scaffolds depended on the hydrophilicity of the media, the stereoregularity of the polymer matrix and the potential establishment of intermolecular interactions in dual drug-loaded scaffolds. In particular, percentages of released drugs and release rates were lower in dual drug-loaded scaffolds than in single systems. All TCS-loaded scaffolds exhibited antibacterial properties independently of the selected PLA grade and the presence of KTP. In addition, KTP-loaded scaffolds also showed bacteriostatic activity, which was more significant at higher D-lactide content of PLA.

Cytotoxicity of TCS-loaded scaffolds could be suppressed and bactericide activity maintained when KTP was also incorporated into the microfibers due to the slower and reduced release from these dual drug-loaded systems.

4.1.5 References

[1] L.T. Lim, R. Auras, M. Rubino, Prog Polym Sci, 33 (2008) 820-852.

[2] O. Wolf, M. Crank, M. Patel, F. Marscheider-Weidemann, EUR No. 22103 EN. European Commission, 2005.

[3] K.M. Nampoothiri, N.R. Nair, R.P. John, Bioresour Technol, 101 (2010) 8493-8501.

[4] R. Auras, B. Harte, S. Selke, Macromol Biosci, 4 (2004) 835-864.

[5] C.J. Weber, V. Haugaard, R. Festersen, G. Bertelsen, Food Addit Contam. 19 (2002) 172–177.

[6] J.J. Conn, R. Oyasu, M. Welsh, J.M. Beal, Am J Surg, 128 (1974) 19-23.

[7] E.E. Schmitt, R.A. Polistina, in: A.C. Co (Ed.), United States, 1967.

[8] C. Burger, K. Kabir, C. Rangger, M. Mueller, T. Minor, R. Tolba, Arch Orthop Trauma Surg, 126 (2006) 695-705.

[9] B. Dhandayuthapani, Y. Yoshida, T. Maekawa, D.S. Kumar, Int J Polym Sci, (2011) 290602.

[10] J. Heller, CRC Crit Rev Ther Drug Carrier Syst, 1 (1984) 39-90.

[11] J.R. Sarasua, A.L. Arraiza, P. Balerdi, I. Maiza, J Mater Sci, 40 (2005) 1855.

[12] J.K. Lee, K.H. Lee, B.S. Jin, Eur Polym J, 37 (2001) 907-914.

[13] Z.W. Ma, M. Kotaki, R. Inai, S. Ramakrishna, Tissue Eng, 11 (2005) 101-109.

[14] J. Zeng, X. Xu, X. Chen, Q. Liang, X. Bian, L. Yang, X. Jing, J Control Release, 92 (2003) 227-231.

[15] W.J. Li, C.T. Laurencin, E.J. Caterson, R.S. Tuan, F.K. Ko, J Biomed Mater Res, 60 (2002) 613-621.

[16] A.M. Piras, F. Chiellini, E. Chiellini, L. Nikkola, N. Ashammakhi, J Bioact Compat Pol, 23 (2008) 423-443.

[17] B. Song, C. Wu, J. Chang, J Biomed Mater Res Part B, 100B (2012) 2178-2186.

[18] Y. Wang, W. Qiao, B. Wang, Y. Zhang, P. Shao, T. Yin, Polym J, 43 (2011) 478-483.

[19] E. Llorens, M.M. Perez-Madrigal, E. Armelin, L.J. del Valle, J. Puiggali, C. Aleman, RSC Adv, 4 (2014) 15245-15255.

[20] T. Okuda, K. Tominaga, S. Kidoaki, J Control Release, 143 (2010) 258-264.

[21] A. Schneider, X.Y. Wang, D.L. Kaplan, J.A. Garlick, C. Egles, Acta Biomater, 5 (2009) 2570-2578.

[22] J. Cailloux, O.O. Santana, E. Franco-Urquiza, J.J. Bou, F. Carrasco, J. Gamez-Perez, M.L. Maspoch, Express Polym Lett, 7 (2013) 304-318.

[23] J. Cailloux, O.O. Santana, E. Franco-Urquiza, J.J. Bou, F. Carrasco, M.L. Maspoch, J Mater Sci, 49 (2014) 4093-4107.

[24] R. Zurita, J. Puiggali, A. Rodriguez-Galan, Macromol Biosci, 6 (2006) 58-69.

[25] D. Li, Y.N. Xia, Adv Mater, 16 (2004) 1151-1170.

[26] S.R. Dhakate, B. Singla, M. Uppal, R.B. Mathur, Adv Mater Lett, 1 (2010) 200-204.

[27] E. Luong-Van, L. Grondahl, K.N. Chua, K.W. Leong, V. Nurcombe, S.M. Cool, Biomaterials, 27 (2006) 2042-2050.

[28] G. Buschle-Diller, J. Cooper, Z. Xie, Y. Wu, J. Waldrup, X.J. Ren, Cellulose, 14 (2007) 553-562.

[29] E. Llorens, L.J. del Valle, A. Diaz, M.T. Casas, J. Puiggali, Macromol Res, 21 (2013) 775-787.

[30] L.J. del Valle, R. Camps, A. Diaz, L. Franco, A. Rodriguez-Galan, J. Puiggali, J Polym Res, 18 (2011) 1903-1917.

[31] L.J. del Valle, A. Diaz, M. Royo, A. Rodriguez-Galan, J. Puiggali, Express Polym Lett, 6 (2012) 266-282.

[32] D. Karst, Y. Yang, J Appl Polym Sci, 96 (2005) 416-422.

[33] D.M. Aragón, D.A. Chiappetta, J. Degrossi, E.F. Vargas, C. Bregni, A. Sosnik, F. Martínez, Rev Colomb Cienc Quím Farm, 37 (2008) 241-257.

[34] J. Zeng, X. Chen, Q. Liang, X. Xu, X. Jing, Macromol Biosci, 4 (2004) 1118-1125.

[35] H. Urayama, S.-I. Moon, Y. Kimura, Macromol Mater Eng, 288 (2003) 137-143.

[36] A. Celebioglu, O.C.O. Umu, T. Tekinay, T. Uyar, Colloid Surface B, 116 (2014) 612-619.

[37] M.L. Vueba, M.E. Pina, F. Veiga, J.J. Sousa, L.A.E.B. de Carvalho, Inter J Pharm, 307 (2006) 56-65.

[38] M.L. Cerrada, G.B. McKenna, Macromolecules, 33 (2000) 3065-3076.

[39] T.Y. Cho, G. Strobl, Polymer, 47 (2006) 1036-1043.

[40] J.R. Sarasua, R.E. Prud'homme, M. Wisniewski, A. Le Borgne, N. Spassky, Macromolecules, 31 (1998) 3895-3905.

[41] J.G. Wagner, J Pharm Sci, 58 (1969) 1253-1257.

[42] T. Higuchi, J Pharm Sci, 52 (1963) 1145-1149.

[43] R.W. Baker, in, John Wiley & Sons, New York, USA, 1987.

[44] H.N. Bhargava, P.A. Leonard, Am J Infect Control, 24 (1996) 209-218.

[45] L.M. McMurry, M. Oethinger, S.B. Levy, Nature, 394 (1998) 531-532.

[46] C.W. Levy, A. Roujeinikova, S. Sedelnikova, A.R. Stuitje, A.R. Salabas, D.W. Rice, J.B. Rafferty, Nature, 398 (1999) 383-384.

[47] S.G. Dastidar, K. Ganguly, K. Chaudhuri, A.N. Chakrabarty, Int J Antimicrob Ag, 14 (2000) 249-251.

[48] H.A. Abbas, F.M. Serry, E.M. El-Masry, Asian J Res Pharm Sci, 2 (2012) 66-72.

4.2 Electrospun Ternary Drug-Loaded Multiactive Scaffolds

Multifunctional electrospun scaffolds were prepared from two PLA grades having slightly different D-lactide content (4.2 wt-% and 2.0 wt-%). Triclosan (TCS), ketoprofen (KTP) and p-coumaric acid (CUM) were selected as bactericide, anti-inflammatory and antioxidant agents, respectively. Single, binary and ternary drug-loaded microfibers having a unimodal diameter distribution could be prepared using a common chloroform:acetone:dimethylsulfoxide mixture and similar operational parameters (i.e., voltage, flow rate and tip-collector distance). FTIR spectra were sensitive to the low amount of drugs loaded and even showed slight differences in PLA conformation. DSC heating scans clearly demonstrated the ability of electrospinning to induce molecular orientation of PLA and also the nucleation effect of incorporated drugs to induce crystallization. Thus, crystallinity of binary drug-loaded scaffolds was significantly higher than observed for unloaded samples.

Release behavior of the three drugs from loaded scaffolds and PLA matrices in PBS:ethanol medium was evaluated. A rapid release was always detected, together with partial drug retention which was higher when the more stereoregular PLA matrix was employed. A strong bactericide effect was found when scaffolds were loaded with 3 wt-% of TCS, but incorporation of when a small percentage of KTP (i.e. 1 wt-%) had a bacteriostatic effect even in the absence of TCS. The inherent cytotoxicity of TCS could be well neutralized by enhancing cell viability by incorporation of CUM and/or KTP.

4.2.1 Introduction

The principle of tissue engineering and regenerative medicine is the application of material scaffolds to develop biomimic and bioinspired materials. These scaffolds can be specifically prepared to display biological activities that induce regeneration of both tissues and organs and restore the function of diseased or traumatized tissues in the human body.[1]

Scaffolds are defined as three-dimensional porous solid biomaterials which should offer a unique combination of inherent properties, such as physical stability within implanted injury site. Besides promoting tissue regeneration, scaffolds have other very important characteristics/functions: (i) capability to favor cell-biomaterial interactions (i.e. cell adhesion and extracellular matrix (ECM) deposition), (ii) enhancement of cell survival (proliferation and differentiation), (iii) compatibility of biodegradation rate with required time for tissue regeneration and (iv) ability to cause minimum inflammation or toxicity *in vivo* resulting from toxic metabolic byproducts.[1] In addition, scaffolds can be used as carriers and/or delivery system of drugs or biomolecules to palliate different stages during replacement and regeneration of tissue or to avoid rejection of implanted biomaterial.

Natural and synthetic polymers have been widely used as biomaterials for medical devices and tissue engineering scaffolds.[2, 3] The most commonly used synthetic polymers in tissue engineering are polylactide (PLA), polyglicolide (PGA) and their copolymers (PLGA).[4] These materials provide synthetic scaffolds characterized by excellent mechanical properties, highly interconnected porous structure, ability to activate their surfaces to yield specific chemical properties, and geometry adapted to direct tissue regeneration.[5]

Different techniques to prepare scaffolds are currently available, but electrospinning is probably one of the simplest processes to obtain porous matrices constituted by fibers in the micrometer or nanometer scales. Furthermore, since fibers can be easily loaded with drugs during their preparation, electrospinning provides the most promising results for tissue engineering, tissue regeneration and drug delivery applications.[6, 7] Specifically, electrospun scaffolds can be used for musculoskeletal tissue engineering include bone and cartilage, and also as control delivery systems for drugs, proteins and DNA.[8] Electrospinning has been widely applied to obtain scaffolds from natural polymers such as collagen,[9] gelatin,[10] chitosan,[11] HA,[12] and silk fibroin,[13] and well as from synthetic polymers like polylactide,[14] polyurethane,[15] polycaprolactone,[16] poly(lactide-co-glicolide),[17] polyvinilalcohol,[18] and poly(lactide-*co*-caprolactone).[5]

Several health problems have been associated with the use of biomaterials, for example infecrion related to the use of catheters[19] or prosthetic bones[20] among others. Other problems concerning damaged tissue, such as inflammation produced by cell necrosis, must be considered, too. Inflammation and oxidative stress are two cellular processes in the tissue that must be treated to restart rapid recovery from tissue injury. In this sense, scaffolds should be designed to be used not only as appropriate platforms to support cell proliferation but also as active elements to mediate cell recovery through local tissue medication.

The goal of this work is the preparation of improved multiactive electrospun scaffolds for regeneration and repair of damaged tissue that are not rejected by the human body and can reduce possible bacterial activity and inflammation during tissue regeneration. To this end, triclosan (TCS), *p*-coumaric acid (CUM) and ketoprofen (KTP) (**Figure 4.2.1**), with antimicrobial, antioxidant, anti-inflammatory activities, respectively, were loaded into two polylactide (PLA) grades having slightly different stereoregularity, and consequently different thermal, degradation and mechanical properties.[21, 22] Scaffold morphology, physicochemical properties, drug release profiles, antimicrobial activity and biocompatibility of scaffolds are presented.

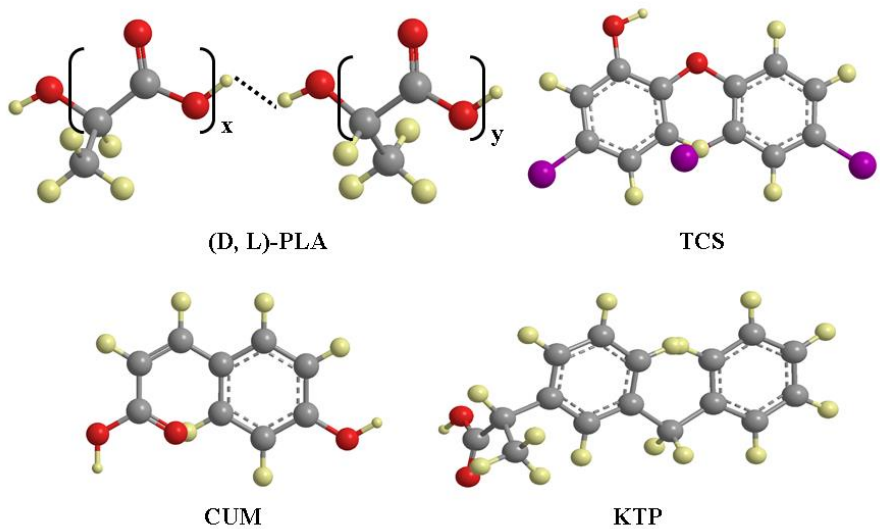

FIGURE 4.2.1

Chemical structures of polylactide (PLA 2002D and PLA 4032D), triclosan (TCS), p-coumaric acid (CUM) and ketoprofen (KTP).

TCS has a well demonstrated antimicrobial activity against both Gram-negative and Gram-positive bacteria. Thus, TCS has been extensively used for topical applications, and its controlled release from biomaterials evaluated.[23, 24] CUM is a hydroxycinnamic acid with recognized activity as scavenger for prevention of oxidative stress damage caused by free radicals.[25, 26] KTP is a non-steroidal anti-inflammatory drug (NSAID) used to control pain and inflammation in rheumatic diseases, as well as inflammation in flogistic diseases.[27, 28]

4.2.2 Experimental Section

Materials

Two commercial PLA grades from Natureworks® with 95.8 and 98 *wt*-% of L-lactic isomer content were used; i.e. PLA 2002D and PLA 4032D, respectively. According to the manufacturer, PLA 2002D is a transparent solid with a density of 1.24 g·cc^{-1}. Its calorimetric and mechanical properties are defined by a glass transition temperature (T_g) of 58 ºC, a melting point (T_m) of 153 ºC, a tensile modulus (E) of 3500 MPa, a tensile strength (σ) of 53-60 MPa and a tensile elongation (γ) of 6%. PLA 4032D has a translucent appearance, a density of 1.24 g·cc^{-1} and highly different properties from those of the sample with higher D content. Thus, T_g, T_m, E, σ and γ values were reported to be 70 ºC, 160 ºC, 3440-3784 Ma, 103.2-144.5 MPa, 100-180%, respectively. Molecular weights determined by GPC were quite similar, and specifically M_n, M_w and polydispersity index were 98,100 g·mol^{-1}, 181,000 g·mol^{-1} and 1.85 for PLA 2002D and 84,200 g·mol^{-1}, 179,400 g·mol^{-1} and 2.13 for PLA 4032D.[21, 22]

Trichloromethane (TCM), acetone (AC), dimethylsulfoxide (DMSO), Triclosan (Irgasan™) (TCS), ketoprofen (KTP) 3-(4,5-dimethylthiazol-2-yl)-2,5-diphenyl-2H-tetrazolium bromide (MTT) were purchased from Sigma-Aldrich (St. Louis, USA) and *p*-coumaric acid (CUM) were purchased from Acros Organics (New Jersey, USA). VERO (African green monkey kidney epithelial cells), MDCK (Madin-Darby canine kidney epithelial cells) were purchased from ATCC (USA).

Preparation of fibers by electrospinning

Both PLA 2002D and PLA 4032D (1 g) were dissolved in 9 mL of a chloroform-acetone mixture (2:1 *v*/*v*). Then, 1 mL of dimethysulfoxide (DMSO) containing the drugs was added and the mixture was homogenized by vortex to obtain an electrospinable solution of 10 *w*/*v*-% PLA, and 3 *w*/*v*-% TCS, 1 *w*/*v*-% KTP and 1 *w*/*v*-% CUM. Furthermore, PLA samples loaded with one single drug and dual-drug combinations (e.g., TCS/CUM and KTP/CUM) were also prepared as controls.

A plastic syringe of 5 mL (Becton Dickson, Spain) was filled with the corresponding PLA drug solution. Electrospinning was carried out between the needle (18G; Terumo, Belgium) connected to the anode and the static collector connected to the cathode. The voltage was applied by a high voltage supply (Gamma High Voltage Research, ES30-5W model). The flow rate was controlled using a KD100 infusion syringe pump (KD Scientific Inc., USA). All electrospinning experiments were conducted at room temperature (aprox. 25ºC).

Morphology and crystallinity of drug loaded PLA nanofibers

Diameter measurements and inspection of fiber surfaces were performed by scanning electron microscopy using a Focus Ion Beam Zeiss Neon 40 instrument (Carl Zeiss, Germany). Carbon coating was accomplished with a Mitec K950 Sputter Coater (dotted with a film thickness monitor *k*150x). Samples were viewed at an accelerating voltage of 5 kV.

Calorimetric data were obtained by differential scanning calorimetry with a TA Instruments Q100 series equipped with a refrigeration cooling system (RCS). Experiments were conducted under a flow of dry nitrogen with a sample weight of approximately 5 mg and calibration was performed with indium. Heating and cooling runs were carried out at a rate of 20 $^{o}C \cdot min^{-1}$ and 10 $^{o}C \cdot min^{-1}$, respectively.

FTIR spectra of CUM, KTP, TCS and unloaded and drug loaded PLA both PLA 4032D and PLA 2002D grades were recorded on a Jasco FTIR 4100 spectrophotometer. Samples were placed on an attenuated total reflection accessory with thermal control and a diamond crystal (Specac MKII Golden Gate Heated Single Reflection Diamond ATR).

Release experiments

Controlled release experiments were performed with electrospun scaffolds cut into small square pieces (20x20x0.1 mm^3). The samples were weighed and placed into polypropylene tubes. A typical phosphate buffer saline (PBS) supplemented with 70 *v*/*v*-% of ethanol was used as the release medium. This medium, which is less hydrophilic than PBS, was interesting to simulate the usual serum supplemented medium.[23] Drug release was carried out in 50 mL of the release medium at 25 ^{o}C for 1 week. Drug concentration in the release medium was evaluated by UV-Vis spectroscopy using a UV-3600 spectrophotometer (Shimadzu, Japan). Calibration curves were obtained by plotting the absorbance measured at the corresponding wavelengths against drug concentration. Samples (1 mL) were drawn from the release medium at predetermined intervals and an equal volume of fresh medium was added to the release vessel. All the drug release tests were carried out using three replicates to control release homogeneity, and the results obtained from the samples were averaged.

Antimicrobial test: assay of bacterial growth and adhesion

Escherichia coli (*E.coli*) and *Micrococcus luteus* (*M.luteus*) were selected as representative of Gram-negative and Gram-positive bacteria, respectively, to evaluate the antimicrobial effect of CUM, TCS/CUM, KTP/CUM and TCS/KTP/CUM loaded electrospun scaffolds. The bacteria were previously grown aerobically to exponential phase in broth culture (5 $g \cdot L^{-1}$ beef extract, 5 $g \cdot L^{-1}$ NaCl, 10 $g \cdot L^{-1}$ peptone, pH 7.2).

Growth experiments were performed in tubes of 15 mL. 10^3 CFU (colony forming units) were seeded in 5 mL of broth culture in the presence of the electrospun scaffolds. The cultures were incubated at 37 ºC and agitated at 80 rpm. After incubation for 24 and 48 h, an aliquot of 100 µL was diluted 10 times with distilled water and absorbance at 600 nm was measured. The bacterial number was determined using a McFarland curve scale.

Adhesion experiments were carried out by seeding 10^7-10^8 CFU in 5 mL of broth culture in the presence of the electrospun scaffolds. The cultures were incubated at 37 ºC and agitated at 80 rpm. After incubation, the cultures were aspired and the material washed once with distilled water. Then, 1 mL of sterile 0.01 M sodium thiosulfate was added and the mixture was vortexed for 2 min and left to repose for 30 min in order for the bacteria to be removed. Finally, 4 mL of broth culture was added and the tubes were incubated at 37 ºC for 24 h and agitated at 80 rpm. The bacterial number was determined as above described.

All assays were performed in triplicate and the results averaged. ANOVA followed by *t*-Student test were conducted as statistical analyses at a confidence level of 95 % ($p < 0.05$). Additionally, correlation coefficients (r) were calculated to evaluate the relation between the antibacterial effect and the drug release.

In-vitro biocompatibility assays: cell adhesion and proliferation

MDCK, and VERO cells were cultured in Dulbecco's modified Eagle Medium (DMEM) supplemented with 10% fetal bovine serum, 1% penicillin/streptomycin and 2 mM L-glutamine at 37ºC in a humidified atmosphere with 5% CO_2 and 95% air. The culture medium was changed every two days and, for sub-culture, cell monolayers were rinsed with phosphate buffered saline (PBS) and detached by incubation with trypsin-EDTA (0.25%) at 37ºC for 2-5 min. Cell concentration was determined by counting with a Neubauer camera using 4% trypan-blue as dye vital. Detached cells with viability ≥ 95% were used for biocompatibility assays.

Unloaded and drug-loaded PLA electrospun microfibers were cut into square pieces (10x10x 0.1 mm^3). These samples were placed into the wells of a multi-well culture plate and sterilized by UV-radiation in a laminar flux cabinet for 15 min. To fix the samples in the well, a small drop of silicone (Silbione® MED ADH 4300 RTV, Bluestar Silicones France SAS, Lyon, France) was used as the adhesive. Samples were incubated in 1 mL of the culture medium under culture conditions for 30 min to equilibrate the material. Finally, the medium was aspired and

the material was evaluated for cell adhesion and proliferation by exposing cells to direct contact with the material surface.

To assess cell adhesion, aliquots of 50-100 µL containing $5x10^4$ cells were seeded onto the electrospun scaffolds placed in the wells. The plate was incubated in culture conditions for 30 min to allow cell attachment to the material surface. Then, 1 mL of the culture medium was added to each well and the plate was incubated for 24 h. Finally, cell viability was determined by the MTT assay. Positive controls were performed on unloaded PLA electrospun scaffolds by cell culture, whereas those loaded with 3 *w/v*-% of TCS were used as negative controls.

Cell proliferation was evaluated by a similar procedure to the adhesion assay, but the aliquot of 50-100 µL contained $2x10^4$ cells. The cultures were maintained for 7 days to allow cell growth and adequate cell confluence in the well. The medium were renewed every two days. Finally, cell viability was determined by the MTT assay.

Each sample was evaluated using five replicates and the results were averaged and graphically represented. The statistical analysis was performed by one-way ANOVA to compare the means of all groups; *t*-Student test was then applied to determine a statistically significant difference between two studied groups. The tests were performed with a confidence level of 95% ($p < 0.05$).

4.2.3 Results and Discussion

Morphology of PLA Multifunctional Electrospun Scaffolds

The success of electrospinning process requires strict control of the operational parameters of each polymer (e.g., strength of the applied electrical field, tip-collector distance and flow rate) and solution properties (e.g., viscosity, surface tension, dielectric constant, volatility, and concentration).[29-31] Selection of an appropriate solvent system is probably one of the most crucial points, especially when compounds of highly different characteristics (e.g., polylactides samples and the above selected drugs) must be electrospun.[32] Note, for example, the large difference between reported Hildebrand parameters for PLA[33] (i.e., 9.87 $(cal \cdot cm^{-3})^{0.5}$) and TCS[34] (i.e., 14.38 $(cal \cdot cm^{-3})^{0.5}$). In addition, a relatively high polymer concentration is required to avoid formation of drops or beads[35] and obtain continuous fibers in a micrometer scale, which appears more appropriate for sustained drug release. These factors made us select a chloroform:acetone:dimethylsulfoxide mixture with a 6:3:1 *v*/*v*/*v* ratio, specifically, the two first solvents were appropriate to obtain PLA electrospun microfibers,[24] whereas the third solvent was essential to allow dissolution of the three selected drugs (TCS, CUM and KTP).

With regard to operational parameters, the selection of the spinning voltage (15 kV) was essential to ensure a stable, conical liquid jet which minimized bead formation. The distance between the target and the syringe tip was kept close to 12.5 cm, and the flow rate was found to be drastically affected by the viscosity of the final solution. Thus, a flow rate of 10 $mL \cdot h^{-1}$ was chosen except when the three drugs dissolved simultaneously. In this case, it was necessary to reduce the flow rate to 5 $mL \cdot h^{-1}$ due to increased viscosity of the final solution.

Figure 4.2.2 shows low magnification SEM images of electrospun fibers obtained under the selected conditions for the different PLA grades and loaded drugs (in particular, single, binary and ternary drug-loaded scaffolds with CUM as a common drug). Analysis of these images revealed that fibers had a unimodal Gaussian diameter distribution (**Figure 4.2.3**) with average diameters between 1.7 µm and 3.8 µm, as summarized in **Table 4.2.1**.

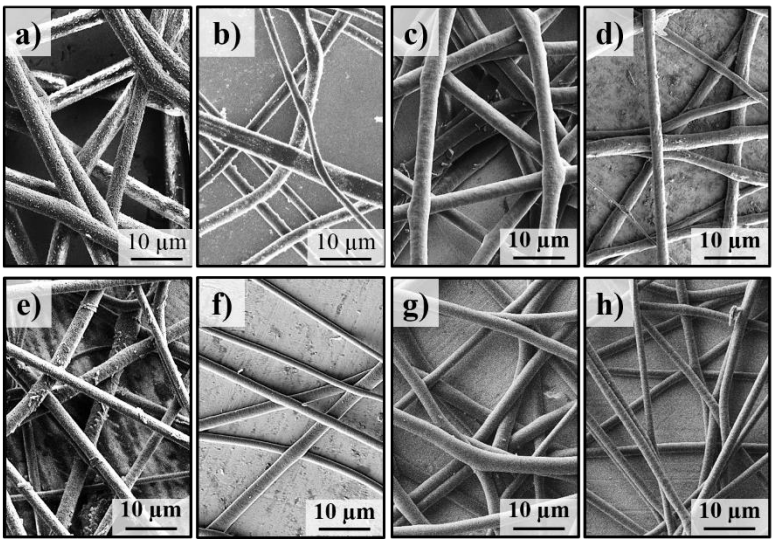

FIGURE 4.2.2

Low magnification SEM micrographs of PLA 2002D + CUM (a), PLA 4032D + CUM (b), PLA 2002D + TCS/CUM (c), PLA 4032D + TCS/CUM (d), PLA 2002D + KTP/CUM (e), PLA 4032D + TCS/CUM (f), PLA 2002D+ TCS/KTP/CUM (g) and PLA 4032D+ TCS/KTP/CUM (h) samples.

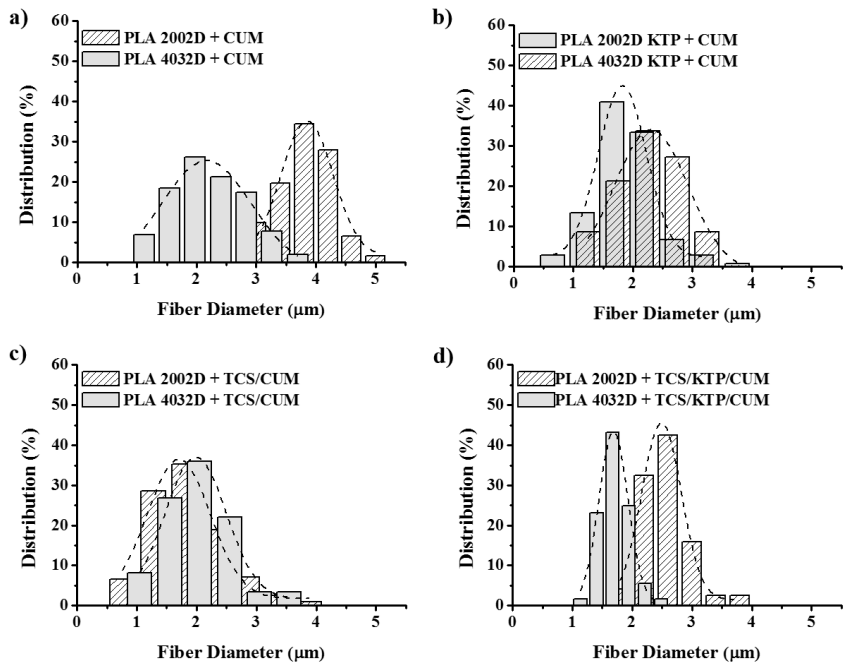

FIGURE 4.2.3

Diameter distribution for electrospun PLA + CUM (a), PLA + KTP/CUM (b), PLA + TCS/CUM (c) and PLA + TCS/KTP/CUM (d) microfibers.

TABLE 4.2.1. Diameters of unloaded and drug loaded electrospun PLA fibers.

Sample	Diameter[a,b] (μm)
PLA 2002D	1.86 ± 0.06
PLA 4032D	1.66 ± 0.05
PLA 2002D + CUM	3.85 ± 0.01
PLA 4032D + CUM	2.14 ± 0.03
PLA 2002D + TCS/CUM	3.23 ± 0.01
PLA 4032D + TCS/CUM	1.92 ± 0.06
PLA 2002D + KTP/CUM	2.28 ± 0.01
PLA 4032D + KTP/CUM	1.82 ± 0.03
PLA 2002D + TCS/KTP/CUM	2.54 ± 0.01
PLA 4032D + TCS/KTP/CUM	1.70 ± 0.01

[a]Fibers were obtained using the following electrospinning operational parameters: applied voltage of 15 kV, tip-collector distance of 12.5 cm and flow rate of 10 $mL \cdot h^{-1}$ except for ternary drug-loaded fiber that decreased to 5 $mL \cdot h^{-1}$.
[b]Mean value ± standard deviation.

The observed variations in the diameter size can be summarized as follows: a) Microfibers prepared from the more stereoregular PLA 4032D sample always had smaller diameters than determined for PLA 2002D compared to fibers with a similar drug load, b) incorporation of CUM gave rise to a significant diameter increase (e.g., from 1.93 to 3.80 mm and from 1.79 to 2.26 μm for single drug-loaded PLA2002D and PLA 4032D samples, respectively), which seems more significant when the more amorphous PLA grade was employed. c) binary drug-loaded samples showed a diameter decrease compared to single drug-loaded fibers, with the effect being less pronounced upon addition of TCS. Note, however, that the percentage of loaded TCS was higher than that of KTP (i.e. 3 *w/v*-% respect to 1 *w/v*-%) and d) the diameter of ternary drug-loaded samples increased compared to unloaded samples, as above indicated, but the trend was not clear since flow rate conditions were changed. In summary, the presence of drugs modified the physicochemical characteristics of the dissolution (e.g., viscosity was seriously affected for ternary TCS/KTP/CUM loaded mixtures in such a way that the flow rate had to be modified) and influenced the morphology of electrospun samples significantly even when processed under the same set of operational parameters.

Texture of microfibers was slightly different depending on the loaded drugs, as shown in the high magnification SEM micrographs of **Figure 4.2.4**. In general, microfibers had a porous structure, as is also commonly observed in unloaded PLA electrospun fibers.[35] The presence of longitudinal striations was also usual in most samples (**Figure 4.2.4**, see red arrows). Surfaces became smoother when TCS was loaded since pores were less defined in the ternary drug-loaded systems (**Figures 4.2.4 g** and **4.2.4 h**) and even difficult to detect in the binary drug-loaded fibers (**Figure 4.2.4 c** and **4.2.4 d**). CUM loaded samples were also characterized by the presence of embedded crystals (withe arrows), which highlighted the difficulty of *p*-coumaric molecules to mix with the PLA matrix. Nevertheless, these crystals were hardly detected in the ternary drug-loaded systems although their fiber usually had the lowest diameter values. This may be an indication of improved mixing with PLA in the presence of the other two drugs (TCS and KTP).

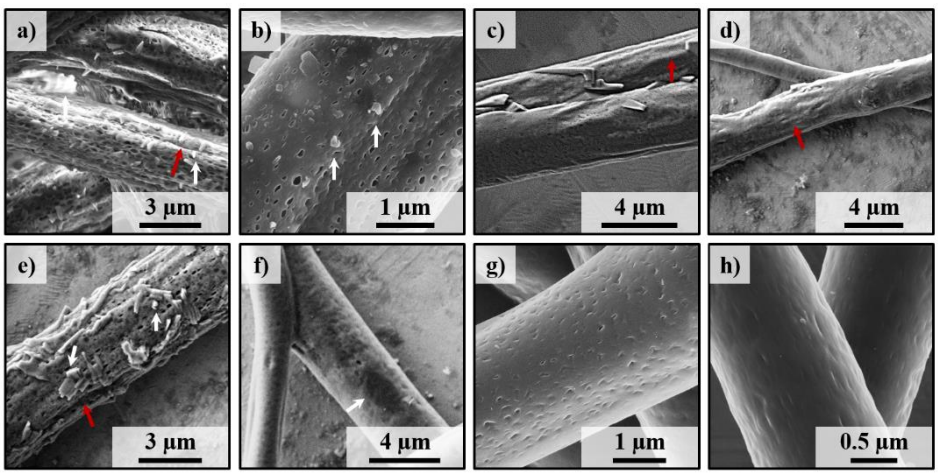

FIGURE 4.2.4

High magnification SEM micrographs of PLA 2002D + CUM (a), PLA 4032D + CUM (b), PLA 2002D + TCS/CUM (c), PLA 4032D + TCS/CUM (d), PLA 2002D + KTP/CUM (e), PLA 4032D + TCS/CUM (f), PLA 2002D+ TCS/KTP/CUM (g) and PLA 4032D+ TCS/KTP/CUM (h) samples. Red arrows pointed out longitudinal striations wheres CUM crystals are indicated by withe arrows.

FTIR Analysis of Electrospun Drug Loaded Samples

PLA is a semicrystalline polymer that exhibits polymorphism, with different crystalline arrangements depending on the crystallization conditions having been described.[26] Usually, the polymer crystallizes in a 10_7 helical conformation that gives rise to the so-called α-,[36-38] α'-[39] and α''-[40] forms and the ε-crystals[41] when the polymer is complexed with solvents like dimethylformamide. Furthermore, PLA can adopt a 3_2 molecular conformation, as reported for β[42,43] and γ[44] structures prepared by stretching or by epitaxial crystallization. Nevertheless,

PLA hardly crystallizes under usual processing conditions, and therefore no crystallization peaks are usually observed in DSC cooling traces from the melt or even during a subsequent heating run. Thus, commercial semicrystalline samples are obtained after subjecting samples to an annealing process which favors crystallization. It has been reported that the electrospinning technique facilitates molecular orientation, hence, the derived microfibers can be easily cold crystallized during a subsequent heating run. This final molecular orientation should depend on solution properties like viscosity, operational parameters (e.g., flow rate and applied voltage), diameter of electrospun fibers and even the presence of drugs that could act as nucleating agents.[24]

FTIR spectroscopy can give information on molecular conformation and crystallinity although interpretation is difficult for PLA due to its different molecular conformations and packing arrangements. Nevertheless, several observation can made: a) The absorbance of the carbonyl band around 1753 cm^{-1} has a smaller correlation with conformational changes of the main chain. Hence, this band can be used as the reference band to correct absorbance fluctuations due to differences in scaffold thickness,[45] b) comparison between absorbance of bands at 1263 cm^{-1} (ν(CH) + ν(C-O-C) for a random conformation) and 1209 cm^{-1} (ν_{as} (C-O-C) + $r_{as}(CH_3)$ for a 10_7 helical conformation) has been reported to be highly relevant because bands should decrease and increase, respectively, when molecules adopt the more ordered helical conformation,[46] c) relative intensities between bands at 1385 cm^{-1} ($\delta_s(CH_3)$, amorphous form) and 1363 cm^{-1} (δ (CH), semycrystalline form) and bands at 1134 cm^{-1} ($r_s(CH_3)$) and 1092 cm^{-1} (ν_{as}(C–O–C)) changed upon annealing of samples (i.e. when crystallinity increased). Specifically, the relative intensity of bands at 1363 cm^{-1} and 1134 cm^{-1} was increased[47] and d) the 921 cm^{-1} absorption band is characteristic of the α-form and corresponds to the coupling of C-C backbone with CH_3 rocking.[48]

Figure 4.2.5 compares the FTIR spectra (1800-900 cm^{-1}) of the two PLA electrospun samples and the PLA 4032D sample loaded with the different combinations of drugs. No significant differences (not shown) were detected between spectra of samples from the two PLA matrices independently of the loaded drugs. Therefore, the difference in stereoregularity (i.e. from 2 to 4.2 *wt*-% of D-lactide) was smaller than spectral sensitivity to chain randomness. On the contrary, spectra of both PLA 2002D (not shown) and 4032D samples showed significant changes with respect to the above indicated b-d points which clearly suggested an increase of crystallinity and the ratio of the 10_7 helical conformation when, for example, PLA 2002D fibers were simultaneously loaded with different drugs (i.e. a decrease of 1263 cm^{-1} band and an increase of 1363. 1209, 1134 and 921 cm^{-1} bands were observed for all loaded samples except the single CUM loaded sample).

FTIR spectrum was sufficiently sensitive to detect the presence of drugs despite the low amount loaded. Basically, multiple peaks were observed in the 1670-1470 cm^{-1} range where bands associated to carbonyl groups and aromatic rings should appear. These rings were common for the three loaded drugs (**Figure 4.2.1**) and consequently additional signals detected in the spectra of drug-loaded scaffolds were always quite similar (i.e. circles in **Figure 4.2.5**).

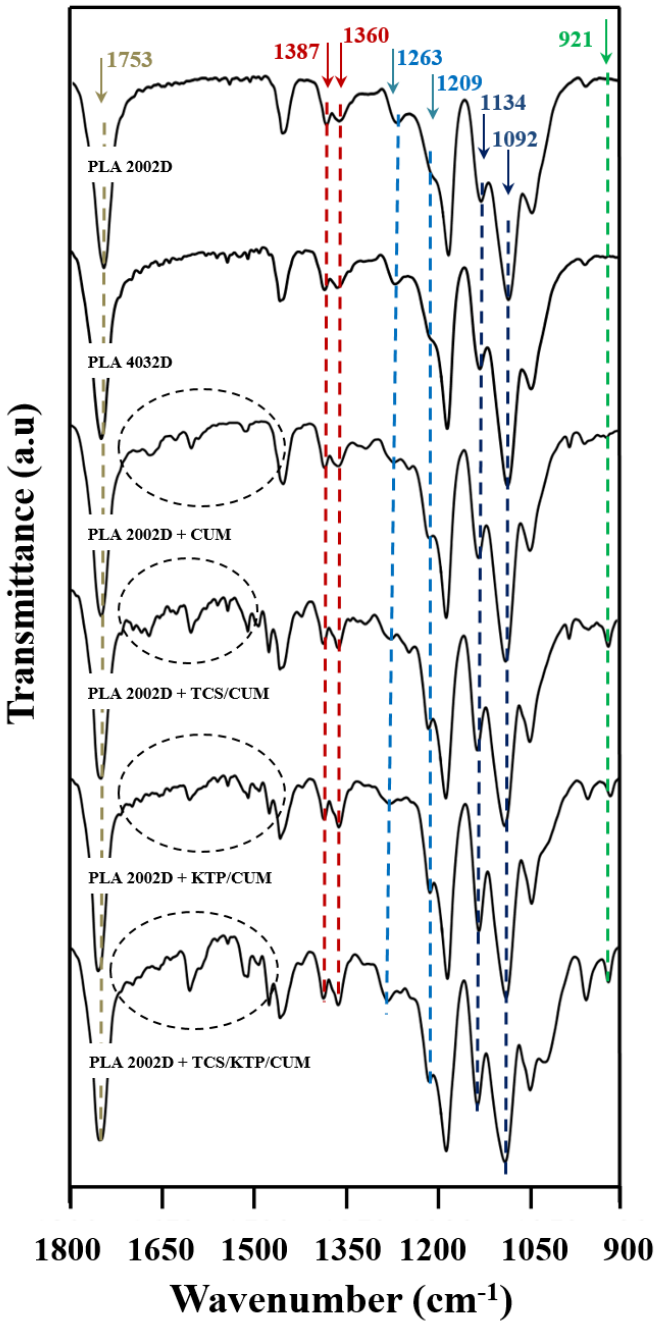

FIGURE 4.2.5

FTIR spectra (1800-900 cm^{-1} region) of PLA 2002D, PLA 4032D, PLA 2002D + CUM, PLA 2002D + TCS/CUM, PLA 2002D + KTP/CUM and PLA 2002D + TCS/KTP/CUM scaffolds.

Thermal Analysis of Electrospun Drug Loaded Samples

The slight difference on the D-lactide content (i.e. 4.2 *wt*-% compared to 2.0 *wt*-%) affected thermal properties significantly, as depicted in **Table 4.2.2** for the commercial pellet samples, which were expressly subjected to an annealing process to increase crystallinity. DSC heating traces of the corresponding electrospun scaffolds (**Figures 4.2.6 a** and **4.2.6 b**) revealed again differences between the two PLA grades and also interesting consequences of the different processing methods. Thus, after electrospinning samples became practically amorphous but could be easily cold crystallized during a subsequent heating run, reaching typical crystallinity values of commercial annealed samples. A cold crystallization peak was hardly observed in the heating run of samples cooled from the melt state (i.e. not subjected to a specific annealing treatment), as also previously reported.[24, 49] Therefore, the capability of the electrospinning technique to render highly aligned and oriented molecules able to easily cold crystallize has been postulated by different authors.[24, 49]

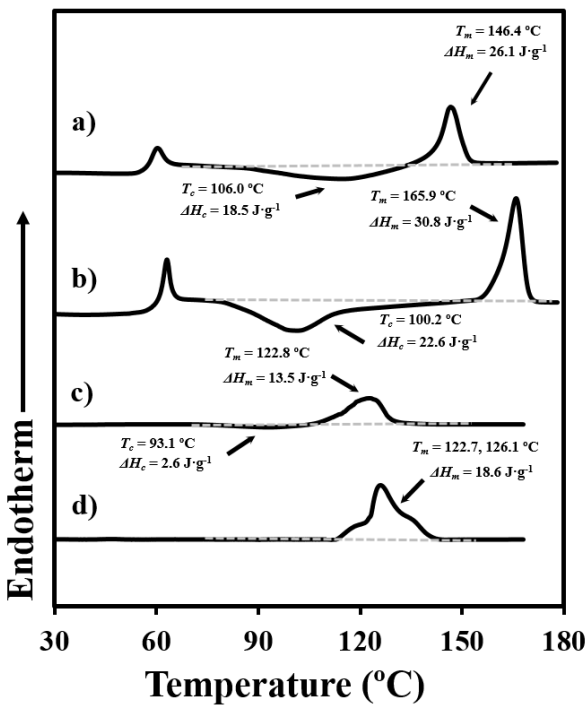

FIGURE 4.2.6

DSC heating runs (20 °C·min^{-1}) of PLA 2002D (a), PLA4032D (b), PLA 2002D + TCS/KTP/CUM (c) and PLA 4032D + TCS/KTP/CUM (d) electrospun scaffolds.

TABLE 4.2.2. Calorimetric data from the heating scan performed in the electrospun samples prepared with amorphous and crystalline PLA.[a]

Sample	T_g [ºC]	T_c [ºC]	$\Delta H_c{}^b$ [J·g^1]	$T_m{}^c$ [ºC]	$\Delta H_m{}^b$ [J·g^{-1}]	ΔH_m - $\Delta H_c{}^b$ [J·g^{-1}]	$\chi_c{}^d$
PLA 2002D[a]	59.6	-	-	149.3	29.2	29.2	0.28
PLA 2002D	59.3	106.0	18.5	146.4	26.1	7.6	0.07,0.25
PLA 4032D[a]	69.3	-	-	167.0	35.0	35.0	0.33
PLA 4032D	62.4	100.2	22.6	165.9	30.8	8.2	0.08,0.29
PLA 2002D + CUM	54.2	94.6	24.0	136.5	24.1	0.1	0.00,0.27
PLA 4032D + CUM	55.0	75.1	24.5	156.3	31.7	7.2	0.07,0.30
PLA 2002D + TCS/CUM	48.6	92.7	6.1	132.2	21.5	15.4	0.16,0.22
PLA 4032D + TCS/CUM	44.1	65.9	10.2	147.2	28.9	18.7	0.19,0.27
PLA 2002D + KTP/CUM	43.5	60.0	5.2	112.9	28.1	22.9	0.22,0.27
PLA 4032D + KTP/CUM	44.2	52.2	3.8	138.9	28.2	24.4	0.25,0.29
PLA 2002D + TCS/KTP/CUM	43.0	93.1	2.6	122.8	13.5	10.9	0.10,0.13
PLA 4032D + TCS/KTP/CUM	43.0	-	-	122.7,**126.1**	18.6	18.6	0.18

[a]Data obtained from commercial pellet samples.
[b]Values have been rescaled considering the theoretical content of TCS (i.e. 3 wt-%) ,aKTP (i.e., 1 wt-%) and CUM (i.e. 1 wt-%).
[c]Shoulders are rather frequent at a lower temperature than that indicated for the predominant melting peak.
[d]Determined by considering an estimated melting enthalpy of 106 J/g for a 100% crystalline sample[50, 51]. Left and right values correspond to crystallinities deduced for the as electrospun material (i.e. considering ΔH_m - $\Delta H_c{}^b$ as the enthalpy associated to crystalline phase of the electrospun sample) and those attained after cold crystallization (i.e. considering ΔH_m as the enthalpy associated to the final crystalline phase), respectively.

DSC heating runs of drug-loaded samples are more complex, especially those of ternary drug-loaded systems (**Figures 4.2.6 c** and **4.2.6 d**). The main thermal characteristics deduced from the different loaded scaffolds (summarized in **Table 4.2.2**) allow the following general remarks to be made:

- The glass transition temperature decreases compared to that observed for the corresponding unloaded scaffolds, suggesting a plasticizing effect caused by the incorporation of the small drug molecules. In addition, the enthalpic relaxation peak tended to be supressed, in contrast with unloaded samples. Therefore, the compact arrangement characteristic of an equilibrium condition is less favored.
- The melting peak temperature decreases dramatically compared to the value of unloaded scaffolds. Furthermore, this decrease is more and less significant for ternary and single drug-loaded scaffolds, respectively. In addition, multiple peaks could be observed for the more complex loaded systems. These features suggest that drugs can be partially incorporated into the crystalline structure and even led to different degrees of perfection. It should be pointed out that the melting peaks could only be associated with the PLA polymer matrix because the melting temperatures of TCS and KTP were lower (55-57 ºC and 93-96 ºC, respectively), whereas *p*-coumaric acid melted at a clearly higher temperature (i.e, 208-217 ºC).
- Binary and ternary drug-loaded systems became highly crystalline after the electrospinning process. Note the reduced cold crystallization enthalpy and the high melting enthalpy (i.e. the relatively high ΔH_m - ΔH_c values). The degrees of crystallinity are clearly higher than determined from unloaded samples, suggesting a nucleating effect of incorporated drugs. This effect was more pronounced when the more regular PLA 4032D sample is used. Logically, all studied samples showed a degree of crystallinity after cold crystallization slightly lower than determined for the commercial annealed samples. The temperature of the cold crystallization peak tends to diminish for drug-loaded samples, suggesting again a nucleating effects of drugs.

Drug Release from Binary and Ternary Drug Loaded PLA Electrospun Scaffolds

Drug release from electrospun fibers in a given medium is intimately related to their morphology and crystallinity and to possible intermolecular interactions between drugs and the polymer matrix. Therefore, a quantitative release study was performed considering both PLA 2002D and PLA 4032D matrices and single, binary and ternary drug-loaded systems. According to our previous studies, we selected a phosphate buffer saline (PBS) supplemented with ethanol (PBS:EtOH 3:7 *v*/v) 70%) to facilitate the delivery of highly hydrophobic molecules such as TCS, KTP and CUM and avoid the establishment of equilibrium conditions that typically limit their release when only PBS is employed.[23]

Figures 4.2.7 a and **4.2.7 b** show the release peofile of CUM from the single drug-loaded PLA 2002D and PLA 4032D scaffolds, respectively. It can be observed that a higher release percentage was attained from the less stereoregular PLA matrix (i.e., 80% compared to 60%), indicating that CUM was better retained in the presence of polymer crystalline domains. In any case, the release of CUM was very fast and reached values of 60-50% after only one hour of exposure to the medium.

Figures 4.2.7 c-4.2.7 h show the release profiles of TCS, KTP and CUM drugs in the binary and ternary drug-loaded systems. The following observation can be made: a) The release profiles for a given scaffold are similar for the three dugs independently of the PLA grade and the kind of system (binary or ternary), b) the maximum release percentage is always greater from PLA 2002D scaffolds than from the corresponding PLA 4032D scaffolds; c) release percentages increase slightly when more drugs were simultaneously loaded in PLA 4032D scaffolds (i.e., 60%, 60-70% and 80% for CUM in single, binary and ternary drug-loaded scaffolds, respectively), whereas percentages remain practically constant for PLA 2002D scaffolds. It seems that a slight synergic effect and the release are increased in complex systems and matrices that had higher encapsulation efficiency (e.g., PLA 4032D). This is interesting since it suggests that binary and ternary drug-loaded scaffolds have greater availability for their local action in the host tissue.

Release rates can be quantitatively compared considering postulated theoretical kinetic models in order to fit the experimental release profiles. Release generally occurs in two different steps, with the fast release initially observed (0-60%) being well-described by the Higuchi **Equation 1**:[52, 53]

$$M_t / M_0 = k_H \, t^{(1/2)} \qquad (0 \leq M_t / M_0 \leq 0.6) \qquad (\mathbf{1})$$

where k_H is the Higuchi release constant, M_t is the percentage of drug released at time t and M_0 is the drug equilibrium percentage (considered as the maximum drug percentage).

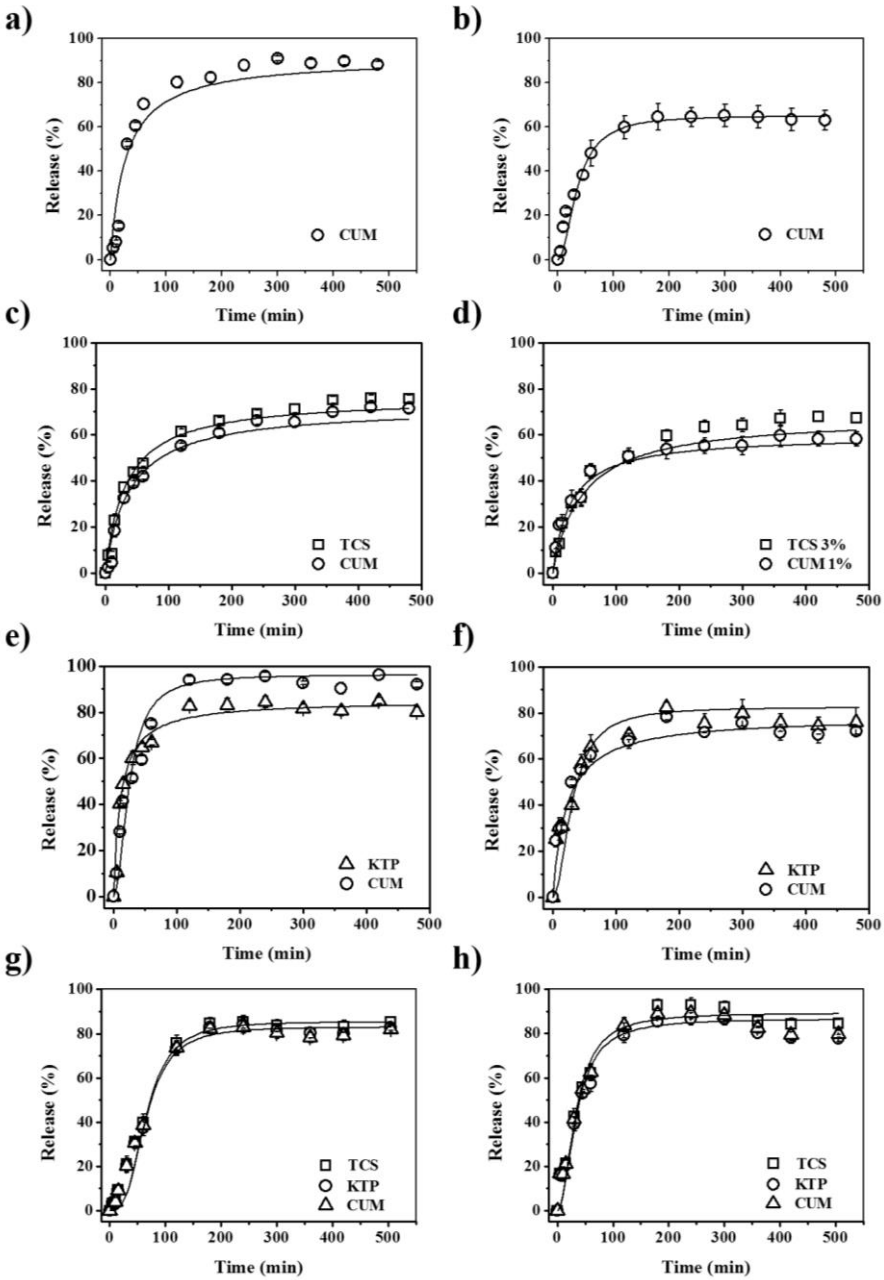

FIGURE 4.2.7

Release curves in a PBS:EtOH medium of CUM (a,b), TCS/CUM (c,d), KTP/CUM (e,f) TCS/KTP/CUM (g,h) drug loaded PLA 2002D (a,c,e,g) and PLA 4032D (b,d,f,h) electrospun scaffolds.

Table 4.2.3 summarizes the values of k_H determined for CUM from the loaded scaffolds. The results show small differences in the release rate but no specific trend linked to the degree of crystallinity, fiber diameter and complexity of the system (single, binary or ternary) can be derived, probably due to the multiple factors with different impact on molecular diffusion that are involved.

TABLE 4.2.3. Higuchi kinetic constant and correlation factor for the first part (0-60%) of the CUM release from the different loaded scaffolds.

Sample	k_H ($h^{-0.5}$)	r
PLA 2002D + CUM	0.76	0.989
PLA 4032D + CUM	0.69	0.990
PLA 2002D + TCS/CUM	0.57	0.990
PLA 4032D + TCS/CUM	0.72	0.986
PLA 2002D + KTP/CUM	1.07	0.991
PLA 4032D + KTP/CUM	0.89	0.982
PLA 2002D + TCS/KTP/CUM	0.41	0.985
PLA 4032D + TCS/KTP/CUM	0.67	0.998

Antibacterial Properties of Single, Binary and Ternary CUM Loaded Multifunctional Electrospun Scaffolds

Bacterial growth curves for *E.coli* (**Figures 4.2.8 a** and **4.2.8 b**) and *M.luteus* (**Figures 4.2.8 c** and **4.2.8 d**) in the presence of unloaded and single, binary and ternary drug-loaded scaffolds of PLA 2002D and PLA 4032D were evaluated as an indication of the bactericide activity of loaded matrices.

Results clearly indicate that bacterial growth was inhibited for both binary and ternary TCS-loaded scaffolds. This is a consequence of the well-known ability of TCS to block the active site of the enol-acyl carrier protein reductase enzyme, which is essential in the synthesis of fatty acids in bacteria.[54] Thus, after 24 hours of culture, *E.coli* and *M.luteus* bacterial growths were 8-10% and 10-12% of the corresponding growths determined for the positive control, respectively. Curves were essentially independent of the polymer matrix and the additional incorporation of CUM and KTP drugs. It seems that sufficient release was achieved by the high TCS content of scaffolds (i.e. 3 *w/v*-%) to inhibit bacterial growth. Also, this effect could not be improved by the presence of the other two drugs and was not influenced by morphologic and crystallinity changes of electrospun scaffolds.

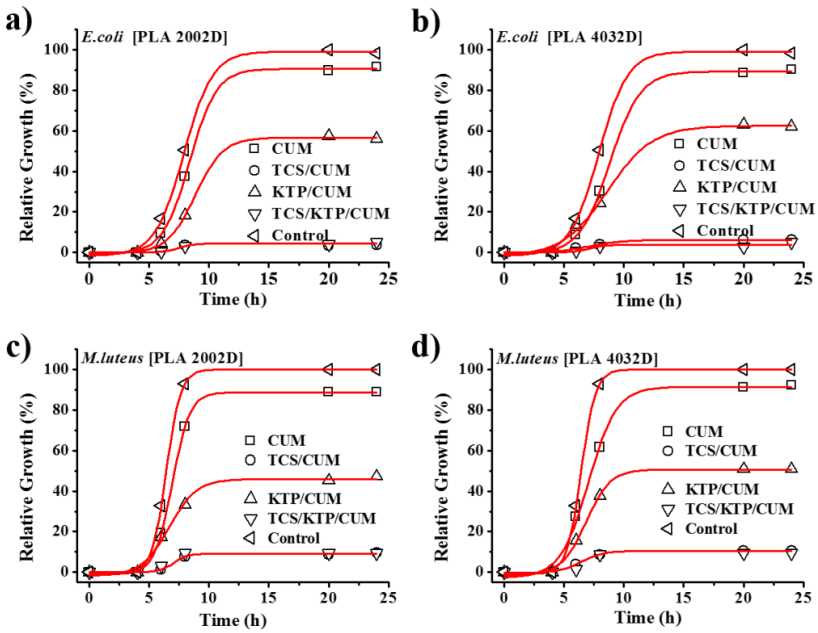

FIGURE 4.2.8

Relative growth of Escherichia coli (a,b) and Micrococcus luteus (c,d) on binary and ternary drug-loaded PLA 2002D (a,c) and PLA 4032D (b,d) electrospun scaffolds.

Figure 4.2.8 also shows typical bacterial growth curves for single CUM-loaded scaffolds. Thus, after an initial lag phase (4-5 hours), an exponential phase associated with binary fission was observed during which Gram-negative and Gram-positive bacterial growth stopped at a value close to 90% with respect to that found for the positive control. More interestingly, the binary KTP/CUM-loaded scaffolds showed moderate inhibition that was slightly dependent on the PLA grade and the type of bacteria. Specifically, growth percentages decreased compared to the positive control to 40% and 50% for Gram-negative bacteria grown on matrices based on PLA 2002D and PLA 4032D, respectively, and to 50% and 60% for Gram-positive bacteria grown on matrices based on PLA 2002D and PLA 4032D, respectively. From these results two conclusions can be drawn: a) KTP has a bacteriostatic effect with a not yet fully clarified mechanism,[55, 56] and b) the less stereoregular PLA matrix has a higher inhibition effect, in agreement with the enhanced drug release (**Figures 4.2.8 c** and **4.2.8 d**).

Bactericide activity was also evaluated by quantification of bacterial adhesion, as shown in **Figure 4.2.9**. Single CUM-loaded scaffolds had a similar percentage of bacterial adhesion than the positive control, as expected from the bacterial growth results. In the same way, practically complete inhibition of bacterial adhesion was found for TCS/CUM and TCS/KTP/CUM loaded scaffolds. Intermediate adhesion values f were obtained for binary KTP/CUM-loaded scaffolds, with significant differences again being observed depending on the PLA grade. Thus, adhesions

of 40% and 70% were determined for PLA 2002D (**Figure 4.2.9 a**) and PLA 4032D (**Figure 4.2.9 b**) scaffolds. The higher percentage found for the latter is in agreement with the differences in the release and bacterial growth. Adhesion results were similar for both Gram-negative and Gram-positive bacteria.

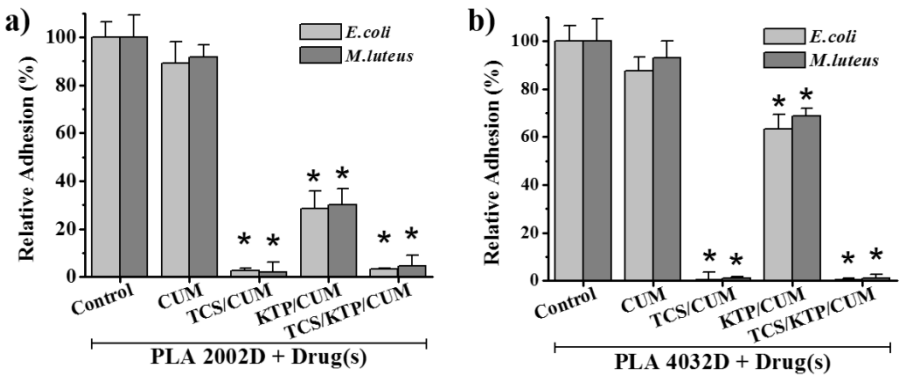

FIGURE 4.2.9

Escherichia coli (blue) and Micrococcus luteus (pink) adhesion on polystyrene plate as positive control and binary and ternary drug-loaded PLA 2002D (a) and PLA 4032D (b) electrospun scaffolds (*p<0.05 *vs.* control, Tukey's test).

Cell Viability on Single, Binary and Ternary CUM Loaded Multifunctional Electrospun Scaffolds

Figure 4.2.10 illustrates cell adhesion and proliferation behavior of two epithelial cell lines (MDCK and VERO) in loaded PLA 2002D and PLA 4032D electrospun scaffolds. A good cell response was expected for CUM and KTP according to their antioxidant and anti-inflammatory activity, respectively. MDCK and VERO cell lines were selected for their epithelial morphology and typical adherent grown which leads to formation of cell monolayers highly sensitive to cell damage due to their flake detachment from the culture plate.

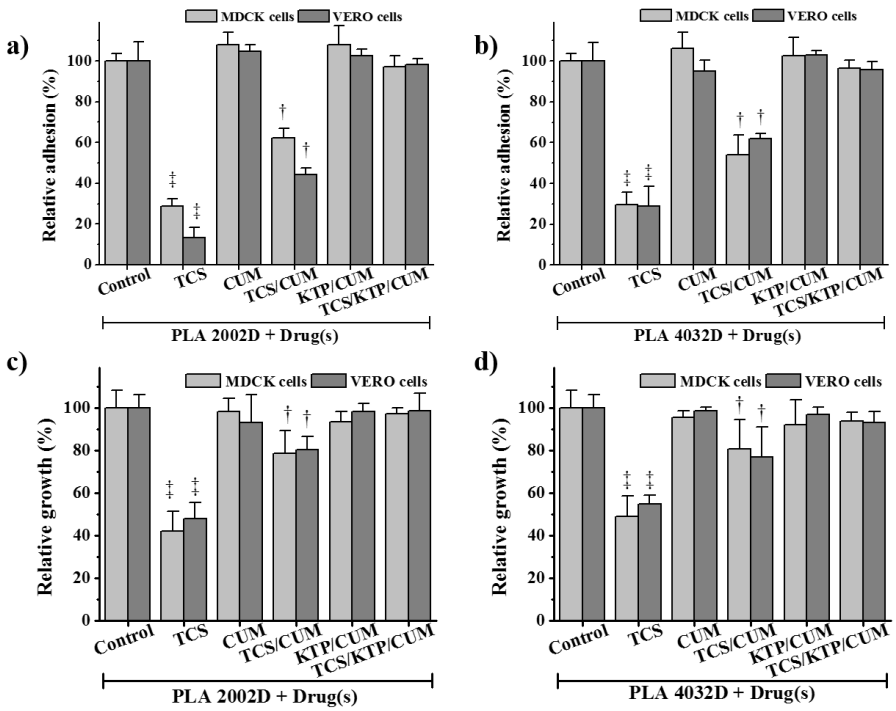

FIGURE 4.2.10

Adhesion (a,b) and proliferation (c,d) of MDCK (blue) and VERO (red) cells on polystyrene plate as positive control and TCS, CUM, TCS/CUM, KTP/CUM and TCS/KTP/CUM PLA 2002D (a,b) and PLA 4032D (c,d) electrospun scaffolds from PLA 2002D and 4032D grades (†p<0.05; ‡p<0.01 *vs.* positive control, ANOVA-Tukey's test).

Scaffolds loaded with 3 *w/v*-% of TCS were used as negative control since this concentration was previously found to be cytotoxic for loaded PLA scaffolds.[24] Cell adhesion on these scaffolds decreased to 20-30% compared to unloaded PLA scaffolds (positive control) after 24 h of culture. Note that this significant difference ($p < 0.001$) was independent of the PLA grade (**Figures 4.2.10 a,** and **4.2.10 b**). It is highly interesting that incorporation of CUM reduced cell damage caused by TCS and favored cell viability. Thus, cell adhesion on binary TCS/CUM-loaded scaffolds was increased by ca. 30% with respect to the negative control. Anti-inflammatory KTP had a similar, additive effect. In this way, cell adhesion on ternary TCS/KTP/CUM-loaded scaffolds clearly increased and reached the same values as positive unloaded scaffolds and also as single drug-loaded PLA scaffolds (**Figures 4.2.10 a** and **4.2.10 b**).

Adhered cells kept their proliferative activity and ultimately were able to colonize the material, forming a monolayer tissue. **Figures 4.2.10 c** and **4.2.10 d** shows the quantification of cell growth, which was clearly related to the previous cell adhesion event. The cytotoxic effect of TCS can be reverted by the renewal of culture medium. Thus, cell viability increased, as demonstrated by values of 40% and 50% determined with respect to the unloaded scaffolds

after 7 days of culture, which were higher that the above adhesion percentages. Nevertheless, viability was still significantly lower ($p < 0.01$) than determined for the control. Again, positive effects on cell proliferation ($p > 0.95$) were found for binary TCS/CUM-scaffolds compared to the negative TCS-loaded control, resulting in an increase cell viability up to 80%. This represents an increase close to 30% with respect to the viable cells measured in single TCS-loaded scaffolds. Cell proliferation in ternary TCS/KTP/CUM-loaded scaffolds was similar to that of positive controls, as expected from the cell adhesión results, demonstrating that cell damage caused by TCS could be neutralized by the positive effect on cell viability caused by the incorporation of CUM and KTP. Finally, it should be indicated that no significant differences were observed between scaffolds prepared from the two PLA grades despite slight differences on drug release.

4.2.4 Conclusions

Bactericide, anti-inflammatory and antioxidant drugs like triclosan, ketoprofen and *p*-coumaric acid, respectively, could be simultaneously loaded into PLA microfibers by the electrospinning technique. Porous and continuous microfibers with an unimodal diameter distribution could be prepared from a 10 *w*/*v*-% solution of PLA in a chloroform:acetone:dimethylsulfoxide mixture and using electrospinning parameters of 15 kV, 12.5 cm and 5-10 $mL \cdot h^{-1}$ for voltage, tip-collector distance and flow rate, respectively.

Electrospun scaffolds had highly variable crystallinity which depended slightly on the PLA grade (at least when D-lactide content varied only from 4.2 to 2.0 *wt*-%) and strongly on the incorporation drugs. Thus, drugs seemed to produce a nucleating effect that, in some cases, led to crystallization levels of commercial annealed samples even for binary drug-loaded systems. Drug-loaded scaffolds also showed a decrease in the glass transition temperature that favored molecular diffusion processes and a decrease in the melting temperature as a consequence of incorporation of drugs in amorphous and crystalline phases, respectively.

The three drugs were released in a similar and fast way from a given scaffold (i.e. for a selected PLA matrix and a single, binary or ternary drug-loaded system) in a PBS:ethanol medium that mimics a typical serum supplemented PBS medium. In all cases, a significant amount of drug was retained inside PLA microfibers, especially the more relevant when the more stereoregular polymer. The entrapping efficiency of PLA was limited and the release of a specific drug seemed to increase with the complexity of the system (i.e. from single to ternary drug-loaded scaffolds), suggesting a synergic effect. New multifunctional scaffolds appear highly interesting since, besides imparting their expected and specific properties (i.e., antioxidant and anti-inflammatory), KTP and CUM can neutralize the cytotoxic effect caused by a moderate/high triclosan load. In summary, multifunctional PLA scaffolds with both high cell viability and protection against microorganism can be easily prepared by the electrospinning technique.

4.2.5 References

[1] R. Sahay, P.S. Kumar, R. Sridhar, J. Sundaramurthy, J. Venugopal, S.G. Mhaisalkar, S. Ramakrishna, J Mater Chem, 22 (2012) 12953-12971.

[2] L.S. Nair, C.T. Laurencin, Prog Polym Sci, 32 (2007) 762-798.

[3] Y. Ji, K. Ghosh, X.Z. Shu, B. Li, J.C. Sokolov, G.D. Prestwich, R.A. Clark, M.H. Rafailovich, Biomaterials, 27 (2006) 3782-3792.

[4] P.X. Ma, Mater Today, 7 (2004) 30-40.

[5] B. Dhandayuthapani, Y. Yoshida, T. Maekawa, D.S. Kumar, Inter J Polym Sci, (2011).

[6] Z.W. Ma, M. Kotaki, R. Inai, S. Ramakrishna, Tissue Eng, 11 (2005) 101-109.

[7] S.R. Bhattarai, N. Bhattarai, H.K. Yi, P.H. Hwang, D.I. Cha, H.Y. Kim, Biomaterials, 25 (2004) 2595-2602.

[8] R. Vasita, D.S. Katti, Int J Nanomedicine, 1 (2006) 15-30.

[9] X. Geng, O.H. Kwon, J. Jang, Biomaterials, 26 (2005) 5427-5432.

[10] I.C. Um, D. Fang, B.S. Hsiao, A. Okamoto, B. Chu, Biomacromolecules, 5 (2004) 1428-1436.

[11] H.J. Jin, J.S. Chen, V. Karageorgiou, G.H. Altman, D.L. Kaplan, Biomaterials, 25 (2004) 1039-1047.

[12] F. Yang, R. Murugan, S. Wang, S. Ramakrishna, Biomaterials, 26 (2005) 2603-2610.

[13] S.A. Riboldi, M. Sampaolesi, P. Neuenschwander, G. Cossu, S. Mantero, Biomaterials, 26 (2005) 4606-4615.

[14] W.J. Li, K.G. Danielson, P.G. Alexander, R.S. Tuan, J Biomed Mater Res A, 67A (2003) 1105-1114.

[15] K. Uematsu, K. Hattori, Y. Ishimoto, J. Yamauchi, T. Habata, Y. Takakura, H. Ohgushi, T. Fukuchi, M. Sato, Biomaterials, 26 (2005) 4273-4279.

[16] E.R. Kenawy, G.L. Bowlin, K. Mansfield, J. Layman, D.G. Simpson, E.H. Sanders, G.E. Wnek, J Control Release, 81 (2002) 57-64.

[17] X.M. Mo, C.Y. Xu, M. Kotaki, S. Ramakrishna, Biomaterials, 25 (2004) 1883-1890.

[18] G. Verreck, I. Chun, J. Rosenblatt, J. Peeters, A. Van Dijck, J. Mensch, M. Noppe, M.E. Brewster, J Control Release, 92 (2003) 349-360.

[19] S.M. Jacobsen, D.J. Stickler, H.L.T. Mobley, E. Shirtliff, Clin Microbiol Rev, 21 (2008) 26-59.

[20] D. Fuster, J. Duch, A. Soriano, S. García, X. Setoain, G. Bori, S. Rubí, D. Rodríguez, B. Doménech, C. Piera, J. Mensa, F. Pons, Rev Esp Med Nucl Imagen Mol, 27 (2008) 430-435.

[21] J. Cailloux, O.O. Santana, E. Franco-Urquiza, J.J. Bou, F. Carrasco, J. Gamez-Perez, M.L. Maspoch, Express Polym Lett, 7 (2013) 304-318.

[22] J. Cailloux, O.O. Santana, E. Franco-Urquiza, J.J. Bou, F. Carrasco, M.L. Maspoch, J Mater Sci, 49 (2014) 4093-4107.

[23] R. Zurita, J. Puiggali, A. Rodriguez-Galan, Macromol Biosci, 6 (2006) 58-69.

[24] L.J. del Valle, R. Camps, A. Diaz, L. Franco, A. Rodriguez-Galan, J. Puiggali, J Polym Res, 18 (2011) 1903-1917.

[25] E. Llorens, L.J. del Valle, A. Diaz, M.T. Casas, J. Puiggali, Macromol Res, 21 (2013) 775-787.

[26] E. Llorens, L.J. del Valle, J. Puiggalí, Macromol Res, 22 (2014) 388-396.

[27] P.P. Shah, P.R. Desai, M. Singh, J Control Release, 158 (2012) 336-345.

[28] M.L. Vueba, M.E. Pina, F. Veiga, J.J. Sousa, L.A.E.B. de Carvalho, Int J Pharm, 307 (2006) 56-65.

[29] D. Li, Y.N. Xia, Adv Mater, 16 (2004) 1151-1170.

[30] S.R. Dhakate, B. Singla, M. Uppal, R.B. Mathur, Adv Mater Lett, 1 (2010) 200-204.

[31] E. Luong-Van, L. Grondahl, K.N. Chua, K.W. Leong, V. Nurcombe, S.M. Cool, Biomaterials, 27 (2006) 2042-2050.

[32] G. Buschle-Diller, J. Cooper, Z. Xie, Y. Wu, J. Waldrup, X. Ren, Cellulose, 14 (2007) 553-562.

[33] D. Karst, Y. Yang, J Appl Polym Sci, 96 (2005) 416-422.

[34] D.M. Aragón, D.A. Chiappetta, J. Degrossi, E.F. Vargas, C. Bregni, A. Sosnik, F. Martínez, Rev Col Cienc Quím Farm, 37 (2008) 241-257.

[35] E. Llorens, L.J. Valle, R. Ferrán, A. Rodríguez-Galán, J. Puiggalí, J Polym Res, 21 (2014) 1-15.

[36] P. De Santis, A.J. Kovacs, Biopolymers, 6 (1968) 299-306.

[37] C. Alemán, B. Lotz, J. Puiggali, Macromolecules, 34 (2001) 4795-4801.

[38] S. Sasaki, T. Asakura, Macromolecules, 36 (2003) 8385-8390.

[39] J. Zhang, K. Tashiro, A.J. Domb, H. Tsuji, Macromol Symp, 242 (2006) 274-278.

[40] H. Marubayashi, S. Akaishi, S. Akasaka, S. Asai, M. Sumita, Macromolecules, 41 (2008) 9192-9203.

[41] H. Marubayashi, S. Asai, M. Sumita, Macromolecules, 45 (2012) 1384-1397.

[42] B. Eling, S. Gogolewski, A.J. Pennings, Polymer, 23 (1982) 1587-1593.

[43] J. Puiggali, Y. Ikada, H. Tsuji, L. Cartier, T. Okihara, B. Lotz, Polymer, 41 (2000) 8921-8930.

[44] L. Cartier, T. Okihara, Y. Ikada, H. Tsuji, J. Puiggali, B. Lotz, Polymer, 41 (2000) 8909-8919.

[45] T. Fujiwara, M. Miyamoto, Y. Kimura, S. Sakurai, Polymer, 42 (2001) 1515-1523.

[46] H. Urayama, S.-I. Moon, Y. Kimura, Macromol Mater Eng, 288 (2003) 137-143.

[47] C. Ribeiro, V. Sencadas, C.M. Costa, J.L.G. Ribelles, S. Lanceros-Mendez, Sci Technol Adv Mat, 12 (2011).

[48] S.O. Kang, S.L. Hsu, H.D. Stidham, P.B. Smith, M.A. Leugers, X. Yang, Macromolecules, 34 (2001) 4542-4548.

[49] J. Zeng, X. Chen, Q. Liang, X. Xu, X. Jing, Macromol Biosci, 4 (2004) 1118-1125.

[50] T.Y. Cho, G. Strobl, Polymer, 47 (2006) 1036-1043.

[51] J.R. Sarasua, R.E. Prud'homme, M. Wisniewski, A. Le Borgne, N. Spassky, Macromolecules, 31 (1998) 3895-3905.

[52] T. Higuchi, J Pharm Sci, 52 (1963) 1145-1149.

[53] R.W. Baker, in, John Wiley & Sons, New York, USA, 1987.

[54] C.W. Levy, A. Roujeinikova, S. Sedelnikova, A.R. Stuitje, A.R. Salabas, D.W. Rice, J.B. Rafferty, Nature, 398 (1999) 383-384.

[55] S.G. Dastidar, K. Ganguly, K. Chaudhuri, A.N. Chakrabarty, Int J Antimicrob Ag, 14 (2000) 249-251.

[56] H.A. Abbas, F.M. Serry, E.M. El-Masry, Asian J Res Pharm Sci, 2 (2012) 66-72.

5.

Preparation of biodegradable scaffolds incorporating non-electrospinable polymers

The work described in this chapter previously appeared in:

[1] Llorens, E.; Calderón, S.; Rodríguez-Galán, A.; del Valle, L. J.; Puiggalí, J. *Mater. Sci. Eng. C.* Submitted.

[2] Llorens, E.; Pérez-Madrigal, M. M.; Armelin, E.; Alemán, C.; del Valle, L.; Puiggalí, J. *R. Soc. Chem. Adv.* **2014**, *4*, 15245-15255.

5.1 PLA Scaffolds Incorporating Bactericide Polybiguanide (PHMB)

Polyhexamethylenebiguanide hydrochloride (PHMB), a low molecular weight polymer related to chlorohexidine (CHX), is a well-known antibacterial agent. In this study, polylactide (PLA) nanofibers loaded with PHMB were produced by electrospinning to obtain 3D biodegradable scaffolds with antibacterial properties. PLA fibers loaded with CHX were used as control. The electrospun fibers were studied and analyzed by SEM, FTIR, DSC and contact angle measurements. PHMB and CHX release from loaded scaffolds was evaluated, as well as their antibacterial activity and biocompatibility. The results showed that the nanofibers became smoother and their diameter smaller with increasing the amount of loaded PHMB, which also led to increased hydrophobicity of scaffolds due to the increase in scaffold surface roughness. PHMB release was highly dependent on the hydrophilicity of the medium and differed from that determined for CHX. Lastly, PHMB-loaded PLA scaffolds showed antibacterial properties since they inhibited adhesion and bacterial growth, and exhibited biocompatible characteristics for the adhesion and proliferation of both fibroblast and

5.1.1 Introduction

Topical formulations containing antimicrobial agents (e.g., mouthwashes, gels or toothpastes) are commonly used for the treatment of infections and burn injuries.[1-3] These formulations ensure direct access of high concentrations of the antimicrobial agent to the site of infection. The agent acts locally or systematically inhibiting microorganism growth around the wound, reducing the probability of resistance development, minimizing deleterious host responses, and reducing the risk of environmental pollution.[4-6]

Several compounds have been extensively studied for their antibacterial activity, with benzalkonium chlorides, cetylpyridinium chloride, aldehydes, anilides, diamidines and silver being the most representative examples.[7-9] Biguanide, commonly known as chlorhexidine (1,1′-hexamethylene- bis-5-(4-chlorophenyl) biguanide, CHX), is also a widely employed antimicrobial agent.[10] Specifically, CHX is an important antiseptic, disinfectant, pharmaceutical and cosmetic preservative and antiplaque agent. The high activity of this drug towards microorganisms is due to the presence of secondary amines that can be protonated, and therefore positively charged under normal pH conditions.[11] Immobilized antimicrobial agents offer an alternative which eliminates patient exposure to active agents and potentially increases the duration of antimicrobial efficacy.[12, 13] Agents can be immobilized on a wide variety of materials including metals and plastics, as well as natural and man-made fabrics such as electrospun scaffolds (specifically, inside constituent micro/nanofibers).

Additional advantages of biguanide compounds are related to their ability to form quadricovalent cationic complexes with silver ions which are stable in ambient conditions. In this way, a synergic effect can be derived from the combination of biguanide and silver antimicrobial activities.[1]

Other chemical compounds also bearing biguanide groups, such as polyhexamethylenebiguanide hydrochloride (PHMB), have been developed.[14, 15] Specifically, PHMB is a cationic oligomer having with a average of 7-11 biguanide groups spaced by flexible hexamethylene segments. PHMB has chemical stability, low toxicity, high effectiveness against microorganisms and reasonable cost.[16, 17] Gilbert *et al.* demonstrated that activity increased with the number of biguanide groups and that maximum biocidal efficiency was obtained when the hexamethylene group was employed as spacer.[18, 19]

In a recent paper, Koburger *et al.*[20] compared the antiseptic efficacy of several antibacterial agents such as triclosan, octenidine, PHMB, PVP-Iodine and chlorhexidine digluconate, concluding that PHMB was the best antiseptic in prolonged use. PHMB action against microorganisms was described as a consequence of its binding to the negatively charged phosphate head groups of phospholipids at the bacterial cell wall. Binding increased rigidity, sank non-polar segments into hydrophobic domains, and disrupted the membrane with subsequent cytoplasmic shedding that culminated in cell death.[18, 19]

Recently, micro/nanofiber nonwoven membranes produced by electrospinning have shown great potential in applications such as biomedical devices (e.g., scaffolds for tissue engineering) due to their typically high surface area and porosity. Furthermore, the unique properties of electrospun fibers have triggered a broad range of other potential applications, including composites, sensors, protective clothing, filtration membranes, magneto-responsive fibers and superhydrophobic membranes.[4] In addition, the electrospinning process provides a simple way to encapsulate drugs within a micro/nanofiber matrix that can lead to a controlled and sustained release.

Several natural and synthetic biodegradable polymers have been successfully electrospun (e.g., polyglycolide,[21] polylactide,[21, 22] polycaprolactone,[23] collagen[24, 25] and chitosan[25, 26]). Polylactide (PLA) is one of the most widely used materials in biomedical applications due to the combination of interesting characteristics like tunable mechanical properties, degradation into natural metabolites, biocompatibility and low cost. Thus, biodegradable polymers containing active ingredients, such as antimicrobials and antibiotics, were also studied in wound dressing materials to protect against contaminations and infections.[27, 28] Specifically, PHMB has been employed as a highly effective antimicrobial agent for composites of cellulose acetate and polyester urethane.[29] The reported results have opened highly interesting perspectives for the use of PHMB in biomedical applications where a rapid release in hydrophilic systems is desired. In this study, the antimicrobial PHMB agent was incorporated into electrospun PLA micro/nanofibers to evaluate the potential application of these materials as temporary and medicated scaffolds. For this purpose, electrospinning conditions were optimized, morphology of micro/nanofibers studied and physicochemical characterization of scaffolds performed. Release kinetics, antimicrobial activity against Gram negative and positive bacteria (i.e. *E. coli* and *M. luteus*) and biocompatibility were also evaluated.

5.1.2 Experimental Section

Materials

Polylactide (PLA), a product of Natureworks (polymer 2002D), was kindly supplied by Nupik International (Polinyà, Spain). According to the manufacturer, this PLA has a D content of 4.25%, a residual monomer content of 0.3%, a density of 1.24 $g \cdot cc^{-1}$, a glass transition temperature (T_g) of 58 ºC and a melting point of 153 ºC.

All solvents, clorhexidine (CHX), 3-(4,5-dimethylthiazol-2-yl)-2,5-diphenyl-2H-tetrazolium bromide (MTT) and cell culture labware were purchased from Sigma-Aldrich (Spain). Cosmocil® (polyhexamethylenebiguanide hydrochloride, PHMB) was kindly provided by B. BRAUN Surgical S.A. The microbial culture was prepared with reagents and labware from Scharlab (Spain).

Escherichia coli CECT 101 and *Micrococcus luteus* CECT 245 bacterial strains were obtained from Spanish Collection of Type Culture (Valencia, Spain). MDCK (Madin-Darby canine kidney) epithelial cells and MRC5 (human fetal lung fibroblast) cells were purchased from ATCC (USA).

Electrospinning

Mixtures of PLA with CHX or PHMB were electrospun from chloroform/acetone mixtures (1:2 *v*/*v*) supplied with formic acid (10:1 *v*/*v*). PLA concentration in the solution was 10 *w*/*v*-%, whereas CHX and PHMB concentrations were 0.5 *w*/*v*-% and 0.02-0.25 *w*/*v*-%, respectively. Thus, processed fibers should contain 5 and 0.2-2.5 *wt*-% of CHX and PHMB, respectively. Samples will be named using the drug abbreviation and percentage, i.e. PLA-CHX 5 and PLA-PHMB 2.5 correspond to PLA scaffolds loaded with 5 and 2.5 *wt*-% of CHX and PHMB, respectively.

Electrospun fibers were collected on a target placed at different distances (10-25 cm) from the needle tip (inside diameter of 0.84 mm). The voltage was varied between 10 and 30 kV and applied to the target using a high-voltage supply (Gamma High Voltage Research, ES30-5W). Polymer solutions were delivered via a KDS100 infusion syringe pump (KD Scientific, USA) to control the mass-flow rate (from 0.5 to 10 $mL \cdot h^{-1}$). All electrospinning experiments were carried out at room temperature. Electrospun unloaded and CHX and PHMB loaded fibers were prepared using optimized parameters (e.g., height, voltage and flow) and solvent conditions (e.g., solvent ratio, and polymer and drug concentration).

Morphology and properties of electrospun PLA-CHX and PLA-PHMB mixtures

Optical and scanning electron microscopy

Optical microscopy studies were performed with a Zeiss Axioskop 40 microscope. Micrographs were taken with a Zeiss AxiosCam MRC5 digital camera.

Detailed inspection of texture and morphology of electrospun samples was conducted by scanning electron microscopy using a Focus Ion Beam Zeiss Neon 40 instrument (Carl Zeiss, Germany). Carbon coating was accomplished by using a Mitec K950 Sputter Coater fitted with a film thickness monitor *k*150x. Samples were visualized at an accelerating voltage of 5 kV. Diameter of electrospun fibers was measured with the SmartTiff software from Carl Zeiss SMT Ltd.

Fourier transform infrared spectroscopy (FTIR)

Infrared absorption spectra were recorded with a Fourier Transform FTIR 4100 Jasco spectrometer in the 1850-950 cm^{-1} range. A Specac model MKII Golden Gate attenuated total reflection (ATR) equipment with a heated Diamond ATR Top-Plate was used.

Differential scanning calorimetry (DSC)

Calorimetric data were obtained by differential scanning calorimetry with a TA Instruments Q100 series equipped with a refrigeration cooling system (RCS). Experiments were conducted under a flow of dry nitrogen with a sample weight of approximately 5 mg and calibration of equipment was performed with indium. Heating runs were carried out at a rate of 20 $^{o}C \cdot min^{-1}$.

Contact angle (CA)

Contact angles (CA) were measured at room temperature with sessile drops using an OCA-15 plus Contact Angle Microscope (Dataphysics, USA) and SCA20 software. Contact angle values of the right and left sides of distilled water drops were measured and averaged. Measurements were performed 10 s after the drop (5 μL) was deposited on the sample surface. All CA data were an average of six measurements on different surface locations.

Release experiments

Controlled release measurements were made with square pieces (20 x 20 x 0.1 mm^3) of the electrospun scaffolds. These pieces were weighed and incubated at 37 ^{o}C in an orbital shaker at 200 rpm in tubes of 50 mL for 1 week. PBS buffer (hydrophilic medium) and alternatively its mixture with different ratios of ethanol (i.e. 9:1 *v*/*v*, 5:5 *v*/*v*, 3:7 *v*/*v* and 1:9 *v*/*v*) as a more hydrophobic component were employed as release media. Drug concentration was evaluated by UV spectroscopy using a Shimadzu 3600 spectrometer. Calibration curves were obtained by

plotting the absorbance measured at 252 and 234 nm versus CHX and PHMB concentration, respectively, in the hydrophilic medium, whereas 261 (for CHX) and 236 nm (for PHMB) were considered when ethanol was added. Samples were withdrawn from the release medium at predetermined time intervals. The volume was kept constant by addition of fresh medium. All drug release tests were carried out using three replicates and the results were averaged.

Antimicrobial test

Escherichia coli (*E. coli*) and *Micrococcus luteus* (*M. luteus*) bacteria were selected to evaluate the antimicrobial effect of electrospun CHX and PHMB loaded fibers. The bacteria were previously grown aerobically to exponential phase in broth culture (5 $g \cdot L^{-1}$ beef extract, 5 $g \cdot L^{-1}$ NaCl, 10 $g \cdot L^{-1}$ peptone, pH 7.2).

Growth experiments were performed on a 24-well culture plate. Square pieces ($10 \times 10 \times 0.1$ mm^3) of the electrospun scaffolds were placed into each well. Then, 1 mL of broth culture containing 10^3 CFU was seeded on the electrospun fiber mats. The cultures were incubated at 37 ºC and agitated at 200 rpm. Aliquots of 50 µL were taken at predetermined time intervals for absorbance measurement at 650 nm in a plate reader. Thus, turbidity was directly related to bacterial growth.

Bacterial adhesion onto scaffolds was also determined. The culture media were aspirated after incubation and the material washed once with distilled water. Then, 0.5 mL of sterile 0.01 M sodium thiosulfate was added to each well. After addition of 4 mL of broth culture, the plate was incubated at 37 ºC and agitated at 200 rpm for 24 h. The bacterial number was determined as above indicated. All assays were conducted in triplicate and the results averaged.

Scaffolds were fixed with 2.5 *w/v*-% formaldehyde at 4 ºC overnight. Then, they were washed three times with distilled water and Gram stained for observation by light microscopy.

Cellular adhesion and proliferation assays

MDCK and MRC-5 cells were cultured in Dulbecco's modified Eagle medium (DMEM) as previously reported.[30] Electrospun unloaded and drug loaded PLA scaffolds were collected on round coverslips (diameter 1.5 cm) that were placed into the wells of a multiwell culture plate. Samples were fixed in the wells with a small drop of silicone (Silbione® MED ADH 4300 RTV, Bluestar Silicones France SAS, Lyon, France) and then sterilized by UV-radiation in a laminar flux cabinet for 15 min. For the cell adhesion assay, aliquots of 50-100 µL containing 5×10^4 cells were seeded onto the electrospun samples in each well and incubated for 24 h (adhesion assay) or 4 days (proliferation assay).

Samples were evaluated by the standard adhesion and proliferation method[30] using five replicates and the results were averaged. Samples with adhered and grown cells on the mats were

fixed with 2.5 *w/v*-% glutaraldehyde at 4 ºC overnight. They were subsequently dehydrated and processed for observation by scanning electronic microscopy.

Statistical analysis

Values were averaged and graphically represented, together with their respective standard deviations. Statistical analysis was performed by one-way ANOVA test to compare the means of all groups, and then Tukey's test was applied to determine a statistically significant difference between two groups. The test confidence level was set at 95% ($p < 0.05$).

5.1.3 Results and Discussion

Electrospinning of PLA-CHX and PLA-PHMB Mixtures

Several solvents and binary solvent mixtures were tested at different voltages, flow rates, polymer concentrations and needle tip-collector distances in order to determine the optimal conditions to obtain continuous fibers from all PLA-PHMB and PLA-CHX mixtures.

In fact, the solvent plays a fundamental role in continuous micro/nanofiber production.[31, 32] A relatively high polymer concentration is typically required to avoid formation of droplets and electrospun beads when a good solvent is selected.[33] Because PLA is highly soluble in chloroform,[30, 34] it was selected as a starting point in the optimization of processing conditions. However, solubilization of CHX and PHMB required more hydrophilic solvents (e.g., DMSO, formic acid, water or ethanol). It is known that the alternating chemical structure of hydrophilic-hydrophobic segments in PHMB can give rise to peculiar characteristics such as micelle formation in aqueous media with methylene segments pointing toward the center of the micelle and hydrophilic biguanide groups pointing outward. This arrangement was not found in solvents that establish lower interactions, for example ethanol.[16] Thus, the selection of an appropriate solvent system is crucial for a successful electrospinning process of the polymer loaded with the PHMB drug.

CHX and PHMB have a different number of biguanide groups in their chemical structure (**Figure 5.1.1 a**) and slightly different solubility. While CHX is soluble in chloroform upon addition of acetone, PHMB requires an additional percentage of formic acid. Therefore, experiments were carried out using a common solvent mixture (i.e. chloroform/acetone/formic acid (1:2:0.3 *v*/*v*/*v*)) for PLA, CHX and PHMB.

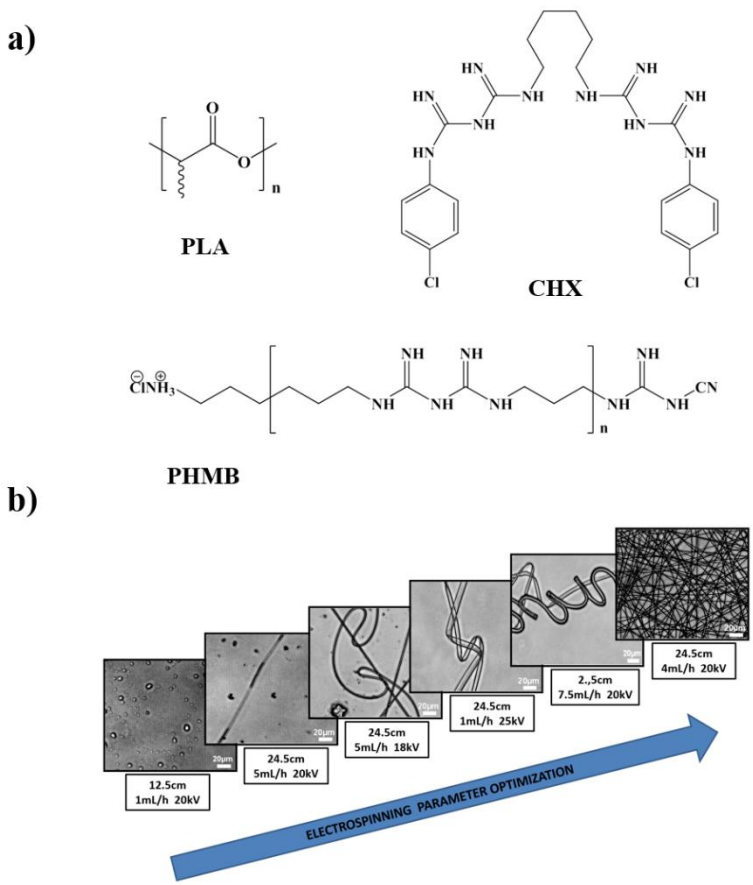

FIGURE 5.1.1

a) Chemical structures of polylactide, chlorhexidine and polyhexamethylenebiguanide hydrochloride. b) Optical micrographs of typical morphologies (e.g., drops, ribbons and nanofibers) of PLA-CHX 5 obtained byelectrospinning under different operational parameters and using a chloroform/acetone/formic acid mixture (1:2:0.3 *v/v/v*) as the solvent.

The electrospinning process was hampered by the drastic increase in viscosity of the PLA solution upon addition of CHX and PHMB. Maximum allowed concentrations were 0.5 *w/v*-% and 0.25 *w/v*-% for CHX and PHMB, respectively. Operational parameters were subsequently varied to avoid drop formation and produce continuous, homogeneous fibers (**Table 5.1.1**). **Figure 5.1.1 b** briefly illustrates all morphologies obtained and the optimization procedure where needle tip-collector distance, voltage and flow rate were varied in the 12.5-24.4 cm, 15-30 kV and 1-10 $mL \cdot h^{-1}$ ranges, respectively.

TABLE 5.1.1. Average diameter of electrospun samples processed in this study. Scaffold obtained under voltage, collector distance and flow rate of ([a]) 15 kV, 5 mL·h^{-1} and 12.5 cm, and ([b]) 20 kV, 4 mL·h^{-1} and 24.5 cm, respectively.

Sample	Ø(nm)
PLA[a]	1565 ± 22
PLA[b]	756 ± 80, 1350 ± 55
PLA-CHX 5[b]	627 ± 4
PLA-PHMB 0.2[b]	565 ± 2
PLA-PHMB 0.75[b]	589 ± 3
PLA-PHMB 1.5[b]	595 ± 4
PLA-PHMB 2.5[b]	610 ± 6

Morphology of PLA-PHMB Fibers

Figure 5.1.2 shows representative optical SEM micrographs of electrospun samples with different compositions and processed under optimal conditions. In general, long continuous micro/nanofibers could be obtained without bead formation. Their diameters varied in a relatively narrow range and showed a monomodal distribution. **Table 5.1.1** summarizes the average diameters, which ranged between 560 and 630 nm for drug loaded samples.

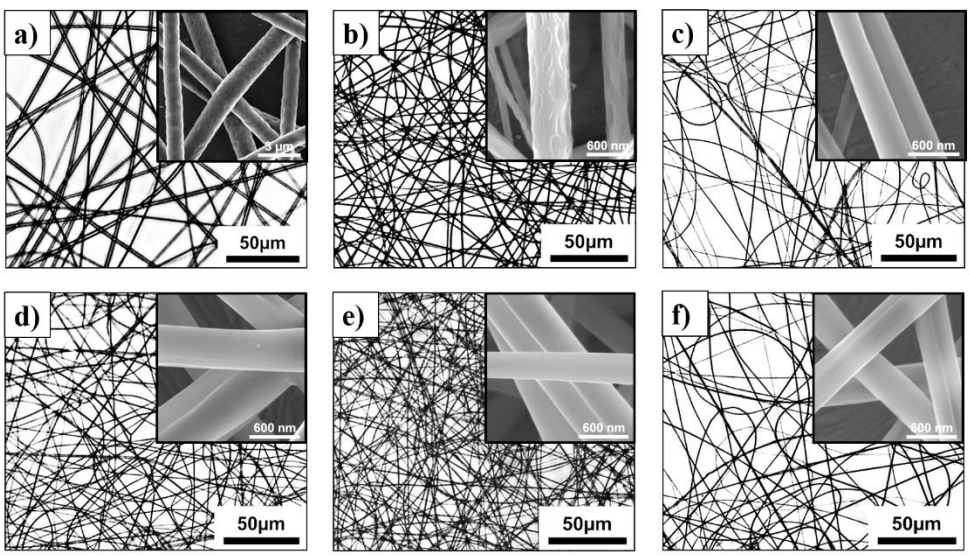

FIGURE 5.1.2

Optical and SEM (insets) micrographs of electrospun nanofibers obtained from a chloroform/acetone/formic acid mixture (1:2:0.3 *v*/*v*/*v*) using optimized concentration, voltage, needle tip-collector distance and flow rate: (a) PLA, (b) PLA-CHX 5 (c) PLAPHMB 2.5, (d) PLA-PHMB 1.5, (e) PLA-PHMB 0.75 and (f) PLA-PHMB 0.2.

It is interesting to note that a higher PHMB content in the electrospinning mixture led to a slight increase in the average diameter (i.e. values progressively increased from 565 to 610 nm when PHMB content increased from 0.2 to 2.5 *wt*-%). In fact, a linear dependence with a correlation coefficient of 0.95 was observed between PHMB concentration and fiber diameter. Surface texture of fibers also changed gradually with composition, as depicted in the high magnification images of the insets of **Figure 5.1.2**. A typical rough/porous surface of PLA fibers[35-37] and even of CHX loaded samples can be observed. However, scaffolds loaded with a relatively low PHMB concentration (e.g., 0.75 *wt*-%) became smooth.

Since fibers became highly heterogeneous (a bimodal distribution could even be envisaged), unloaded PLA was not successfully processed under the operational conditions determined for drug loaded samples (**Figure 5.1.3**). In this case, homogeneous samples were obtained when needle tip-collector distance, voltage and flow rate were 12.5 cm, 15 kV and 5 $mL \cdot h^{-1}$, respectively. It should be pointed out that the average diameter was smaller than previously reported[30] (i.e. 2 μm) due to the presence of formic acid, which probably modified surface tension and polarity.[38]

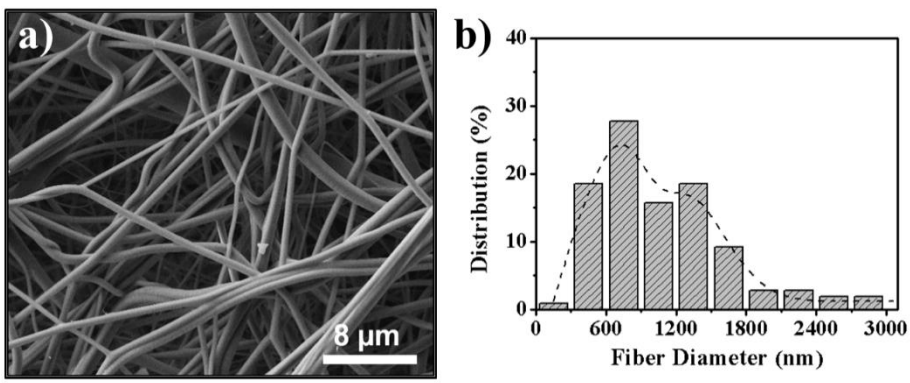

FIGURE 5.1.3

SEM micrograph (a) and diameter distribution (b) of electrospun PLA microfibers obtained at voltage, needle tip-collector distance and flow rate of 20 kV, 24.5 cm and 4 $mL \cdot h^{-1}$, respectively, and using a chloroform/acetone/formic acid mixture (1:2:0.3 *v/v/v*) as the solvent.

FTIR Characterization of PLA-PHMB Scaffolds

FTIR spectra of CHX and PHMB biocides (**Figure 5.1.4 a**) were similar and showed typical biguanide group signals in the 1550-1450 cm^{-1} region (see arrows in **Figure 5.1.4 a**). Thus, a C=N stretching band at 1490 and 1460 cm^{-1} and a strong NH band at 1537-1535 cm^{-1} were observed for PHMB and CHX, respectively.[16, 39]

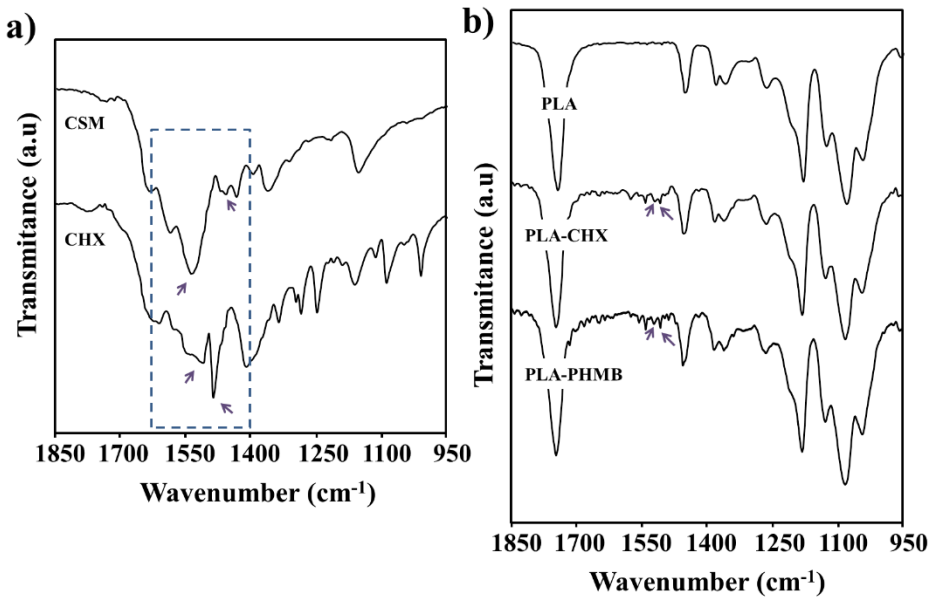

FIGURE 5.1.4

FTIR spectra (1850-950 cm^{-1}) of CHX and PHMB drugs (a) and PLA, PLA-CHX 5 and PLA-PHMB 2.5 scaffolds (b).

FTIR spectra of unloaded PLA, PLA-CHX 5 and PLA-PHMB 2.5 are compared in **Figure 5.1.4 b**. The presence of biguanide bands is corroborated in the loaded samples (see **Figure 5.1.4 a**) despite their low drug content. Characteristic PLA bands[40] are always observed (i.e. -C=O stretching at 1750 cm^{-1}, -CH_3 bending at 1449 cm^{-1} and –COC-vibration at 1181 cm^{-1} and 1083 cm^{-1}), with similar intensities for all bands, as expected for samples of similar crystallinity.

According to literature, the five conjugated amines of biguanide groups can bind neighboring molecules by establishing multiple hydrogen bonding interactions, which may be of interest in supramolecular chemistry.[41] For example, hydrogen bonding between PHMB and cellulose has previously been described.[29, 42]

FTIR spectra of PLA-PHMB and PLA-CHX scaffolds did not reveal any evidence of such interaction (e.g., a shift of the C=O absorption band towards a lower wavenumber), probably because of the low drug content and low sensitivity of the technique.

Thermal Properties of PLA-PHMB Scaffolds

Calorimetric data (i.e. glass transition, cold crystallization and melting temperatures as well as crystallization and melting enthalpies) of all electrospun samples are summarized in **Table 5.1.2**.

TABLE 5.12. Selected calorimetric data from the heating scan performed with the different PLAbiguanideelectrospun samples.

Sample	T_g (ºC)	T_c (ºC)	ΔH_c ($J \cdot g^{-1}$)	T_m (ºC)	ΔH_m ($J \cdot g^{-1}$)	$\Delta H_m - \Delta H_c$ ($J \cdot g^{-1}$)
PLA[o,a]	60.0	-	-	149.8	33.4	33.4
PLA[b]	58.7	113.4	19.8	146.6	20.1	0.3
PLA-CHX 5[b]	58.5	110.6	19.9	146.7	24.3	4.4
PLA-PHMB 0.2[b]	58.8	107.9	16.0	146.5	25.3	9.3
PLA-PHMB 0.75[b]	58.5	103.4	15.2	146.0	24.6	9.4
PLA-PHMB 1.5[b]	58.6	97.5	19.0	147.7	24.9	7.6
PLA-PHMB 2.5[b]	58.4	108.6	18.3	146.6	24.7	7.2

[a] Commercial sample included for comparison purposes.
[b] Scaffold obtained under voltage, collector distance and flow rate of 20 kV, 4 mL, 24.5 cm, respectively.

Several features deserve attention:

a) All samples had a clear glass transition, as expected for practically amorphous samples
b) Addition of CHX and PHMB did not affect the glass transition or melting temperatures,
c) A broad exothermic peak (70-130 ºC) corresponding to cold crystallization of PLA is always observed.

The high molecular orientation obtained in the electrospinning process facilitated PLA crystallization, as previously reported.[42] No samples were able to crystallize when slowly cooled from the melt or not even in a subsequent heating run due to lack of orientation and difficulty of PLA to crystallize, d) Melting enthalpy was slightly higher than crystallization enthalpy, indicating that even some fraction of PLA was able to crystallize during electrospinning. A slight difference was detected between ΔH_m of unloaded and drug loaded PLA. This was mainly due to the lower crystallinity attained in the electrospinning of PLA alone since in this case the operational parameters were modified. In fact, voltage and needle tip-collector distance were reduced and flow rate was increased. No specific trend was observed for cold crystallization enthalpies, suggesting that variation in fiber diameter had very little influence in the range between 550 and 1600 nm.

Contact Angles Measurements on the PLA-PHMB Scaffolds

Although both surface energy and roughness are the dominant factors in wettability of materials, surface roughness is the key factor after selection of the components of materials. To clarify the effect of electrospinning and drug concentration on the surface properties of scaffolds, water contact angles were measured. For the sake of completeness, contact angle was also determined for smooth PLA films, see **Figure 5.1.5 a**.

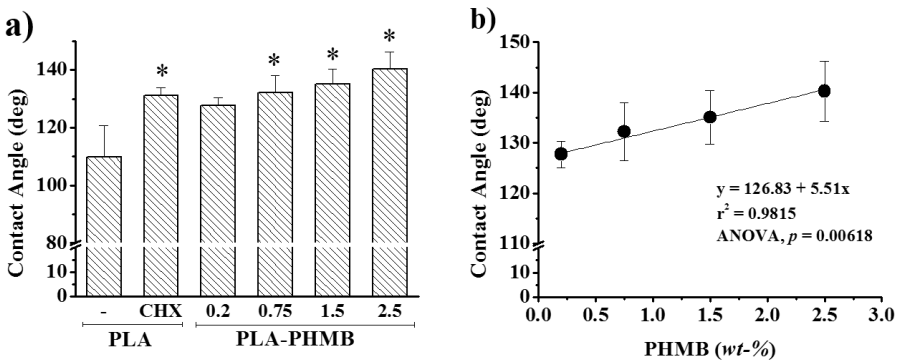

FIGURE 5.1.5

a) Contact angles for PLA, PLA-CHX 5 and PLA-PHMB scaffolds loaded with drug *wt*-% ranging from 0.2 to 2.5 (* $p < 0.05$ vs unloaded PLA, Tukey's test). b) Correlation between contact angle and *wt*-% of PHMB in PLA scaffolds.

Some points are worth noting:

- Contact angle increased drastically in the PLA scaffold constituted by microfibers compared to the film (i.e. from 95º to 110º), showing the increase in surface area caused by roughness. The impact of roughness on the contact angle is given by the Wenzel **Equation 1**:[43]

$$\cos \theta W = r \cos \theta Y \qquad (1)$$

which relates the contact angle on a rough surface, θ_W, with the roughness ratio of the surface, r, and the contact angle on a smooth surface, θ_Y.

Wenzel's relation shows that surface roughness will increase the contact angle for a droplet on hydrophobic surfaces since the ratio between the true surface area of a rough surface and the surface area of a comparably sized smooth surface is always greater than one.

- The contact angle of drug loaded scaffolds increased significantly ($p < 0.05$) compared to the unloaded PLA scaffold. This cannot be justified in terms of roughness as the diameter of loaded fibers was clearly smaller than that of unloaded fibers, and consequently a smoother surface should be expected. The hydrophobicity increase

seems to be a direct consequence of adding biguanide groups able to establish hydrogen bonding interactions with the polylactide ester groups. Note that PLA-CHX 5 and PLAPHMB 1.5 samples have a similar number of biguanide groups, and therefore similar contact angle values (131º ± 3º and 135º ± 5º). The result is surprising since both CHX and PHMB molecules have a hydrophilic character but increase the hydrophobicity of a PLA matrix when mixed.

- The increase in PHMB content led to a linear increase of the contact angle (i.e. from 127.8° to 140.3º for 0.2 to 2 *wt*-% loaded samples, respectively), as shown in **Figure 5.1.5 b**. This reflects again the effect of intermolecular interactions. However, surface roughness should be slightly higher since fiber diameters evolved similarly with PHMB content (**Table 5.1.1**).[44] In any case, this effect should be insignificant due the low range of diameters (565-627 nm) compared with the small change in contact angle between loaded and unloaded PLA samples, whose constituent fibers are highly different in diameter (i.e. 1565 nm and 565-627 nm).

Biguanide Release from Polylactide Scaffolds

The release of biguanide complexes from an electrospun matrix is intimately related to the morphology and structure of constituent fibers and to the release environment. In fact, the rate of diffusion-controlled drug release depends on three main factors: a) Solubility of the drug in the release medium, b) Ability of the medium to penetrate the polymer matrix, and c) Physical interactions between polymer and drug.[45]

The release of CHX and PHMB from PLA scaffolds was studied in media with different hydrophobicity/hydrophilicity ratios (i.e. PBS and PBS-EtOH 9:1, 5:5, 3:7 and 1:9 *v/v* mixtures). Specifically, ethanol has higher affinity with PLA than water and can have a swelling effect that facilitates drug release. To demonstrate the swelling action of ethanol on PLA scaffolds, a 24 h immersion test was carried out with PLA-PHMB 2.5. **Figure 5.1.6** shows that after immersion the average fiber diameter increased from an initial value of 610 nm to 750 nm and maintained a monomodal distribution. Thus, fibers swelled homogeneously, and even the surface texture changed and became rougher.

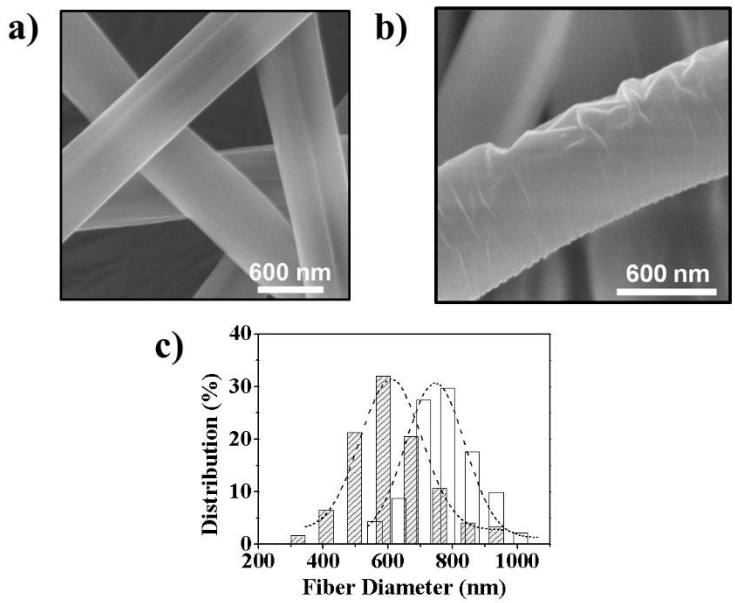

FIGURE 5.1.6

SEM micrographs of morphological details of PHMB 2.5 before (a) and after immersion in ethanol (b). Diameter distributions of PHMB 2.5 nanofibers before and after immersion in ethanol (c).

Figure 5.1.7 compares the release of CHX and PHMB from scaffolds loaded with the maximum amount of drug in a representative hydrophobic medium (PBS-EtOH 3:7 *v*/*v*) and the most hydrophilic one (PBS buffer).

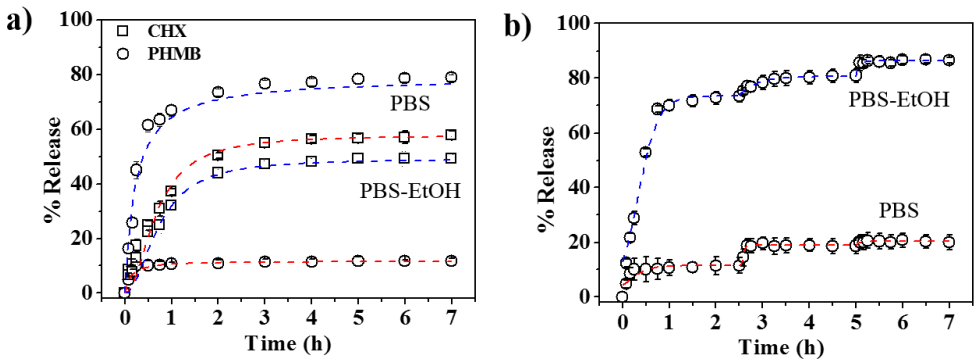

FIGURE 5.1.7

(a) Drug release profiles of PLA-CHX 5 and PLA-PHMB 2.5 in PBS (red line) and PBS-EtOH 3:7 *v*/*v* (blue line). (b) Release profiles of PHMB 2.5 in PBS (red line) and PBS-EtOH 3:7 *v*/*v* (blue line) obtained when the medium was renewed every 2.5 h.

The release kinetics can be calculated from experimental results by several theoretical models, typically first-order[45, 46] and Higuchi[47, 48] models. Drug release generally occurs in two steps, i.e., a rapid release of molecules that should deposit mainly on the high surface area of fibers and a slow release that should involve the diffusion of molecules through the polymer bulk towards the outer medium. In this way, a combined model based on the two above models is usually used to describe the first (0-60%) and second (40-100%) parts of the release,[49, 50] as stated in **Equations 2** (Higuchi model) and **3** (first-order model):

$$M_t/M_0 = k_H t^{1/2} \qquad \left(0 \leq \frac{M_t}{M_0} \leq 0.6\right) \qquad (2)$$

$$\ln\left(1-\frac{M_t}{M_0}\right) = a - k_1 t \qquad \left(0.4 \leq \frac{M_t}{M_0} \leq 1.0\right) \qquad (3)$$

where k_H and k_1 are the Higuchi and first-order release constant, respectively, a takes into account the release in the first step, M_t is the percentage of drug released at time t, and M_0 is the drug equilibrium percentage (considered as the maximum drug percentage).

TABLE 5.1.3. Release kinetic parameters for PLA-CHX 5 and PLA-PHMB 2.5 scaffolds

Drug	Media	k_H ($h^{-0.5}$)	r	k_1 (h^{-1})	r
PHMB	PBS	0.985	0.97	0.568	0.976
	PBS-EtOH 9:1 *v/v*	0.527	0.97	0.679	0.973
	PBS-EtOH 5:5 *v/v*	0.798	0.96	0.676	0.956
	PBS-EtOH 3:7 *v/v*	1.107	0.97	0.756	0.996
	PBS-EtOH 1:9 *v/v*	1.028	0.96	0.824	0.992
CHX	PBS	0.609	0.99	0.737	0.982
	PBS-EtOH 3:7 *v/v*	0.598	0.95	1.149	0.981

Kinetic data in **Table 5.1.3** and release profiles in **Figure 5.1.7** are worth discussing:

- CHX and PHMB showed very different release profiles in the studied media. The fact that each PHMB molecule has several biguanide groups able to interact with all polymer chains of the matrix and the slower diffusion rate through the matrix caused by its higher molecular size play a fundamental role.
- The first part of the release was clearly slower for CHX independent of the hydrophobic/hydrophilic character of the medium. Smaller values were determined for the Higuchi constant, suggesting that a greater ratio of the small CHX molecules was incorporated into the inner part of electrospun nanofibers whereas a higher ratio of PHMB molecules was incorporated into the outer part. Note that just the opposite release behavior was expected considering the higher binding capabilities and diffusion rate of PHMB.

- The release of CHX was similar but slightly greater (i.e. 58% versus 49%) in a more hydrophilic medium (i.e. PBS), in agreement with the hydrophilic character of CHX and its greater solubility in water.
- Release constants for PHMB increased gradually with the ethanol content in release media because of the swelling effect of ethanol.
- A huge difference in the final release of PHMB was found between PBS and PBS/ethanol mixtures. This behavior contrasts with that observed for CHX and seems opposite to the solubility characteristics of PHMB. Interactions of biguanide groups with PLA may explain this phenomenon if a competitive binding exists between PLA and ethanol molecules. Note also that the hydrophobic character of PLA can give rise to a contraction in aqueous media that hinders access of water molecules to the binding sites and PHMB release.

Release profiles always reached an asymptotic value lower than 100% because of the establishment of equilibrium conditions. **Figure 5.1.7 b** clearly demonstrates that release was able to follow a similar profile (i.e. similar release constants) both in hydrophilic and hydrophobic media when the medium was renewed after reaching equilibrium.

Antibacterial Assays of Biguanide Loaded PLA Scaffolds

Chemical-releasing, bacteria-killing capacity of PHMB loaded scaffolds was evaluated, together with their effect to inhibit bacterial adhesion. Specifically, *Escherichia coli* and *Micrococcus luteus* were considered as examples of Gram-negative and Gram-positive bacteria, respectively.

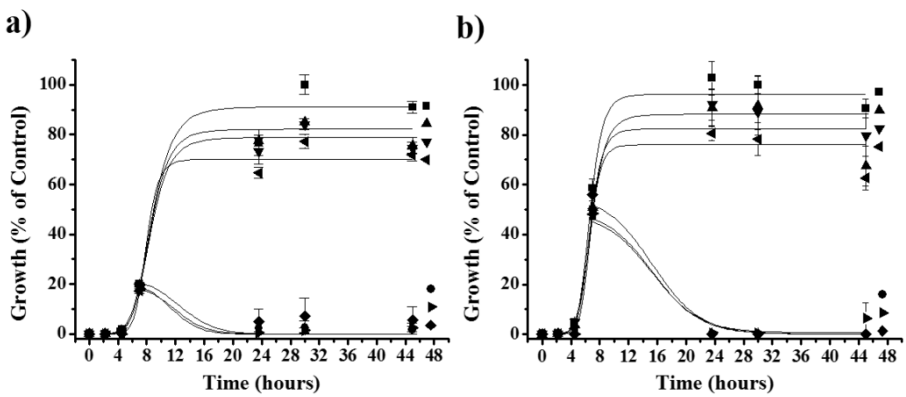

FIGURE 5.1.8

Growth curves of *Escherichia coli* (a) and *Micrococcus luteus* (b) bacteria on the scaffolds. Growth on culture plate (PS) as positive control (■) and scaffolds of PLA (▲), PLA-CHX (▲) and PLA-PHMB 0.2 (▼), PLA-PHMB 0.75 (◄), PLA-PHMB 1.5 (►), PLA-PHMB 2.5 (♦).

Figure 5.1.8 shows the bacterial growth curves for *E. coli* and *M. luteus* culture media in contact with scaffolds loaded with different PHMB contents. Typical bacterial growth dynamics were found with PLA-PHMB 0.2 and PLA-PHMB 0.75 samples. Thus, the initial lag phase (4-5 hours), the exponential phase associated with binary fission, and the death phase associated with loss of viability could be detected. Total growth inhibition (i.e. growth lower than 1% compared to the positive control) was observed for both bacteria after 24 hours of culture. This inhibitory effect was similar for PLA-CHX 5, considered the positive control. It is interesting to remark that the inhibitory effect of bacterial growth did not occur initially, and even the bacteria had the ability to remain viable during the lag phase (4-5 hours) and enter the exponential growth phase reaching relative values of 20% and 50% with respect to the control after 7-8 hours of culture for *E. coli* and *M. luteus*, respectively. Furthermore, during bacterial growth, the beginning of the bacterial death phase was fully coincident with the PHMB release profile (see **Figure 5.1.6**).

Scaffolds loaded with lower PHMB concentrations (i.e. PLA-PHMB 0.2 and PLA-PHMB 0.75) also showed an antibacterial effect, although no death phase could be observed after 45 hours of culture. In these cases, bacterial division ceased and growth curves finished in a stationary phase. Logistic models adjusted for growth of *E. coli* and *M. luteus* (**Figure 5.1.8**) showed maximum growths around 91-88%, 82-83% and 70-76% for the control (polystyrene plate) and scaffolds loaded with 0.2 and 0.75 *wt*-%, respectively. The results demonstrate antibacterial activity of PLA-PHMB scaffolds that was clearly dependent on drug concentration.

Adhesion percentages of *E. coli* and *M. luteus* on PLA scaffolds loaded with different PHMB concentrations and the PLA-CHX 5 positive control are shown in **Figure 5.1.9 a**. The bacterial adhesion rate of this control, as well as the PLA matrices loaded with the higher PHMB concentrations, decreased dramatically (i.e. 1.5 and 2.5 *wt-%*). Thus, relative adhesion of *E. coli* ranged between 3 and 15% while it was slightly lower for *M. luteus* (e.g., 3 and 10% of relative adhesion were determined for the PLA-PHMB 1.5 scaffold). It should pointed out that the similar number of biguanide groups in the PLA-CHX 5 and PLA-PHMB 1.5 scaffolds led to a similar reduction of bacterial adhesion.

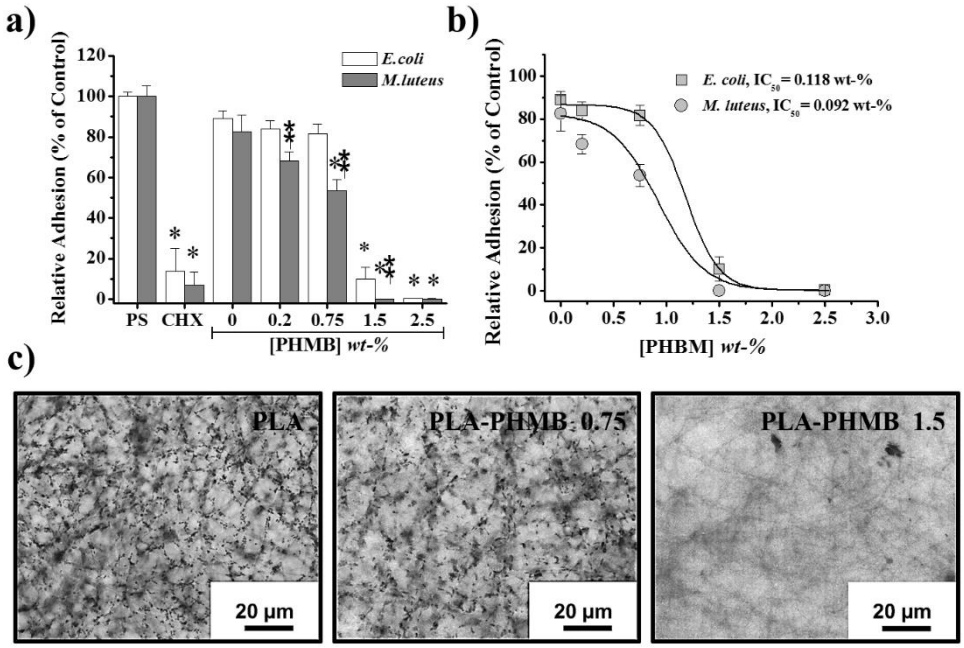

FIGURE 5.1.9

(a) Bacterial adhesion on polystyrene plate (PS) as positive control and PLA, PLA-CHX and PLA-PHMB scaffolds (*$p < 0.05$ *vs.* unloaded PLA matrix, Tukey's test. ‡$p < 0.05$ between two types of bacteria, t-Test). (b) Dose-dependent curves of inhibition of bacterial adhesion on PLA-PHMB scaffolds. (c) Representative optical micrographs of adhesion of *Micrococcus luteus* on PLA and PLA-PHMB scaffolds.

Scaffolds loaded with low PHMB concentration showed a smaller decrease in bacterial adhesion, which became clearly dependent on the type of bacteria (Gram-positive or Gram-negative) and loaded drug percentage. Specifically, *M. luteus* exhibited a notorious and statistically significant ($p < 0.05$) reduction of adhesion compared to unloaded PLA scaffolds. This difference was analyzed with a dose-dependent adhesion model (**Figure 5.1.9 b**), which detected a severe decrease in the bacterial adhesion rate in the PHMB concentration range between 0.75 and 1.5 *wt*-%. Thus, the 50% inhibitory concentration (IC_{50}) of bacterial adhesion can be used as a good indicator of bacterial sensitivity (**Figure 5.1.9 b**). Values of 0.92 *wt*-% and 1.18 *wt*-% were determined using the models adjusted for M. luteus, and E. coli, respectively, with the latter exhibiting higher resistance to the antibacterial agent.

Lastly, PLA scaffolds are highly susceptible to be colonized by bacteria, as can be seen in the micrograph of **Figure 5.1.9 c**. This can be effectively avoided by loading a low PHMB ratio, as also shown in **Figure 5.1.9 c** for a representative sample.

Cell Adhesion and Growth in the Biguanide Loaded PLA Scaffolds

PLA scaffolds prepared from electrospun micro/nanofibers had a 3D pore structure that provided excellent cell adhesion for both types of cells (MRC5 and MDCK), as shown in **Figure 5.1.10** a. The adhesion percentages were higher for fibroblast cells (MRC5) than for epithelial cells (MDCK). Low cell adhesion percentages were determined for both cell lines when cultured over the PLA-PHMB 2.5 scaffold because of the cytotoxic effect produced by the high PHMB concentration. A slightly different cytotoxic behavior was also observed in PHMB and CHX samples since cytotoxicity of PLA-CHX 5 was clearly higher than that of PLA-PHMB 1.5, which had the same number of biguanide groups, and a similar one to that found for PLA-PHMB 2.5. This behavior shows again the difference in release behavior between small and large drugs containing biguanide groups.

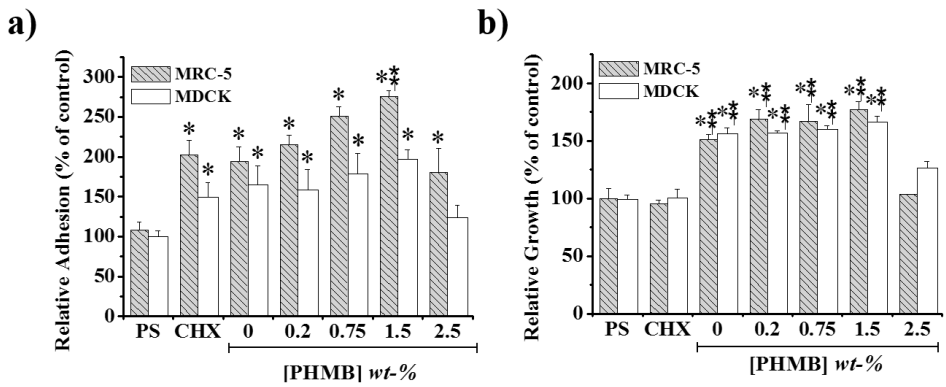

FIGURE 5.1.10

Adhesion (a) and proliferation (b) of MRC-5 and MDCK cells on polystyrene plate (PS, culture plate) as positive control and PLA, PLA-CHX and PLA-PHMB scaffolds ($^{*}p < 0.05$) *vs.* positive control, $^{**}p < 0.05$ *vs.* PLA-CHX; ANOVA-Tukey's test).

The MRC-5 and MDCK cells proliferated on unloaded PLA and PLA matrices loaded with PHMB concentrations lower than 1.5 *wt*-% (**Figure 5.1.10 b**). Growth percentages were significantly ($p < 0.05$) higher than those determined for the positive control (PS plate) and PLA-CHX 5 and PLA-PHMB 2.5 scaffolds. This led to the conclusion that new scaffolds were fully biocompatible provided that drug concentration did not exceed a certain percentage (i.e. 1.5 *wt*-% for PLA-PHMB 1.5 scaffolds). Micrographs of cellular monolayers in the matrices more cytotoxic PLA-CHX 5 and PLA-PHMB 2.5 scaffolds are given in **Figure 5.1.11**.

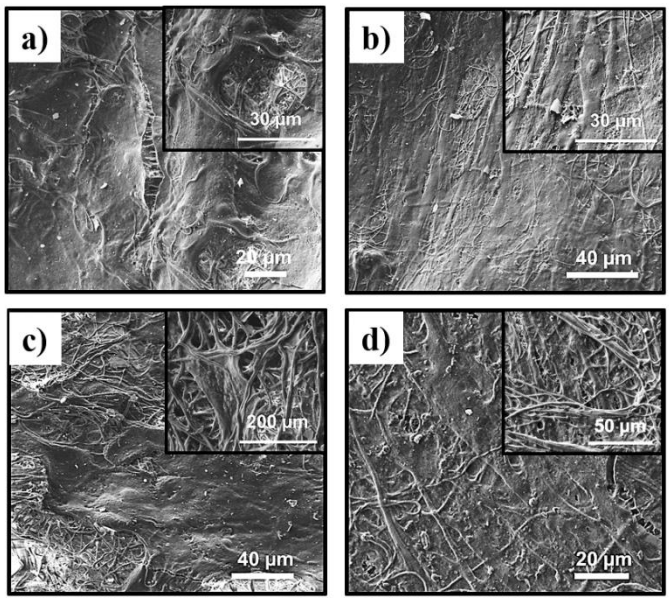

FIGURE 5.1.11

SEM micrographs of the cellular proliferation on representative scaffolds. MDCK cells (a, c) and MRC-5 cells (b, d). The cells monolayer formation is shown on PLA-PHMB 0.75 (a, b), the inset shows detailed of cell spreading. The cellular growth in the PLA-PHMB 2.5 (c,d) scaffold is shown in the inset.

Loaded scaffolds acted as controlled release systems and allowed the addition of an antibacterial amount higher than the cytotoxic value. **Figure 5.1.12 a** summarizes the evaluation results of PHMB cytotoxicity considering two possibilities: a) Addition of a PHMB solution to a fibroblast cell monolayer and b) Addition of a PHMB solution to a fibroblast cell suspension before attachment on the plate. Cytotoxic concentrations to reduce cell population by 50% (CC_{50}) were approximately 0.01 *w/v*-% and 0.03 *w/v*-% for the first and second case, respectively. Results indicate that cells were more sensitive to the oligomeric drug when tissue (i.e. a monolayer) was formed and less sensitive in suspension (e.g., during colonization of material or cell division). These results are in agreement with the oligomeric structure of PHMB, which contains an average number of 7-11 biguanide groups. This molecule established several simultaneous cell interactions on a cell monolayer, facilitating cell death compared to cells in suspension, as schematically shown in **Figure 5.1.12 b**.

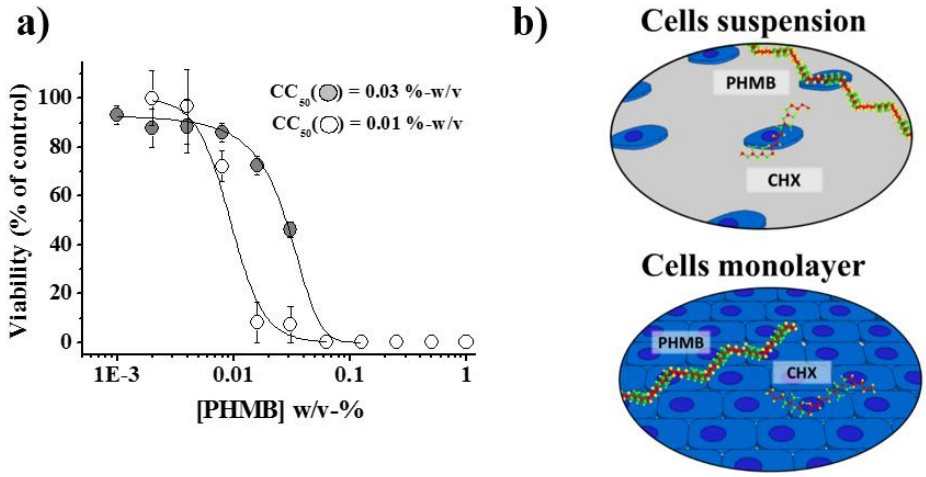

FIGURE 5.1.12

a) Cytotoxicity curves in fibroblast cells (MRC-5 cells) forming a monolayer (○) or in suspension (●) for exposure to PHMB solutions. b) Scheme of the interaction of oligomeric PHMB and monomeric CHX with cells forming a monolayer or in suspension.

5.1.4 Conclusions

PLA nanofibers loaded with PHMB and having average diameters ranging between 560 and 630 nm were obtained by electrospinning and using a chloroform/acetone/formic acid mixture (1:2:0.3 *v*/*v*/*v*) as a solvent. The fiber diameter increased and the surface texture became smoother with increasing the loaded PHMB concentration. Nanofibers had a high molecular orientation that facilitated PLA cold crystallization during heating.

Addition of PHMB to PLA scaffolds increased the hydrophobicity of the sample, which was surprising considering the hydrophilic character of PHMB. The highly-hydrophobicity of these scaffolds conditioned PHMB release, which was prevented in the hydrophilic medium and was facilitated when hydrophobicity was more hydrophobic. The molecular size of PHMB also resulted in a clearly different release behavior from that of the biguanide monomer. PHMB released from PLA scaffolds inhibited bacterial growth and prevented cell adhesion and colonization due to controlled and sustained release. The significant inhibition of bacterial growth required a PHMB concentration higher than 0.75 *wt*-%.

PHMB loaded scaffolds were fully biocompatible and led to significant adhesion and proliferation of both fibroblast and epithelial cell lines. Controlled release made it possible to load scaffolds with a large amount of PHMB, which was higher than the cytotoxic dose (CC_{50}).

In summary, addition of PHMB to PLA scaffolds resulted in characteristics different from those obtained by addition of small drugs (CHX) containing a single biguanide group. These PHMB loaded scaffolds are particularly interesting because of their potential biomedical applications.

5.1.5 References

[1] R. Ben-Knaz, R. Pedahzur, D. Avnir, Adv Funct Mater, 20 (2010) 2324-2329.

[2] R.J.W. Lambert, M.D. Johnston, G.W. Hanlon, S.P. Denyer, J App Microbiol, 94 (2003) 747-759.

[3] H. Behar-Levy, D. Avnir, Chem Mater, 14 (2002) 1736-1741.

[4] S. Pal, E.J. Yoon, S.H. Park, E.C. Choi, J.M. Song, J Antimicrob Chemoth, 65 (2010) 2134-2140.

[5] D.S. Jones, A.F. Brown, A.D. Woolfson, A.C. Dennis, L.J. Matchett, S.E.J. Bell, J Pharm Sci, 89 (2000) 563-571.

[6] M. Addy, Adv Drug Deliver Rev, 13 (1994) 123-134.

[7] G.E. McDonnell, First Edition ed., ASM Press, Washington D.C., 2007.

[8] D.R. Monteiro, L.F. Gorup, A.S. Takamiya, A.C. Ruvollo, E.R. Camargo, D.B. Barbosa, Int J Antimicrob Ag, 34 (2009) 103-110.

[9] M. Zilberman, J.J. Elsner, J Control Release, 130 (2008) 202-215.

[10] K. Kaehn, Skin Pharmacol Phys, 23 (2010) 7-16.

[11] J.B.D. Green, T. Fulghum, M.A. Nordhaus, First Edition ed., Formatex, Badajoz, 2011.

[12] K. Vasilev, J. Cook, H.J. Griesser, Expert Rev Med Devic, 6 (2009) 553-567.

[13] M. Charnley, M. Textor, C. Acikgoz, React Funct Polym, 71 (2011) 329-334.

[14] A.M. Milstone, C.L. Passaretti, T.M. Perl, Clin Infect Dis, 46 (2008) 274-281.

[15] K.S. Lim, P.C.A. Kam, Anaesth Intens Care, 36 (2008) 502-512.

[16] G.F. de Paula, G.I. Netto, L.H.C. Mattoso, Polymers, 3 (2011) 928-941.

[17] B. Roth, F.H.H. Brill, Skin Pharmacol Phys, 23 (2010) 4-6.

[18] M.J. Allen, G.F. White, A.P. Morby, Microbiology, 152 (2006) 989-1000.

[19] P. Gilbert, D. Pemberton, D.E. Wilkinson, J App Bacteriol, 69 (1990) 593-598.

[20] T. Koburger, N.O. Hubner, M. Braun, J. Siebert, A. Kramer, J Antimicrob Chemoth, 65 (2010) 1712-1719.

[21] Y. You, B.M. Min, S.J. Lee, T.S. Lee, W.H. Park, J Appl Polym Sci, 95 (2005) 193-200.

[22] S.G. Cao, B.H. Hu, H.Q. Liu, Acta Polym Sin, (2010) 1193-1198.

[23] V. Thomas, M.V. Jose, S. Chowdhury, J.F. Sullivan, D.R. Dean, Y.K. Vohra, J Biomat Sci Polym E, 17 (2006) 969-984.

[24] S.A. Sell, M.J. McClure, K. Garg, P.S. Wolfe, G.L. Bowlin, Adv Drug Deliver Rev, 61 (2009) 1007-1019.

[25] Z.G. Chen, X.M. Mo, F.L. Qing, Mater Lett, 61 (2007) 3490-3494.

[26] H. Homayoni, S.A.H. Ravandi, M. Valizadeh, Carbohyd Polym, 77 (2009) 656-661.

[27] N. Hiraishi, C.K.Y. Yiu, N.M. King, F.R. Tay, D.H. Pashley, Dent Mater, 24 (2008) 1391-1399.

[28] Y.N. Lin, K.M. Chang, S.C. Jeng, P.Y. Lin, R.Q. Hsu, J Mater Sci Mater M, 22 (2011) 571-577.

[29] X. Liu, T. Lin, Y. Gao, Z. Xu, C. Huang, G. Yao, L. Jiang, Y. Tang, X. Wang, J Biomed Mater Res B Appl Biomater, 100 (2012) 1556-1565.

[30] L.J. del Valle, R. Camps, A. Diaz, L. Franco, A. Rodriguez-Galan, J. Puiggali, J Polym Res, 18 (2011) 1903-1917.

[31] S.V. Fridrikh, J.H. Yu, M.P. Brenner, G.C. Rutledge, Phys Rev Lett, 90 (2003) 144502-144504.

[32] M.G. McKee, C.L. Elkins, T.E. Long, Polymer, 45 (2004) 8705-8715.

[33] C.J. Luo, M. Nangrejo, M. Edirisinghe, Polymer, 51 (2010) 1654-1662.

[34] E. Armelin, A.L. Gomes, M.M. Perez-Madrigal, J. Puiggali, L. Franco, L.J. del Valle, A. Rodriguez-Galan, J.S.D. Campos, N. Ferrer-Anglada, C. Aleman, J Mater Chem, 22 (2012) 585-594.

[35] A. Agrawal, A.D. Saran, S.S. Rath, A. Khanna, Polymer, 45 (2004) 8603-8612.

[36] Z.G. Wang, L.S. Wan, Z.M. Liu, X.J. Huang, Z.K. Xu, J Mol Catal B-Enzym, 56 (2009) 189-195.

[37] Z.M. Huang, Y.Z. Zhang, M. Kotaki, S. Ramakrishna, Compos Sci Technol, 63 (2003) 2223-2253.

[38] N. Bhardwaj, S.C. Kundu, Biotech Adv, 28 (2010) 325-347.

[39] L. Chen, L. Bromberg, T.A. Hatton, G.C. Rutledge, Polymer, 49 (2008) 1266-1275.

[40] G. Kister, G. Cassanas, M. Vert, Polymer, 39 (1998) 3335-3340.

[41] O. Lebel, T. Maris, J.D. Wuest, Can J Chem, 84 (2006) 1426-1433.

[42] R.S. Blackburn, A. Harvey, L.L. Kettle, J.D. Payne, S.J. Russell, Langmuir, 22 (2006) 5636-5644.

[43] R.N. Wenzel, Ind Eng Chem, 28 (1936) 988-994.

[44] S.B. Zhou, H.S. Peng, X.J. Yu, X.T. Zheng, W.G. Cui, Z.R. Zhang, X.H. Li, J.X. Wang, J. Weng, W.X. Jia, F. Li, J Phys Chem B, 112 (2008) 11209-11216.

[45] H. Liu, K.K. Leonas, Y.P. Zhao, J Eng Fiber Fabr, 5 (2010) 10-19.

[46] M. Gibaldi, S. Feldman, J Pharm Sci, 56 (1967) 1238-1242.

[47] J.G. Wagner, J Pharm Sci, 58 (1969) 1253-1257.

[48] T. Higuchi, J Pharm Sci, 50 (1961) 874-875.

[49] T. Higuchi, J Pharm Sci, 52 (1963) 1145-1149.

[50] R.W. Baker, John Wiley & Sons, New York, USA, 1987.

5.2 Electrospun Nanofibers from Biodegradable Polylactide and Conducting Poly(3-Thiophene Methyl Acetate) Mixtures

Hybrid scaffolds constituted by polylactide (PLA) as a biodegradable polymer and poly(3-thiophene methyl acetate) (P3TMA) as an electroactive polymer were prepared and studied. Both polymers had a similar solubility and consequently could be easily electrospun using a common solvent. Electrospinning operational parameters were optimized to get continuous micro/nanofibers with a homogeneous diameter that ranged between 600 and 900 nm depending on the PLA/P3TMA ratio. Electrospinning was only effective when the P3TMA content was at maximum 50 wt-%. The incorporation of P3TMA slightly decreased the fibre diameter, led to smoother fibre surfaces and gave rise to some heterogeneous clusters inside the fibers. PLA was highly oriented inside the electrospun fibers and able to easily cold crystallize by heating. Thermal degradation was not highly influenced by the presence of P3TMA, although the onset temperature slightly increased since the first decomposition step of PLA was prevented. New scaffolds had promising electrochemical properties and even provided a good substrate for cell adhesion and cell proliferation. Therefore, these hybrids materials are suitable to improve the cellular response towards physiological processes.

5.2.1 Introduction

Polymeric materials with both biodegradable and electrically conducting properties have a growing interest in biomedical applications because of both the lack of long-term health risk and their good behavior as supportive matrix for tissue regeneration. The electrochemical response of conducting polymers makes feasible the local stimulation of desired tissue and the enhancement of either the proliferation or differentiation of various cell types.[1-4] Nevertheless, it remains a considerable challenge to synthesize an ideal electroactive polymer that meets the biocompatibility and biodegradability requirements to minimize the inflammatory reaction in the host tissue that could be raised by the use of non-degradable materials. An alternative strategy is the use of conducting polymer/biopolymer blends since unique properties that justify their potential technological applications in biomedical devices can be achieved.

The requirements for materials used in tissue engineering applications are biocompatibility and biodegradability since they should degrade with time and should be replaced with newly regenerated tissues. The architecture of the biomaterial is also very important and, specifically, scaffolds constituted by electrospun nanofibers have promising features, such as big surface area for absorbing proteins and abundance of binding sites for cell membrane receptors.

Ultrathin fibers from a wide range of polymer materials can be easily prepared by electrospinning.[5-11] This electrostatic technique involves the use of a high voltage field to charge the surface of a polymer solution droplet, held at the end of a capillary tube, and induce the ejection of a liquid jet towards a grounded target (collector).

Two different approaches have been applied to develop scaffolds constituted by conducting and biodegradable polymers: a) By coating an electrospun mat of a well-known biocompatible and reabsorbable biomaterial with the conducting polymer; and b) By direct electrospinning of a conducting/biodegradable polymer mixture. The second option is easier to perform but requires a good solubility of the conducting polymer in the electrospinning solution and gives rise to scaffolds with lower conductivity.

First works providing novel conductive materials well suited as biocompatible scaffolds for tissue engineering involved polyaniline-gelatin blend nanofibers.[12] Picciani *et al*.[13] considered the use of poly(L-lactide) as the support polymeric matrix for the preparation of polyaniline-based conducting nanofibers and evaluated the influence of operational parameters on the morphology of electrospun fibers. Several polyaniline and poly(D,L-lactide) mixtures at different weight percents were also successfully electrospun from 1,1,1,3,3,3-hexafluoroisopropanol solutions and their conductivity and biocompatibility evaluated.[14] Nanofibrous blends of HCl-doped poly(aniline-co-3-aminobenzoic acid) copolymer and poly(lactic acid) (PLA) were fabricated by electrospinning solutions of the polymers in a dimethyl sulfoxide/tetrahydrofuran mixture.[15] Scarce works concern the electrospinning of mixtures based on polypyrrole and basically deal with scaffolds constituted by polypyrrole/polycaprolactone (PCL)/gelatin nanofibers.[16] Specifically, conductive nanofibers

containing 15% polypyrrole exhibited the most suitable balance of electrical conductivity, mechanical properties and biodegradability, matching the requirements for the regeneration of cardiac tissue. Furthermore, such scaffold promoted cell attachment and proliferation as well as the interaction and expression of cardiac-specific proteins.

Polythiophenes constitute a group of conducting polymers with high technological potential due to their optical, electroluminescents, electronic and, specially, electrochemical properties.[17, 18] Different derivatives can be considered and, specifically, several works were focused on the preparation of nanofibers from mixtures of poly(3-hexylthiophene) (P3HT) and PCL or poly(lactic-co-glycolic acid) (PLGA) as biodegradable polymers.[19, 20] Thus, P3HT domains in concentrated PCL solution were highly stretched from the electrospinning electrode and formed fibrils with very small diameters (i.e. ~30 nm) embedded inside PCL composite fibers. Interestingly, fibrils became connected one to another during the volume shrinkage of the solution by solvent evaporation, generating PCL composite fibers with continuous P3HT fibrils embedded inside. On the other hand, it was found that PLGA–P3HT nanofibers have a significant influence on cell adhesion and proliferation. These new electrically conducting axially aligned nanofibers provided both electrical and structural cues and could be potentially used as scaffolds for neural regeneration.

Poly(3-thiophene methyl acetate) (P3TMA) is another polythiophene derivative that is characterized by bearing carboxylate substituents in the 3-position of the heterocyclic ring. The polymer can be easily prepared via oxidative chemical[21] and photochemical[22] reactions and appears a suitable candidate for being processed by electrospinning since has a good solubility in organic solvents like chloroform. Furthermore, it has currently been demonstrated that very stable free-standing nanomembranes with electroactive and biodegradable properties can be prepared by combining P3TMA and polyesters, such as poly(tetramethylene succinate), and even thermoplastic polyurethanes and poly(vinylidene fluoride).[21-24]

The main goal of the present work is the establishment of the electrospun conditions required to get continuous micro/nanofibers from mixtures of P3TMA with PLA as well as to perform a basic characterization of morphology and properties (e.g., ability to store charge and biocompatibility) of the derived scaffolds. PLA has been just selected as the biodegradable component due to its excellent properties and its wide use in the biomedical field.

5.2.2 Experimental Section

Materials

3-Thiophene acetic acid (3TAA) (98.0%) was purchased from Fluka (Sigma-Aldrich). Iron chloride anhydrous (97.0%), dry methanol (99.5%), chloroform (99.9%) were purchased from Panreac Quimica S.A.U. (Spain) and used as received without further purification. PLA, a product of Natureworks (polymer 2002D), was kindly supplied by Nupik International (Polinyà, Spain). According to the manufacturer, this PLA has a D content of 4.25%, a residual monomer content of 0.3%, a density of 1.24 $g \cdot cc^{-1}$, a glass transition temperature (T_g) of 58 ºC and a melting point of 153 ºC.
Kidney epithelial cells derived from African green monkey (VERO) were purchased from ATCC (USA).

Synthesis of poly(3-thiophene methyl acetate)

The 3-thiophene methyl acetate (3TMA) monomer was obtained with a 74% yield by refluxing 3TAA in dry methanol for 24 hours at a temperature of 90 ºC.[21] The polythiophene derivative, P3TMA, was subsequently prepared by a chemical oxidative coupling in dry chloroform following the procedure described by Kim *et al*.[25] Anhydrous ferric chloride ($FeCl_3$) was used as oxidant and dopant. The polymerization yield was ca. 61% after removing the residual oxidant and oligomers.
Molecular weights and polydispersity index (PDI) were estimated by size exclusion chromatography (SEC) using a liquid chromatograph (Shimadzu, model LC-8A) equipped with an Empower computer program (Waters). A PL HFIP gel column (Polymer Lab) and a refractive index detector (Shimadzu RID-10A) were employed. Polymers were dissolved and eluted in 1,1,1,3,3,3-hexafluoroisopropanol at a flow rate of 0.5 $mL \cdot min^{-1}$ (injected volume 100 µL, sample concentration 1.5 $mg \cdot mL^{-1}$). The number and weight average molecular weights were calculated using polymethyl methacrylate standards. The resulting number and weight average molecular weights were [Mn = 59,300 $g \cdot mol^{-1}$ and Mw = 117,500 $g \cdot mol^{-1}$] and [Mn = 10,700 $g \cdot mol^{-1}$ and Mw = 22,500 $g \cdot mol^{-1}$] for PLA and P3TMA, respectively.

Electrospinning

Mixtures of PLA and P3TMA were electrospun from different solvents such as chloroform, acetone and chloroform/acetone mixtures at polymer concentrations of 5 *w/v*-% and 1-5 *w/v*-% for PLA and P3TMA, respectively. Samples will be named indicating only the PLA weight percentage (e.g., PLA/P3TMA-100, and PLA/P3TMA-67 corresponds to PLA alone, and a mixture with 67% PLA and 33% P3TMA, respectively).
The electrospun fibers were collected on a target, which was placed at different distances (10-20 cm) from the syringe tip (inside diameter of 0.84 mm). The voltage was varied between 10 and 30 kV and applied to the collecting target using a high-voltage supply (Gamma High Voltage Research, ES30-5W). The polymer solutions were delivered via a KDS100 infusion syringe

pump from KD Scientific to control the mass-flow rate (from 0.5 to 10 $mL \cdot h^{-1}$). All electrospinning experiments were carried out at room temperature.

Composition, morphology and properties of electrospun polylactide/poly(3-thiophene methyl acetate) mixtures

^{1}H-NMR spectra were acquired with a Bruker AMX-300 spectrometer operating at 300.1 MHz. Chemical shifts were calibrated using tetramethylsilane as an internal standard. Deuterated chloroform was used as the solvent.

Infrared absorption spectra were recorded with a Fourier Transform FTIR 4100 Jasco spectrometer in the 4000-600 cm^{-1} range. A Specac model MKII Golden Gate attenuated total reflection (ATR) with a heated Diamond ATR Top-Plate was used.

Optical morphologic observations were performed using a Zeiss Axioskop 40 microscope. Micrographs were taken with a Zeiss AxiosCam MRC5 digital camera.

Inspection of the morphology of electrospun samples was conducted by scanning electron microscopy using a Focus Ion Beam Zeiss Neon 40 instrument (Carl Zeiss, Germany). Carbon coating was accomplished by using a Mitec K950 Sputter Coater fitted with a film thickness monitor k150x. Samples were visualized at an accelerating voltage of 5 kV. Diameter of electrospun fibers was measured with the SmartTiff software from Carl Zeiss SMT Ltd.

Calorimetric data were obtained by differential scanning calorimetry with a TA Instruments Q100 series equipped with a refrigeration cooling system (RCS). Experiments were conducted under a flow of dry nitrogen with a sample weight of approximately 5 mg and calibration was performed with indium. Heating runs were carried out at a rate of 20 $^{o}C \cdot min^{-1}$ with both electrospun and samples slowly cooled (10 $^{o}C \cdot min^{-1}$) from the melt state.

Thermal degradation was studied at a heating rate of 20 ^{o}C/min with around 5 mg samples in a Q50 thermogravimetric analyzer of TA Instruments and under a flow of dry nitrogen. Test temperatures ranged from 50 to 600 ^{o}C.

X-ray powder diffraction patterns were obtained with a PANalytical X´Pert diffractometer with Cu Kα radiation (λ = 0.1542 nm) and a silicium monocrystal sample holder.

Electrochemical characterization

In order to assess the electrochemical behavior of the PLA/P3TMA scaffolds cyclic voltammetry (CV) studies were conducted with an Autolab PGSTAT302N galvanostat equipped with the ECD module (Ecochimie, The Netherlands). Measurements were performed on fiber mats, which were deposited by electrospinning on both sides of steel AISI 316 sheets of 1×1 cm^2. All

electrochemical assays were performed using a threeelectrode two compartment cell under nitrogen atmosphere and at room temperature.

The cell was filled with 50 mL of phosphate buffered saline (PBS, pH=7.4) with 0.1 M $LiClO_4$ as supporting electrolyte. Steel sheets were used as working electrode, while an Ag|AgCl electrode containing KCl saturated aqueous solution was the reference electrode (offset potential versus the standard hydrogen electrode, E_0 = 0.222 V at 25 ºC). Steel AISI 316 sheets of 1×1 cm^2 were used as counter electrode.

PLA/P3TMA fiber mats were deposited by electrospinning onto both sides of stainless steel sheets and electrochemical measurements were carried out i from -0.4 V to 1.1V, at scan rate of 50 $mV \cdot s^{-1}$.

Five consecutive oxidation-reduction cycles were conducted to assess the loss of electrochemical activity, which was determined as:

$$LEA\ (\%) = \Delta Q/Q_1 \cdot 100 \qquad (\mathbf{1})$$

where ΔQ is the difference of anodic voltammetric charge between the first cycle and the last cycle and Q_1 is the anodic voltammetric charge corresponding to the first cycle.

Wettability

Contact angle measurements were performed using the water drop method at room temperature. Images of 0.5 µL distilled water drops were recorded after stabilization (30 s) using an OCA 20 (DataPhysics Instruments GmbH, Filderstadt). The contact angle values were obtained as the average of eight independent measures for each sample. The software SCA 20 was used to analyze the images and acquire the contact angle values.

Cellular adhesion and proliferation assays

Vero cells were cultured in Dulbecco's modified Eagle medium (DMEM) supplemented with 10% fetal bovine serum, 1% penicillin/streptomycin and 2 mM L-glutamine at 37ºC in a humidified atmosphere with 5% CO_2 and 95% air. The culture medium was changed every two days and, for sub-culture, the cell monolayers were rinsed with phosphate buffered saline (PBS) and detached by incubation with trypsin-EDTA (0.25%) for 2-5 min at 37ºC. Cell concentration was established by count with the Neubauer camera using 4% trypan-blue as dye vital. The detached cells with viability ≥ 95% were used for cultures following the conditions for biocompatibility assays.

PLA/P3TMA electrospun nanofibers were collected on circular coverslips (diameter 1.5 cm). These samples were placed into the wells of a multiwell culture plate and then sterilized by UV-radiation for 15 min in a laminar flux cabinet. For fixing the samples on the well, a small drop of silicone (Silbione® MED ADH 4300 RTV, Bluestar Silicones France SAS, Lyon, France) was used as adhesive. Samples were incubated with 1 mL of culture medium during 30 min under culture conditions to equilibrate the material. Finally, the medium was aspired and the

material was evaluated for cell adhesion and proliferation by exposing cells to direct contact with the material surface.

For the cellular adhesion assay, aliquots of 50-100 µL containing 5×10^4 cells were seeded onto the electrospun samples placed in each well. The plate was incubated under culture conditions for 30 min to allow cellular attachment onto the material surface. Then, 1 mL of the culture medium was added to each well, and the plate was incubated during 24 h.

Finally, the cell viability was determined by the MTT (3-(4,5-dimethylthiazol-2-yl)-2,5-diphenyl-2H-tetrazolium bromide) assay. The controls were realized by cells culture on self-polystyrene surface of the plate (TCPS).

For the cellular proliferation assay, the procedure was similar to the adhesion assay, but the aliquot of 50-100 µL contained 2×10^4 cells. Cultures were maintained during 7 days to allow the cellular growth and an adequate cellular confluence in the well. The media were renewed each two days; and finally, the viability was determined by the MTT assay.

Each sample was evaluated using five replicates, results being averaged and graphically represented. The statistical analysis was performed by one-way ANOVA test to compare the means of all groups. The *t*-Test was applied to determine a statistically significant difference between different groups. The tests were performed with a confidence level of 95% ($p < 0.05$).

5.2.3 Results and Discussion

Electrospinning of Polylactide/Poly(3-Thiophene Methyl Acetate) Mixtures

In order to select the most appropriate conditions to obtain continuous PLA/P3TMA microfibers, several solvents and binary mixtures were tested at different voltages, flows, polymer concentrations and needle tip-collector distances. Although the chemical structure (**Figure 5.2.1 a**) of both polymers was quite different, their solubility characteristics were similar and, consequently, a common solvent could be selected for the electrospinning process.

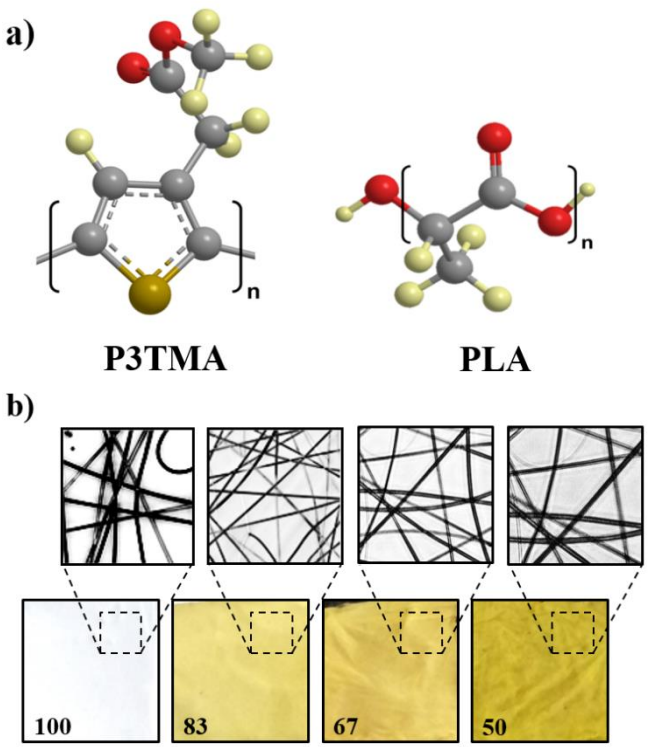

FIGURE 5.2.1

Chemical structures of poly(3-thiophene methyl acetate) and polylactide (a) and optical pictures of conducting scaffolds with the corresponding optical micrographs (b).

In fact, solvent plays a fundamental role for the continuous micro/nanofiber production[26, 27] and, in general, a relatively high polymer concentration is required to avoid the formation of droplets and electrospun beads when a good solvent is selected.[28] Both PLA and P3TMA are highly soluble in chloroform[21] and, therefore, this solvent was selected as a starting point in the optimization of processing conditions. However, quality of fibers improved over a wide range of polymer compositions when chloroform/acetone mixtures were employed. Although chloroform seems more appropriate for PLA considering the reported Hildebrand solubility parameters[29] (i.e. 18.83 $MPa^{0.5}$, 19.98 $MPa^{0.5}$ and 17.64 $MPa^{0.5}$ for chloroform, acetone and

PLA, respectively), the best results were achieved when a small percentage of acetone was added. In fact, Hansen parameters[30] determined for dispersion, polar and hydrogen-bonding components suggests that the addition of acetone improves polar interactions (**Table 5.2.1**). Thus, a chloroform/acetone (70:30 *v/v*) mixture had closer parameters to PLA than the individual solvents and gave good electrospun fibers for all assayed PLA/P3TMA polymer blends. In fact, this solvent mixture was also previously selected as the best solution for electrospinning other PLA/polymer mixtures.[31]

TABLE 5.2.1. Hansen parameters of polylactide and selected electrospinning solvents.

Sample	δ_d ($MPa^{0.5}$)	δ_p ($MPa^{0.5}$)	δ_h ($MPa^{0.5}$)	δ_T ($MPa^{0.5}$)
Chloroform	17.8	3.1	7.0	18.9
Acetone	15.0	10.4	5.5	19.9
Chloroform/Acetone 70:30 *v/v*	17.0	5.3	6.5	19.2
Polylactide	17.6	5.3	5.8	19.3

The low molecular weight of P3TMA precluded its processability into micro/nanofibers since chain entanglements were insufficient to stabilize the jet. Therefore spraying of droplets that coalesced into ill-defined shapes was observed (data not shown). PLA was essential to both render a scaffold with biodegradable properties and improve processability by increasing the average molecular weight of the polymer mixture. In fact a PLA content higher than 50% was necessary even in the most favorable electrospinning conditions to completely avoid the formation of droplets. **Figure 5.2.2** illustrates the optimization process when a deposition distance of 12 cm was chosen according to a first screening, also in the **Figure 5.2.1 b** an optical pictures of conducting scaffolds with the corresponding optical micrographs are shown with the increasing content of conductive polymer affects to the increase colour. It can be observed that big drops corresponding to the conducting polymer were obtained when a relatively high flow (i.e. 10 $mL \cdot h^{-1}$) and low voltage (i.e. 15 kV) were employed. At an intermediate voltage (25 kV) the drop size decreased and at a high voltage (30 kV) beads were characteristic. The decrease of the flow up to 4 $mL \cdot h^{-1}$ improved considerably the morphology and, specifically, a low voltage led to small beads whereas continuous and homogeneous size fibers could be attained at an intermediate voltage. The selected electrospinning conditions for the different conducting/biodegradable polymer mixtures are summarized in **Table 5.2.2**.

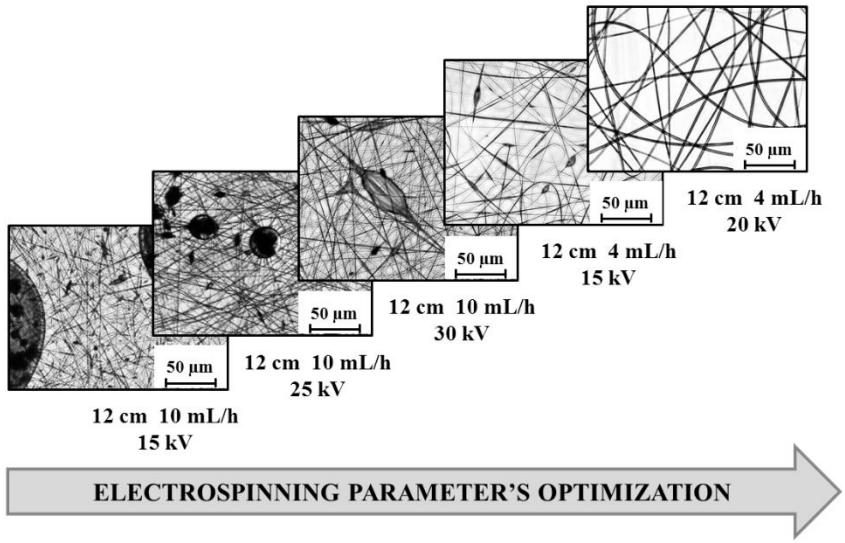

FIGURE 5.2.2

Optical micrographs showing typical morphologies obtained by electrospinning a PLA/P3TMA 67 mixture from a chloroform/acetone (70:30 *v/v*) solution and a deposition distance of 12 cm.

TABLE 5.2.2. Optimal electrospinning conditions for the different studied samples.[a]

Sample	Voltage (kV)	Flow Rate ($mL \cdot h^{-1}$)
PLA/P3TMA 100	15-20	4-10
PLA/P3TMA 83	20-25	4-10
PLA/P3TMA 67	20-25	4
PLA/P3TMA 50	20-25	4

Morphology of Polylactide/Poly(3-Thiophene Methyl Acetate) Nanofibers

Figure 5.2.3 shows representative SEM micrographs of electrospun samples with different compositions. In general, long micro/nanofibers with a cylindrical morphology and randomly distributed in the fibrous mats could be attained. Fibers were adhered to each other forming a dense but porous structure. Diameter distribution was relatively wide. This feature was particularly remarkable for the PLA/P3TMA 50 sample, in which significant amounts of fibers with diameters so different as 250 nm and 2 µm were clearly distinguished. However, in all cases the most predominant size was in the 600-900 nm range. **Figure 5.2.4** shows the monomodal distributions observed for the samples prepared under the optimized conditions. It is interesting

to note that the increase on the P3TMA ratio in the electrospinning mixture led to a slight decrease on the average diameter (i.e. values progressively decreased from 864 to 633 when P3TMA content increased from 0 to 50 *wt*-%).

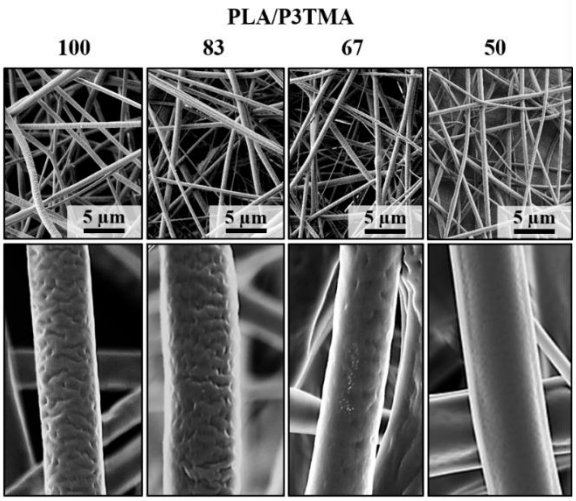

FIGURE 5.2.3

SEM micrographs taken at low (top) and high (bottom) magnification of electrospun nanofibers of PLA/P3TMA samples obtained from a chloroform/acetone (70:30 *v/v*) solution using optimized concentration, voltage, needle-collector distance and flow.

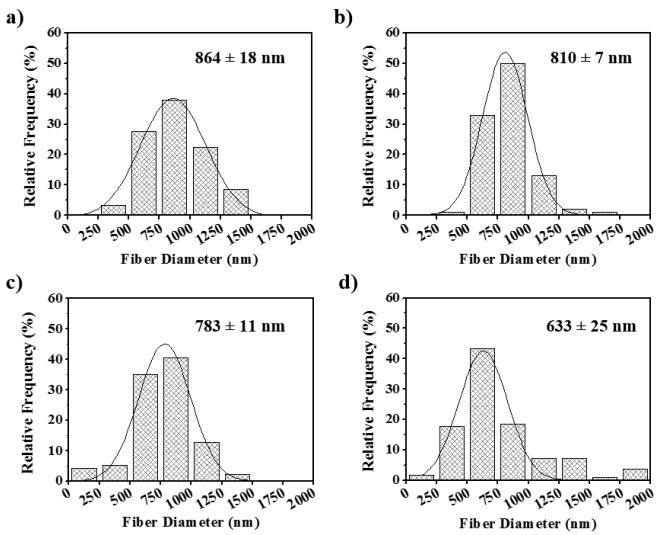

FIGURE 5.2.4

Diameter distribution of electrospun nanofibers of PLA/P3TMA samples obtained from a chloroform/acetone (70:30 *v/v*) solution using optimized concentration, voltage, needle-collector distance and flow.

Surface texture of fibers changed also gradually with composition as depicted in the high magnification images of **Figure 5.2.3**. It is clear that the typical rough/porous surface of PLA fibers progressively became smooth as the P3TMA content increased (e.g., an almost completely smooth texture was observed for PLA/P3TMA 50). Nanofibers were cut with the focused ion beam in order to evaluate their homogeneity through the visualization of the generated cross sections. **Figure 5.2.5 a** clearly shows that PLA nanofibers had an irregular shape as expected from their rough surface texture and also that the section was relatively homogeneous. However, the cross sections of fibers prepared from polymer mixtures (i.e. PLA/P3TMA 50 shown in **Figure 5.2.5 b**) were completely different since in some cases a relative thick and bright outer part could be clearly distinguished. It is possible that the inner part was constituted by some clusters richer in a conductive P3TMA phase, giving place to the observed contrast. In order to verify that fibers were not hollow, a water jet was headed towards their cross section centre. The inset of **Figure 5.2.5 b** illustrated the apparition of a small hole caused by the impact of the jet and consequently demonstrated a compact fibre structure. It should be pointed out that cross sections taken at different places of the microfibers were rather variable since homogeneous and heterogeneous distributions were detected, suggesting that the indicated aggregates are randomly distributed along themicro/nanofibers.

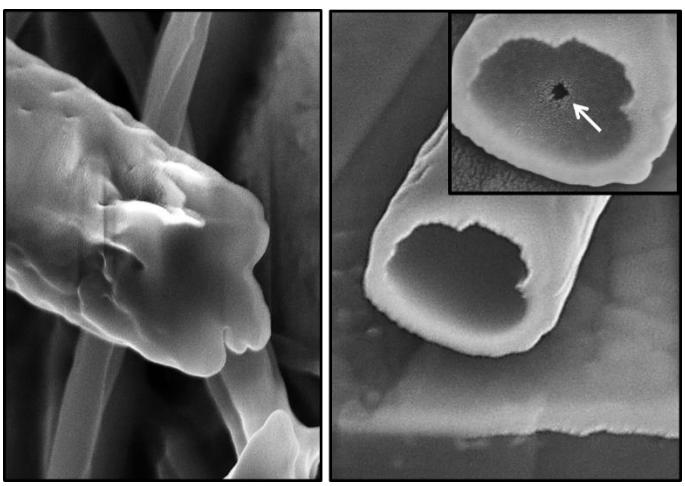

FIGURE 5.2.5

High magnification SEM micrographs showing the cross section of electrospun PLA (left) and PLA/P3TMA 50 (right) nanofibers. The inset shows the corresponding cross section after being exposed to a water jet.

Characterization of Electrospun Polylactide/Poly(3-Thiophene Methyl Acetate) Mixtures

NMR and FTIR spectroscopies were used to assess the composition of the electrospun hybrid scaffolds. Thus NMR spectra revealed the presence of characteristic signals of each homopolymer (**Figure 5.2.6**), the corresponding areas being in agreement with the theoretical composition of the sample. Spectra always showed the characteristic quadruplet at 5.21, 5.19, 5.17 and 5.15 ppm associated to the proton of the PLA methine group and the doublet at 1.60 and 1.58 ppm associated to the protons of the PLA methyl group. In addition complex signals, which reflect sequence sensitivity, were also observed and attributed to P3TMA. Thus, thiophene protons gave rise to an isolated multiplet (7.18-7.15 ppm) whereas signals of methylene and methyl lateral groups appeared overlapped as a double duplet (3.82-3.80 ppm and 3.62-3.60 ppm) and a duplet (3.77 and 3.72 ppm), respectively. Splitting of the CH_3 signal reflects the head-to-head (HH) and head-to-tail (HT) dyads produced during the chemical polymerization as has been previously reported.[25] Areas of dyad signals were practically identical, demonstrating a non-regioregular structure with a statistical disposition of the monomer units. HT and HH dyads corresponding to the methylene protons were splitted again demonstrating triad sensitivity (e.g., splitting of HH dyad gave rise to HHT and THH triads, whereas THT and HHT triads were derived for the HT dyad). The complex signal associated to the CH group can be interpreted in a similar way, the highest chemical shifts corresponding to the TH dyad.

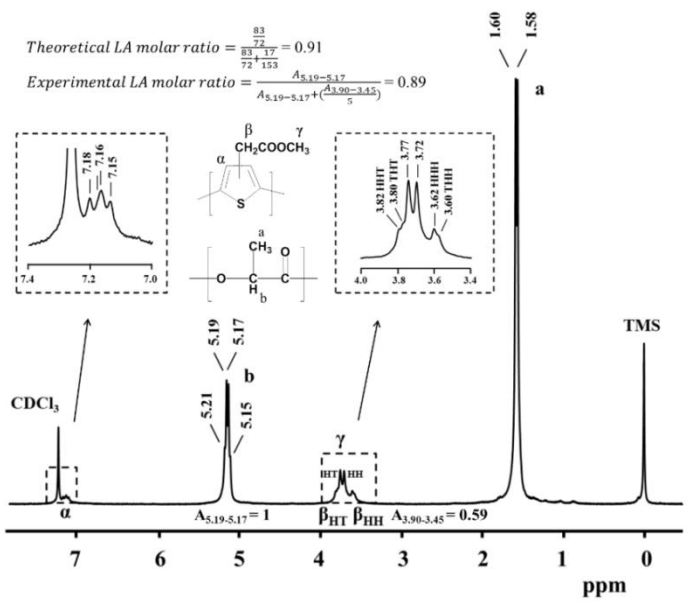

FIGURE 5.2.6

NMR spectra of a representative electrospun PLA/ P3TMA 83 sample.

FTIR spectra of P3TMA samples coming directly from synthesis and from electrospinning were identical and showed a single C=O signal at 1732 cm^{-1} (**Figure 5.2.7**). Therefore, ester groups were not cleaved during processing, supporting the interpretation of the complex NMR spectra on the basis of sequence sensitivity. Furthermore, a broad band associated to OH groups could not be detected in the 3300-2500 cm^{-1} FTIR region (not shown). The spectra of the conducting polymer showed also typical signals at 1435 cm^{-1} (thiophene ring stretching), 1322 cm^{-1} (methyl deformation), 1198 and 1167 cm^{-1} (asymmetric and symmetric C-O stretching), 1012 cm^{-1}, 839 cm^{-1} (aromatic CH out of plane deformation) and 741 cm^{-1} (methyl rocking).

The spectra of the scaffold samples were highly similar to that corresponding to the neat PLA (**Figure 5.2.7**), the C=O stretching vibration at 1759 cm^{-1} and the asymmetric and symmetric C-O stretching at 1183 and 1082 cm^{-1}, respectively, being the most intense bands. The intensity of the characteristic signals of P3TMA decreased with its ratio in the scaffold (e.g., bands at 1322 and 839 cm^{-1}). It should be pointed out that the strong P3TMA band at 1167 cm^{-1} could not be observed in the spectra of scaffolds even for the highest P3TMA content. This suggests a change in the environment of the ester groups when the P3TMA was processed together with PLA. However, it is also significant that the transmittance measured at 1167 cm^{-1} was clearly lower for the hybrid scaffold than for the neat PLA (see blue arrows in **Figure 5.2.7**), even though this wavenumber still corresponded to a transmittance maximum. For the sake of completeness, **Figure 5.2.7 e** shows the spectrum of a powder mixture composed by 50 *wt*-% of each polymer where the two strong PLA bands at 1183 and 1082 cm^{-1} can be clearly observed together with the strongest P3TMA band. However, the latter appears slightly shifted due to its overlapping with a medium intensity PLA band at 1129 cm^{-1}. Differences between the spectra of electrospun samples and polymer mixtures are evident and suggest the occurrence of some specific interactions in the processed samples.

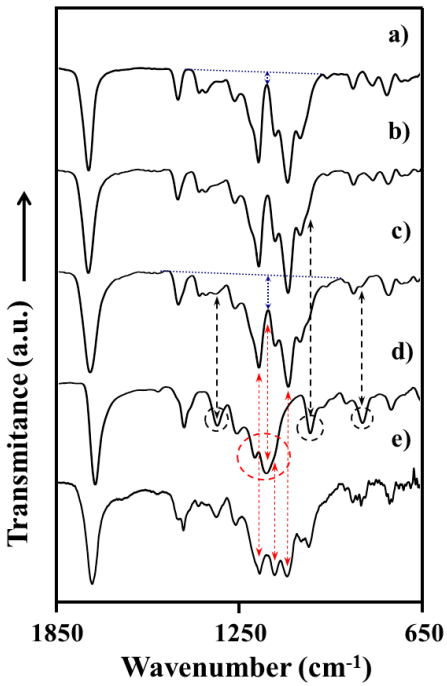

FIGURE 5.2.7

FTIR (2000-600 cm^{-1}) spectra of electrospun PLA (a), PLA/P3TMA 67 (b), PLA/P3TMA 50 (c) and P3TMA (d). For comparison purposes the spectrum of a blend containing 50 *wt*-% of each homopolymer is shown in (e).

TABLE 5.2.3. Selected calorimetric data from the heating scan performed with the different PLA/P3TMA electrospun samples.

Sample	T_g (°C)	T_c (°C)	ΔH_c ($J \cdot g^{-1}$)	T_m (°C)	ΔH_m ($J \cdot g^{-1}$)	$\Delta H_m - \Delta H_c$ ($J \cdot g^{-1}$)	X_c[a]
PLA[b]	60.0	-	-	149.8	33.4	33.4	31.5
PLA/P3TMA 100	61.7	96.6	17.4	146.2	22.0	4.6	4.3, 20.7
PLA/P3TMA 83	59.5	96.4	14.0	147.2	17.5	3.5	4.0, 19.9
PLA/P3TMA 67	59.4	96.5	14.3	147.5	17.8	3.5	4.9, 25.1
PLA/P3TMA 50	60.4	94.1	12.0	145.7	16.2	4.2	7.9, 30.6
P3TMA	67.2	-	-	111.3	11.6	11.6	-

[a] Degree of crystallinity referred to the PLA content and using a heat of fusion of 106 J/g for a 100% crystalline sample.[32] Values on the left correspond to the crystallinity of as electrospun samples whereas those on the right correspond to the crystallinity attained during the heating scan.
[b] Commercial sample included for comparison purposes.

Table 5.2.3 contains the main calorimetric data (i.e. glass transition, cold crystallization and melting temperatures as well as crystallization and melting enthalpies) obtained from the heating run of all electrospun scaffolds, whereas heating traces of representative samples can be seen in **Figure 5.2.8**.

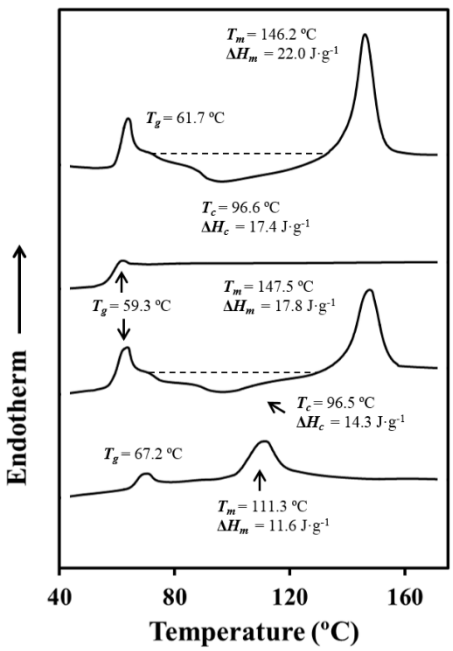

FIGURE 5.2.8

DSC heating (a) and cooling (b) scans performed with electrospun PLA/P3TMA 100 (a,b) and PLA/P3TMA 67 (c) samples obtained under the corresponding optimized processing conditions. For comparison purposes the heating scan of a P3TMA powder sample is shown in (d).

Several features deserve attention:

- A broad exothermic peak (70-130 ºC) corresponding to the cold crystallization of PLA is always observed. The high molecular orientation attained in the electrospinning process facilitated the PLA crystallization, as previously reported.[32] On the contrary, amorphous samples (**Figure 5.2.8 c**) were always attained when samples were slowly cooled from the melt due to the lack of orientation and the difficulty of PLA to crystallize.
- The degree of crystallinity referred to the PLA content tends to increase when nanofibers are obtained from mixtures with a higher P3TMA content, which is probably due to the higher orientation attained when the fibre diameter decreased. This trend was observed in both samples from direct electrospun (i.e. calculated through the difference between melting and crystallization enthalpies) and samples obtained after cold crystallization (i.e. considering only the melting enthalpy).

- All samples show a clear glass transition, as could be presumed for amorphous samples, and a typical relaxation endothermic peak, which indicates that metastable PLA glassy material achieves equilibrium thermodynamic conditions with a lower specific volume, enthalpy and entropy.[33]
- Incorporation of P3TMA has a scarce influence on the characteristic glass transition, crystallization and melting temperatures of the final scaffold. In fact, neither the glass transition nor the melting peak of P3TMA (**Figure 5.2.8 d**) were detected in the heating runs of the resulting scaffolds.

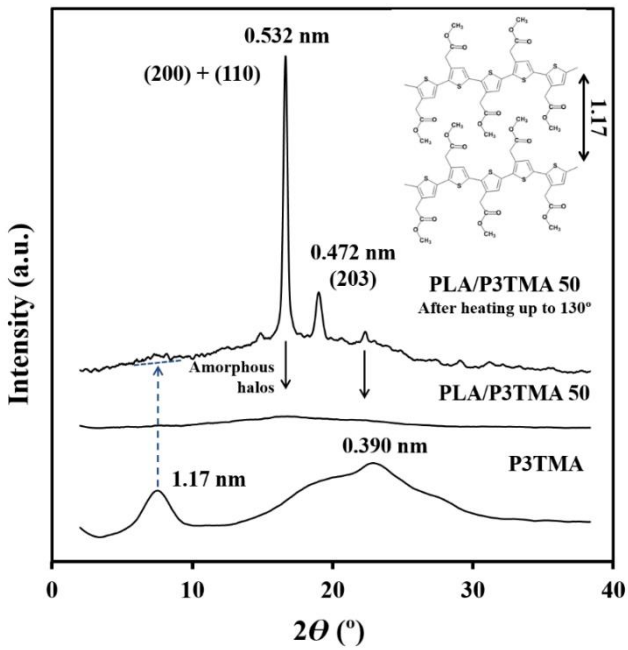

FIGURE 5.2.9

X-ray power difractograms of a P3TMA powder sample and an electrospun P3TMA 50 scaffold before and after being heated up to 130 ºC. Inset shows a scheme of the molecular arrangement where for the sake of simplicity only a heat-to-heat distribution has been represented.

It is interesting to note that P3TMA obtained from chemical polymerization was semicrystalline despite the random disposition of its repeating unit. The X-ray diffraction profile (**Figure 5.2.9**) is characterized by a strong and well defined peak at 1.17 nm that is related to the interchain distance (inset of **Figure 5.2.9**). Profiles of electrospun samples showed only amorphous halos without Bragg reflections associated to any of the two homopolymers. However, crystallization took place when the sample was heated up to 130 ºC and the diffraction profile clearly showed the two strongest reflections of the α-form of PLA (i.e. those appearing at 0.542 and 0.472 nm that correspond to the (200)+(110) and (203) indices, respectively).[34,35] Therefore, crystallization involved only the PLA since the main reflection of P3TMA can only be guessed.

Scaffolds were thermally stable up to more than 200 ºC, as deduced from TGA and DTGA curves (**Figure 5.2.10**). Incorporation of P3TMA slightly modified the degradation process, leading to a regular increase of both the char yield at 600 ºC and the onset degradation temperature. Thermal degradation of PLA has previously been explained according to a complex reaction process with the participation of at least two different mechanisms.[36] The DTGA curve of PLA is clearly asymmetric showing a shoulder in the low temperature region, which is associated with a minor degradation process. This shoulder disappears in the DTGA curves of scaffolds suggesting that the first degradation step is hindered by the presence of P3TMA. It is also clear that the DTGA maximum is slightly shifted to a lower temperature, which coincides with one of the two degradation processes observed also for P3TMA. In addition, the scaffold has a hardly observed minor decomposition process that corresponds to the higher temperature degradation step of P3TMA.

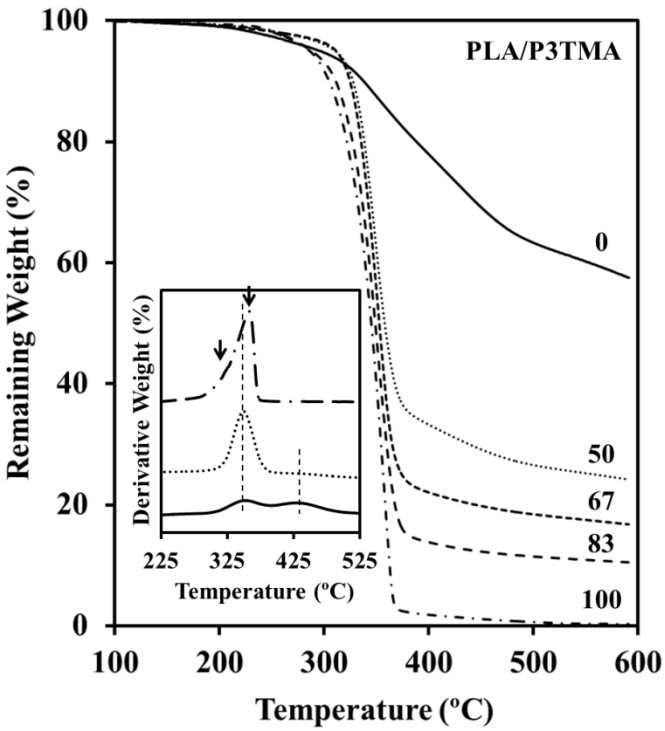

FIGURE 5.2.10

TGA degradation curves of the different electrospun PLA/P3TMA samples. Inset compares DTGA curves of PLA, PLA/P3TMA 50 and P3TMA.

Electrochemical Characterization of Electrospun Polylactide/Poly(3-Thiophene Methyl Acetate) Mixtures

The low molecular weight of P3TMA makes unfeasible to get electrospun mats and to carry out the corresponding CV measurements from the neat polymer. Processability has been demonstrated to be possible when a high molecular weight polymer (e.g., PLA) is incorporated as it was also demonstrated in previous works concerning the electrochemical characterization of P3TMA nanomembranes prepared by spin coating.[21, 22]

The control voltammogram recorded for PLA fibers (**Figure 5.2.11 a**) shows an oxidation shoulder with anodic potential $E_p^a(O_1)$ of 0.86 V and an oxidation peak with $E_p^a(O_2)$ higher than 1.1 V. Both peaks have been assigned to the formation of irreversible polarons and bipolarons. Besides, the cathodic scan shows a weak reduction shoulder R_1 with a cathodic peak potential $E_p^c(R_1)$ of -0.08 V.

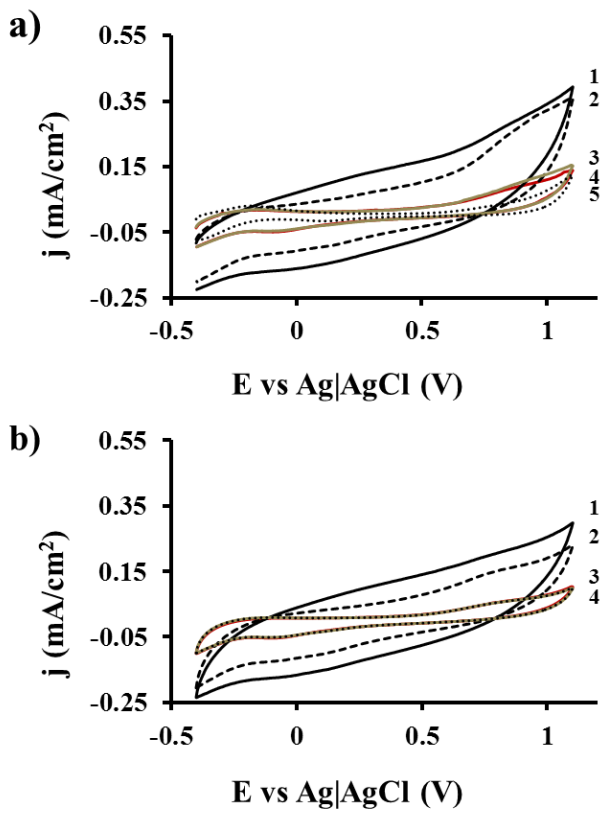

FIGURE 5.2.11

(a) Control voltammograms collected using scan rates of 50 mV/s for electrospun mats of PLA (curve 4) and PLA/P3TMA with 50 *wt*-% (curve 1), 67 *wt*-% (curve 2) and 83 *wt*-% (curve 3) in a PBS solution containing 0.1 M $LiClO_4$. Curve 5 corresponds to a steel sheet used as control. (b) Cyclic voltammograms of the same species after 5 consecutive oxidation–reduction cycles.

The voltammogram recorded for the PLA/P3TMA 83 hybrid was highly similar to that obtained for PLA (**Figure 5.2.11 a**, curves 3 and 4), but interestingly the hybrids with a lower PLA content (i.e. PLA/P3TMA 50 and 67 samples) showed clearly improved electrochemical properties (**Figure 5.2.11 a**, curves 1 and 2). Thus, E_p^a (O_1) and E_p^a (O_2) anodic potentials increased up to 0.75 and 1.40 V for the 67 *wt*-% sample and 0.82 and 1.08 V for the 50 *wt*-% sample, respectively, and pointed out an increased irreversibility for the oxidation process. Furthermore, the weak R_1 reduction shoulder was always observed (i.e. cathodic peak potentials of -0.04 V and -0.05 V for the PLA/P3TMA 50 and 67, respectively). Current densities (j) determined at 1.10 V were 0.152 $mA \cdot cm^{-2}$ and 0.394 $mA \cdot cm^{-2}$ for PLA/P3TMA 83 and 50, samples, respectively.

The electroactivity, which refers to the ability to store charge, was evaluated by integrating the cathodic and anodic areas of the voltammograms displayed in **Figure 5.2.11**. Specifically, the electroactivity increases with the similarity between such areas. Results indicate that the electroactivity increases significantly upon the incorporation of P3TMA, especially when the concentration of conducting polymer is higher than 30 *wt*-%. Thus, the electroactivity measured for PLA/P3TMA 83, 67 and 50 is 17%, 190% and 289% higher than those of PLA. In order to investigate the electrochemical stability of the samples, five consecutive cycles were applied by varying the potential in the interval defined by -0.4 V (initial and final potential) and 1.1 V (reversal potential) at 50 $mV \cdot s^{-1}$. The electroactivity decreases with the oxidation and reduction areas of consecutive voltammograms. The voltammograms recorded after such five cycles, which are shown in **Figure 5.2.11 b**, indicate that the oxidation/reduction peak distributions are highly similar. As it can be seen, the reduction of the cathodic and anodic areas, which reflects a loss of electroactivity, depends on the P3TMA content. More specifically, the LEA determined for PLA/P3TMA 50 and PLA/P3TMA 83 samples is 27% and 38%, respectively, evidencing that the electrostability increases with the P3TMA content.

Table 5.2.4 summarizes the cyclic voltammogram peak description for all samples including the values of the current densities measured at 1.10 V for the first and fifth cycles. Major differences in the electrochemical behavior were found when the integrated area and the current density were considered. Thus, independently of the number of cycle, charge and current density increased when the P3TMA content did. Results indicate that the incorporation of P3TMA into the PLA matrix provided fibers with interesting electrochemical features since an increase of both the electroactivity and electrostability were clearly observed.

TABLE 5.2.4. Electrochemical behavior of PLA and PLA/P3TMA 83 *wt*-%, 67 *wt*-%, and 50 *wt*-% samples: current density at 1.1 V and charge for the 1st cycle and the 5th oxidation-reduction cycles, and loss of electrochemical stability after 5 consecutive cycles (LEA).

Sample	*j* at 1.1 V ($mA \cdot cm^{-2}$)		*Q* (mc)		*LEA* (%)
	1st cycle	5th cycle	1st cycle	5th cycle	
PLA	0.138	0.102	2.9	2.0	31
PLA/P3TMA 83	0.152	0.098	3.1	1.9	38
PLA/P3TMA 67	0.355	0.223	8.4	5.5	34
PLA/P3TMA 50	0.394	0.290	11.3	8.3	27

Wettability of Polylactide/Poly(3-Thiophene Methyl Acetate) Mixtures

Figure 5.2.12 compares the contact angle measured for the different systems studied in this work. The average value of the contact angle determined for PLA (133.4º ± 1.5º) and P3TMA (88.6º ± 2.6º) reflects the hydrophobic character of the polyester and the slightly hydrophilic nature of the polythiophene derivative. It should be noted that the contact angle found for PLA is similar to that recently reported by Liu et al. for PLA nanofibers prepared using a similar technique.[37] The very low wetting ability of electrospun PLA nanofibers should be attributed to the combined effect of the surface roughness and morphology for these particular nanostructures. Addition of P3TMA to PLA does not produce changes in the contact angle of the latter, values obtained for PLA/P3TMA 83, 67 and 50 mixtures being 134.5º ± 2.4º, 135.1º ± 1.6º and 128.7º ± 0.8º, respectively. The similarity between the contact angles of PLA and PLA/P3TMA combined with the electrochemical results displayed in the previous subsection suggest that the behavior of the mixtures as supportive matrix for the cell growth should be better than that of the homopolymer. Thus, the incorporation of P3TMA to the PLA matrix is expected to mainly affect the hydrophilicity of the surface, which in fact remains practically unaltered, and the ability of exchange ions across cell membranes, which was shown to be enhanced (see previous subsection).

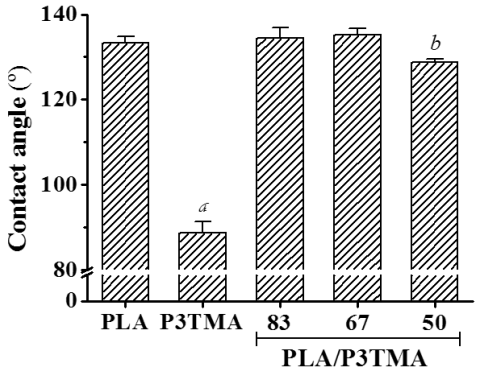

FIGURE 5.2.12

Graphical representation of the contact angles measured for PLA, P3TMA and PLA/P3TMA mixtures with 83 *wt*-%, 67 *wt*-% and 50 *wt*-%. Tukey test, $p < 0.05$; a, b *vs.* other materials.

Cell Adhesion and Growth in the PLA/P3TMA Hybrid Scaffolds

SEM images of VERO cells adhered and grown on the PLA (control) and PLA/P3TMA matrices were qualitatively very similar (**Figure 5.2.13**).

The VERO cells cultured during 24 h on the 3D surfaces led always to a homogeneous distribution and rounded morphologies (**Figures 5.2.13 a** and **5.2.13 c**), which should correspond to individual cells or small groups of a few cells (insets of **Figures 5.2.13 a** and **5.2.13 c**). Cells appeared also adhered to the fibers by small filopodia. Cells cultured during 7 days on the mats surface were able to form monolayers (**Figures 5.2.13 b** and **5.2.13 d**), a typical indicator of cell viability and proliferation. The surface colonization progressed through a suitable cellular extension, which apparently was facilitated and guided by the fiber array (inset in the **Figures 5.2.13 b** and **5.2.13 d**).

In quantitative terms, the P3TMA content in the fibers did not affect the cell adhesion (**Figure 5.2.13 e**) but interestingly the cellular proliferation was slightly improved in the scaffolds with a higher P3TMA content (**Figure 5.2.13 f**). In this way, the new electrospun micro/nanofibers constituted by the hybrid materials may improve the electrochemical properties and the cellular response (frequently mediated by ionic channels) to several physiological processes such as membrane depolarization during cell division.[38]

In conclusion, PLA/P3TMA micro/nanofibers were well suited to provide a good substrate for cell adhesion and cell proliferation and offered an appropriate 3D environment.
Furthermore, cells developed in the PLA/P3TMA matrices showed always a healthy morphology.

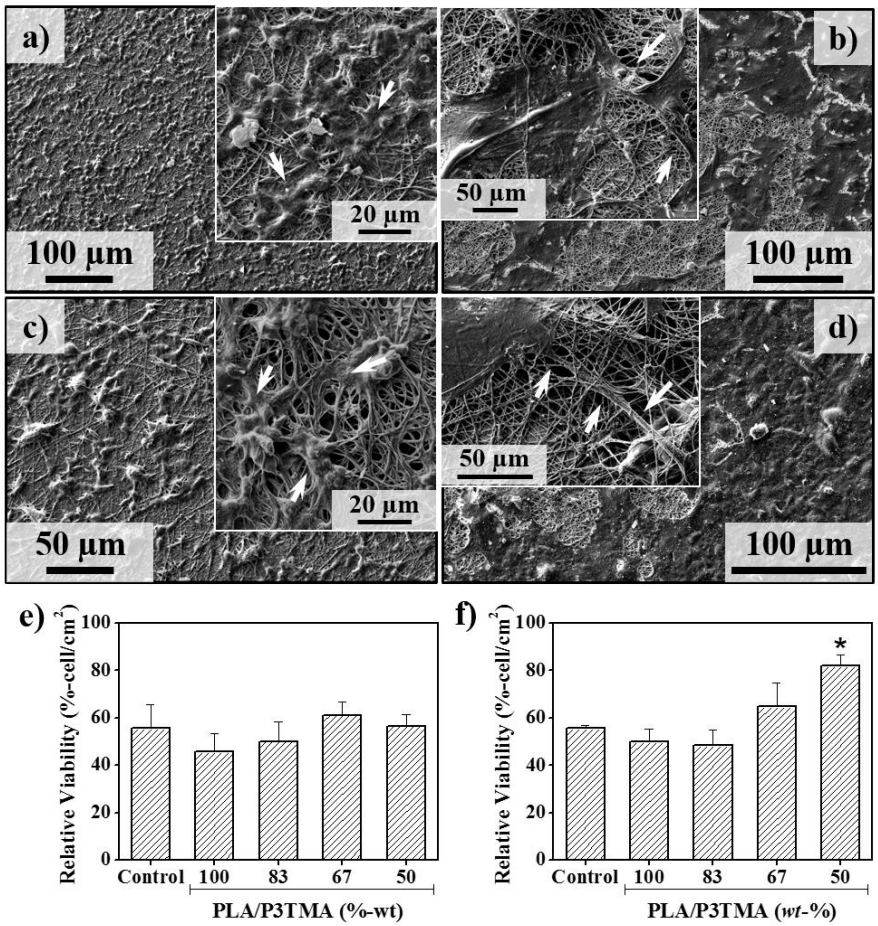

FIGURE 5.2.13

SEM images of VERO cells adhering (a and c) and growing (b and d) on electrospun fibers of PLA (a and c) and PLA/P3TMA 50 *w*/*w*-% (b and d). The arrows indicate morphological details of the cellular extensions. Quantitative data of the relative adhesion (e) and proliferation (f) of cells onto the fibers mats. * $p < 0.05$ vs others fibersmats and control (tissue culture plate), Tukey test for n = 4 replicates.

5.2.4 Conclusions

Mixtures of PLA and P3TMA can be effectively electrospun to render hybrid micro/nanofibers that combine the biocompatibility and electrochemical properties of each homopolymer. Processing conditions (solvent, concentration, flow, voltage, collector distance) were optimized to allow incorporating up to 50 *wt*-% of P3TMA and keeping continuous fiber morphology. Increasing contents of the conducting polymer gave rise to smoother fiber surfaces, smaller diameters, higher orientation of PLA chains and the sporadic formation of cluster aggregates inside the fibers.

Incorporation of P3TMA into the PLA matrix provided an increase of the electroactivity and electrostability, both charge and current intensity clearly increasing with the P3TMA content. Current density determined at 1.10 V was as high as 0.394 $mA \cdot cm^{-2}$ for fiber mats containing 50 *wt*-% of P3TMA while the electroactivity of such hybrid was 289% higher than that of PLA. The electrostability of samples was probed since the average charge loss was less than 27% after performing five consecutive oxidation-reduction cycles. New hybrid scaffolds were good substrates for cell adhesion and cell proliferation and even the last was clearly enhanced respect to the parent PLA scaffolds. Cellular response to physiological processes seemed to be improved by the incorporation of P3TMA.

5.2.5 References

[1] Y. Wei, P.I. Lelkes, A.G. MacDiarmid, E. Guterman, S. Cheng, K. Palouian, Peking University Press, Beijing, 2004.

[2] P.R. Bidez, S.X. Li, A.G. MacDiarmid, E.C. Venancio, Y. Wei, P.I. Lelkes, J Biomat Sci-Polym E, 17 (2006) 199-212.

[3] A. Kotwal, C.E. Schmidt, Biomaterials, 22 (2001) 1055-1064.

[4] R.F. Valentini, CRC Press LLC, Boca Raton, 2000.

[5] D.H. Reneker, I. Chun, Nanotechnology, 7 (1996) 216-223.

[6] A. Frenot, I.S. Chronakis, Curr Opin Colloid In, 8 (2003) 64-75.

[7] Y. Dzenis, Science, 304 (2004) 1917-1919.

[8] D. Li, Y.N. Xia, Adv Mater, 16 (2004) 1151-1170.

[9] K. Jayaraman, M. Kotaki, Y.Z. Zhang, X.M. Mo, S. Ramakrishna, J Nanosci Nanotechno, 4 (2004) 52-65.

[10] R. Dersch, M. Steinhart, U. Boudriot, A. Greiner, J.H. Wendorff, Polym Advan Technol, 16 (2005) 276-282.

[11] J.M. Deitzel, J.D. Kleinmeyer, J.K. Hirvonen, N.C.B. Tan, Polymer, 42 (2001) 8163-8170.

[12] M.Y. Li, Y. Guo, Y. Wei, A.G. MacDiarmid, P.I. Lelkes, Biomaterials, 27 (2006) 2705-2715.

[13] P.H.S. Picciani, E.S. Medeiros, Z.L. Pan, W.J. Orts, L.H.C. Mattoso, B.G. Soares, J Appl Polym Sci, 112 (2009) 744-753.

[14] K.D. McKeon, A. Lewis, J.W. Freeman, J Appl Polym Sci, 115 (2010) 1566-1572.

[15] M. Gizdavic-Nikolaidis, S. Ray, J.R. Bennett, A.J. Easteal, R.P. Cooney, Macromol Biosci, 10 (2010) 1424-1431.

[16] D. Kai, M.P. Prabhakaran, G.R. Jin, S. Ramakrishna, J Biomed Mater Res A, 99A (2011) 376-385.

[17] J. Roncali, Chem Rev, 97 (1997) 173-205.

[18] O. Bertran, E. Armelin, F. Estrany, A. Gomes, J. Torras, C. Aleman, J Phys Chem B, 114 (2010) 6281-6290.

[19] S. Lee, G.D. Moon, U. Jeong, J Mater Chem, 19 (2009) 743-748.

[20] A. Subramanian, U.M. Krishnan, S. Sethuraman, J Mater Sci-Mater M, 23 (2012) 1797-1809.

[21] E. Armelin, A.L. Gomes, M.M. Perez-Madrigal, J. Puiggali, L. Franco, L.J. del Valle, A. Rodriguez-Galan, J.S.D. Campos, N. Ferrer-Anglada, C. Aleman, J Mater Chem, 22 (2012) 585-594.

[22] A.L. Gomes, M.B.P. Zakia, J. Filho, E. Armelin, C. Aleman, J.S.D. Campos, Polym Chem-Uk, 3 (2012) 1334-1343.

[23] M.M. Perez-Madrigal, E. Armelin, L.J. del Valle, F. Estrany, C. Aleman, Polym Chem-Uk, 3 (2012) 979-991.

[24] M.M. Perez-Madrigal, M.I. Giannotti, G. Oncins, L. Franco, E. Armelin, J. Puiggali, F. Sanz, L.J. del Valle, C. Aleman, Polym Chem-Uk, 4 (2013) 568-583.

[25] B.S. Kim, L. Chen, J.P. Gong, Y. Osada, Macromolecules, 32 (1999) 3964-3969.

[26] S.V. Fridrikh, J.H. Yu, M.P. Brenner, G.C. Rutledge, Phys Rev Lett, 90 (2003) 144502-144504.

[27] M.G. McKee, C.L. Elkins, T.E. Long, Polymer, 45 (2004) 8705-8715.

[28] C.J. Luo, M. Nangrejo, M. Edirisinghe, Polymer, 51 (2010) 1654-1662.

[29] D.W. van Krevelen, Elsevier, Amsterdam, 1990.

[30] C.M. Hansen, CRC Press, Florida, 2000.

[31] A. Agrawal, A.D. Saran, S.S. Rath, A. Khanna, Polymer, 45 (2004) 8603-8612.

[32] L.J. del Valle, R. Camps, A. Diaz, L. Franco, A. Rodriguez-Galan, J. Puiggali, J Polym Res, 18 (2011) 1903-1917.

[33] J.R. Sarasua, R.E. Prud'homme, M. Wisniewski, A. Le Borgne, N. Spassky, Macromolecules, 31 (1998) 3895-3905.

[34] P. De Santis, A.J. Kovacs, Biopolymers, 6 (1968) 299-306.

[35] W. Hoogsteen, A.R. Postema, A.J. Pennings, G. Tenbrinke, P. Zugenmaier, Macromolecules, 23 (1990) 634-642.

[36] K. Chrissafis, Thermochim Acta, 511 (2010) 163-167.

[37] W.Y. Liu, J.C. Wei, Y.W. Chen, P. Huo, Y. Wei, Acs Appl Mater Inter, 5 (2013) 680-685.

[38] M.H. Bolin, K. Svennersten, X.J. Wang, I.S. Chronakis, A. Richter-Dahlfors, E.W.H. Jager, M. Berggren, Sensor Actuat B-Chem, 142 (2009) 451-456

6.

Biodegradable polymer matrices incorporating polyethylene glycol as a sacrificial polymer

The work described in this chapter previously appeared in:

[1] Llorens, E.; del Valle, L. J.; Ferran, R.; S.; Rodríguez-Galán, A.; Puiggalí, J. *J. Polym. Res.* **2014**, *21* (2), 360-375.

[2] Llorens, E.; Bellmunt, S.; del Valle, L.; Puiggalí, J. *J. Polym. Res.* Submitted.

[3] Llorens, E.; Ibañez, H.; del Valle, L.; Puiggalí, J. *Mater. Sci. Eng. C.* Submitted.

6.1

Scaffolds with Tuneable Hydrophilicity from Electrospun Microfibers of Polylactide and Poly(Ethylene Glycol) Mixtures: Morphology, Drug Release Behavior and Biocompatibility

Electrospun mats were obtained from different mixtures of polylactide (PLA) and poly(ethylene glycol) (PEG). Processing conditions were optimized for all compositions and the resulting micro/nanofiber morphologies (i.e. diameter size and surface texture) were characterized by scanning electron microscopy (SEM). NMR and FTIR spectroscopies were employed to verify the final composition and thermal properties were evaluated by DSC and TGA. XPS spectroscopy revealed that PEG was mainly deposited on the surface of electrospun micro/nanofibers, leading to smooth textures. Interestingly, PLA/PEG scaffold solubility in ethanol was very different to that in water, since a significant amount of PEG was effectively retained in the PLA matrix after immersion in ethanol whereas only a low level of PEG was retained in the PLA matrix after immersion in water. The hydrophilicities of the scaffolds obtained from PLA/PEG mixtures were consequently higher than that of the PLA, even after the exposure to water.

As PEG can be used as a sacrificial polymer because of its high solubility in water, it was possible to increase the porosity of PLA/PEG scaffolds. PLA/PEG scaffolds loaded with triclosan (TCS) had very different release profiles in hydrophilic (e.g., PBS) and hydrophobic (e.g., Sörensen/ethanol (30:70 v/v) mixture) media, while differences were small between scaffolds having different PLA/PEG ratios. TCS loaded scaffolds exhibited good antibacterial properties for all compositions and allowed adhesion of epithelial cells (i.e. MDCK and VERO). Significant differences in cell proliferation were found between unloaded and TCS loaded scaffolds due to the clear improvement of cell colonization by increasing PEG content.

6.1.1 Introduction

Scaffolds based on biodegradable and/or biocompatible polymers for tissue engineering applications are receiving much attention because of their potential use as temporary templates for cell seeding, migration, proliferation and differentiation prior to regeneration of the natural extracellular matrix (ECM) or a biological functional tissue.[1-4] Several methodologies have been developed to prepare suitable scaffold structures, including electrospinning techniques.[5, 6] This electrostatic process involves the use of a high voltage field to charge the surface of a polymer solution droplet held at the end of a capillary tube and induce the ejection of a liquid jet towards a grounded target (collector). Selection of appropriate experimental conditions for a given polymer (i.e. solvent, polymer concentration and operational parameters such as strength of the applied electric field, deposition distance and flow) can lead to fibers with diameters ranging from several micrometers to a few nanometres in an extremely rapid process (millisecond scale).[7-10]

The deposition of electrospun micro/nanofibers can give rise to interconnected porous networks, which are interesting substrates for tissue regeneration and even for drug delivery. In fact, these scaffolds have morphologies similar to the structures of natural ECM, as well as large surface area-to-volume ratios that facilitate cell adhesion and proliferation, provide an ideal porous structure for nutrient and metabolic waste exchange, and promote vascularization.[11]

Several biodegradable polymers coming from both synthetic and natural routes have been successfully electrospun (e.g., polyglycolide,[12] polylactide,[12-15] polycaprolactone,[16] collagen[17, 18] and chitosan[15, 18, 19]). Polylactide (PLA) (**Figure 6.1.1 a**) is one of the most widely used materials in clinical applications due to the combination of interesting characteristics like tuneable mechanical properties, degradation into natural metabolites, biocompatibility and low cost. However, PLA has some problems associated with its inherent hydrophobic nature which may reduce expression of phenotypic markers and hinder cell attachment and proliferation.[20, 21] In order to solve this problem, chemical modifications (e.g., grafting hydrophilic moieties[22] or incorporating hydrophilic blocks[23] into the PLA main chain) as well as the use of amphiphilic mixtures like its blends with poly(ethylene glycol) (PEG) have been considered (**Figure 6.1.1 a**).[24-26] In fact, PEG is also widely employed in the biomedical field due to its lack of toxicity, good biocompatibility and elimination from human body when its molecular weight is low.[27]

Spasova *et al*.[24] were the first to prepare electrospun mats from chloroform solutions of PLA and a maximum PEG content of 30 *wt*-%. Interestingly, the scaffolds with the highest PEG content facilitated the arrangement of osteoblast-like cells in tissue-like structures. It was also demonstrated that the incorporation of PEG can favor the electrospinning process and particularly the production of regular and continuous fibers due to the reduction of solution viscosity caused by the low molecular weight PEG.[25] Finally, it should be pointed out that

PLA scaffolds containing 5 *wt*-% of PEG had excellent *in-vitro* osteogenic potential and *in vivo* biocompatibility with the surrounding tissues.[26]

The present work studies the electrospinning conditions to obtain PLA/PEG scaffolds over a wide range of compositions (i.e. a PEG content from 10 to 70 *wt*-%) and characterizes the resulting scaffolds. Moreover, it evaluates the solubility of the newly prepared scaffolds in both water and a less hydrophilic medium (e.g., ethanol) since scaffold texture may be drastically affected (e.g., porosity may increase, favouring subsequent cell colonization processes) and biocompatibility may be altered depending on composition and washing process. Another goal of the study is to obtain information concerning the distribution of PEG and PLA phases. Finally, several issues related to drug loading and release are discussed, i.e. distribution of a hydrophobic drug like triclosan (**Figure 6.1.1 a**) in the hybrid PLA/PEG two-phase system, release profile in media with different hydrophilicity, and influence of the hybrid composition on the pharmacological effect.

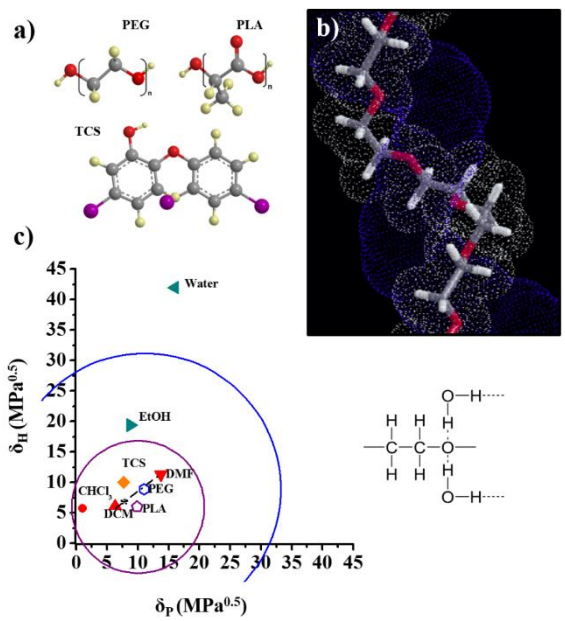

FIGURE 6.1.1

Chemical structures of PEG, PLA and TCS (a). Coil of water molecules (blue) around a PEG molecular chain (top) and scheme of hydrogen bonding interactions between water molecules and PEG (bottom) (b). Projection into the hydrogen-dispersion (δ_h-δ_p) plane of the Hansen parameter solubility sphere for PEG (blue), PLA (garnet), solvents used in this work and TCS (c).

6.1.2 Experimental Section

Materials

Polylactide (PLA), a product of Natureworks (polymer 2002D), was kindly supplied by Nupik International (Polinyà, Spain). Poly(ethylene glycol) (PEG) of number average molecular weights of 10.000 and 35.000 $g \cdot mol^{-1}$ were purchased from Sigma-Aldrich. Solvents and triclosan were purchased from Sigma Aldrich and used as received.

Escherichia coli CECT 101 and Micrococcus luteus CECT 245 bacterial strains were obtained from Spanish Collection of Type Culture (Valencia, Spain). MDCK (kidney epithelial cells derived from Madin-Darby canine) and VERO (kidney epithelial cells derived from African green monkey) were purchased from ATCC (USA).

Electrospinning

Polylactide (PLA), poly(ethylene glycol) (PEG) and their mixtures were electrospun from different solvents such as chloroform, dichloromethane and dichloromethane/ dimethylformamide mixtures, and using a polymer weight percentage of 7% for PLA, 35% for PEG and between 7-35% for the studied mixtures. Samples will be named indicating only the polylactide weight percentage (i.e. PLA/PEG-100, PLA/PEG-60 and PLA/PEG-0 correspond to PLA alone, a blend with 60% PLA and 40% PEG, and PEG alone, respectively). The electrospun fibers were collected on a target placed at different distances (10-20 cm) from the syringe tip (inside diameter of 0.84 mm). The voltage was varied between 10 and 30 kV, and the polymer solutions were delivered via infusion syringe pump with mass-flow rate from 0.5 to 10 $mL \cdot h^{-1}$. All electrospinning experiments were carried out at room temperature. Triclosan loaded electrospun fibers were prepared under optimized conditions determined for the corresponding polymer solutions. The triclosan contents of these solutions were 3 and 0.5 *w/v*-% for samples used for release and antibacterial assays, and for cytotoxicity assays, respectively.

Composition, morphology and thermal properties of PLA/PEG scaffolds

Optical morphological observations were made using a Zeiss Axioskop 40 microscope, during the electrospun optimization. Then, morphological details of electrospun samples was conducted by scanning electron microscopy using a Focus Ion Beam Zeiss Neon 40 (Carl Zeiss, Germany). The mats were coating with carbon and visualized at 5 kV.

Calorimetric data were obtained by DSC with a TA Instruments Q100 series equipped with a refrigeration cooling system (RCS). Experiments were conducted under a flow of dry nitrogen with a sample weight of approximately 5 mg, and calibration was performed with indium. Heating runs were carried out at a rate of 20 $^{o}C \cdot min^{-1}$.

Thermal degradation was studied at a heating rate of 20 ºC·min^{-1} with around 5 mg samples in a Q50 thermogravimetric analyzer of TA Instruments and under a flow of dry nitrogen. Test temperatures ranged from 50 to 600 ºC.

Infrared absorption spectra were recorded in the 3600 - 600 cm^{-1} range with a FTIR 4100 Fourier Transform spectrometer from Jasco. A MKII Golden Gate attenuated total reflection (ATR) accessory from Specac was employed.

^{1}H-NMR spectra were acquired with a Bruker AMX-300 spectrometer operating at 300.1 MHz. Chemical shifts were calibrated using tetramethylsilane as an internal standard. Deuterated chloroform ($CDCl_3$) was used as the solvent at room temperature.

X-ray photoelectron spectroscopy (XPS) was performed with a SPECS system equipped with an Al anode XR50 source operating at 200 W and a Phoibos 150 MCD-9 detector XP. The overview spectra were taken with pass energy of 25 eV at 0.1 eV steps at a pressure below 7.5x10^{-9} mbar and binding energies were referred to the C1s and O1s signals.

Porosity of PLA/PGE scaffolds and PEG removal

The porosity of microfiber scaffolds was measured by the liquid intrusion method. Scaffolds (n = 3) were weighed prior to immersion in ethanol or water (liquid intrusion). Vacuum was applied for 10 min, and the scaffolds were left for 1 h on a shaker table to allow diffusion of ethanol into the void volume. The scaffolds were taken out and reweighed before and after drying at vacuum. Porosity (P) was calculated according to **Equation 1**:

$$P = \frac{\left[\frac{(m_w - m_d)}{d_s}\right]}{\left\{\left[\frac{(m_w - m_d)}{d_s}\right] + \left[\frac{(m_d^{PLA})}{d_{PLA}}\right] + \left[\frac{(m_d^{PEG})}{d_{PEg}}\right]\right\}} \qquad (1)$$

where m_w, m_d, m_d^{PLA}, m_d^{PEG} are the weights of the wet scaffold, dry scaffold, PLA fraction and PEG fraction in the dry scaffold, respectively, and d_s, dPLA and dPEG refer to the densities of the solvent (i.e. 1.0 and 0.789 g·mL^{-1} for water and ethanol, respectively), amorphous PLA (1.24 g·mL^{-1}) and semicrystalline PEG (1.07 g·mL^{-1}), respectively. The last densities were estimated using DSC data of scaffolds which point to high and low crystallinity for PEG and PLA phases, respectively.

Capability of water and ethanol to remove PEG from scaffolds was evaluated by the ratio of the initial weight and the weight after drying sample previously immersed for 24 hours in the selected solvent.

Release experiments

Controlled release measurements were made with mats of electrospun samples cut into square pieces (20 x 20 x 0.1 mm^3). They were weighed and incubated at 37 ºC in an orbital shaker at 60 rpm in vessels with 50 mL of phosphate buffered saline release medium (pH 7.4). After 24

h this hydrophilic medium was replaced by the more hydrophobic Sörensen/ethanol (30:70 *v*/*v*) medium. The triclosan concentration in the release media was carried out by UV spectroscopy. Calibration curves were obtained by plotting the absorbance measured at 283 nm against triclosan concentration. All drug release tests were carried out using six replicates to control the homogeneity of the drug release, and the results were averaged.

Antimicrobial test: Assay of Bacterial Growth and Adhesion

Escherichia coli (*E. coli*) and *Micrococcus luteus* (*M. luteus*) bacteria were selected to evaluate the antimicrobial effect of triclosan loaded electrospun fibers.

Growth experiments were performed by seeding 10^3 CFU (colony forming units) in 5 mL of broth culture (Luria-Bertani medium) in the presence of the electrospun fiber mats. The cultures were incubated at 37 ºC and agitated at 200 rpm. After incubation for 24 and 48 h, an aliquot of 100 µL was diluted 10 times with distilled water and absorbance at 600 nm measured. The bacterial number was determined by absorbance measurements at 600 nm and using a McFarland curve.

Adhesion experiments were carried out by seeding 10^7-10^8 CFU in 5 mL of broth culture in the presence of the electrospun fiber mats. The cultures were incubated at 37 ºC and agitated at 200 rpm. After incubation (24 h), the cultures were aspired and the material washed one time with distilled water. Then, 1 mL of sterile 0.01 M sodium thiosulfate was added and the mixture vortexed for 2 min and kept in repose for 30 min to remove the bacteria. Finally, tubes were incubated at 37 ºC and agitated at 200 rpm for 24 h after addition of 4 mL of broth culture. The bacterial number was determined as above indicated.

All assays were conducted in triplicate and the results averaged. *t*-Student test was performed as statistical analysis at a confidence level of 95% ($p < 0.05$).

In-vitro biocompatibility assays: adhesion and cellular proliferation

MDCK and VERO cells were cultured in Dulbecco's modified Eagle medium (DMEM) supplemented with 10% fetal bovine serum, 1% penicillin/streptomycin and 2 mM L-glutamine at 37 ºC in a humidified atmosphere with 5% CO_2 and 95% air.

Unloaded and triclosan loaded PLA/PEG electrospun nanofibers were collected on circular coverslips (diameter 1.5 cm), placed into the wells of a multiwell culture plate and sterilized by UV-radiation in a laminar flux cabinet for 15 min. The samples were fixed in the well using a small drop of silicone (Silbione® MED ADH 4300 RTV, Bluestar Silicones France SAS, Lyon, France) as adhesive. The samples were then incubated in 1 mL of culture medium under culture conditions for 30 min to stabilize the material. Finally, the medium was aspired and the material was evaluated for cell adhesion and proliferation by exposing cells to direct contact with the material surface.

For cell adhesion assay, aliquots of 50-100 µL containing $5x10^4$ cells were seeded onto the electrospun samples in the wells. The plate was incubated under culture conditions for 30 min to allow cell attachment to the material surface. Then, 1 mL of the culture medium was added to each well and the plate incubated for 24 h. Finally, cell viability was determined by MTT (3-(4,5-dimethylthiazol-2-yl)-2,5-diphenyl-2H-tetrazolium bromide) assay. Controls were conducted by cell culture on the polystyrene surface of the plate (TCPS).

The cell proliferation assay was similar to the adhesion assay, but the aliquot of 50-100 µL contained $2x10^4$ cells. Cultures were maintained for 7 days to allow cell growth and adequate cell confluence. The media were renewed every two days. Finally, viability was determined by the MTT assay.

All samples were evaluated using five replicates and the results were averaged and graphically represented. The statistical analysis was performed by one-way ANOVA test to compare the means of all groups. A statistically significant difference between the studied groups was determined by t-Test, which was performed with a confidence level of 95% ($p < 0.05$).

6.1.3 Results and Discussion

Electrospinning Conditions

Several solvents and binary mixtures were tested at different voltages, flows, polymer concentrations and needle-collector distances in order to select the most appropriate conditions to obtain continuous microfibers from all PLA/PEG mixtures. It is well known that for a given polymer (i.e. with a defined chemical constitution and molecular weight) the choice of a "good" solvent plays a fundamental role in the success of the electrospinning process for micro/nanofiber production.[28, 29] It has recently been postulated that solubility and spinability can be correlated in such a way that solvents of high solubility require a high polymer concentration to avoid formation of droplets and electrospun beads, whereas the use of solvents of partial solubility may be appropriate to work with more diluted solutions.[30] Similar solubility parameters have been reported for PLA[31] (i.e. 20.18 $MPa^{0.5}$) and PEG[32] (i.e. 20.08-20.90 $MPa^{0.5}$), and therefore it seems feasible to choose a common solvent for all the mixtures studied in this work. Suitable solvents[33, 34] are dichloromethane (DCM) and chloroform since their solubility parameters (i.e. 20.31 $MPa^{0.5}$ and 18.83 $MPa^{0.5}$, respectively) are close enough to those of the two studied polymers. As explained below, we also tried to use less volatile solvents. Thus, mixtures with dimethylformamide (DMF) (δ = 24.83 $MPa^{0.5}$) were assayed. The final DMF content should be relatively low to obtain a final solubility parameter (e.g., 21.66 $MPa^{0.5}$ was calculated for a DCM/DMF 70:30 *v/v* mixture) close enough to those corresponding to PEG and PLA. Triclosan (TCS) loaded samples were also prepared by electrospinning. A higher solubility parameter[35] (i.e. 29.41 $MPa^{0.5}$) was in this case estimated by van Krevelen's group contribution method;[36] however, the above solvents also seem appropriate because of the low TCS concentration in the solution.

It is interesting to note that PEG can be dissolved in ethanol (δ = 26.42 $MPa^{0.5}$) and is completely soluble in water despite its significantly different solubility parameter (i.e. 47.85 $MPa^{0.5}$). No better agreement was found, even when Hansen parameters determined by the Hoftyzer-Van Krevelen[37] method for dispersion, polar and hydrogen-bonding components (i.e. 16.99, 10.70, 8.88 $MPa^{0.5}$, respectively) were considered (**Figure 6.1.1 c**). In fact, the high solubility was explained by the formation of a coil of water molecules around the PEG chain. In particular, hydrogen bonds were postulated to be established at two sites of each ether oxygen atom of PEG chains with a helical conformation (**Figure 6.1.1 b**).[38]

Figure 6.1.2 shows the importance of the choice of solvent and polymer concentration to obtain good electrospinning results. Specifically, it was unfeasible to get low molecular weight fibers from PEG (e.g., M_n = 10.000 g·mol^{-1}), but continuous fibers were obtained when M_n increased to 35.000 g·mol^{-1} if the polymer concentration in the solution was sufficiently high. Note, for example, that droplets (**Figure 6.1.2 a**) were characteristic when this concentration was low (e.g., close to 10 *wt*-%). Electrospun microfibers could be prepared when PEG (even for low molecular weight samples) was mixed with PLA. Thus, good solvents like DCM rendered fibers even at a relatively low concentration but some aggregates were also frequently formed (**Figure 6.1.2 b**) due to the high volatility of the solvent. The best results were obtained when DMF was added to the solvent to prevent its rapid evaporation (i.e. **Figure 6.1.2 c**). The electrospinning conditions selected for mixtures containing the same amount of PLA are summarized in **Table 6.1.1**. It can be observed that polymer mixtures with increasing PEG content required a higher PEG concentration in the solution, higher voltage and even higher flow (note that only the PEG sample, which had the highest molecular weight, exhibited a different behavior concerning the selected flow.

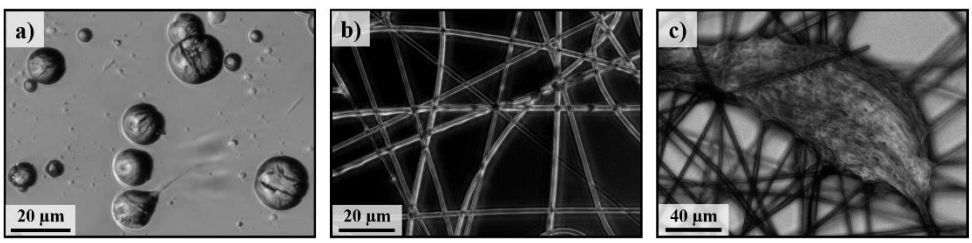

FIGURE 6.1.2

Optical micrographs of typical morphologies of PEG (Mn 35.000 g·mol^{-1}) (a) and PLA/PEG 50 samples (b,c) obtained by electrospinning from polymer solutions in chloroform (a), dichloromethane (b) and a dichloromethane/dimethylformamide (70:30 *v*/*v*) mixture. Polymer concentrations were 10 *wt*-%, 9 *wt*-% and 14 *wt*-% for a), b) and c), respectively.

Figure 6.1.3 shows SEM micrographs of electrospun samples prepared under the selected conditions and the corresponding monomodal diameter distribution, which is also summarized in **Table 6.1.2**. As expected, a higher polymer concentration led to an increase in diameter with the PEG content. Again, PEG fibres did not follow this trend because of the use of a higher molecular weight sample.

TABLE 6.1.1. Hansen parameters of polylactide and selected electrospinning solvents.

Sample	Composition Electrospinning solution[a] (*w*/*w*/*w*)	Polymer Concentration[b] (*wt*-%)	Voltage (kV)	Flow Rate (mL·h^{-1})
PLA/PEG 100	7.0 : 0.0 : 93.0	7.0	16	0.8
PLA/PEG 90	7.0 : 0.8 : 92.2	7.8	17	2.0
PLA/PEG 70	7.0 : 3.0 : 90.0	10.0	18	3.0
PLA/PEG 50	7.0 : 7.0 : 86.0	14.0	18	3.0
PLA/PEG 40	7.0 : 10.5 : 82.5	17.5	18	3.0
PLA/PEG 30	7.0 : 16.3 : 79.7	23.3	20	4.0
PLA/PEG 0	7.0 : 35.0 : 65.0	35.0	20	0.8

Optimal distance between spinneret and collector was 15 cm.
[a]PEG/PLA/(DCM/DMF) weight ratio. DCM/DMF corresponds to a 70:30 *v*/*v* solvent mixture.
[b]Weight of PEG + PLA respect to the total weight of the solution.

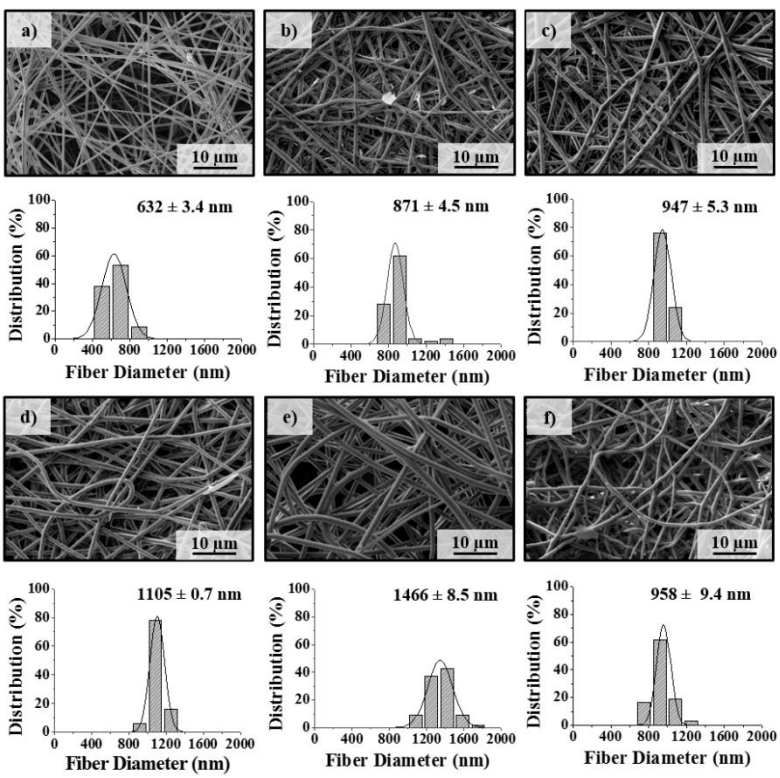

FIGURE 6.1.3

SEM micrographs and diameter distribution of PLA/PEG 100 (a), PLA/PEG 70 (b), PLA/PEG 50 (c), PLA/PEG 40 (d), PLA/PEG 30 (e) and PLA/PEG 0 electrospun micro/nanofibers (f) obtained from a dichloromethane/dimethylformamide (70:30 *v*/*v*) mixture using concentration, voltage, needle-collector distance and flow conditions optimized for each composition.

TABLE 6.1.2. Variation of the fiber diameter size of electrospun PLA/PEG samples after extraction with water and ethanol.

Sample	$Ø_0$ (nm)	After immersion in water[a]			After immersion in ethanol	
		$Ø$ (nm)	$Ø_e$ (nm)	$(Ø_0 - Ø)$ (nm)	$Ø$ (nm)	$(Ø_0 - Ø)$ (nm)
PLA/PEG 100	632 ± 3.39	624 ± 6.54	632	8	588 ± 7.99	44
PLA/PEG 90	648 ± 3.91	451 ± 5.61	610	197	458 ± 2.50	190
PLA/PEG 70	871 ± 4.46	511 ± 0.76	713	360	650 ± 4.52	221
PLA/PEG 50	947 ± 5.30	622 ± 0.05	644	325	700 ± 1.26	247
PLA/PEG 40	1105 ± 0.74	653 ± 0.59	670	452	885 ± 3.40	220
PLA/PEG 30	1466 ± 8.50	933 ± 4.66	763	533	1198 ± 2.09	268
PLA/PEG 0	958 ± 9.38	-	-	-	-	-

[a]$Øe$ is the diameter estimated as $[Ø_0^2 \cdot \rho_m \cdot x/\rho_{PLA}]^{0.5}$, where ρ_m, ρ_{PLA} and x are the density of the initial mixture, the density of PLA and the PLA *wt*-%, respectively.

The capability to obtain continuous microfibers even at a PEG content as high as 70 *wt*-% and using the low molecular weight fraction is worth mentioning. High-magnification SEM micrographs revealed that PLA fibers had a typical rough surface that became progressively smooth with increasing the PEG content (**Figure 6.1.4**). In fact, the PLA/PEG 40 mixture rendered completely smooth fibers, as is also characteristic of PEG. These observations suggest that PEG was predominantly deposited on the outer part of the fiber.

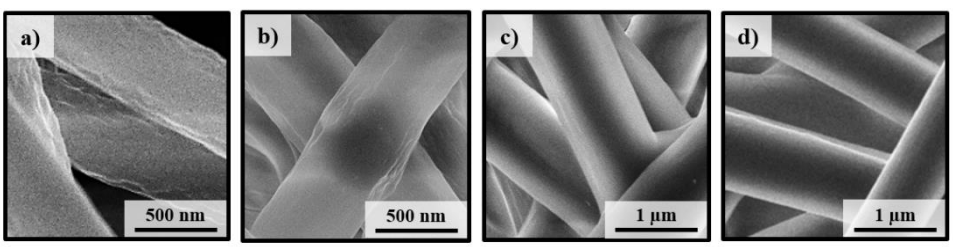

FIGURE 6.1.4

High-magnification SEM micrographs of the surface texture of PLA/PEG 100 (a), PLA/PEG 90 (b), PLA/PEG 50 (c), PLA/PEG 40 (d) samples obtained under optimized conditions for each sample.

Composition and Thermal Properties of Electrospun PLA/PEG Mixtures

FTIR spectra of the electrospun mixtures showed characteristic peaks associated with PLA (e.g., 1753 and 1182 cm^{-1}) or PEG (e.g., 961 and 834 cm^{-1}) (**Figure 6.1.5 a**) with a variable intensity ratio that depended on the composition. Although the absorbance ratio between, for example, 1753 and 834 cm^{-1} bands could be used to evaluate the final composition of the mixture, analysis of the ^{1}H-NMR spectrum (**Figure 6.1.5 b**) was obviously a more precise tool. Thus, areas corresponding to PLA methine (quadruplet at 5.19-5.13 ppm), PEG methylene (singlet at 3.64 ppm) and PLA methyl (doublet at 1.59-1.57 ppm) protons were used to determine the molar PLA content of the electrospun fibers (**Table 6.1.3**) as showed in the **Equation 2**:

$$\text{PLA } (\textit{molar}\text{-}\%) = 100 \cdot \left[\left(\frac{A_{1.59\text{-}1.57}}{3}\right) + \left(\frac{A_{5.18\text{-}5.15}}{1}\right)\right] / \left[\left(\frac{A_{1.59\text{-}1.57}}{3}\right) + \left(\frac{A_{3.64}}{4}\right) + \left(\frac{A_{5.18\text{-}5.15}}{1}\right)\right] \qquad (2)$$

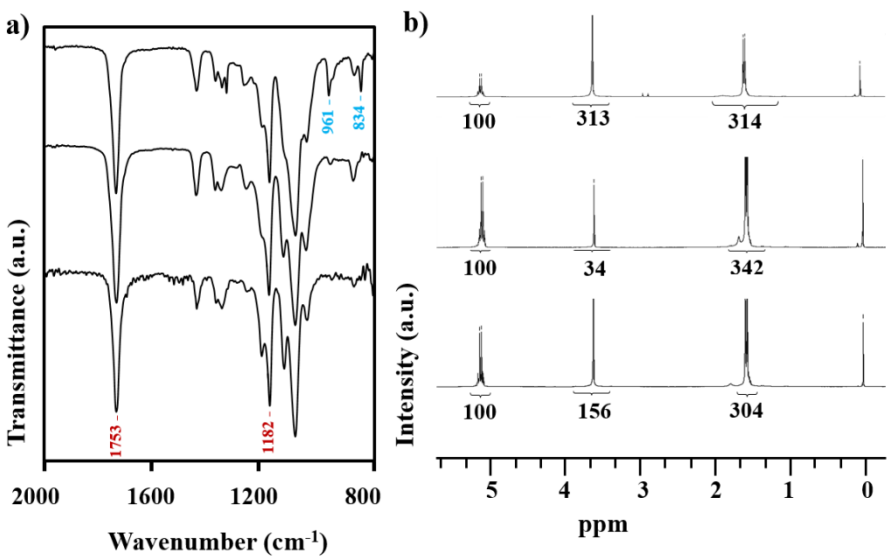

FIGURE 6.1.5

FTIR (2000-800 cm^{-1}) (a) and NMR (b) spectra of PLA/PEG 70 electrospun samples before (top) and after immersion in water (middle) and ethanol (bottom).

Values in **Table 6.1.3** show good agreement with the molar feed ratio in the initial electrospinning solutions.

TABLE 6.1.3. Composition of PLA/PEG samples before and after being immersed in water and ethanol for 24 hours.

Sample	PLA (*molar*-%)[a]	PLA (*molar*-%)[b]	After immersion in water		After immersion in ethanol	
			PLA (*molar*-%)[b]	Extracted PEG (*molar*-%)[b]	PLA (*molar*-%)[b]	Extracted PEG (*molar*-%)[b]
PLA/PEG 100	100.0	100.0	-	-	-	-
PLA/PEG 90	84.6	83.3	93.0	54.5	96.8 : 3.2	78.9
PLA/PEG 70	58.8	56.5	92.9	83.4	72.1 : 27.9	35.2
PLA/PEG 50	37.9	35.7	92.8	88.5	66.5 : 33.5	46.6
PLA/PEG 40	28.9	27.0	91.2	88.0	63.3 : 36.7	50.0
PLA/PEG 30	20.7	19.2	95.2	93.9	64.8 : 35.2	55.6
PLA/PEG 0	0.0	0.0	-	-	-	-

[a]Theoretical value from the composition of the electrospinning solution.
[b]Experimental composition from analysis of ^{1}H-RMN spectra.
[c]Calculated from the final (PEG_f) and the initial (PEG_0) molar percentages of PEG as $100 \cdot PEG_f/PEG_0$.

Figure 6.1.6 shows heating and cooling runs of all electrospun samples whereas melting and crystallization data are summarized in **Table 6.1.4**. In general, distinctive peaks associated with melting/crystallization of each homopolymer are easily distinguished.

Several points can be made:

- The melting temperature and enthalpy associated with the PEG peak decreases with the PLA content, the change in enthalpy being highly significant, especially when PLA content increased from 50 to 70 *wt*-%. Note also that PEG was not able to crystallize at higher PLA contents;
- The melting temperature associated with PLA remained practically constant for all samples but interestingly the melting enthalpy reached a high value when the PEG content was above 10 *wt*-% (i.e. similar to the semicrystalline commercial sample before electrospinning). It seems that PEG facilitated the orientation of PLA molecules in the electrospinning process, making it possible to achieve maximum crystallinity. It is interesting to note that the PLA cold crystallization peak was only detected for the PLA-rich electrospun samples, and consequently the crystallinity observed for samples with a PEG content equal to or above 30 *wt*-% was attained in the electrospinning process (i.e. not during the DSC heating scan);
- The PEG (PLA/PEG 0) electrospun sample and the non-processed sample (commercial PEG) showed similar melting behaviors whereas crystallinity was lower for the PLA (i.e. PLA/PEG 100) electrospun sample than for the commercial sample.

TABLE 6.1.4. Selected calorimetric data from the heating and cooling scans performed with the different PLA/PEG electrospun samples before and after being molten, respectively.

Sample	T_m^{PEG} [ºC]	ΔH_m^{PEG} [J·g^1]	T_c^{PEG} [ºC]	ΔH_c^{PEG} [J·g^1]	T_m^{PLA} [ºC]	ΔH_c^{PLA} [J·g^{-1}]	T_m^{PLA} [ºC]	ΔH_m^{PLA} [J·g^{-1}]
PLA[a]	-	-	-	-	-	-	149.8	33.4
PLA/PEG 100	-	-	-	-	111.5	19.8	149.6	20.1
PLA/PEG 90	-	-	-	-	110.9	10.5,11.7	149.0	15.1,16.8
PLA/PEG 70	55.4	16.0,53.3	-	-	-	-	150.1	22.3,31.8
PLA/PEG 50	61.6	73.8,147.6	39.4	63.9,127.8	-	-	149.4	15.7,31.4
PLA/PEG 40	62.6	94.9,158.2	40.3	83.6;139.3	-	-	150.4	14.5,36.2
PLA/PEG 30	62.5	107.0,152.9	41.9	101.7;145.3	-	-	148.8	10.0,33.3
PLA/PEG 0	63.8	170.1	44.7	165.7	-	-	-	-
PEG[a]	65.0	177.2	44.4	177.2	-	-	-	-

Melting and crystallization data of PLA corresponds to the first heating scan. Melting and crystallization data of PEG corresponds to the heating and cooling scans, respectively. Pair of values reported in the enthalpy data columns refer to the total weight and the specific PLA or PEG weight of samples, respectively.
[a]Pellets of the commercial sample corresponds to the 35000 g·mol^{-1} sample.

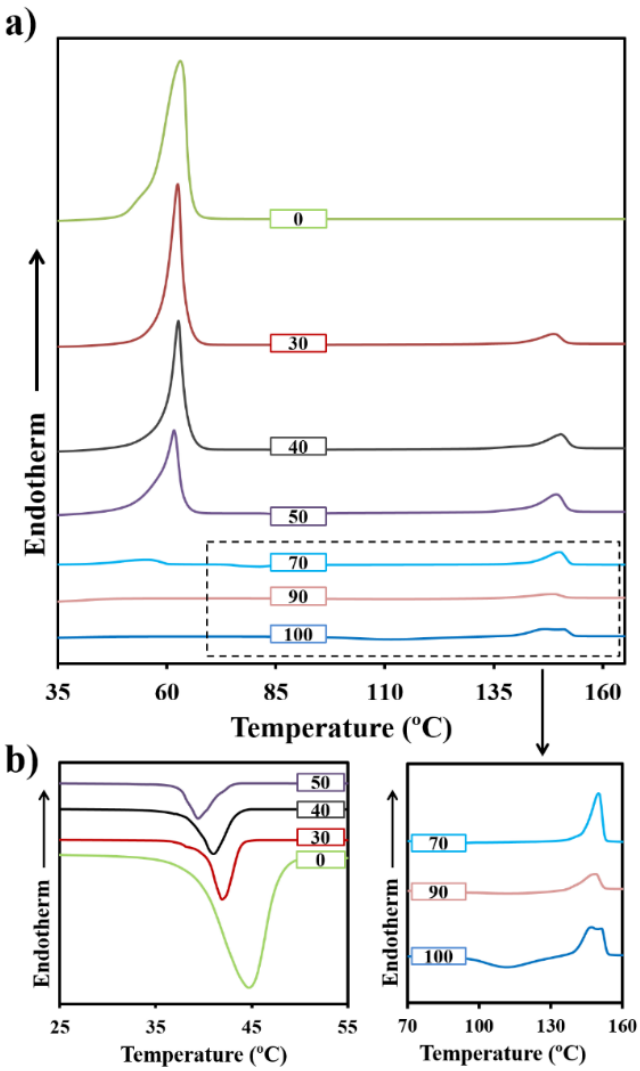

FIGURE 6.1.6

DSC heating (a) and cooling (b) runs performed with electrospun samples obtained under the corresponding optimized processing conditions. Curves are labelled indicating the PLA *wt*-% in each mixture.

Thermal degradation of PLA/PEG samples occurred in two steps whose maximum weight losses at a heating rate of 20 ºC/min corresponded to 369 and 423 ºC, as is characteristic of degraded PLA[39] and PEG[40] homopolymers, respectively. Logically, the weight losses associated with each step were proportional to the content of the corresponding homopolymer in the mixture (**Figure 6.1.7**). Despite the close contact between all molecules after the electrospinning process, the degradation behavior of each polymer was clearly unaltered; even the former decomposition of PLA, which mainly gives rise to lactide, did not affect the stability of the remaining PEG. This is not always true, as recently reported for mixtures of polytrimethylene carbonate and PLA.[41]

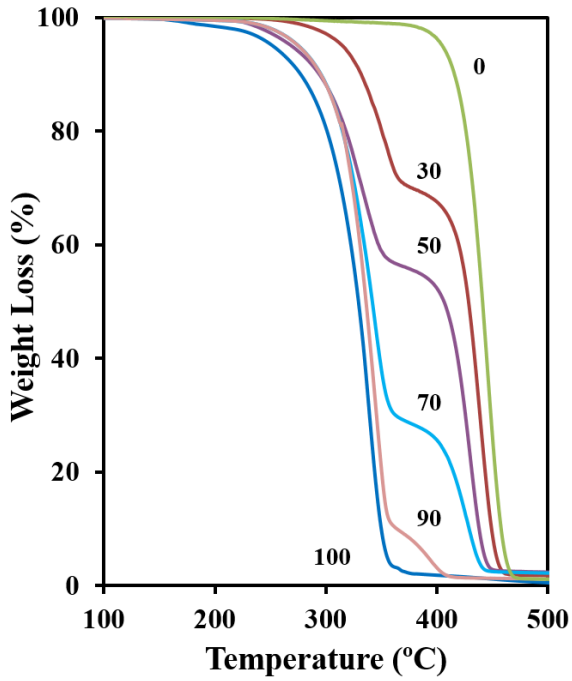

FIGURE 6.1.7

TGA degradation curves of all PLA/PEG electrospun samples. Curves are labelled indicating the PLA *wt*-% in each mixture.

Solubility of PLA/PEG Scaffolds in Water and Ethanol

PEG is a polymer that is completely soluble in water, so it was interesting to study the effect of this solvent on the morphology of electrospun micro/nanofibers. FTIR (**Figure 6.1.5 a**) and NMR (**Figure 6.1.5 b**) spectra showed a clear decrease in the intensity of typical PEG signals after immersion of the samples in water. **Figure 6.1.8 a** illustrates the good correlation of weight loss after immersion with the initial PEG content, although the final molar compositions determined from NMR data and summarized in **Table 6.1.3** demonstrate that a small amount of PEG always remained in the PLA matrix. This value increased with the PLA content in the

initial scaffold, as expected for high trapping efficiency (e.g., PLA/PEG 90 and PLA/PEG 70 samples retained 55.5% and 8.1% of the initial PEG, respectively).

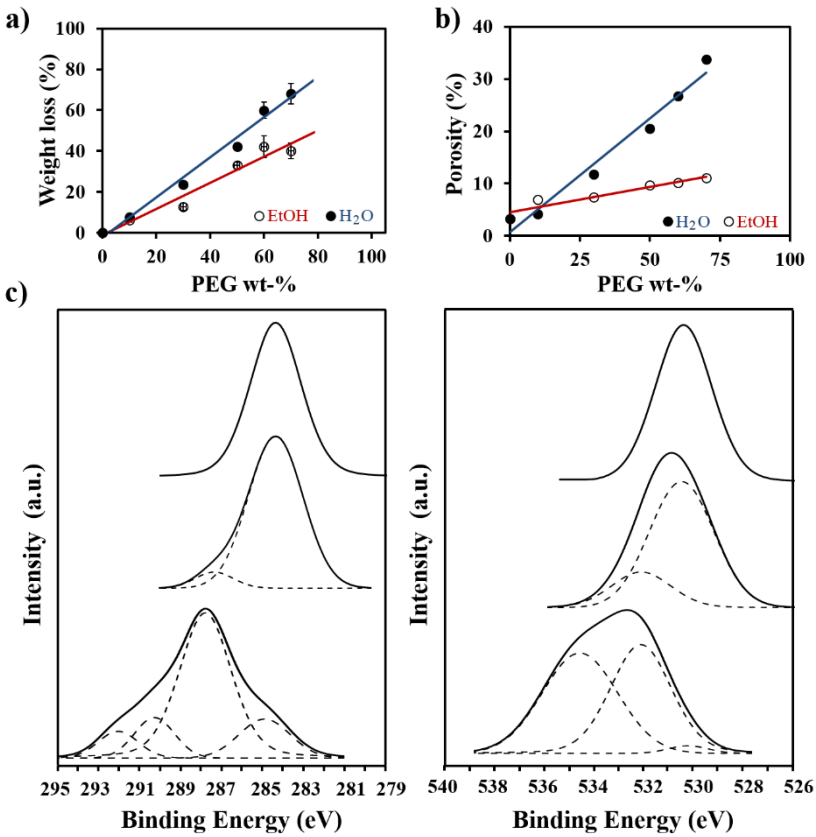

FIGURE 6.1.8

a) Weight loss of all PLA/PEG electrospun samples after immersion in water (*black circles*) and ethanol (*white circles*). b) Plot of porosity (%) versus initial PEG *wt*-% of electrospun samples after immersion in water (*black circles*) and ethanol (*white circles*). c) Carbon (*left*) and oxygen (*right*) XPS signals of PEG (*top*), and PLA/PEG 70 electrospun samples before (*middle*) and after (*bottom*) immersion in water.

A fiber morphology was still observed after exposure to water, as shown in **Figure 6.1.9** for a representative sample. A significant decrease in the fiber diameters was logically detected, with the final values being in relatively good agreement with those calculated from the measured weight losses and polymer densities (**Table 6.1.3**). A slight swelling effect was generally found, although a clear contraction was detected for the mixture with the highest PEG content. Roughness of fiber surfaces increased after water exposure, as shown in the high-magnification SEM micrographs (**Figure 6.1.9**) of samples with an initial smooth texture. It is clear that a significant fraction of PEG was deposited on the fiber surfaces. The reported data demonstrate that a small fraction of PEG can be retained in the micro/nanofibers. Thus, even after water exposure hydrophilicity can be enhanced compared to that of PLA samples. Furthermore, and more important, the size of fibers diminished drastically. Consequently, the scaffolds should

have bigger pores that could facilitate cell in growth. **Figure 6.1.8 b** illustrates this linear increase in scaffold porosity with the PEG content after immersion in water.

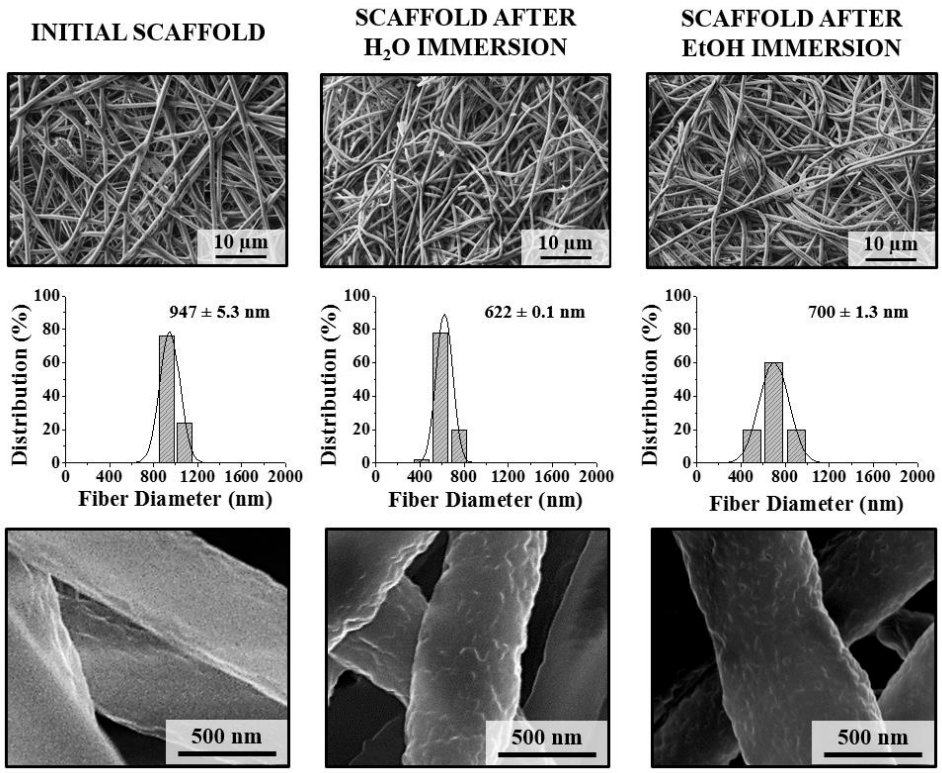

FIGURE 6.1.9

Low-magnification SEM micrographs (top row), diameter distribution (middle row) and high-magnification SEM micrographs (bottom row) of PLA/PEG 50 electrospun samples before (left column) and after immersion in water (middle column) and ethanol (right column).

When they were immersed in ethanol, the scaffolds behaved completely differently, despite this solvent's ability to dissolve PEG. Spectroscopic data (**Figure 6.1.5**, **Table 6.1.3**) clearly indicate that a maximum of 55% of the initial PEG was dissolved when PLA content in the samples was lower than 90 *wt*-%. Moreover, the weight loss after immersion was clearly less than the initial PEG content (**Figure 6.1.8 a**). A fiber morphology of all PLA/PEG samples was logically maintained (**Figure 6.1.9**) although in this case a slight decrease in the fiber diameter was detected (**Table 6.1.2**). Fiber surface texture was again characterized by a roughness which was demonstrative of the solubilization of the PEG deposited on their surfaces. Ethanol was not able to form a coil of solvent molecules around the PEG chain, which could facilitate the diffusion of PEG outside the PLA matrix. Thus, when using ethanol instead of water, PEG was effectively trapped inside fibers and scaffold porosity was barely affected (**Figure 6.1.8 b**).

The composition of the surface layer of each PLA/PEG scaffolds (i.e. the surface of the constitutive micro/nanofibers) was studied from the analysis of C1s and O1s peaks of the XPS spectra (**Figure 6.1.8 c**). PEG spectra were characterized by C1s and O1s peaks at binding energies of 284.6 eV and 532 eV, respectively, whereas PLA spectra were more complicated since three C1s peaks were observed at 292.0 eV (CO), 290.0eV (CH) and 287.7 eV (CH_3) and two O1 peaks at 534.8 eV (O-C) and 532.4 eV (O=C) in the deconvoluted spectra. **Figure 6.1.8 c** clearly shows the correspondence of XPS spectra of PLA/PEG 70 to PEG, which strongly supports the idea that this polymer was preferentially deposited on the fiber surface during electrospinning. Note that this mixture had the highest PLA content, and is therefore the best sample to demonstrate a preferential deposition of PEG on the surface. Logically, XPS spectra of scaffolds with a higher PEG content also revealed that the fiber surface was mainly constituted by PEG. The spectra changed dramatically when scaffolds were immersed in water due to the solubilization of PEG. Thus, practically only the signals attributed to PLA were detected after immersion, as shown in **Figure 6.1.8 c** (bottom). However, very small signals attributed to PEG could still be observed, in agreement with NMR data, demonstrating the retention of a small amount of PEG in the PLA matrix.

Triclosan Loading and Release from PLA/PEG Scaffolds

The micro/nanofibers of samples were easily loaded with triclosan by adding the appropriate amount of the drug (3 *w/v*-%) in the initial electrospinning solutions. In this way, triclosan-loaded scaffolds were prepared under the same processing conditions determined for the unloaded samples. **Figure 6.1.10** illustrates the final morphology of the representative PLA/PEG 50 sample. The diameters of loaded fibers were generally rather similar to those previously determined for the unloaded samples. Variations were not significant (e.g., 947 nm versus 913 nm and 1105 nm versus 1181 nm for unloaded and TCS loaded PLA/PEG 50 and PLA/PEG 40 samples, respectively). Furthermore, the diameters were found to increase or decrease slightly (i.e. with no specific trend) for different compositions of the polymer mixture. More interestingly, the roughness of the fiber surface increased upon the addition of triclosan, as can be deduced by comparing the TCS loaded PLA/PEG 50 sample with the unloaded one, which was characterized by a smooth surface (**Figure 6.1.10 c** and **6.1.10 d**). This change in the fiber surface morphology may play an important role in supporting cell attachment.

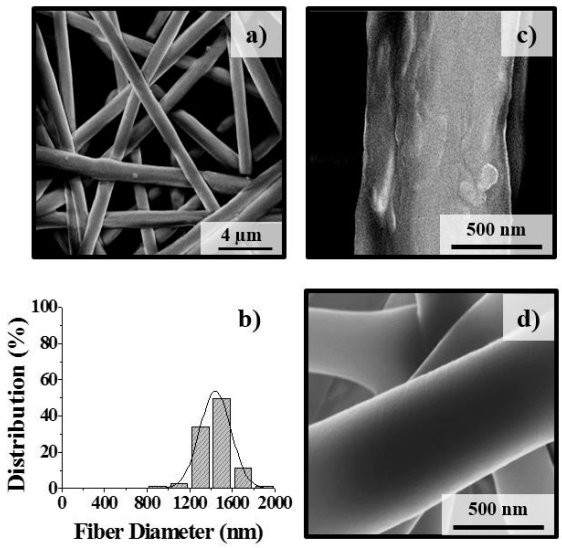

FIGURE 6.1.10

Low-magnification SEM micrograph (a), diameter distribution (b) and high-magnification SEM micrographs (c) of triclosan loaded PLA/PEG 50 samples. For the purpose of comparison, a high-magnification micrograph of unloaded PLA/PEG 50 samples is shown in (d).

Figure 6.1.11 illustrates the release behaviors of several PLA/PEG samples when they were successively exposed to a hydrophilic PBS medium and then to a more hydrophobic Sörensen/ethanol (30:70 *v/v*) solution. Interestingly, the release profiles of all samples were highly similar, and therefore practically independent of the fiber composition. Profiles showed four different steps. First, a progressive release up to 10% of the loaded drug that extended over a period of 8-10 h was observed. As previously deduced for other TCS loaded matrices,[42, 43] it seems that an equilibrium condition was reached when the medium was highly hydrophilic and released triclosan reached a saturation level. Note that composition of samples varied during the indicated period since practically all PEG was dissolved in the medium, as previously demonstrated. This means that triclosan incorporated into the PEG rich phases was still retained in the final PLA rich micro/nanofiber. It is clear that the coil of water molecules around the PEG chain allowed its solubilization but did not affect the triclosan incorporated into the two component fiber system. In addition, TCS release profiles during this period were slightly different for samples containing different amounts of PEG. Thus, the inset of **Figure 6.1.11** shows that release was slightly enhanced for higher PEG contents, suggesting that TCS was effectively incorporated into the PEG phase on the surface, and could therefore solubilize with no chance of being trapped in the PLA matrix. Note also that solubility parameters (**Figure 6.1.1 c**) indicate a similar interaction between triclosan and the two polymers considered.

Second, after the initial period the amount of released triclosan was constant while the medium did not change (during the period between 10 and 24 h), in agreement with the establishment of an equilibrium condition. Third, a fast release was observed when the medium was replaced with the Sörensen/ethanol mixture. The release period extended over 2-5 h and a new saturation

level which increased slightly by reducing the PLA content (76% and 78% for PLA/PEG 100 and PLA/PEG 40, respectively) was reached. Minor differences can be explained by the increase in the fiber diameter with PEG content, which could hinder the diffusion of TCS from PEG rich samples. Fourth, the amount of released triclosan remained constant as the exposure time was increased. It seems that an equilibrium condition was again established in the new more hydrophobic medium, and that the PLA content of PLA/PEG 40 micro/nanofibers was sufficient to retain a significant percentage (i.e. ~25%) of loaded triclosan.

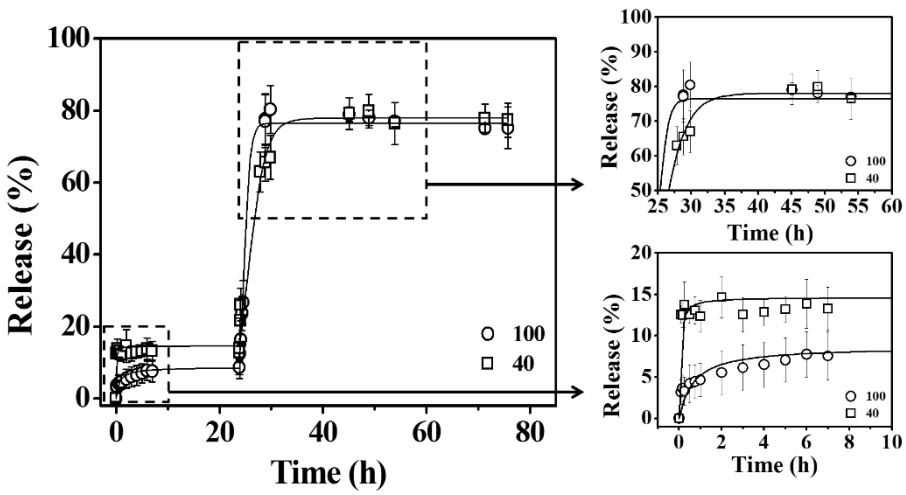

FIGURE 6.1.11

Triclosan release curves for PLA/PEG 100 (*circles*), PLA/PEG 40 (*squares*) electrospun samples. Release was conducted in a PBS medium for the first 24 h and then in a Sörensen/ethanol mixture (30:70 *v*/*v*).

Antibacterial Properties of Triclosan-Loaded PLA/PEG Scaffolds

Triclosan is a broad-spectrum antiseptic with documented safety and efficacy against Gram-positive and Gram-negative bacteria (e.g., *M.luteus* and *E.coli*, respectively). The antibacterial effect of triclosan released from micro/nanofiber mats was determined by studying bacterial growth and adhesion inhibition in broth medium. As shown in **Figure 6.1.12** for unloaded samples, scaffold composition had a small effect on *E.coli* growth and adhesion that gradually diminished with increasing PEG content when *M.luteus* was assayed. It has been reported that Gram-positive bacteria were unable to metabolize PEG due to the lack of appropriate enzymes,[44] which is probably the main reason for the enhanced growth of Gram-positive bacteria in non-PEG materials. Thus, a high PEG content in the material could be beneficial in avoiding bacterial growth. The effect of triclosan was clearly enhanced for the Gram-negative bacterium (i.e. *E.coli*) due to its higher sensitivity to the drug. In summary, all loaded scaffolds were found to be unable to support bacterial adhesion since the relative values always decreased up to approximately 85%. The result is significant because it demonstrates the capability of the hydrophobic medium to facilitate TCS release and the effective avoidance of the formation of bacterial biofilms.

PEG is also an interesting component for use as a sacrificial polymer since it can be easily removed by solubilization in water, leading to samples with increased porosity. **Figure 6.1.11 e** and **6.1.11 f** compare the antibacterial growth effect of TCS loaded scaffolds before and after immersion in water (i.e. samples without the predominant PEG component) for both Gram-positive and Gram-negative bacteria. No statistical differences between the two kinds of samples were found. Thus, triclosan could be effectively retained in the micro/nanofibers after removing PEG, in agreement with the above release experiments. Results also point out that the negative effect of PEG on *M. luteus* growth is insignificant compared with that of loaded TCS.

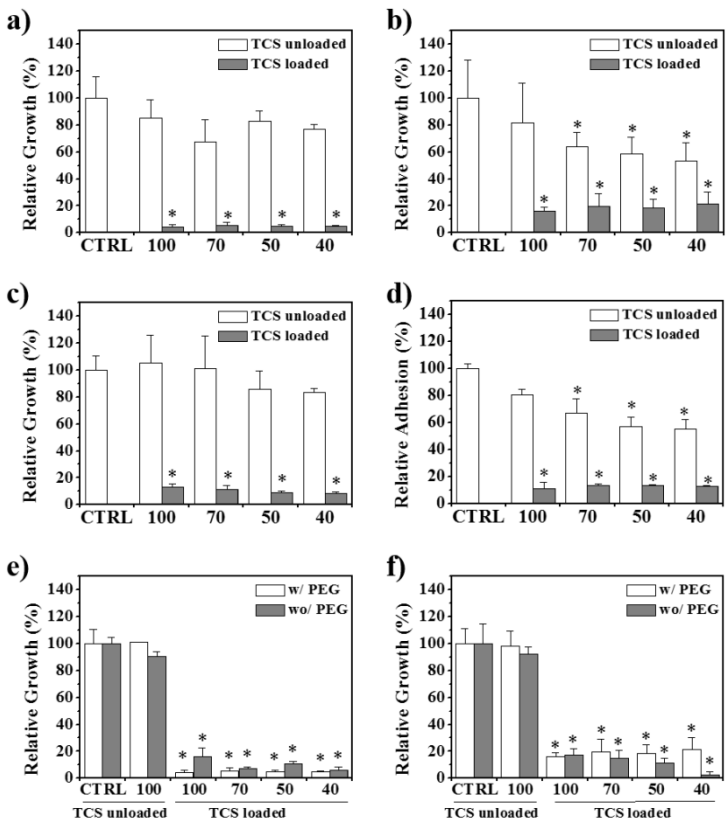

FIGURE 6.1.12

Relative growth (a,b) and adhesion (c,d) of *Escherichia coli* (a,c) and *Micrococcus luteus* (b,d) on control surfaces and unloaded and TCS loaded PLA/PEG electrospun samples. Plots of the relative growth of *Escherichia coli* (e) and *Micrococcus luteus* (f) before (w/PEG) and after immersion in water (wo/PEG) are also shown. ($^{*}p < 0.05$) *vs.* positive control.

Biocompatibility of Unloaded and Triclosan Loaded PLA/PEG Scaffolds

The triclosan antibacterial effect must be harmonized with the safety of eukaryotic cells because these should receive the antibacterial protection. Thus, adhesion and proliferation of two epithelial cells (MDCK and VERO) were studied for unloaded and TCS loaded scaffolds. Both experiments are important to follow cell development since adhesion is an early cellular event whereas proliferation is an evidence of metabolic cell activity. **Figure 6.1.13 a** compares the results on relative adhesion for all materials studied. No significant differences were found between the control, unloaded sample and TCS loaded samples. Furthermore, adhesion was largely independent of the cell (MDCK or VERO) and scaffold composition. In contrast, statistically significant differences in proliferation were observed (**Figure 6.1.13 b**). Thus, colonization increased by 20-40% in PLA/PEG scaffolds compared to the control, irrespective of the incorporation of triclosan. More interestingly, proliferation was enhanced for higher PEG contents in the initial scaffold. This is in agreement with increased porosity of scaffolds caused by the solubilization of PEG (used as a sacrificial polymer) and the formation of 3D structures that are more favorable for rapid cell colonization of the material. Other less influential factors include greater roughness of nanofiber surfaces and increased hydrophilicity due to the small amount of PEG that is always present in the PLA matrix, as mentioned above.

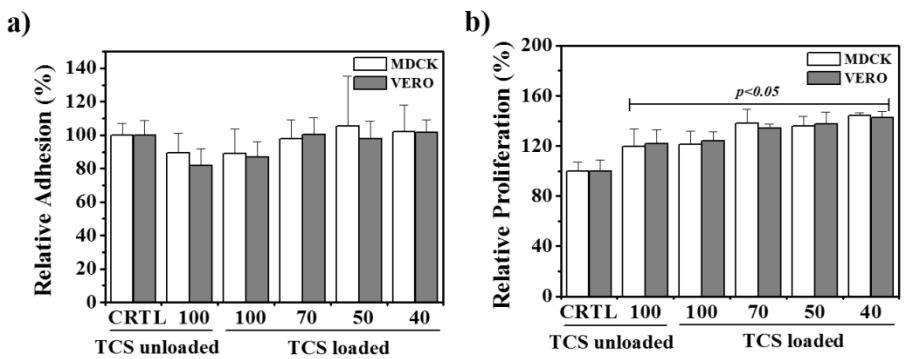

FIGURE 6.1.13

Adhesion (a) and proliferation (b) of MDCK and VERO cells on control plate surfaces and unloaded and TCS loaded PLA/PEG electrospun samples.

6.1.4 Conclusions

Scaffolds constituted by a variable ratio of poly(ethylene glycol) and polylactide in various ratios were prepared by the electrospinning technique using dicloromethane/dimethylformamide (70:30 *v/v*) as the solvent. The resulting micro/nanofibers were found to be continuous even at a high PEG content (i.e. 70 *wt*-%) and have smoother surfaces as this content was increased. A preferential deposition of PEG on the outermost part of each fibers was inferred, as also demonstrated by XPS analysis.

Most of the PEG was easily removed by exposure to water, although a small amount was always found to be retained in the PLA matrix. Scaffolds with different hydrophilicity, and even with high porosities, were thus obtained if PEG was used as a sacrificial polymer. A completely different behavior was observed for scaffolds exposed to ethanol as a large amount of PEG was retained inside the fibers and practically only the PEG deposited on the surface was effectively solubilized.

The roughnesses of the triclosan-loaded samples increased, and release was marked by the achievement of an equilibrium condition that varied significantly with the hydrophilicity of the exposure medium. Slight differences in the release behavior were detected depending on the composition; specifically, an increase in PLA content resulted in higher retention of the drug, especially in a hydrophilic medium.

Triclosan-loaded PLA/PEG scaffolds exhibited antibacterial activity regardless of the composition, although a slight decreasing trend with the PEG content was detected for the Gram-positive bacteria. Cell adhesion and proliferation were well supported by PLA/PEG scaffolds, even when they were loaded with triclosan. Cell proliferation was significantly dependent on the initial PEG content; in particular, cell colonization was enhanced in the more porous 3D structures attained after solubilization of PEG.

6.1.5 References

[1] E.S. Place, J.H. George, C.K. Williams, M.M. Stevens, Chem Soc Rev, 38 (2009) 1139-1151.

[2] P.A. Madurantakam, C.P. Cost, D.G. Simpson, G.L. Bowlin, Nanomedicine (Lond), 4 (2009) 193-206.

[3] M.P. Lutolf, J.A. Hubbell, Nat Biotechnol, 23 (2005) 47-55.

[4] K.F. Leong, C.K. Chua, N. Sudarmadji, W.Y. Yeong, J Mech Behav Biomed Mater, 1 (2008) 140-152.

[5] D.H. Reneker, I. Chun, Nanotechnology, 7 (1996) 216-223.

[6] S.F. Badylak, D.O. Freytes, T.W. Gilbert, Acta Biomater, 5 (2009) 1-13.

[7] Y. Dzenis, Science, 304 (2004) 1917-1919.

[8] D. Li, Y.N. Xia, Adv Mater, 16 (2004) 1151-1170.

[9] K. Jayaraman, M. Kotaki, Y.Z. Zhang, X.M. Mo, S. Ramakrishna, J Nanosci Nanotechno, 4 (2004) 52-65.

[10] D.H. Reneker, A.L. Yarin, H. Fong, S. Koombhongse, J Appl Phys, 87 (2000) 4531-4547.

[11] J. Rouwkema, N.C. Rivron, C.A. van Blitterswijk, Trends Biotechnol, 26 (2008) 434-441.

[12] Y. You, B.M. Min, S.J. Lee, T.S. Lee, W.H. Park, J Appl Polym Sci, 95 (2005) 193-200.

[13] O. Suwantong, P. Pankongadisak, S. Deachathai, P. Supaphol, J Polym Res, 19 (2012) 9896-9886.

[14] J.Y. Park, I.H. Lee, J Polym Res, 18 (2011) 1287-1291.

[15] M. Peesan, R. Rujiravanit, P. Supaphol, J Biomat Sci-Polym E, 17 (2006) 547-565.

[16] Y.H. Nien, C.Y. Shih, C.Y. Yang, C.J. Lu, Q.X. Ye, J Polym Res, 20 (2013) 166-171.

[17] S.A. Sell, M.J. McClure, K. Garg, P.S. Wolfe, G.L. Bowlin, Adv Drug Deliver Rev, 61 (2009) 1007-1019.

[18] Z.G. Chen, X.M. Mo, F.L. Qing, Mater Lett, 61 (2007) 3490-3494.

[19] H. Homayoni, S.A.H. Ravandi, M. Valizadeh, Carbohyd Polym, 77 (2009) 656-661.

[20] S.N. Stephansson, B.A. Byers, A.J. Garcia, Biomaterials, 23 (2002) 2527-2534.

[21] Y. Lin, L.L. Wang, P.B. Zhang, X. Wang, X.S. Chen, X.B. Jing, Z.H. Su, Acta Biomater, 2 (2006) 155-164.

[22] X.W. Jiang, E.B. Vogel, M.R. Smith, G.L. Baker, J Polym Sci Pol Chem, 45 (2007) 5227-5236.

[23] Y.K. Luu, K. Kim, B.S. Hsiao, B. Chu, M. Hadjiargyrou, J Control Release, 89 (2003) 341-353.

[24] M. Spasova, O. Stoilova, N. Manolova, I. Rashkov, G. Altankov, J Bioact Compat Pol, 22 (2007) 62-76.

[25] B.Y. Wang, S.Z. Fu, P.Y. Ni, J.R. Peng, L. Zheng, F. Luo, H. Liu, Z.Y. Qian, J Biomed Mater Res A, 100A (2012) 441-449.

[26] P.Y. Ni, S.Z. Fu, M. Fan, G. Guo, S.A. Shi, J.R. Peng, F. Luo, Z.Y. Qian, Int J Nanomed, 6 (2011) 3065-3075.

[27] D.A. Herold, K. Keil, D.E. Bruns, Biochem Pharmacol, 38 (1989) 73-76.

[28] S.V. Fridrikh, J.H. Yu, M.P. Brenner, G.C. Rutledge, Phys Rev Lett, 90 (2003).

[29] M.G. McKee, C.L. Elkins, T.E. Long, Polymer, 45 (2004) 8705-8715.

[30] C.J. Luo, M. Nangrejo, M. Edirisinghe, Polymer, 51 (2010) 1654-1662.

[31] D. Karst, Y.Q. Yang, J Appl Polym Sci, 96 (2005) 416-422.

[32] M.J. Fernández-Berridi, T.F. Otero, G.M. Guzman, J.M. Elorza, Polymer, 23 (1982) 1361-1366.

[33] J. Brandrup, E.H. Immergut, E.A. Grulke, A. Abe, D.R. Bloch, Fourth ed., John Wiley & Sons, New York, 2003.

[34] R.C. Weast, M.J. Astle, 60th ed., CRC Press Inc., Boca Raton. Florida, 1980.

[35] D.M. Aragón, D.A. Chiappetta, J. Degrossi, E.F. Vargas, C. Bregni, A. Sosnik, F. Martínez, Rev Col Cienc Quím Farm, 37 (2008) 241-257.

[36] A. Barton, 2nd ed., CRC Press Inc. , New York, 1991.

[37] D.W. van Krevelen, P.J. Hoftyzer, Angew Makromol Chem, 52 (1976) 101-109.

[38] Y. Aray, M. Manuel, J. Rodriguez, D. Vega, Y. Simon-Manso, S. Coll, C. Gonzalez, D.A. Weitz, J Phys Chem B, 108 (2004) 2418-2424.

[39] F.D. Kopinke, M. Remmler, K. Mackenzie, M. Moder, O. Wachsen, Polym Degrad Stabil, 53 (1996) 329-342.

[40] S.L. Madorsky, S. Straus, J Polym Sci, 36 (1959) 183-194.

[41] Y. Marquez, L. Franco, J. Puiggali, Thermochim Acta, 550 (2012) 65-75.

[42] R. Zurita, J. Puiggali, A. Rodriguez-Galan, Macromol Biosci, 6 (2006) 58-69.

[43] L.J. del Valle, R. Camps, A. Diaz, L. Franco, A. Rodriguez-Galan, J. Puiggali, J Polym Res, 18 (2011) 1903-1917.

[44] A.I. Lopez, R.Y. Reins, A.M. McDermott, B.W. Trautner, C.Z. Cai, Mol Biosyst, 5 (2009) 1148-1156.

6.2 Scaffolds Constituted by Mixed Polylactide and Poly(Ethylene Glycol) Electrospun Microfibers

Scaffolds constituted by different ratios of poly(ethylene glycol) (PEG) and polylactide (PLA) electrospun fibers have been prepared by using a single rotatory collector. Electrospinning parameters and solution conditions were optimized to obtain continuous fibers and a homogeneous distribution of both polymers in the final scaffold. Short needle-collector distances allowed good overlapping of the two incident and independent jets. The composition of the scaffold was effectively tuned by varying the flow rate of the PLA solution. PEG and PLA fibers could be well distinguished in the scaffold because of their smooth and rough textures, and diameters in the nanometric and micrometer range. Greater sizes corresponded to polylactide and clearly depended on the flow rate. Drugs such as triclosan and polyhexamethylene biguanide hydrochloride, which have different hydrophilic/hydrophobic character and molecular size, were loaded into PLA microfibers by electrospinning. The high water solubility of PEG justified its use as a sacrificial polymer. Thus, it was possible to prepare scaffolds with tuned porosity (from 40 to 80%) by water immersion of dual samples having different PEG content. Porosity greatly affected the release rate; specifically a practically instantaneous or a sustained release were determined for triclosan in an appropriate medium. Drug loaded scaffolds had a clear bactericidal effect that was more effective for Gram-positive bacteria. Cell proliferation studies indicate that fibroblast colonization increased by 20-25% in PLA/PEG scaffolds with high PEG content compared to the

6.2.1 Introduction

Electrospinning is one of the simplest procedures for generating 3D scaffolds for tissue engineering applications. This technique is highly versatile because it allows fibers with diameters varying from the micrometer to the nanometer range to be obtained from a wide diversity of polymers. Basically, a polymer solution is ejected from a capillary by a strong electrostatic potential and collected as a non-woven fibrous mat on an electrically grounded target. Selection of appropriate experimental conditions for a given polymer (i.e. solvent, polymer concentration and operational parameters such as strength of the applied electric field, needle-collector distance and flow rate) are basic to get homogeneous and continuous fibers with a selected diameter.[1-4] Furthermore, it is possible to prepare core-shell structures by using a coaxial spinneret[5] or even by replacing the electrospinning solution by a water-in-oil (W/O) emulsion.[6]

Scaffolds usually employed in the biomedical field are based on biodegradable polyesters such as polycaprolactone and polylactide (PLA). However, these polymers generally have problems related to their inherent hydrophobic nature that may reduce expression of phenotypic markers and hinder cell attachment and proliferation.[7, 8] Among approaches that have been proposed to increase hydrophilicity of electrospun fibers, some consider the use of polyethylene glycol (PEG). This polymer can be easily eliminated from human body, is biocompatible and shows interesting properties for biomedical applications.[9] Efforts have mainly focused on decreasing the hydrophobicity of polylactide due to its excellent combination of characteristics like tunable mechanical properties, degradation into natural metabolites, biocompatibility and low cost. Thus, scaffolds with increased hydrophilicity have been obtained by: a) Electrospinning of diblock or triblock copolymers having PEG segments,[10-12] b) Emulsion electrospinning of PEG and PLA-*b*-PEG diblock copolymers,[13] c) Electrospinning of solution mixtures of PLA and PEG.

Spasova *et al*.[14] demonstrated the possibility to easily modulate the hydrophilicity of PLA nanofibers by adding PEG to the spinning solutions. They also reported that osteoblasts tended to arrange in tissue-like structures for long-term cultures, especially in scaffolds with the highest PEG content. An excellent *in-vitro* osteogenic potential and *in vivo* biocompatibility with the surrounding tissues was found for PLA scaffolds containing 5 *wt*-% of PEG.[15] Electrospinning of PLA could also be improved by addition of low molecular weight PEG because regular and continuous fibers were produced due to the reduction of solution viscosity.[16] These fibers could be prepared up to a 79 *wt*-% of PEG and rendered scaffolds with enhanced cell proliferation because of the more porous 3D structures obtained after solubilization of PEG.[17] On the other hand, the use of PLA/PEG mixtures has inherent problems related to the difficulty of electrospinning PEG.

The high water solubility of PEG indicates that scaffolds constituted from either uniaxial or coaxial electrospun fibers based on PEG and PLA are rapidly enriched in the PLA component after exposure to a physiologic medium. Therefore, PEG can be considered as a sacrificial polymer with a remarkable function in the early stages of implantation because its hydrophilicity may favor cell adhesion, and also in the later stages because the increasing porosity of scaffolds should enhance cell colonization. Therefore, preparation of PEG/PLA scaffolds merits attention. Specifically, the first goal of this work evaluates a different approach where each polymer is independently electrospun and the resultant fibers collected together in a rotatory collector (**Figure 6.2.1**). In this case, electrospinning of PEG requires using high molecular weight samples (i.e. M_n greater than 30,000 g·mol^{-1}). The method allows easy modulation of the ratio between PLA and PEG without any restriction and even determination of the final characteristics of each fiber (e.g., diameter and texture). The only limitation resulted from the intrinsic difficulty in electrospinning PEG because of high molecular weight samples (i.e. M_n close to 35,000 g·mol^{-1}).

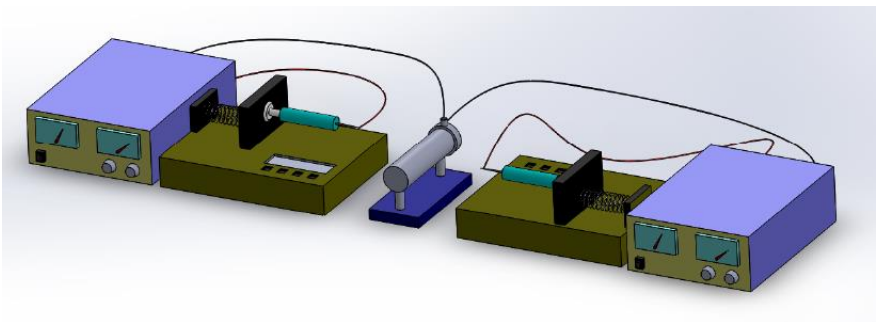

FIGURE 6.2.1
Graphical representation of dual electrospinning.

The second goal of this work is to evaluate the biocompatibility of new scaffolds and the bactericide effect caused by incorporation of drugs with well-differentiated hydrophobic/hydrophilic character. Physicochemical interactions between drug molecules and polymer matrix play a fundamental role, and specifically the hydrophobic/hydrophilic properties of drug and polymer should be matched to achieve good drug encapsulation into electrospun nanofibers. Triclosan (TCS) and polyhexamethylene biguanide hydrochloride (PHMB) (**Figure 6.2.2**) were chosen as model drugs. The first is a well-known antibacterial and antifungal agent[18] scarcely soluble in water but well soluble in ethanol. The second is a hydrophilic cationic oligomer having an average of 7-11 biguanide groups spaced by flexible hexamethylene segments.[19-21] PHMB action against microorganisms is consequence of its binding to the negatively charged phosphate head groups of phospholipids on the bacterial cell wall.

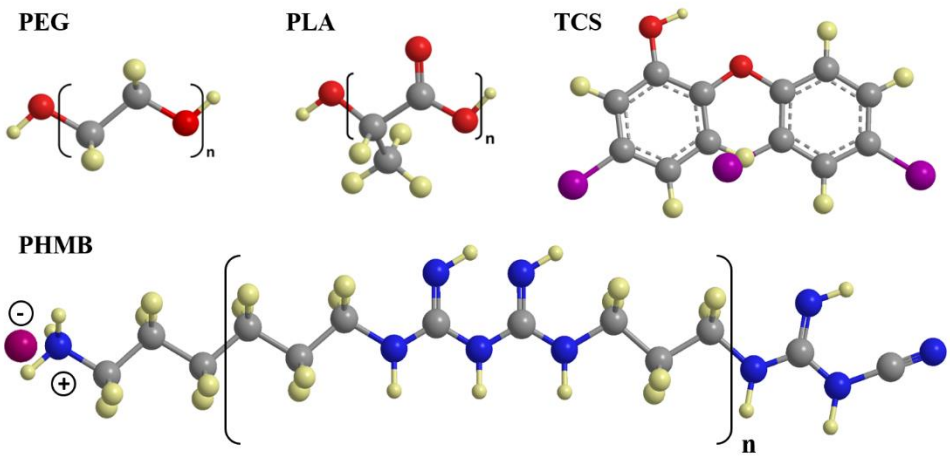

FIGURE 6.2.2
Chemical structures of PLA, PEG, TCS and PHMB.

6.2.2 Experimental Section

Materials

PEG with number average molecular weight of 35,000 g·mol^{-1} was purchased from Sigma-Aldrich. Polylactide (PLA), a product of Natureworks (polymer 2002D), was kindly supplied by Nupik International (Polinyà, Spain). According to the manufacturer, this PLA has a D content of 4.25%, a residual monomer content of 0.3%, a density of 1.24 g·cc^{-1}, a glass transition temperature (T_g) of 58 ºC and a melting point of 153 ºC. Solvents, Triclosan (TCS) and cell culture labware were purchased from Sigma-Aldrich (USA). Polyhexamethylene biguanide hydrochloride (PHMB) was kindly provided by B. Braun Surgical S.A. (Rubí, Spain).

Escherichia coli CECT 101 and *Micrococcus luteus* CECT 245 bacterial strains were obtained from Spanish Collection of Type Culture (Valencia, Spain). Human fetal lung fibroblast cells (MRC-5) and African green monkey kidney epithelial cells (VERO) were from ATCC (USA).

Electrospinning

A dual electrospinning system was used to prepared scaffods constituted by a mixture of PEG and PLA microfibers, as depicted in **Figure 6.2.1**. Samples will be denoted by the experimental polylactide molar percentage (i.e. PLA/PEG-100, PLA/PEG-67 and PLA/PEG-0 correspond to PLA alone, a blend with 67 *molar*-% of PLA and 33 *molar*-% of PEG, and PEG alone, respectively). Electrospun fibers were collected on a rotary ground collector operating at 30 rpm and placed at a variable distance (6-25 cm) from two equidistant needle tips (inside diameter of 0.84 mm). The needles were placed facing each other in order to minimize disturbing effects between the two electrically charged jets of PLA and PEG solutions. The voltage was varied between 10 and 30 kV and applied to the collector using two high-voltage suppliers (Gamma High Voltage Research, ES30-5W). Polymer solutions were delivered via two KDS100 infusion syringe pumps (KD Scientific, USA) to control the flow rate (from 0.5 to 10 mL·h^{-1}). All electrospinning experiments were carried out at room temperature. Unloaded and TCS and PHMB loaded electrospun fibers were prepared using optimized parameters (e.g., needle-collector distance, voltage and flow rates) and solvent conditions (e.g., solvent ratio, and polymer and drug concentrations). The TCS and PHMB contents of the electrospinning solutions were 1 and 0.25 *w/v*-%, respectively.

Morphology and properties of electrospun scaffolds

Optical microscopy studies were performed with a Zeiss Axioskop 40 microscope. Micrographs were taken with a Zeiss AxiosCam MRC5 digital camera.

Detailed inspection of texture and morphology of electrospun samples was conducted by scanning electron microscopy using a Focus Ion Beam Zeiss Neon 40 instrument (Carl Zeiss, Germany). Carbon coating was accomplished by using a Mitec K950 Sputter Coater fitted with a *k*150x film thickness monitor. Samples were visualized at an accelerating voltage of 5 kV.

The diameter of electrospun fibers was measured with the SmartTiff software from Carl Zeiss SMT Ltd.

Contact angles (CA) were measured at room temperature with sessile drops using an OCA-15 plus Dynamic Contact Angle Microscope (Dataphysics, USA) and SCA20 software. Contact angle values of the right and left sides of distilled water drops were measured and averaged. Measurements were performed 10 s after the drop (5 mL) was deposited on the sample surface. All CA data were an average of six measurements on different surface locations.

Calorimetric data were obtained by differential scanning calorimetry (DSC) with a TA Instruments Q100 series equipped with a refrigeration cooling system (RCS). Experiments were conducted under a flow of dry nitrogen with a sample weight of approximately 5 mg, and calibration was performed with indium. Heating runs were carried out at a rate of 20 ºC·min^{-1}. Thermal degradation was studied at a heating rate of 20 ºC·min^{-1} with around 5 mg samples in a Q50 thermogravimetric analyzer (TGA) of TA Instruments and under a flow of dry nitrogen. Test temperatures ranged from 50 to 600 ºC.

Porosity of PLA/PEF scaffolds

The porosity of scaffolds was measured by the liquid intrusion method. Scaffolds (n = 3) were weighed prior to immersion in water (intrusion liquid). Vacuum was applied for 10 min, and the scaffolds were placed on a shaker table for 1 h to allow diffusion of water into the avoid volume. The scaffolds were taken out and reweighed. Porosity was calculated according to **Equation 1**:

$$P = [(m_w - m_d) / d_w)] /[(m_w - m_d) / d_w] + [m_d^{PLA} / d_{PLA}] + [m_d^{PEG} / d_{PEG}] \quad (\mathbf{1})$$

where m_w, m_d, m_d^{PLA}, m_d^{PEG} are the weights of the wet scaffold, dry scaffold, PLA fraction and PEG fraction in the dry scaffold, respectively, and d_w, d_{PLA} and d_{PEG} refer to the densities of the solvent (i.e. 1.0 g·mL^{-1} for water), amorphous PLA (1.24 g·mL^{-1}) and semicrystalline PEG (1.07 g·mL^{-1}), respectively. The last two densities were estimated using DSC data of scaffolds which point to high and low crystallinity of PEG and PLA homopolymers, respectively.

Release experiments

Controlled release measurements were made with square pieces (weighting approximately 200 mg) of the electrospun scaffolds. These pieces were weighed and incubated at 37 ºC in an orbital shaker at 200 rpm in tubes of 50 mL for 1 week. PBS buffer (hydrophilic medium) and alternatively its mixture with ethanol (i.e. 3:7 *v*/*v* ratio) as a more hydrophobic component were employed as release media. Drug concentration was evaluated by UV spectroscopy using a Shimadzu 3600 spectrometer. Calibration curves were obtained by plotting the absorbance measured at 281 and 236 nm versus TCS and PHMB concentration. Samples were withdrawn from the release medium at predetermined time intervals. The volume was kept constant by

addition of fresh medium. All drug release tests were carried out using three replicates and the results were averaged.

Antimicrobial test

Escherichia coli (*E. coli*) and *Micrococcus luteus* (*M. luteus*) bacteria were selected to evaluate the antimicrobial effect of TCS and PHMB loaded electrospun fibers. The bacteria were previously grown aerobically to exponential phase in broth culture (5 $g \cdot L^{-1}$ beef extract, 5 $g \cdot L^{-1}$ NaCl, 10 $g \cdot L^{-1}$ peptone, pH 7.2).

Bacterial adhesion experiments were performed on a 24-well culture plate. Square pieces (0.5×0.5×0.1 mm^3) of the electrospun scaffolds were placed into each well. Then, 1 mL of broth culture containing 10^3 CFU was seeded on the electrospun fiber mats. The cultures were incubated at 37 ºC and agitated at 200 rpm. The culture media were aspirated after incubation and the material washed once with distilled water. Then, 0.5 mL of sterile 0.01M sodium thiosulfate was added to each well. After addition of 4 mL of broth culture, the plate was incubated at 37 ºC and agitated at 200 rpm for 24 h. The bacterial number was determined as above indicated. All assays were conducted in triplicate and the results averaged.

Cellular adhesion and proliferation assays

MRC-5 and VERO cells were cultured in Dulbecco's modified Eagle medium (DMEM) as previously reported.[22]

Square pieces (0.5×0.5×0.1 mm^3) of the electrospun scaffolds were placed into the wells of a multiwell culture plate. Samples were fixed in the wells with a small drop of silicone (Silbione® MED ADH 4300 RTV, Bluestar Silicones France SAS, Lyon, France) and then sterilized by UV-radiation in a laminar flux cabinet for 15 min. For the cell adhesion and proliferation assays, aliquots of 50-100 µL containing $5x10^4$ (adhesion assay) and $2x10^4$ (proliferation assay) cells were seeded onto the electrospun samples in each well and incubated for 24 h (adhesion assay) or 4 days (proliferation assay).

Samples were evaluated by the standard adhesion and proliferation method[22] using MTT reactive. The experiments were carried out using three replicates and the results were averaged. Samples with adhered and grown cells on the mats were fixed with 2.5 *w/v*-% formaldehyde at 4 ºC overnight. They were subsequently dehydrated and processed for observation by scanning electronic microscopy.

Statistical analysis

The statistical analysis was performed by one-way ANOVA followed by Tukey test. The analyses were performed with a confidence level of 95% ($p < 0.05$).

6.2.3 Results and Discussion

Electrospinning Conditions

Solvent and polymer concentration conditions could be selected from previous works on PLA and PEG because each polymer was electrospun independently. Chloroform/acetone 2:1 *v*/*v* and dichloromethane/dimethylformamide 7:3 *v*/*v* mixtures were employed for PLA and PEG, respectively.[17, 22] PLA required a low polymer concentration (5-7 *wt*-%) due to the high viscosity of the final solution, whereas PEG was difficult to electrospun and a minimum concentration of 35 *wt*-% was necessary for the commercial sample with a molecular weight of 35,000 $g \cdot mol^{-1}$. This forced the use of a PLA flow rate higher than that of PEG when scaffolds had to keep a structural consistency capable of dissolving PEG after exposure to aqueous environments. Experiments were performed with maximum (i.e. 10 *wt*-%) and minimum (i.e. 35 *wt*-%) PLA and PEG concentrations, respectively, to minimize the difference between flow rates. Scaffolds with variable composition were prepared by varying the PLA flow rate (from 0.8 to 10 $mL \cdot h^{-1}$) and keeping the rate of PEG at a minimum value (0.8 $mL \cdot h^{-1}$) to maintain good fiber morphology.

The distance between the needles and the rotary collector was also fundamental to obtain scaffolds with a homogeneous composition. For example, ejected jets did not perfectly overlap onto the collector when distances were greater than 10 cm. High dispersion of compositions was therefore found after NMR analysis of specimens taken along a diagonal of the obtained scaffold. Short distances (e.g., 3 cm) were also inappropriate because of considerable defects in fibers caused by poor solvent evaporation.

Optimization of the electrospinning process indicated that a needle-collector distance of 6 cm and voltages of 20 and 15 kV for PEG and PLA, respectively, were adequate for all the indicated flow rates. PLA and PEG fibers could easily be distinguished on account of their morphology as shown in **Figures 6.2.3** and **6.2.4**.

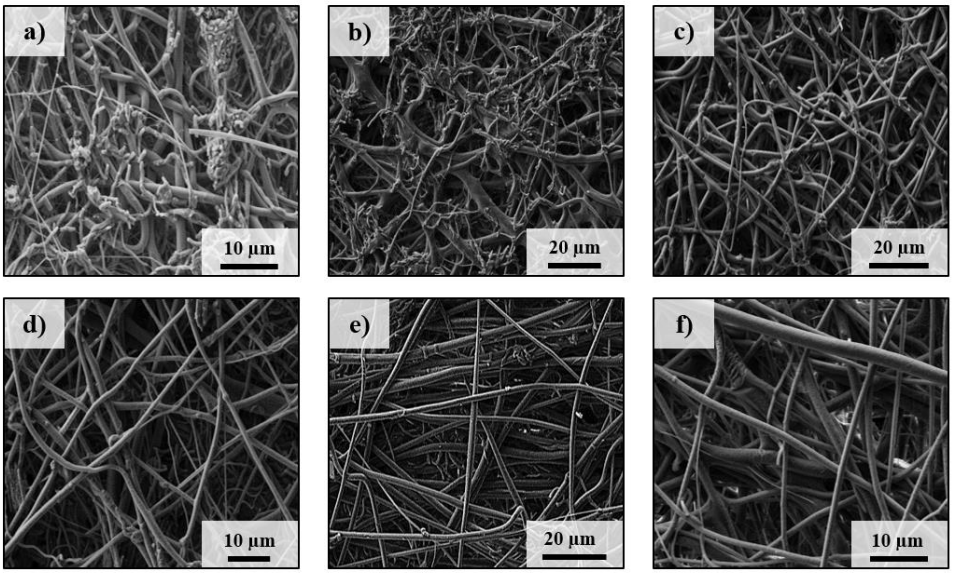

FIGURE 6.2.3

Low-magnification SEM micrographs of PLA/PEG-14 (a), PLA/PEG-31 (b) PLA/PEG-48 (c), PLA/PEG-59 (d), PLA/PEG-67 (e) and PLA/PEG-77 (f) samples.

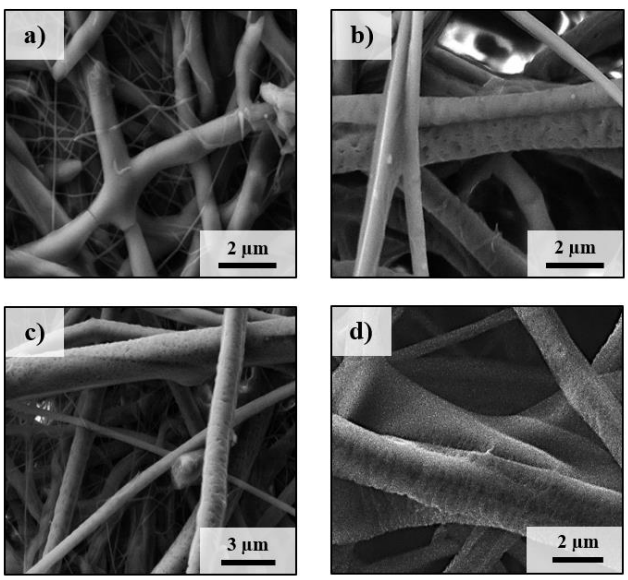

FIGURE 6.2.4

High magnification SEM micrographs showing the surface texture of PLA/PEG-14 (a), PLA/PEG-31 (b), PLA/PEG-48 (c) and PLA/PEG-77 (d) samples.

Thus, a gradual change of the scaffold morphology according to the polymer composition can be clearly observed in the low magnification images. Specifically, samples with a high PEG content had a higher ratio of narrow and tortuous fibers. High magnification micrographs indicate that these PEG fibers had a smooth texture and high diameter distribution. In fact, two populations of fibers in the nanometric (100-300 nm) and micrometric (850-1200 nm) size range could be seen in the micrographs of samples with a high PEG content (e.g., **Figure 6.2.4 a**). On the contrary, rigid microfibers having a rather homogeneous diameter distribution and a rough texture with abundant pores and tranversal striations were typically observed for PLA-rich samples (**Figure 6.2.4 d**). Since PLA and PEG fibers could be differentiated according to their morphology (**Figures 6.2.4 b** and **6.2.4 c**) a statistical analysis of their diameter distribution was performed, see **Table 6.2.1** for PLA. Average diameters of the unimodal distributions were found to increase gradually from 1185 to 1830 nm with the flow rate.

Scaffold Composition and Properties

The experimental PLA/PEG ratio was determined from ^{1}H-NMR spectra (**Figure 6.2.5**) because well differentiated signals could be assigned to each polymer (**Figure 6.2.5**). Homogeneity in composition was also verified with spectra from several specimens regularly distribute along the diagonal of each scaffold. Areas corresponding to PLA methine (quadruplet at 5.19-5.13 ppm), PEG methylene (singlet at 3.64 ppm) and PLA methyl (doublet at 1.59-1.57 ppm) protons were used to determine the molar PLA content of the electrospun scaffolds (**Table 6.2.1**) according to **Equation 2.**

$$\text{PLA } (\textit{molar}\text{-}\%) = 100 \cdot \left[\left(\frac{A_{1.59\text{-}1.57}}{3}\right) + \left(\frac{A_{5.18\text{-}5.15}}{1}\right)\right] / \left[\left(\frac{A_{1.59\text{-}1.57}}{3}\right) + \left(\frac{A_{3.64}}{4}\right) + \left(\frac{A_{5.18\text{-}5.15}}{1}\right)\right] \qquad (2)$$

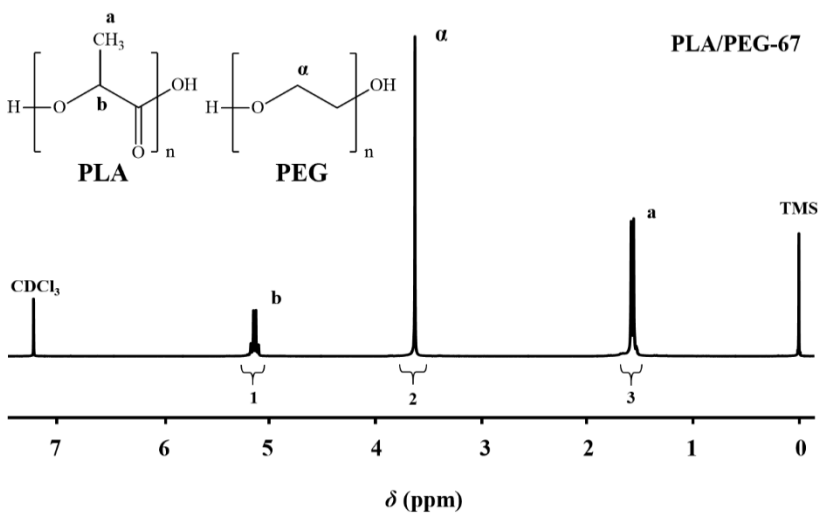

FIGURE 6.2.5

^{1}H-NMR spectra of PLA/PEG-67 electrospun samples.

Values summarized in **Table 6.2.1** show relatively good agreement with the molar feed ratio in the initial electrospinning solutions. A slight deficit in the PEG content was detected in most cases.

TABLE 6.2.1. Fiber diameter and composition of PLA/PEG scaffolds obtained from the indicated flow rates of the PLA solution.[a]

Sample	PLA flow rate ($mL \cdot h^{-1}$)	PLA (*mol*-%)		Ø (nm)
		Feed	Scaffold	
PLA/PEG-0	0	0	0	958 ± 9[b]
PLA/PEG-14	0.8	19.3	14	1185 ± 6[c]
PLA/PEG-31	2.0	37.3	31	1195 ± 24[c]
PLA/PEG-48	4.0	54.3	48	1210 ± 43[C]
PLA/PEG-59	6.0	64.1	59	1273 ± 15[C]
PLA/PEG-67	8.0	70.4	67	1465 ± 17[C]
PLA/PEG-77	10.0	74.9	77	1501 ± 41[C]
PLA/PEG-100	10.0	100	100	1830 ± 10[C]

[a]The flow rate of the PEG solution was 0.8 $mL \cdot h^{-1}$ for all scaffolds except for PLA/PEG-100.
[b]Average diameter of PEG microfiber population.
[c]Average diameter of PLA fibers.

Composition was also evaluated from the melting enthalpies measured in the DSC heating scans of the different scaffolds (**Table 6.2.2**). Calorimetric traces showed melting peaks at 62-65 ºC and 150-153 ºC associated to PEG and PLA homopolymers, respectively. PEG weight percentages of all scaffolds could also be estimated from the melting enthalpy of the low temperature peak and that determined for the PLA/PEG-0 sample. Values summarized in **Table 6.2.2** indicate again good agreement with theoretical percentages and even with values calculated from NMR spectra.

TGA traces of PLA/PEG-*x* samples (**Figure 6.2.6**) showed two degradation steps which maximum weight losses at a heating rate of 20 ºC·min^{-1} corresponding to 369 and 423 ºC, as characteristic for the decomposition of PLA[23] and PEG[24] homopolymers, respectively. Logically, the weight loss associated with each step was proportional to the content of the corresponding homopolymer in the mixture and could be used as an additional indication of scaffold composition.

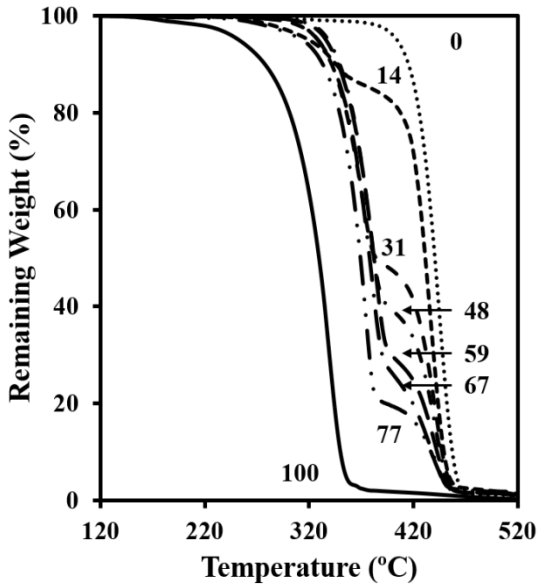

FIGURE 6.2.6

TGA degradation curves of PLA/PEG-*x* electrospun samples. Curves are labelled indicating the *mol*-% of PLA in each sample.

TABLE 6.2.2. Selected calorimetric data from the heating scan of PLA/PEG-*x* electrospun samples and estimation of their PEG content.

Sample	T_{mPEG} (ºC)	ΔH_{mPEG} ($J \cdot g^{-1}$)	T_{mPLA} (ºC)	ΔH_{mPLA} ($J \cdot g^{-1}$)	PEG (*wt*-%)[a]	PEG (*wt*-%)[b]	PEG (*wt*-%)[c]
PLA/PEG-0	63.8	170.1	-	-	100	100	100
PLA/PEG-14	65.7	138.3	151.7	2.5	81.3	77.8	83.7
PLA/PEG-31	62.2	102.1	151.9	8.9	60.0	58.3	65.0
PLA/PEG-48	62.0	87.9	152.3	10.1	51.7	41.2	47.4
PLA/PEG-59	64.3	64.2	152.6	12.1	37.8	31.8	36.7
PLA/PEG-67	63.2	48.2	152.2	13.2	28.3	25.9	29.1
PLA/PEG-77	63.1	40.1	151.9	15.8	23.6	21.9	19.9
PLA/PEG-100	-	-	149.6	20.1	0	0	0

[a]From calorimetric data.
[b]Theoretical values according to electrospinning flow rates.
[c]From ^{1}H-NMR spectra.

Contact angle measurements could only be performed onto PLA-rich scaffolds because the high hydrophilicity of PEG caused spread and sorption of the sessile drop. As can be seen in **Figure 6.2.7**, the sample with 77 *mol*-% of PLA had a similar contact angle to the PLA scaffold (125º). No measurements could be made on scaffolds having a lower PLA content (e.g., 65%). PLA rich scaffolds were more hydrophobic than PLA melt-pressed films, whose contact angle was close to 93º since surface roughness also becomes a dominant factor in wettability of materials. It is well reported that the surface area of a rough surface is greater than the surface area of a comparably sized smooth surface, and consequently an increase of the contact angle should be expected.[25] Contact angles measurements performed on samples previously immersed in water were in the 115º-130º for all compositions, showing the solubilization of PEG and the attainment of a typical PLA scaffold.

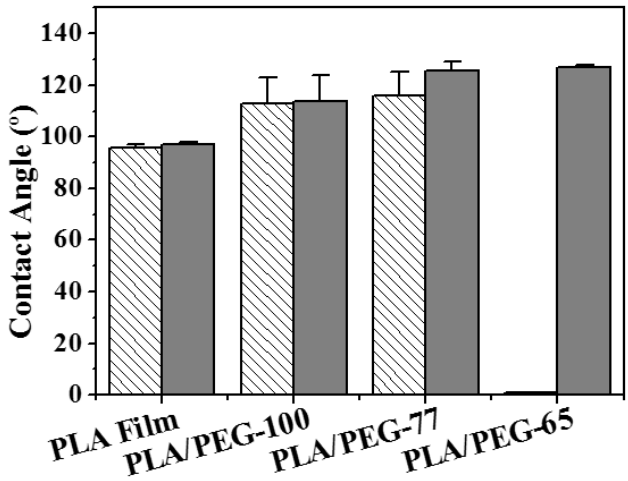

FIGURE 6.2.7

Contact angles of representative PLA/PEG-*x* scaffolds and a PLA film (sparsed bars). Data after immersion on water are also given for scaffolds.

PEG could be effectively removed by immersion of the scaffold in water, as demonstrated by NMR spectra (not shown). Thus, the percentage of PEG removed was practically 100% except for the PLA-rich scaffold (i.e. PLA/PEG 77), which had a retention or trapping efficiency close to 6%. Porosity of samples clearly increased after solubilization of PEG, and logically the effect was more significant as the initial content of PEG increased (**Figure 6.2.8**). A series of scaffolds with tuned porosity from 40 to 80% could thus be easily obtained by using PEG as a sacrificial polymer, which is an interesting feature for tissue engineering applications because cell growth is facilitated.

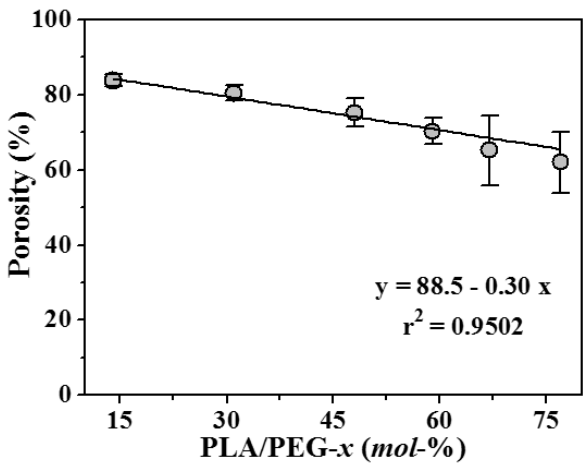

FIGURE 6.2.8

Plot of porosity (%) of PLA/PEG-*x* scaffolds after immersion in water versus initial molar percentage of PLA in the scaffold sample.

Triclosan and PHMB Release from PLA/PEG-*x* Scaffolds and Bactericide Properties

PLA microfibers were easily loaded with TCS and PHMB bactericide agents by adding the appropriate amount of the drug (1 *w/v*-% and 0.25 *w/v*-% for TCS and PHMB, respectively) in the corresponding electrospinning solution. A small percentage of dimethylsulfoxide (10 *v/v*-%) was also incorporated into the drug containing solutions to solubilize both drugs. In the case of PHMB, the process was hampered by the drastic increase in viscosity of the solution that limited the maximum load to a value of 0.25 *w/v*-%. Operational parameters previously optimized for the electrospinning process could still be applied for new solutions. On the contrary, morphology of samples was affected by the change of solvent and the presence of the drug. Specifically, moderate and remarkable diameter decreases were detected for all TCS and PHMB loaded scaffolds, respectively. For instance, the diameter decreased from 1185 nm to 762 nm and 319 nm for PLA/PEG-14 scaffolds loaded with TCS and PHMB, respectively, as summarized in **Table 6.2.3**. The rough texture of electrospun PLA was not modified when fibers were loaded with TCS. However, a drastic change was observed for PHMB loaded samples. In this case, the obtained nanofibers had a smooth surface and could not be distinguished in terms of size and texture from the typical PEG nanofibers (**Figure 6.2.9**).

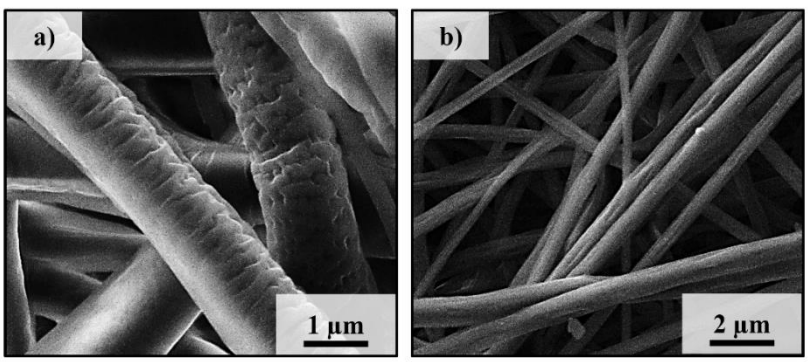

FIGURE 6.2.9

High magnification SEM micrographs of a PLA/PEG-48 electrospun sample loaded with TCS (a) and PHMB (b).

The release of TCS and PHMB from PLA/PEG scaffolds was studied in the hydrophilic PBS medium and also in its mixture with 70 *v*/*v*-% of ethanol, which could have greater affinity with hydrophobic drugs and even with PLA. Ethanol could also produce a swelling effect that facilitates drug release.

TABLE 6.2.3. Diameters of PLA microfibers in unloaded and TCS and PHMD loaded PLA/PEG scaffolds. 999999

Sample	$Ø_{unloaded}$ (nm)	$Ø_{TCS}$ (nm)	$Ø_{PHMB}$ (nm)
PLA/PEG-14	1185 ± 7	762 ± 38	319 ± 7
PLA/PEG-48	1210 ± 43	1158 ± 24	542 ± 5
PLA/PEG-77	1501 ± 41	1305 ± 13	1002 ± 5

Figure 6.2.10 compares the release profiles from representative PLA/PEG scaffolds. A similar behavior is observed for all scaffolds when PBS was employed. An asymptotic value close to 25% was quickly reached in the case of TCS (70 min) due to the achievement of equilibrium conditions. The release of PHMB was slower but increased steadily and reached a similar value (i.e. 20-25%) after 490 min of exposure to the medium. Probably, the big size of PHMB molecules hindered their diffusion through the PLA fiber.

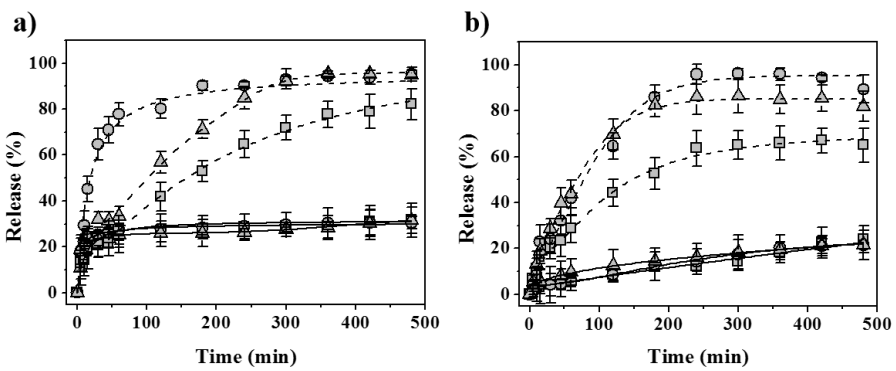

FIGURE 6.2.10

TCS (a) and PHMB (b) release curves in a PBS/ethanol mixture (30:70 *v*/*v*) (dashed line) and PBS medium (solid line) for PLA/PEG-14 (○), PLA/PEG-48 (Δ) and PLA/PEG-77 (□).

Profiles of release in the medium containing ethanol were clearly different from PBS and, in this case, revealed differences between scaffolds. Hence, a gradual increase in the TCS release rate by increasing the PEG content in the scaffold, which means an increase of porosity and a decrease on PLA diameter size, can be seen in **Figure 6.2.10 a**. Thus, TCS release from

PLA/PEG-14 and PLA/PEG-77 scaffolds was practically instantaneous and sustained, respectively. Specifically, a 70% release required 70 and 400 min when bicomponent scaffolds had the highest and lowest PEG content, respectively.

Release of PHMB seemed to proceed at a slower rate than that TCS despite the clearly lower diameter of PLA electrospun fibers loaded with PHMB. This behavior is again a consequence of the greater molecular size of the drug, which hinders its molecular motion through the fiber matrix. **Figure 6.2.10 b** reveals that PHMB release differences between scaffolds were small although logically the lowest rate was observed for the least porous scaffold (i.e. that having the highest PLA content).

Differences on the release rate were quantified considering the kinetic constant deduced for the first and fast release step, which could be fitted to a Higuchi **Equation 3**:[26]

$$M_t / M_0 = k_H\, t^{1/2} \qquad (0 \leq M_t / M_0 \leq 0.6) \qquad \textbf{(3)}$$

where k_H is the Higuchi constant, M_t is the percentage of drug released at time t, and M_0 is the drug equilibrium percentage (considered as the maximum drug percentage).

TABLE 6.2.4. Higuchi kinetic parameter for the release of TCS and PHMB from representative PLA/PEG scaffolds in a PBS/ethanol 3:7 *v/v* mixture at 37 ºC.

Sample	TCS		PHMB	
	k_H ($h^{-0.5}$)	*r*	k_H ($h^{-0.5}$)	*r*
PLA/PEG-14	0.906	0.960	0.520	0.980
PLA/PEG-48	0.424	0.949	0.474	0.961
PLA/PEG-77	0.371	0.982	0.381	0.993

Values reported in **Table 6.2.4** indicate variations of the Higuchi constant from 0.906 to 0.371 $h^{-0.5}$ and from 0.520 to 0.381 $h^{-0.5}$ for bicomponent scaffolds loaded with TCS and PHMB, respectively. In summary, the release of a given drug, especially those with a small molecular size, can be tuned by controlling the size of PLA microfibers and by modifying the PLA/PEG ratio of the initial scaffold because of its influence on the final porosity. Therefore, a method to modulate release in function of the required application is provided.

TCS and PHMB are broad-spectrum antiseptics with documented safety and efficacy against Gram-positive and Gram-negative bacteria (e.g., *M.luteus* and *E.coli*, respectively). The bactericide effect of both drugs released from PLA/PEG scaffolds was determined by studying bacterial growth in broth medium. As shown in **Figure 6.2.11** for unloaded samples, a high

growth of both bacteria was observed for all scaffolds. Similar results were obtained for the control, probably as a consequence of the low porosity of the scaffolds.

Growth measurements performed with TCS and PHMB loaded scaffolds demonstrated their bactericide activity and indicated slightly greater efficiency for TCS. In addition to the difference in inherent activity between the studied drugs, the faster release of the smaller TCS molecules is worth noting. **Figure 6.2.11** also shows a slightly different behavior between PLA/PEG scaffolds, with the bactericide activity being greater for those having a high ratio of PLA loaded microfibers. Finally, bacterial growth of PHMB loaded scaffolds was slightly dependent on the type of bacteria, and in particular *M. luteus* exhibited a higher reduction of growth.

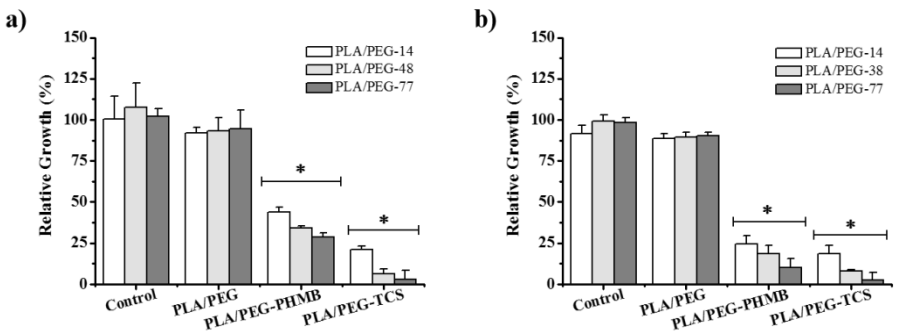

FIGURE 6.2.11

Relative growth of *Escherichia coli* (a) and *Micrococcus luteus* (b) on control surfaces and PLA/PEG-*x* electrospun samples loaded with TCS or PHMB (*$p < 0.05$ *vs.* control; ANOVA-Tukey's test).

Biocompatibility of PLA/PEG Scaffolds

Adhesion and proliferation of fibroblast and epithelial cells (MRC-5 and VERO cells, respectively) were studied for dual PLA/PEG scaffolds. Both experiments are important to follow cell development since adhesion is an early cellular event whereas proliferation is an evidence of metabolic cell activity. **Figure 6.2.12 a** compares the results on relative adhesion for the studied materials and shows higher adhesion of fibroblast cells onto the PLA/PEG scaffolds compared to the control. Moreover, proliferation studies (**Figure 6.2.12 b**) indicate that fibroblast colonization increased by 20-25% in the PLA/PEG scaffolds compared to the control when PEG content was high. This feature is in agreement with the higher porosity of scaffolds caused by the solubilization of PEG (used as sacrificial polymer) and the achievement of 3D structures more favorable for a rapid colonization of the material by fibroblast cells. Adhesion of epithelial cells seems slightly favored in the case of PLA/PEG scaffolds, the highest increase (18%) being observed for the PLA-rich scaffold. It is important to remark that these cells paved the surface of the scaffold and were not able to enter the porous 3D structure.

Thus, no significant increase of proliferation was detected for dual scaffolds and even negative results were detected when the PEG content was high, a feature that may be related to a surface instability caused by the solubilization of PEG. **Figure 6.2.13** shows the development of epithelial film monolayers onto representative PLA/PEG scaffolds and the impossibility of these cells to penetrate in the porous structure.

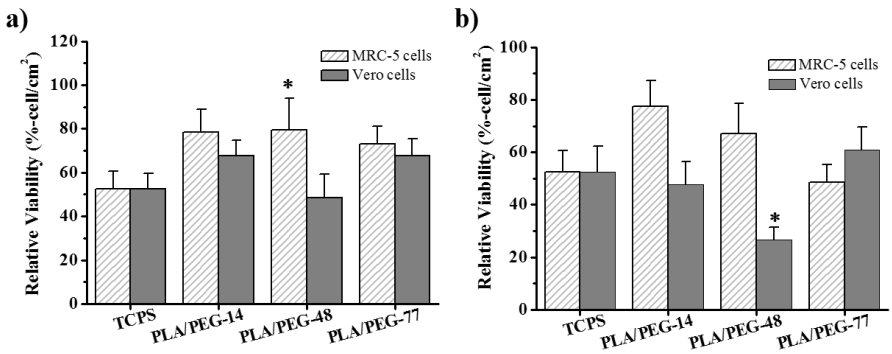

FIGURE 6.2.12

Adhesion (a) and proliferation (b) of cells on control plate surfaces and not loaded scaffolds (*$p < 0.05$ *vs.* positive control; ANOVA-Tukey's test).

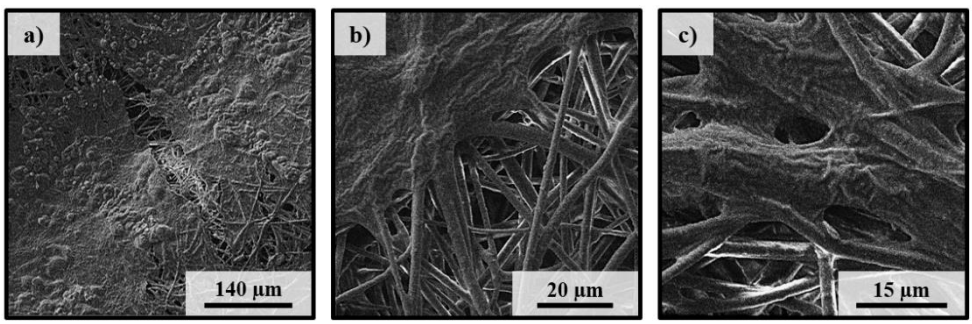

FIGURE 6.2.13

Low-magnification (a) and high-magnification (b,c) SEM micrographs showing proliferation of VERO cells on representative PLA/PEG-77 (a,b) and PLA/PEG-77 (c) scaffolds.

6.2.4 Conclusions

Homogeneous scaffolds constituted by PLA and PEG continuous fibers could be satisfactorily prepared by the electrospinning technique when independent jets produced from each homopolymer solution were overlapped over a single rotary collector. Final scaffold compositions were easily tuned by modifying the PLA flow rate while a constant and low rate was preferred for PEG considering the significant difference on polymer concentrations (i.e. 10 and 35 *wt*-% for PLA and PEG, respectively) required to obtain electrospinable solutions. PLA and PEG fibers could be well distinguished in the final scaffold according to surface texture (rough or smooth) and diameter rage. This was clearly dependent and increased with the flow rate.

Drugs of different size and hydrophilic/hydrophobic character were easily loaded into PLA nanofibers although a slight solvent modification that influenced fiber morphology was required. This change was drastic in the case of cationic PHMB that led to nanofibers instead of microfibers.

The high water solubility of PEG allowed tuning scaffold porosity by varying the ratio between fibers of the two components and using PEG as a sacrificial polymer. The release from the different scaffolds was also modulated from a practically instantaneous to a sustained delivery according to porosity and fiber size if an appropriate release medium was selected. TCS and PHMB drugs loaded drugs had a bactericide effect that was lower for PHMB because only a limited amount of drug could be incorporated in the scaffold. The increase in the scaffold porosity favored rapid fibroblast cell colonization whereas a contrary effect was observed when epithelial like cells.

In summary, the reported method based on the use of PEG as a sacrificial polymer allows preparing scaffolds with tuned porosity (from 40 to 80%) and different drug release kinetics and susceptibility to fibroblast cell colonization.

6.2.5 References

[1] D.H. Reneker, I. Chun, Nanotechnology, 7 (1996) 216-223.

[2] Y. Dzenis, Science, 304 (2004) 1917-1919.

[3] D. Li, Y.N. Xia, Adv Mater, 16 (2004) 1151-1170.

[4] K. Jayaraman, M. Kotaki, Y.Z. Zhang, X.M. Mo, S. Ramakrishna, J Nanosci Nanotechno, 4 (2004) 52-65.

[5] Z.C. Sun, E. Zussman, A.L. Yarin, J.H. Wendorff, A. Greiner, Adv Mater, 15 (2003) 1929-1932.

[6] Y. Liao, L. Zhang, Y. Gao, Z.-T. Zhu, H. Fong, Polymer, 49 (2008) 5294-5299.

[7] S.N. Stephansson, B.A. Byers, A.J. Garcia, Biomaterials, 23 (2002) 2527-2534.

[8] Y. Lin, L.L. Wang, P.B. Zhang, X. Wang, X.S. Chen, X.B. Jing, Z.H. Su, Acta Biomater, 2 (2006) 155-164.

[9] D.A. Herold, K. Keil, D.E. Bruns, Biochem Pharmacol, 38 (1989) 73-76.

[10] Y.K. Luu, K. Kim, B.S. Hsiao, B. Chu, M. Hadjiargyrou, J Control Release, 89 (2003) 341-353.

[11] X. Xu, L. Yang, X. Xu, X. Wang, X. Chen, Q. Liang, J. Zeng, X. Jing, J Control Release, 108 (2005) 33-42.

[12] X.H. Zong, H. Bien, C.-Y. Chung, L.F. Yin, D. Fang, B.S. Hsiao, B. Chu, E. Entcheva, Biomaterials, 26 (2005) 5330-5338.

[13] X. Xu, X. Zhuang, X. Chen, X. Wang, L. Yang, X. Jing, Macromol Rapid Comm, 27 (2006) 1637-1642.

[14] M. Spasova, O. Stoilova, N. Manolova, I. Rashkov, G. Altankov, J Bioact Compat Pol, 22 (2007) 62-76.

[15] P.Y. Ni, S.Z. Fu, M. Fan, G. Guo, S.A. Shi, J.R. Peng, F. Luo, Z.Y. Qian, Int J Nanomed, 6 (2011) 3065-3075.

[16] B.Y. Wang, S.Z. Fu, P.Y. Ni, J.R. Peng, L. Zheng, F. Luo, H. Liu, Z.Y. Qian, J Biomed Mater Res A, 100A (2012) 441-449.

[17] E. Llorens, L.J. Valle, R. Ferrán, A. Rodríguez-Galán, J. Puiggalí, J Polym Res, 21 (2014) 1-15.

[18] A.D. Russell, J AntimicrobChemoth, 53 (2004) 693-695.

[19] G.F. de Paula, G.I. Netto, L.H.C. Mattoso, Polymers, 3 (2011) 928-941.

[20] B. Roth, F.H.H. Brill, Skin Pharmacol Phys, 23 (2010) 4-6.

[21] P. Gilbert, D. Pemberton, D.E. Wilkinson, J App Bacteriol, 69 (1990) 593-598.

[22] E. Llorens, L.J. del Valle, A. Diaz, M.T. Casas, J. Puiggali, Macromol Res, 21 (2013) 775-787.

[23] F.D. Kopinke, M. Remmler, K. Mackenzie, M. Moder, O. Wachsen, Polym Degrad Stabil, 53 (1996) 329-342.

[24] S.L. Madorsky, S. Straus, J Polym Sci, 36 (1959) 183-194.

[25] R.N. Wenzel, Ind Eng Chem, 28 (1936) 988-994.

[26] T. Higuchi, J Pharm Sci, 50 (1961) 874-875.

6.3 Biocompatibility and Drug Release Behavior of Scaffolds Prepared by Coaxial Electrospinning of Poly(Butylene succinate) and Polyethylene Glycol

I

Scaffolds constituted by electrospun microfibers of poly(ethylene glycol) (PEG) and poly(butylene succinate) (PBS) were studied. Specifically, coaxial microfibers having different core-shell distributions and compositions were considered as well as uniaxial micro/nanofibers prepared from mixtures of both polymers. Processing conditions were optimized for all geometries and compositions and resulting morphologies (i.e. diameter and surface texture) characterized by scanning electron microscopy. Chemical composition, molecular interactions and thermal properties were evaluated by means of FTIR, NMR and XPS and differential scanning calorimetry. The PEG component of electrospun fibers could be solubilized by immersion of scaffolds in aqueous medium, giving rise to high porosity and hydrophobic samples. Nevertheless, a small amount of PEG was retained in the PBS matrix, suggesting some degree of mixing. Solubilization was slightly dependent on fiber structure; specifically, the distribution of PEG in the core or shell of coaxial fibers led to higher or lower retention levels, respectively. Scaffolds could be effectively loaded with hydrophobic drugs having antibacterial and anticancerigen activities like triclosan and curcumin, respectively. The release was highly dependent on their chemical structure and the medium composition. Thus, low and high release rates were observed in phosphate saline buffer solution (SS) and SS/ethanol (30:70 v/v), respectively. Slight differences in the release of triclosan were found depending on fiber distribution and composition. Antibacterial activity and biocompatibility were evaluated for both loaded and unloaded scaffolds.

6.3.1 Introduction

Electrospinning is currently one of the simplest methods of drug loading into micro/nanofiber scaffolds. The drug is dissolved or dispersed in a polymer solution that is subsequently exposed to a strong electrical potential. Electrical charges accumulate on the surface of a liquid droplet placed at the tip of a capillary and a charged jet is ejected towards a grounded electrode when the Coulombic repulsion of the charges overcomes the surface tension of the polymer droplet.[1-4] The solvent evaporates as it travels from the tip to the grounded target and fibers with different morphology are collected depending on solution properties (e.g., viscosity, dielectric constant, volatility, concentration, etc.) and operational parameters (e.g., strength of the applied electrical field, deposition distance, flow rate, etc.).[5, 6]

Electrospun scaffolds for tissue regeneration and drug delivery applications have been successfully been prepared from both natural polymers like collagen, gelatin, chitosan, silk fibroin and hyaluronic acid and synthetic homopolymers and copolymers such as poly(lactic acid) (PLA), poly(ε-caprolactone) (PCL), polyethylene glycol (PEG), poly(butylene succinate), poly (L-lactide-*co*-caprolactone) and poly(lactic-*co*-glycolic acid) (PLGA).[7-11]

Drug-loaded micro/nanofibrous scaffolds can be applied topically or as an implant for antibiotic, antifungal, antimicrobial,[12] antioxidant[13] and anticancer[14] drug delivery. Despite the simplicity of this encapsulation procedure based on electrospinning, some requirements should be met to attain optimal results. Thus, release behavior becomes highly dependent on the distribution of drug molecules in electrospun fibers, as well as on the final morphology of the fibers. Physicochemical interactions between drug molecules and the polymer matrix play a fundamental role, and specifically the hydrophobic-hydrophilic properties of drug and polymer should be matched in order to achieve a good drug encapsulation inside the electrospun nanofibers. Lack of good interactions may cause drug migration during electrospinning on or near the fiber surface, resulting in a significant burst effect.[15] In order to achieve sustained release and improve molecular interactions, blending hydrophilic-hydrophobic polymers in different ratios has been considered.[16, 17]

Coaxial electrospinning is a modification of the classical procedure that enables production of micro/nanofibers with a core-shell structure and highly different compositions. In this case, two polymer solutions are supplied by means of two separate syringe pumps and pipelines leading to a core-shell nozzle. At the exit of this special needle a core-shell droplet appears and acquires a shape similar to the Taylor cone. Nevertheless, the core material may be not entrained into the shell jet, giving rise to monolithic instead of core-shell jets.[18] In fact, electric charges escape very rapidly to the outer surface of the forming jet and core entrainment becomes only possible by viscous tractions.[19]. Successful encapsulation of drug to the core of coelectrospun fibers is determined by various parameters (e.g., shell polymer concentration, core polymer concentration, molecular weight and drug concentration) as well as the relative flow rate of the core and shell solutions.[20] Fiber morphology is sometimes critical and incorporation of a highly

hydrophilic and water soluble PEG polymer may accelerate transport of drug molecules into the environment.[20] Coaxial electrospun nanofibers have gained much interest as gene- and growth factor-delivery systems, as well as embedding media of pharmaceutical compounds such as antibiotic or antioxidant drugs.[21, 22]

PEG is a highly hydrophilic polymer widely used in the biomedical field of its lack of toxicity, good biocompatibility and easy elimination from human body.[23] Polybutylene succinate (PBS), a polymer supplied by Showa High Polymers as Bionolle™ is currently the most commonly employed poly(alkylene dicarboxylate) due to its relatively low production cost, good thermal and mechanical properties and easy processability.[24, 25] To the best of our knowledge, no studies have been performed on the preparation of coaxial core-shell structures constituted by these two biocompatible polymers with well-differentiated hydrophilic-hydrophobic properties.

Triclosan (polychlorophenoxy phenol) (**Figure 6.3.1**) is a well-known antibacterial and antifungal agent[26] scarcely soluble in water but well soluble in ethanol. At in-use concentrations, triclosan acts as a biocide, with multiple cytoplasmic and membrane targets.[26] At lower concentrations, however, triclosan appears bacteriostatic and is seen to target bacteria mainly by inhibiting fatty acid synthesis. Curcumin is molecule constituted by two phenol groups connected by α,β-unsaturated carbonyl groups (**Figure 6.3.1**). These diketones can form stable enols and are readily deprotonated to form enolates. Curcumin seems to have beneficial effects on various diseases, including multiple myeloma, pancreatic cancer, myelodysplastic syndromes, colon cancer, psoriasis, and Alzheimer's disease.[27, 28] Curcumin is also a pleiotropic molecule capable of interacting with molecular targets involved in inflammation.

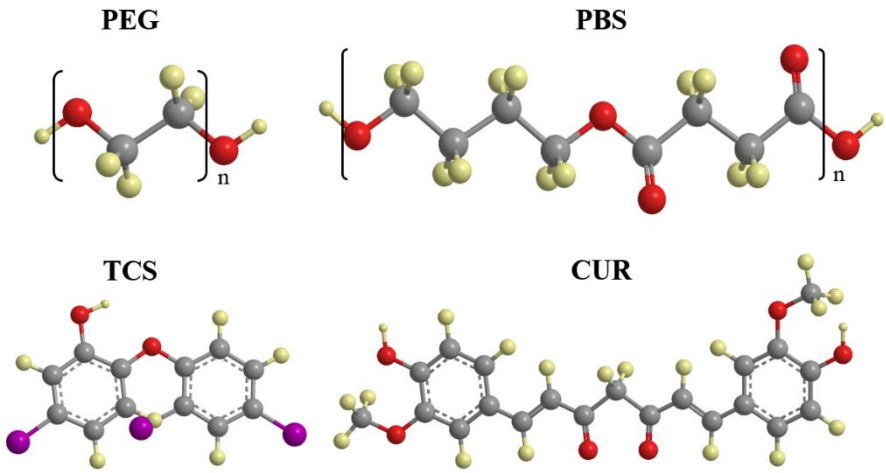

FIGURE 6.3.1
Chemical structures of polymers used to prepare electrospun coaxial microfibers and loaded drugs.

The main goal of the present work is the study of scaffolds constituted by PEG and PBS microfibers. To this end, electrospinning will be performed using a solution mixture of both polymers and compared with coaxial electrospinning having both PEG-PBS and PBS-PEG core-shell distributions. Morphological changes caused by the rapid solubilisation of PEG in aqueous media will also be evaluated since PEG can be used as a sacrificial polymer to modify material porosity and cellular colonization. Finally, scaffolds will be studied as drug delivery systems considering the loading of triclosan and curcumin drugs in PEG and PBS components, respectively. This distribution should probably lead to a fast release of PEG taking into account its solubilisation in aqueous media, and consequently to an immediate antibactericidal effect. On the contrary, loading of curcumin in the non-soluble polymer should result in a slower rate, and therefore in a sustained anticancer effect.

6.3.2 Experimental Section

Materials

Poly(ethylene glycol) samples of number average molecular weight of 35,000 $g \cdot mol^{-1}$ weas purchased from Sigma-Aldrich. Polybutylene succinate is a commercial product (Bionolle® 1001) supplied by Showa Denko K.K. (Germany). The polymer has a melt flow index of 1.6 $g \cdot 10\ min^{-1}$ (measured at 190 ºC under a load of 2.16 Kg according to ASTM-D1238). Solvents, curcumin, triclosan and cell culture labware were purchased from Sigma-Aldrich (USA).
Escherichia coli CECT 101 and *Micrococcus luteus* CECT 245 bacterial strains were obtained from Spanish Collection of Type Culture (Valencia, Spain). Fibroblast-like Cos-7 and ephithelial-like Vero cells from kidney African green monkey were purchased from ATCC (USA).

Electrospinning

Electrospun fibers were collected on a target placed at different distances (10-25 cm) from the needle tip (inside diameter of 0.84 mm) or the core-shell nozzle (inside diameters 1.37 mm and 2.39 mm) for single fiber or core-shell structure preparations, respectively. The voltage was varied between 10 and 30 kV and applied to the target using a high-voltage supply (Gamma High Voltage Research, ES30-5W). Polymer solutions were delivered via a single or two KDS100 infusion syringe pumps (KD Scientific, USA) to control the flow rate (from 1 to 5 $mL \cdot h^{-1}$). All electrospinning experiments were carried out at room temperature. Unloaded and triclosan and curcumin loaded electrospun fibers were prepared using optimized parameters (e.g., collector distance, voltage and flow rate) and solvent conditions (e.g., polymer and drug concentrations). The triclosan and curcumin contents of the electrospinning solutions were 1 and 0.5 *w/v*-% for samples used for release and antibacterial assays, and for cytotoxicity assays, respectively. Coaxial electrospun microfibers will be denoted by subscripts s and c, which indicate the polymer that constitutes the shell and the core, respectively. Absence of these scripts indicates fibers prepared from a polymer mixture. Weight percentages of each polymer in the electrospinning solutions are also given in the sample abbreviation.

Morphology, composition and properties of electrospun scaffolds

Optical microscopy studies were performed with a Zeiss Axioskop 40 microscope. Micrographs were taken with a Zeiss AxiosCam MRC5 digital camera.
Detailed inspection of texture and morphology of electrospun samples was conducted by scanning electron microscopy using a Focus Ion Beam Zeiss Neon 40 instrument (Carl Zeiss, Germany). Carbon coating was accomplished by using a Mitec K950 Sputter Coater fitted with a film thickness monitor *k*150x. Samples were visualized at an accelerating voltage of 5 kV. Diameter of electrospun fibers was measured with the SmartTiff software from Carl Zeiss SMT Ltd.

^{1}H-NMR spectra were acquired with a Bruker AMX-300 spectrometer operating at 300.1 MHz. Chemical shifts were calibrated using tetramethylsilane as an internal standard. Deuterated chloroform ($CDCl_3$) was used as the solvent at room temperature.

Infrared absorption spectra were recorded in the 3600 - 600 cm^{-1} range on a Jasco FTIR 4100 Fourier Transform spectrometer. A Specac MKII Golden Gate attenuated total reflection (ATR) accessory was employed.

X-ray photoelectron spectroscopy (XPS) was performed with a SPECS system equipped with an Al anode XR50 source operating at 200 W and a Phoibos 150 MCD-9 detector XP. Samples were fixed in a special sample holder with double sided carbon adhesive tape. The overview spectra were recorded with pass energy of 25 eV at 0.1 eV steps at a pressure below $7.5x10^{-9}$ mbar, with binding energies being referred to the C1s and O1s signals. The overlapping peaks were deconvoluted using the PeakFit v4 program by Jandel Scientific Software.

Contact angles (CA) were measured at room temperature with sessile drops using an OCA-15 plus Contact Angle Microscope (Dataphysics, USA) and SCA20 software. Contact angle values of the right and left sides of distilled water drops were measured and averaged. Measurements were performed 10 s after the drop (5 mL) was deposited on the sample surface. All CA data were an average of six measurements on different surface locations.

Calorimetric data were obtained by differential scanning calorimetry with a TA Instruments Q100 series equipped with a refrigeration cooling system (RCS). Experiments were conducted under a flow of dry nitrogen with a sample weight of approximately 5 mg, and calibration was performed with indium. Heating and cooling runs were carried out at rates of 20 $^oC \cdot min^{-1}$ and 10 $^oC \cdot min^{-1}$, respectively.

Porosity of PLA/PGE scaffolds

The porosity of electrospun scaffolds was measured by the liquid intrusion method. Vacuum dried scaffolds (n = 3) were weighed prior to immersion in water for 1 h using a shaker table to allow diffusion of water into the void volume. The scaffolds were taken out and reweighed. Porosity was calculated according to **Equation 1**:

$$P = [(m_w - m_d) / d_s)] / (m_w - m_d) / d_s] + [m_d^{PBS} / d_{PBS}] + [m_d^{PEG} / d_{PEG}] \quad (\mathbf{1})$$

where m_w, m_d, m_d^{PBS}, m_d^{PEG} are the weights of the wet scaffold, dry scaffold, PBS fraction and PEG fraction in the dry scaffold, respectively, and d_s, d_{PBS} and d_{PEG} refer to the densities of water (i.e. 1.0 $g \cdot mL^{-1}$), semicrystalline PBS (1.26 $g \cdot mL^{-1}$) and semicrystalline PEG (1.07 $g \cdot mL^{-1}$), respectively. The last densities were estimated using DSC data of scaffolds which pointed to a high crystallinity for both PEG and PBS phases.

Release experiments

Controlled release measurements were made with square pieces (weighting approximately 200 mg) of the electrospun scaffolds. These pieces were weighed and incubated at 37 ºC in an orbital shaker at 200 rpm in tubes of 50 mL for 1 week. Phosphate saline buffer solution (SS) and alternatively its mixture with ethanol (i.e. 3:7 *v/v* ratio) as a more hydrophobic component were employed as release media. Drug concentration was evaluated by UV spectroscopy using a Shimadzu 3600 spectrometer. Calibration curves were obtained by plotting the absorbance measured at 290 and 243 nm versus triclosan and curcumine concentration, respectively, in the hydrophilic medium, whereas 280 nm was considered for triclosan when ethanol was added in the medium. Samples were withdrawn from the release medium at predetermined time intervals. The volume was kept constant by addition of fresh medium. All drug release tests were carried out using three replicates and the results were averaged.

Cellular adhesion and proliferation assays

Human fetal lung fibroblast (MRC-5) and African green monkey kidney epithelial (Vero) cells were cultured in Dulbecco's modified Eagle medium (DMEM) as previously reported.[29]
Square pieces (0.5×0.5×0.1 mm^3) of the electrospun scaffolds were placed into each well of a multiwell culture plate. Samples were fixed in the wells with a small drop of silicone (Silbione® MED ADH 4300 RTV, Bluestar Silicones France SAS, Lyon, France) and then sterilized by UV-radiation in a laminar flux cabinet for 15 min. For the cell adhesion assay, aliquots of 50-100 µL containing $5x10^4$ cells were seeded onto the electrospun samples in each well and incubated for 24 h (adhesion assay) or 4 days (proliferation assay).
Samples were evaluated by the standard adhesion and proliferation method[13] using three replicates and the results were averaged. Samples with adhered and grown cells on the mats were fixed with 2.5 *w/v*-% formaldehyde at 4 ºC overnight. They were subsequently dehydrated and processed for observation by scanning electronic microscopy.

Antimicrobial test

Escherichia coli (*E. coli*) and *Micrococcus luteus* (*M. luteus*) bacteria were selected to evaluate the antimicrobial effect of electrospun CUM and TCS loaded fibers. The bacteria were previously grown aerobically to exponential phase in broth culture (5 $g \cdot L^{-1}$ beef extract, 5 $g \cdot L^{-1}$ NaCl, 10 $g \cdot L^{-1}$ peptone, pH 7.2).
Growth experiments were performed on a 24-well culture plate. Square pieces (0.5×0.5×0.1 mm^3) of the electrospun scaffolds were placed into each well. Then, 1 mL of broth culture containing 10^3 CFU was seeded on the electrospun fiber mats. The cultures were incubated at 37 ºC and agitated at 200 rpm. Aliquots of 50 µL were taken at predetermined time intervals for absorbance measurement at 650 nm in a plate reader. Thus, turbidity was directly related to bacterial growth.

Bacterial adhesion onto scaffolds was also determined. The culture media were aspirated after incubation and the material washed once with distilled water. Then, 0.5 mL of sterile 0.01 M sodium thiosulfate was added to each well. After addition of 4 mL of broth culture, the plate was incubated at 37 ºC and agitated at 200 rpm for 24 h. The bacterial number was determined as above indicated. All assays were conducted in triplicate and the results averaged.

6.3.3 Results and Discussion

Electrospinning Conditions

A common solvent like dichloromethane was chosen for both PEG and PBS polymers and the two drugs (triclosan and curcumin) because its solubility parameter (20.31 $MPa^{0.5}$) is close to those reported for PEG[30] and PBS[31] (around 20 $MPa^{0.5}$). Polymer concentration and operational parameters (voltage and flow) were selected to obtain continuous fibers and avoid formation of droplets and beads, while needle-collector distance could be fixed at a value of 14 cm for all samples. In this way, concentration of the high molecular weight PBS sample was limited to the 5-7 *wt*-% range due to the high viscosity of the final solution, whereas the low molecular weight PEG sample required a concentration of 10-15 *wt*-% to avoid the typical formation of droplets.

Best experimental conditions, together with the average diameter of electrospun fiber, are summarized in **Table 6.3.1**. In all cases, a unimodal narrow distribution (not shown) was observed. Note that fibers prepared from a common solution had significantly smaller diameters than coaxial fibers (0.43-0.75 µm as opposed to 1.8-4.8 µm) due to differences in the size of corresponding needles. Diameters of coaxial microfibers seemed to increase with polymer concentration in the electrospinning solution when PEG was in the fiber shell, whereas an unclear trend was observed when it was in the core since, in this case, a higher variation on processing parameter was required (e.g., flow rate changed from 5 to 1.2 $mL \cdot h^{-1}$). Logically, the increase in polymer concentration and the decrease in the flow rate lead to opposite effects.

TABLE 6.3.1. Optimal electrospinning conditions for the electrospining of PBS/PEG microfibers.[a]

Fiber	PBS/PEG (feed)		Voltage	Flow Rate	Diameter	PBS/PEG (fiber)
	(*w*/*w*)	(mol/mol)	(kV)	$mL \cdot h^{-1}$	(µm)	(mol/mol)
PBS_s/PEG_c	5/10	14.9/85.1	20	5	4.08 ± 0.04	13.4/86.6
	7/10	19.6/80.4	20	2.5	2.76 ± 0.02	19.6/80.4
	5/15	10.4/89.6	15	1.2	3.37 ± 0.04	8.7/91.3
PEG_s/PBS_c	5/10	14.9/85.1	25	3	1.79 ± 0.01	10.5/89.5
	7/10	19.6/80.4	25	5	1.96 ± 0.02	14.4/85.6
	5/15	10.4/89.6	20	5	4.80 ± 0.07	8.1/91.9
PBS/PEG	5/10	14.9/85.1	25	4	0.43 ± 0.01	12.9/87.1
	7/10	19.6/80.4	25	2	0.74 ± 0.02	14.8/85.2
	5/15	10.4/89.6	20	4	0.74 ± 0.01	11.2/88.8

[a]Optical collector distance was always 14 cm.

SEM micrographs of representative samples allow comparing fiber surface textures for some representative samples (see **Figure 6.3.2**). In general, a significant difference can be detected depending on the polymer in the shell of the coaxial fiber. Thus, rough or smooth surfaces were characteristic of fibers having a PBS or PEG shell, respectively. Similarly, the narrowest nanofibers obtained from the polymer mixtures showed the smoothest surfaces, as is characteristic of PEG and also of mixtures with a high PEG content (e.g., higher than 55 *wt*-%).[32]

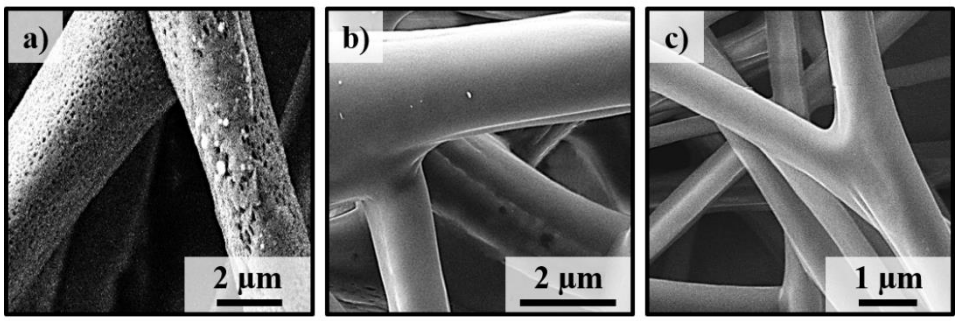

FIGURE 6.3.2

SEM micrographs showin the texture of PBS_s/PEG_c 5/15 (a), PEG_s/PBS_c 10/7 (b) and PBS/PEG 7/10 (c) representative samples obtained from dichloromethane solutions and using optimized concentration conditions of voltage needle-collector distance and flow.

Composition and Properties of Electrospun PBS/PEG Fibres

^{1}H-NMR spectra (**Figure 6.3.3**) was useful to determine the composition of all electrospun samples. Thus, areas corresponding to methylene protons of PBS (4.11, 2.62 and 1.70 ppm) and PEG (3.64 ppm) were used to determine the molar PBS content of electrospun fibers as follows (**Equation 2**):

$$\text{PBS } (\textit{molar}\text{-}\%) = 100 \cdot \left(\frac{A_{4.11} + A_{2.62} + A_{1.70}}{12}\right) / \left[\left(\frac{A_{4.11} + A_{2.62} + A_{1.70}}{12}\right) + \left(\frac{A_{3.64}}{4}\right)\right] \quad (2)$$

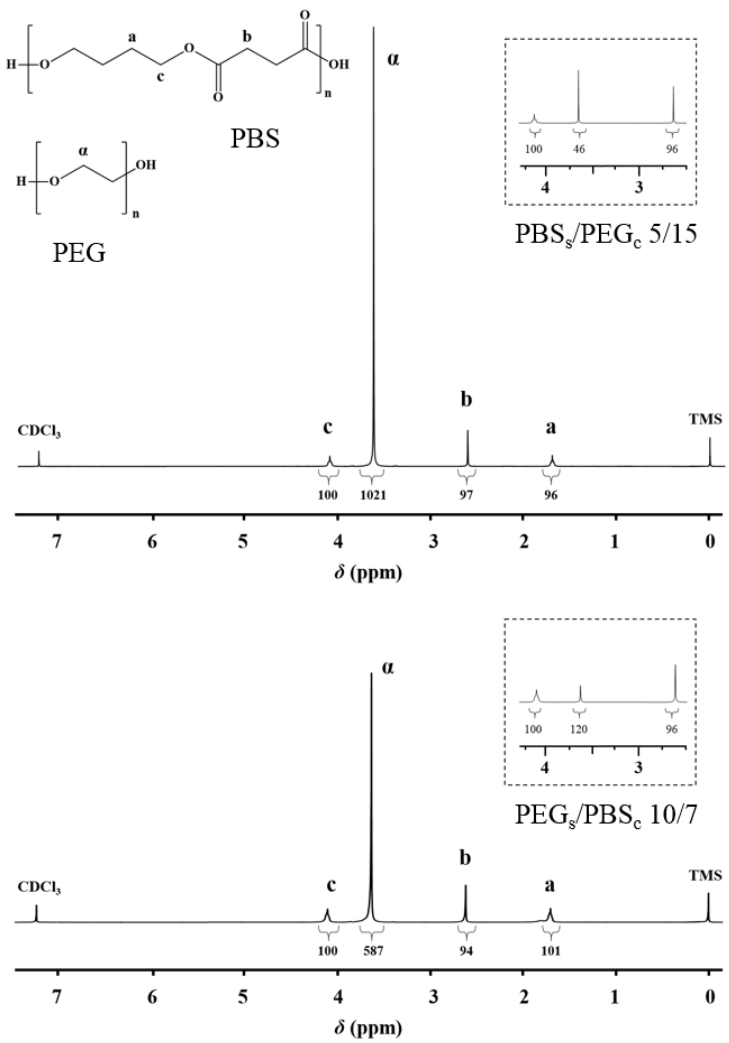

FIGURE 6.3.3

^{1}H-NMR spectra of PBS_s/PEG_c 5/15 (top) and PEG_s/PBS_c 10/7 (bottom) electrospun samples before and after immersion in water (insets).

Composition values summarized in **Table 6.3.1** show relatively good agreement with the polymer molar feed ratio in the initial electrospinning solutions. In particular, it was excellent for the coaxial fibers having PEG confined in their core, whereas a slight deficiency was detected in PEG when it was the component of the shell jet. An unclear trend was observed for uniaxial fibers but again PEG content was slightly lower than expected, chiefly when the PBS/PEG ratio increased.

FTIR spectra of the electrospun fibers logically showed the characteristic peaks associated with PBS (e.g., 1722, 1158, 1044 and 802 cm^{-1}) and PEG (e.g., 961 and 834 cm^{-1}) (**Figure 6.3.4**) with a variable intensity ratio that depended on the composition. The spectra merely corresponded to the superposition of homopolymer spectra since no band displacements indicative of new intermolecular interactions were detected.

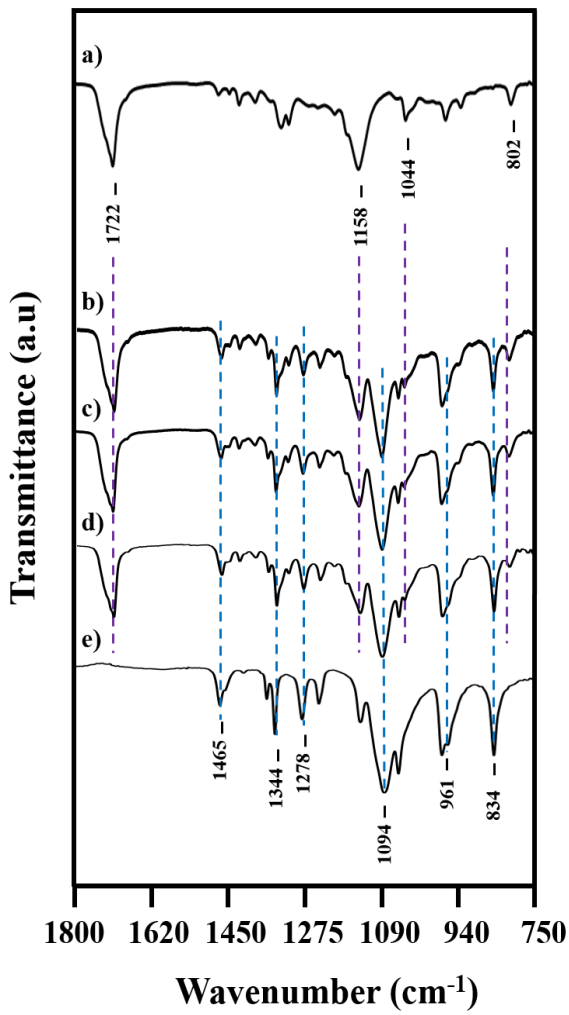

FIGURE 6.3.4

FTIR spectra of electrospun PBS, PBS_s/PEG_c 5/15, PEG_s/PBS_c 15/5, PBS/PEG 5/15 and PEG samples.

On the contrary, XPS spectra were relevant, as shown in **Figure 6.3.5**, because analysis of C1s and O1s peaks showed the establishment of interactions between PEG and PBS molecules in the electrospun fibers. The PBS spectrum was very complicated, as had already been reported,[33] because four C1s and two O_1 peaks were found in the deconvoluted spectrum at 284.5 eV (C_1-CH_2), 285.2-285.6 eV (C_2-C=O), 286.4-286.9 (C_3-O), 289.3 eV (C_4=O), 531.6 eV (O_1=C) and 533.0 eV (O_2-C=O), whereas the PEG spectrum was characterized by single C1s and O1s peaks at binding energies of 285.0 eV (C_5-O) and 532.5 eV (O_3-C).[34] Note in **Figure 6.3.5** that the spectrum of a representative PBS/PEG sample clearly differs from that expected from a weighted addition according to the final composition of the homopolymer spectra. Thus, for example, peak O_1 appeared shifted to a higher binding energy and the intensities of peaks O_3 and C_3 were lower and higher than expected, respectively.

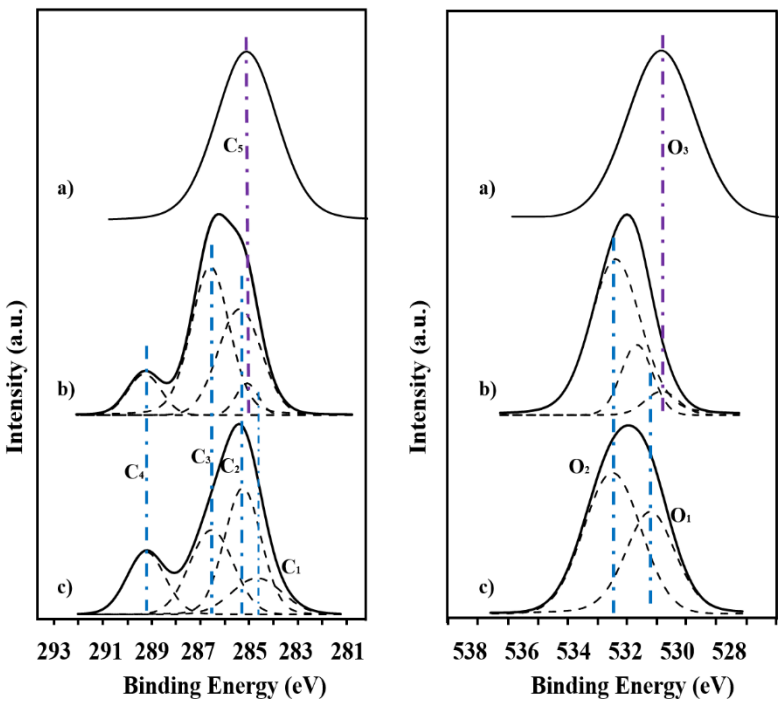

FIGURE 6.3.5

Carbon (left) and oxygen (right) XPS signals of electrospun PEG (top), PBS/PEG 5/15 electrospun samples (middle) and PBS (bottom**)** samples.

TABLE 6.3.2. Selected calorimetric data from the heating and cooling scans performed with the different PBS/PEG electrospun samples.

Sample	PEG Component				PBS Component			
	T_m (ºC)	ΔH_m (J.g^{-1})	T_c (ºC)	ΔH_c (J·g^{-1})	T_m (ºC)	ΔH_m (J·g^{-1})	T_c (ºC)	ΔH_c (J·g^{-1})
PBS[a]	-	-	-	-	111.0	56.9	77.7	59.2
PBS	-	-	-	-	110.3	75.7	79.7	61.4
PEG[a]	65.0	177.2	44.4	177.2	-	-	-	-
PEG	63.8	176.1	44.7	175.7	-	-	-	-
PBS_s/PEG_c 5/10	56.9	90.4	37.7	80.5	109.1	27.5	78.6	30.0
PEG_s/PBS_c 10/5	62.3	125.3	34.6	111.7	106.5	17.7	76.3	19.2
PBS/PEG 5/10	62.5	121.3	34.3	103.5	111.7	28.1	79.4	26.4

[a] Pellets of the commercial sample.

Table 6.3.2 summarizes the main melting and crystallization data of the electrospun samples, including data from the commercial pellet of the homopolymers. Several points merit attention: a) Crystallinity of electrospun PBS was higher than that of the commercial sample and also than that attained after the cooling scan from the melt. Thus, melting enthalpies of 75.7 and 56.9 J·g^{-1} were determined in the heating scans of the electrospun and commercial PBS samples, whereas crystallization enthalpy of 61.4 and 59.2 J·g^{-1} were determined in the corresponding cooling scans. Therefore, the electrospining process seems to favour the orientation of PBS molecules and facilitate the subsequent crystallization. b) Similar melting and crystallization enthalpies were determined for PEG commercial and electrospun samples. c) Characteristic PEG and PBS crystalline domains were observed in the DSC scans of the electrospun PBS/PEG samples. Nevertheless, a slight decrease in the melting point was found for the component distributed in the core of coaxial fibers (i.e. melting points of PEG and PBS decreased from 65.0 ºC and 111.0 ºC to 56.9 and 106.5 ºC, respectively). This feature suggests that the polymer confined in the inner part of the microfiber had greater difficulty in forming more perfect and thicker lamellae as a consequence of significant retention of solvent or even a lower degree of orientation. d) Crystallization enthalpies associated with the PEG component in the binary electrospun samples were clearly lower that the corresponding melting enthalpies detected in the previous heating run (e.g., 103.5 and 121.3 J·g^{-1} for PBS/PEG 5/10, whereas better agreement was found between crystallization and melting enthalpies of the PBS component. In the case of PEG, it is likely that its crystallization from the melt was hindered by constraints imposed by previous crystallization of the higher melting point PBS component.

Water Solubility of PLA/PEG Scaffolds

The high solubility of PEG in water allowed its use as a sacrificial polymer to increase the porosity of the scaffold after exposure to an aqueous medium. The solubilisation of PEG from the different electrospun scaffolds can be evaluated through ^{1}H-NMR spectra for two different composition and core-shell structures, as shown in **Figure 6.3.6.**. A clear decrease in the intensity of the typical PEG signal (3.64 ppm) was always observed after immersion of the samples in water.

TABLE 6.3.3. Diameter and composition of electrospun fibers after removal of PEG removal, variation respect to initial diameter, compositional analysis after immersion en % of PEG removed.

Sample	PBS/PEG (*w/w*-%)	Ø (µm)	ΔØ[a] (µm)	PBS/PEG (mol/mol)	PEG_{rem}[b] (%)
PBS_s/PEG_c	5/10	3.30 ± 0.1	- 0.78	55.0/45.0	87
	7/10	--	--	59.7/40.3	84
	5/15	2.63 ± 0.1	- 0.74	45.0/55.0	88
PEG_s/PBS_c	5/10	1.50 ± 0.01	- 0.29	59.8/40.2	92
	7/10	1.62 ± 0.02	-0.34	68.8/31.2	92
	5/15	3.96 ± 0.03	- 0.84	58.2/41.8	94
PBS/PEG	5/10	0.30 ± 0.01	- 0.13	55.8/44.2	88
	7/10	0.51 ± 0.01	- 0.22	58.0/42.0	87
	5/15	0.45 ± 0.02	- 0.29	60.7/39.3	92

[a]Variation respect to the initial diameter.
[b]Molar percentage of PEG removed respect to the initial PEG content.

Final compositions deduced from NMR spectra are summarized in **Table 6.3.3**, together with the percentage of PEG compared to the initially solubilized content. Although these values were always high and around 90%, some significant amount of PEG was held in the PBS matrix (e.g., 31.2-55.0 *molar*-%). Solubilization slightly depended on the fiber structure, and specifically the lowest and highest average percentages (87 and 94%) were found for coaxial fibers with PEG in the core and the shell, respectively, whereas an intermediate average value of 89% was determined for uniaxial fibers. The fact that no complete PEG removal was observed for the electrospun PEG_s/PBS_c sample suggests the formation of a non-perfect core-shell structure and some degree of mixing between both polymers, probably more significant in the interphase.

The morphology of microfibers was logically affected by solubilisation of PEG for representative uniaxial and coaxial samples, as shown in **Figure 6.3.6**. Thus, the smooth texture of the uniaxial nanofibers became clearly rough (**Figure 6.3.6 a**) after immersion and their average diameter decreased between 29 and 39% of the initial value (**Table 6.3.3**), with the higher percentage being associated with fibers with an initially greater PEG content. Drastic changes occurred after immersion of coaxial PBS_s/PEG_c microfibers since longitudinal slits were usually observed (**Figure 6.3.6 b**). These slits could probably be a direct consequence of the release of the PEG component placed in the inner part of the fiber. Logically, the rough surface associated to the PBS shell remained after immersion. A significant diameter decrease (19-21%) was also observed, although in some cases no measurements could be performed due to the flat appearance of the opened fibers. This percentage was obviously lower than that found for the uniaxial fibers due to the greater diameter of coaxial fibers. Finally, PBS_c/PEG_s fibers exhibited a rough surface after the release of the PEG shell component (**Figure 6.3.6 c**) and a diameter decrease close to 17% comparable with that determined for PBS_s/PEG_c fibers with a similar initial diameter. Note in the given micrograph that PEG was still present in some parts of the fibers, giving rise to local smooth surfaces.

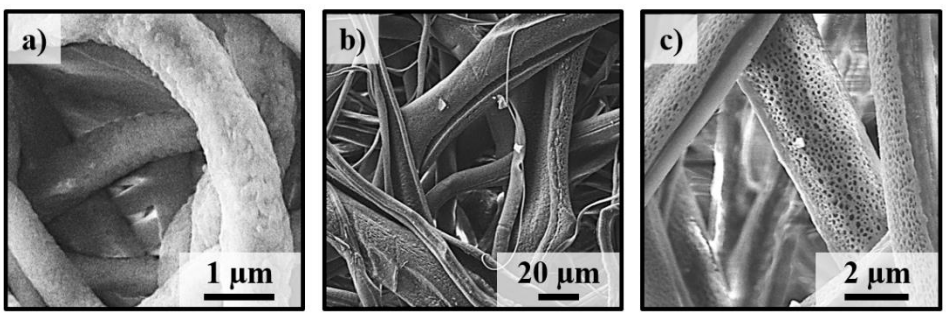

FIGURE 6.3.6.

High magnification SEM micrographs of PBS/PEG 5/15 (a), PBS_s/PEG_c 5/15 (b) and PEG_s/PBS_c 10/7 (c) electrospun samples after immersion in water.

Porosity of electrospun scaffolds was high due to the solubilization of PEG and depended on the initial size of fibers and the distribution of the two components. Thus, lower porosities corresponded to the PBS_s/PEG_c coaxial fibers (0.62-0.77) whereas maximum values (0.77-0.94) were determined for uniaxial nanofibers. It is interesting to note that the core-shell distribution played a significant role, and thus scaffolds derived from microfibers having a PEG shell had significantly higher porosity (0.71-0.88) than related ones having a PEG core. In the last case, the external surface and probably the pore dimension of fibers should be less affected by solubilization.

Contact Angle Measurements

Information about the distribution of hydrophilic PEG and hydrophobic PBS in coaxial electrospun fibers can be verified through contact angle measurements as shown in **Figure 6.3.7**.

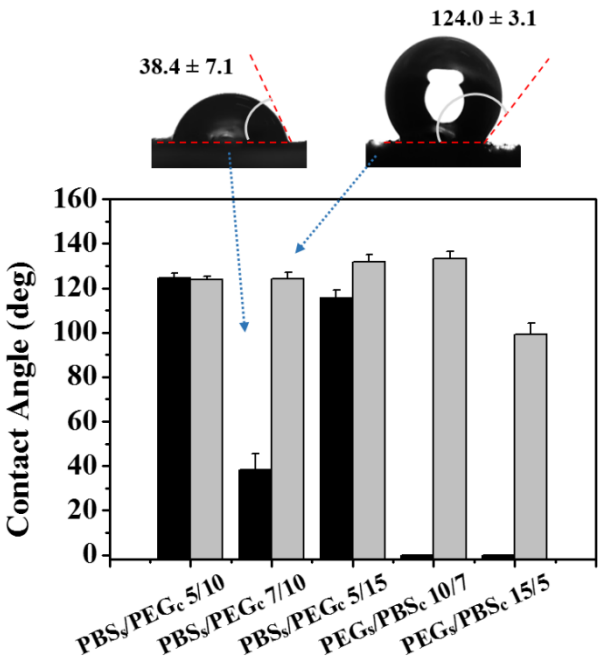

FIGURE 6.3.7

Contact angles for PBS_s/PEG_c 5/10, 7/10 and 5/15 and PEG_s/PBS_c 10/7 and 15/5 scaffolds before and after immersion. Inset show the optical micrographs of a drop deposited on a representative scaffold before (black) and after (grey) being immersed in water.

The high hydrophilicity of PEG caused sessile drop spreading, and consequently angles could not be measured for any PEG_s/PBS_c sample. On the contrary, high contact angles were usually determined for the PBS_s/PEG_c samples, indicating that PEG was well confined in the fiber core. Thus, values between 112º and 122º could be measured because of the correct core-shell structure, with hydrophobic PBS in the outer part of the fiber and the effective confinement of PEG. Note that only the PBS_s/PEG_c 7/10 sample had a non-perfect distribution or confinement since the contact angle decreased to 40º. In fact, measurements performed with melt pressed PBS films indicate a contact angle close to 90º, a value obviously lower than determined for electrospun scaffolds because surface roughness is also a dominant factor in wettability of materials. The surface area of a rough surface is greater than the surface area of a comparably sized smooth surface, and consequently an increase of the contact angle should be expected.[35] The high increase of the contact suggests also that microfiber scaffolds benefit from air pocket formation.[36] Spreading was also characteristic for uniaxial fibers because of good mixing of polymers and the high PEG content.

Figure 6.3.7 also compares contact angle measurements of scaffolds before and after being immersion in water. Results clearly indicate that a hydrophobic PBS surface was attained after the removal of PEG, with the effect being more pronounced for PEG_s/PBS_c samples and even for the defective PBS_s/PEG_c 7/10 scaffold.

Drug Load and Release from PBS/PEG Scaffolds

The micro/nanofibers of the studied samples were easily loaded with triclosan and curcumin by adding the appropriate amount of the drug in the corresponding electrospinning solution (i.e. triclosan in the PEG solution and curcumin in the PBS solution for coaxial fibers). Studies were performed with representative samples of the uniaxial and the two coaxial core-shell structures. Specifically, uniaxial fibers with the lowest and highest PEG content (i.e. PBS/PEG 5/15 and 7/10) were considered, together with the related coaxial samples with PEG placed in the core and the shell when its content was the highest and the lowest, respectively (i.e. PBS_s/PEG_c 5/15 and PEG_s/PBS_c 10/7. In this way, PBS_s/PEG_c 5/15 should have the fastest and the slowest release rate for curcumin and triclosan, respectively, while the opposite would be expected for PEG_s/PBS_c 10/7.

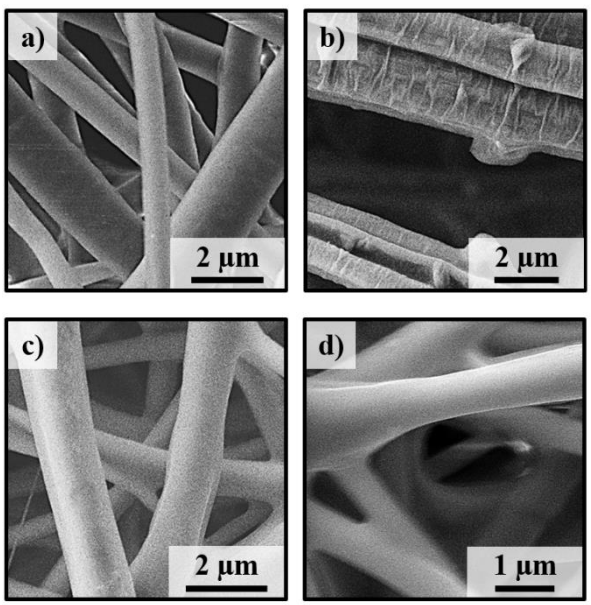

FIGURE 6.3.8

High magnification SEM micrographs of drug loaded PBS_s/PEG_c 5/15 (a). PEG_s/PBS_s 10/7 (b); PBS/PEG 5-15 (c) and PBS/PEG 7-10 (d) scaffolds.

The incorporation of the drug had some influence on the electrospinning process, and consequently operational parameters were slightly modified, as indicated in **Table 6.3.4**. Conditions were also optimized to obtain similar sizes for the two kinds of coaxial fibers (i.e. 1.49-1.58 μm) as well as for the uniaxial fibers with different compositions (i.e. 0.74 μm). **Figure 6.3.8** shows the different textures attained with the drug loaded samples, which, as expected, corresponded to rough and smooth surfaces for the coaxial fibers with a PBS shell and the two uniaxial fibers, respectively. The only significant change was the appearance of transversal ribs in the coaxial sample with a PEG shell, in contrast with the smooth surface of the unloaded sample. Changes in fiber surface morphology may have played a significant role in supporting cell attachment but they not when the polymer in the shell was highly soluble.

Immersion of loaded fibers in aqueous media led to a decrease in the fiber diameter, a rough texture and solubilization of PEG (**Table 6.3.4**), with percentages of removed PEG being similar to those for unloaded samples.

TABLE 6.3.4. Optimal electrospinning conditions applied for the selected drug loaded samples and resulting diameters before and after immersion in water.

Sample	Voltage (kV)	Rate ($mL \cdot h^{-1}$)	Distance (cm)	Ø[a] (μm)	Ø[b] (μm)	$PEG_{removed}$[c] (%)
PBS_s/PEG_c 5/15	25	1.35	17	1.49 ± 0.03	0.86	83
PEG_s/PBS_c 10/7	25	4	24	1.58 ± 0.01	1.14	94
PBS/PEG 7/10	25	1	14	0.74 ± 0.02	0.37	92
PBS/PEG 5/15	20	2	14	0.74 ± 0.01	0.42	91

[a]Before immersion in water.
[b]After immersion in water.
[c]Molar percentage of PEG removed by immersion in water respect to the initial PEG content.

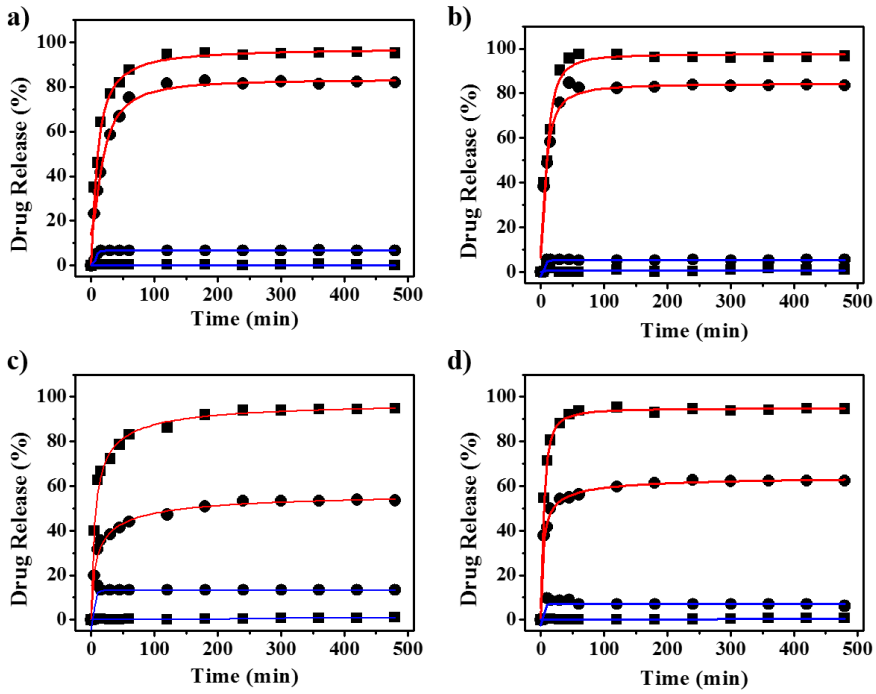

FIGURE 6.3.9

Triclosan (●) and curcumin (■) release curves in Saline Buffer/Ethanol mixture (30/70 *v*/*v*) (red line) and Saline Buffer medium (blue line) for PBS_s/PEG_c 5/15 (a) PEG_s/PBS_s 10/7 (b). PBS/PEG 5/15 (c) and 7/10 (d).

Figure 6.3.9 compares the release behavior of all scaffolds when they were exposed to a hydrophilic SS and to a more hydrophobic SS/ethanol (30:70 *v*/*v*) mixture. Release proceeds at a similarly fast rate for all assayed samples until a limit value is reached. This value is highly dependent on the affinity between the drug and the release medium, and also varies with composition and structure of electrospun fibers. Some interesting features can be pointed out:

- The amount of triclosan released in the SS medium was low (i.e. between 5-13% of the loaded drug) and inferior to the solubility limit. Hence, this hydrophobic drugs was effectively retained/adsorbed in the hydrophobic PBS component. It is remarkable that this adsorption was still found when the drug was only loaded in the water soluble PEG component placed in the shell of the coaxial fibers. Somehow the drug moved towards the hydrophobic component placed in the inner part of fiber. The amount of released drug was higher for the thin uniaxial fibers and slightly with the PEG content (i.e. 14%, 9%, 7 and 5% for PBS/PEG 5/15 and PBS/PEG 7/10, PBS_s/PEG_c 5/15, PEG_s/PBS_c 10/7 samples, respectively).

- The triclosan released in the medium containing ethanol was relatively high and strongly depended on the fiber structure and composition. Therefore, the restriction of maximum amount of triclosan released was not due to limited solubility. Lower release percentages were found for uniaxial fibers (i.e. 52% and 62%, **Figures 6.3.9 c** and **6.3.9 d**) despite their lower diameter, probably as a consequence of the mixed arrangement of PEG and PBS in the fiber. Coaxial structures gave rise to a higher release that was similar for both distributions (i.e. 80% and 82% for fibers having PEG in the core and the shell, respectively, **Figures 6.3.9 a** and **6.3.9 b**).
- The high difference between the release percentages of PBS_s/PEG_c 5/15 depending on the media (i.e. 7% and 82% for SS and SS/ethanol mixture, respectively) made it possible to discard an explanation based on a swelling effect of ethanol since triclosan was loaded into the PEG shell, which is soluble in both aqueous and ethanol solutions.

A minimum release of curcumin in SS medium was observed for all assayed samples (i.e. 1%) due to its high hydrophobicity and excellent interaction with PBS. This high retention was even observed for the thin uniaxial fibers where curcumin was loaded into the matrix constituted by the mixture of PEG and PBS polymers. On the contrary, curcumin was completely released independently of the fiber structure and compostion in the medium containing 70 *v*-% of ethanol. Logically, a tuned release in function of the ethanol ratio in the media should be expected.

Biocompatibility of Unloaded and Triclosan Loaded PLA/PEG Scaffolds

Adhesion and proliferation of fibroblast (MRC-5) and epithelial (Vero) cells were studied for all scaffolds. Both experiments are important to follow cell development since adhesion is an early cellular event whereas proliferation is an evidence of metabolic cell activity. **Figure 6.3.10 a** compares the results on relative adhesion for representative studied materials, which indicate that adhesion of fibroblast-like MRC-5 cells was well supported and even slightly improved when fibres were stabilized by solubilization of PEG or cross-linking with glutaraldehyde. On the other hand, ephitelial cells were more sensitive and in general the adhesion on the studied scaffolds decreased by around 50% compared to the control (**Figure 6.3.10 b**).

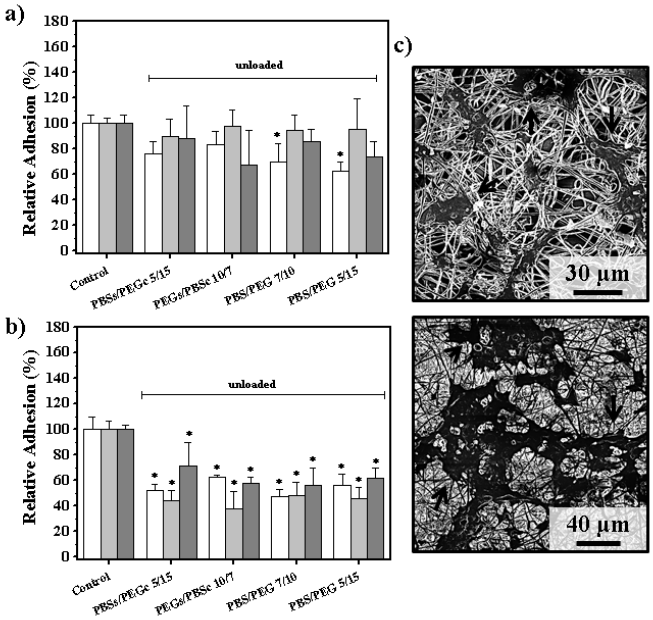

FIGURE 6.3.10

Adhesion of MRC-5 (a) and Vero (b) cells on the control plate surface, selected unloaded scaffolds before (white) and after (light grey) being immersed in water and glutaraldehyde fixed scaffolds (grey) (*$p < 0.05$) *vs*. positive control; ANOVA-Tukey's test) c) SEM micrographs showing adhesion of Vero cells on PEG_s/PBS_c 10/7 scaffolds before (top) and after (bottom) being immersed in water.

Proliferation studies indicated that MRC-5 cells were able to colonize all materials without a statistical difference compared to the control, whereas of Vero cells was proportional to their initial adhesion on the polymer scaffolds (see **Figure 6.3.11**).

SEM microscopy observations of cultures allowed the evaluation of morphological characteristics associated with cell adhesion and proliferation onto the film surfaces (e.g., **Figures 6.3.10 c** and **6.3.11 b** for representative samples and Vero cells). Cells were attached and spread out on film surfaces after a seeding of 24 h, even for the more problematic Vero cells. These exhibited large areas of cytoplasm extending on the scaffold surfaces and promoting their attachment onto the material. Cells proliferated and reached confluence after 4 days of culture. Materials were effectively colonized, and specifically cells formed a monolayer with close contacts between them.

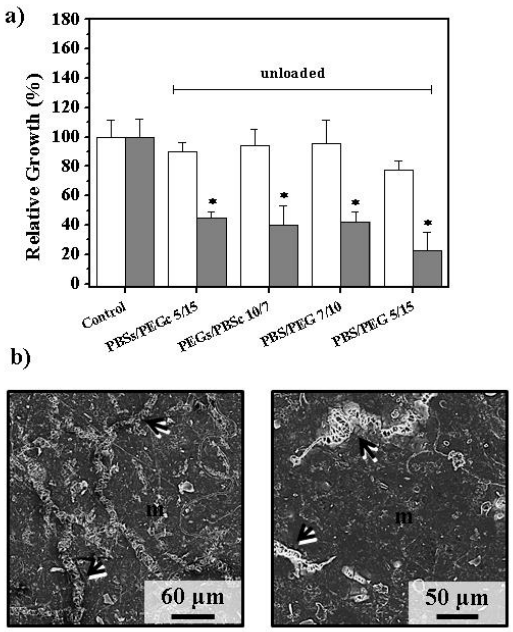

FIGURE 6.3.11

(a) Proliferation of MRC-5 (white) and Vero (grey) cells on control plate surfaces scaffolds (*$p < 0.05$) *vs.* positive control; ANOVA-Tukey's test). (b) SEM micrographs of the cellular proliferation on representative scaffolds/ PEG_s/PBS_c 10/7 (left) and PBS/PEG 7/10 (right).

Figures 6.3.10 and **6.3.11** also revealed that the drug load necessary to perform the release experiments was too high to support cell adhesion and proliferation. This means that both drugs were effectively released during culture and that minimum doses required to produce cell necrosis were always attained. In fact, the required cytotoxic concentrations of curcumine and triclosan to reduce cell population by 50% (CC_{50}) were approximately 14-24 $\mu g \cdot mL^{-1}$ and 6-15 $\mu g \cdot mL^{-1}$, respectively. The given intervals indicated the toxicity for the more sensitive Vero cells (lower values) and the MRC-5 cells (higher values). Experimental cytotoxic concentrations were clearly lower than calculated for complete release of loaded drugs (i.e. 50 and 100 $\mu g \cdot mL^{-1}$ for curcumin and triclosan, respectively).

Antibacterial Properties of Triclosan Loaded PLA/PEG Scaffolds

Triclosan is a broad-spectrum antiseptic with documented safety and efficacy against Gram-positive and Gram-negative bacteria (e.g., *M.luteus* and *E.coli*, respectively). The antibacterial effect of triclosan released from scaffolds constituted by uniaxial and coaxial electrospun fibers was determined by studying bacterial adhesion and growth inhibition in broth medium.

As shown in **Figure 6.3.12** for unloaded samples, high adhesion was measured for all scaffolds of both bacteria. It was considerably greater than that measured for the control, probably as a consequence of the high specific surface and porosity of the scaffolds. Therefore, it seems crucial to prevent bacterial colonization by means of an antiseptic, and in this sense triclosan was highly effective (**Figures 6.3.12 a** and **6.3.12 b**).

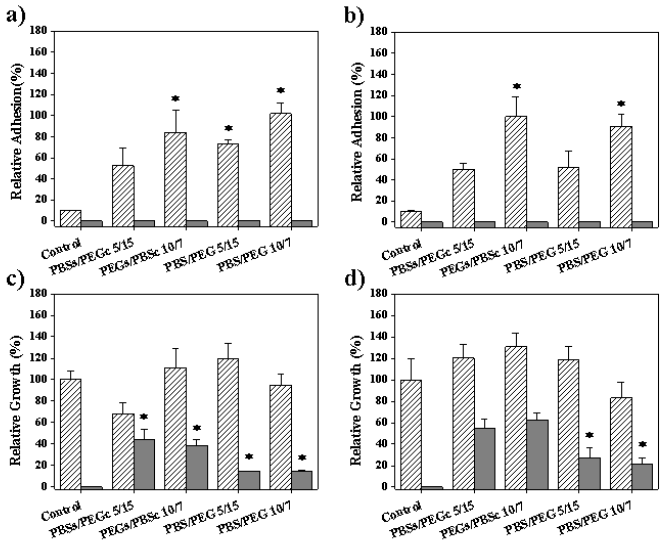

FIGURE 6.3.12

Adhesion (a,b) and relative growth (c,d) of *Escherichia coli* (a,c) and *Micrococcus luteus* (b,d) on control surfaces and unloaded (sparse) and TCS loaded (grey) PBS_s/PEG_c. PEG_s/PBS_c and PBS/PEG electrospun samples.

Growth inhibition measurements made with triclosan loaded scaffolds (**Figures 6.3.12 c** and **6.3.12 d**) demonstrated that those constituted by coaxial fibers were more susceptible to colonization, whereas the core-shell structure had not significant influence. Thus, inhibitions between 60%-40% and 90%-75% were found for scaffolds constituted by coaxial and uniaxial fibre, respectively. These results agree qualitatively with the higher release observed for the thin uniaxial fibers SS medium and demonstrated that the low release was sufficient to inhibit bacterial colonization. The effect of triclosan was clearly enhanced for the Gram-negative bacterium (i.e. *E.coli*) due to its higher sensitivity to the drug.

6.3.4 Conclusions

Coaxial microfibers with different core-shell distributions and constituted by PEG and PBS could be prepared from dichloromethane solutions and optimized processing parameters. These fibers had different surface textures depending on the polymer in the shell (i.e. smooth and rough for PEG and PBS, respectively), suggesting the success of coaxial electrospinning. This was also corroborated by contact angle measurements that demonstrated the hydrophilicity and hydrophobicity of coaxial fibers having a shell of PEG and PBS, respectively.

Calorimetric data indicated a high crystallinity for PBS rich domains caused by a molecular orientation favored by the electrospinning process. A decrease in the corresponding melting temperature also suggested that the polymer confined in the fiber core developed more defective crystals.

XPS spectroscopy revealed that establishment of new interactions between PBS and PEG were established in the uniaxial nanofibers prepared from a common dissolution of both polymers. Thus, a significant amount of PEG remained in the scaffolds after immersion in water. This amount was dependent on the fiber distribution, with higher and lower values being associated with coaxial fibers with a PBS shell and a PEG shell, respectively.

Release of triclosan and curcumin from loaded scaffolds was highly dependent on the media and their hydrophobicity. Slight differences were also detected depending on the structure of the fiber. Specifically, the lowest release was found for PEG-rich uniaxial nanofibers exposed to SS medium whereas the highest value corresponded to coaxial microfibers exposed to SS/ethanol mixtures. Scaffolds constituted by coaxial microfibers were more susceptible to colonization by both Gram-positive and Gram-negative bacteria whereas the core-shell structure had no significant influence.

6.3.5 References

[1] D.H. Reneker, I. Chun, Nanotechnology, 7 (1996) 216-223.

[2] A. Frenot, I.S. Chronakis, Curr Opin Colloid Interface Sci, 8 (2003) 64-75.

[3] Y. Dzenis, Science, 304 (2004) 1917-1919.

[4] K. Jayaraman, M. Kotaki, Y.Z. Zhang, X.M. Mo, S. Ramakrishna, J Nanosci Nanotechno, 4 (2004) 52-65.

[5] S.R. Dhakate, B. Singla, M. Uppal, R.B. Mathur, Adv Mater Lett, 1 (2010) 200-204.

[6] S. Sharma, Adv Mater Lett, 4 (2013) 522-533.

[7] M. Zamani, M.P. Prabhakaran, S. Ramakrishna, Int J Nanomedicine, 8 (2013) 2997-3017.

[8] M. Spasova, O. Stoilova, N. Manolova, I. Rashkov, G. Altankov, J Bioact Compat Pol, 22 (2007) 62-76.

[9] L.J. del Valle, R. Camps, A. Diaz, L. Franco, A. Rodriguez-Galan, J. Puiggali, J Polym Res, 18 (2011) 1903-1917.

[10] E.H. Jeong, S.S. Im, J.H. Youk, Polymer, 46 (2005) 9538-9543.

[11] Y. Liu, J.-H. He, J.-Y. Yu, Fibres Text East Eur, 15 (2007) 30-33.

[12] X. Zong, S. Li, E. Chen, B. Garlick, K.-s. Kim, D. Fang, J. Chiu, T. Zimmerman, C. Brathwaite, B.S. Hsiao, B. Chu, Ann Surg, 240 (2004) 910-915.

[13] E. Llorens, L.J. del Valle, A. Diaz, M.T. Casas, J. Puiggali, Macromol Res, 21 (2013) 775-787.

[14] R. Toshkova, N. Manolova, E. Gardeva, M. Ignatova, L. Yossifova, I. Rashkov, M. Alexandrov, Int J Pharm, 400 (2010) 221-233.

[15] J. Zeng, L.X. Yang, Q.Z. Liang, X.F. Zhang, H.L. Guan, X.L. Xu, X.S. Chen, X.B. Jing, J Control Release, 105 (2005) 43-51.

[16] K. Kim, Y.K. Luu, C. Chang, D. Fang, B.S. Hsiao, B. Chu, M. Hadjiargyrou, J Control Release, 98 (2004) 47-56.

[17] H. Cao, X.G. Jiang, C.L. Chai, S.Y. Chew, J Control Release, 144 (2010) 203-212.

[18] S.N. Reznik, A.L. Yarin, E. Zussman, L. Bercovici, Phys Fluids (1994), 18 (2006).

[19] A.L. Yarin, Polymers Adv Tech, 22 (2011) 310-317.

[20] I.C. Liao, S. Chen, J.B. Liu, K.W. Leong, J Control Release, 139 (2009) 48-55.

[21] C.L. He, Z.M. Huang, X.J. Han, L. Liu, H.S. Zhang, L.S. Chen, J Macromol Sci, Part B, 45 (2006) 515-524.

[22] C.-L. He, Z.-M. Huang, X.-J. Han, J Biomed Mater Res A, 89A (2009) 80-95.

[23] D.A. Herold, K. Keil, D.E. Bruns, Biochem Pharmacol, 38 (1989) 73-76.

[24] T. Fujimaki, Polym Degrad Stabil, 59 (1998) 209-214.

[25] S.M. Lai, C.K. Huang, H.F. Shen, J Appl Polym Sci, 97 (2005) 257-264.

[26] A.D. Russell, J Antimicrob Chemoth, 53 (2004) 693-695.

[27] H. Hatcher, R. Planalp, J. Cho, F.M. Torti, S.V. Torti, Cell Mol Life Sci, 65 (2008) 1631-1652.

[28] Y. Jiao, J. Wilkinson, X. Di, W. Wang, H. Hatcher, N.D. Kock, R. D'Agostino, M.A. Knovich, F.M. Torti, S.V. Torti, Blood, 113 (2009) 462-469.

[29] S.C. Gupta, S. Prasad, J.H. Kim, S. Patchva, L.J. Webb, I.K. Priyadarsini, B.B. Aggarwal, Nat Prod Rep, 28 (2011) 1937-1955.

[30] D. Karst, Y.Q. Yang, J Appl Polym Sci, 96 (2005) 416-422.

[31] M. Imaizumi, T. Nagata, Y. Goto, Y. Okino, T. Takahashi, K. Koyama, Kobunshi Ronbunshu, 62 (2005) 438-440.

[32] E. Llorens, L.J. Valle, R. Ferrán, A. Rodríguez-Galán, J. Puiggalí, J Polym Res, 21 (2014) 1-15.

[33] H.Y. Wang, J.H. Ji, W. Zhang, Y.H. Zhang, J. Jiang, Z.W. Wu, S.H. Pu, P.K. Chu, Acta Biomater, 5 (2009) 279-287.

[34] M. Cerruti, S. Fissolo, C. Carraro, C. Ricciardi, A. Majumdar, R. Maboudian, Langmuir, 24 (2008) 10646-10653.

[35] R.N. Wenzel, Ind Eng Chem, 28 (1936) 988-994.

[36] A.B.D. Cassie, S. Baxter, Trans Faraday Soc, 40 (1944) 546-551.

7.
Conclusions

General Conclusions

First Block: Antioxidant loaded biodegradable scaffolds and potential application

The study of 3D scaffolds from electrospun polylactide nanofibers loaded with antioxidants (i.e., vitamin B_6 in pyridoxine and pyridoxal form and two polyphenols, caffeic and *p*-coumaric acids) prepared by electrospinning under optimized conditions leads to the following conclusions:

i. Fiber morphology (diameter and texture) and crystallinity were dependent on the drug load. Furthermore, the drug release was influenced by the kind of drug and release medium (hydrophobic or hydrophilic medium).
ii. The new loaded PLA scaffolds were suitable to support both cell adhesion and growth, and additionally had a protective activity against the oxidative stress responsible for cell damage and death by necrosis.
iii. New antioxidative scaffolds demonstrated *in-vivo* and *in-vitro* inhibition of the oxidative damage on DNA under both *in-vivo* and *in-vitro* conditions. Thus, they could be used as platform to improve the process of DNA extraction and purification.

Second Block: Multifunctional biodegradable fiber scaffolds

Multifunctional PLA scaffolds were obtained by loading different drugs simultaneously during the process of electrospinning:

i. PLA scaffolds with antibacterial, antioxidant and/or anti-inflammatory activity were obtained by loading triclosan, ketoprofen and/or *p*-coumaric acid, respectively. Thus, the scaffolds obtained were dual or ternary drug-loaded systems.
ii. The drug release from these multifunctional scaffolds was modulated by: first, the PLA enantiomeric grade, because its influence thermal, to the degradation and the mechanical properties of the matrix; second, the chemical structure of the drugs that are combined in the scaffold and their behaviours against the different release media (hydrophilic or hydrophobic medium).
iii. These new materials have therapeutic advantage because they effectively respond to the need of procuring a simultaneous control over potential microbial infections, and inflammatory-oxidative processes that can occur during wound closure and tissue repair.

Third Block: Preparation of biodegradable scaffolds that incorporate non-electrospinable polymers

The development of fiber scaffolds from mixtures of electrospinable and non-electrospinable polymers allowed obtaining new hybrid materials in the biomedical field:

i. Antibacterial scaffolds can be prepared from the mixture of PLA and PHMB (polyhexamethylenebiguanide hydrochloride). The antibacterial activity of PHMB loaded scaffolds is much greater than those loaded with chlorhexidine (CHX) monomer.
ii. Conducting scaffolds were successfully prepared from mixtures of PLA and P3TMA (poly 3-thiophene methyl acetate). These PLA/P3TMA hybrid scaffolds maintained the biocompatible and current conducting (e.g., capability to store charge) properties of each individual component. Thus, these new matrices provide the possibility to get cellular growth and differentiation through electrical stimulation.

Fouth Block: Biodegradable polymer matrices incorporating polyethylene glycol as a sacrificial polymer

Scaffolds containing a sacrificial polymer (e.g., polyethylene glycol (PEG)) are reshaped when this polymer is removed. PEG is considered an appropiate sacrificial polymer in the biomedical field due to its non-toxicity, high biocompatibility and easy removal from the human body. The following specific issues were derived from the study of electrospun using PEG as a sacrificial polymer:

i. Scaffolds having to different ratios of PEG and PLA were easily obtained by electrospinning solution mixtures of both homopolymers. A high amount of PEG (e.g., 70 *wt*-%) can be supported by these fibers, giving rise after its removal to matrices that maintain their ability to support cell adhesion and growth. In addition, fibers can be loaded with hydrophobic drugs achieving a burst effect at the beginning of their release.
ii. Electrospinning from independent solutions of PLA and PEG and using a single rotatory collector gave rise to matrices constituted by well-differentiated fibers of each homopolymer. The process allows an easy control to get homogeneous fibers and scaffolds constituted by variable ratios of PEG and PLA. Furthermore, the process allows loading independently each polymer with different drugs in such a way that a rapid or a sustained release can be achieved. The independent loading process can minimize the effect of the drug on the fiber morphology (e.g., size and texture) by modulating the processing parameters.
iii. Coaxial microfibers with different core-shell distributions and constituted by PEG and poly(butylene succinate) (PBS) were successfully prepared. PEG could be easily solubilized even if it was placed in the core of the fibers. The corresponding electrospun scaffolds appear interesting to get a fast and slow release of drugs loaded

in the highly soluble PEG and the hydrophobic PBS component, respectively. Coaxial microfibers showed a slightly faster release than uniaxial fibers with similar composition and size. Scaffolds constituted by coaxial microfibers were also more susceptible to colonization by both Gram-positive and Gram-negative bacteria, whereas the core-shell structure had no significant influence